Microscopic Analysis of Aerosol Chemical Mixing State in Cold Environments

by

Rachel M. Kirpes

A dissertation submitted in partial fulfillment
of the requirements for the degree of
Doctor of Philosophy
(Chemistry)
in the University of Michigan
2019

Doctoral Committee:

      Assistant Professor Kerri A. Pratt, Chair
      Assistant Professor Andrew P. Ault
      Professor Zhan Chen
      Associate Professor Mark Flanner

Rachel M. Kirpes

rmkirpes@umich.edu

ORCID iD: 0000-0002-2998-0108

Dedication

Laudato Si, per frate Sole e sora Luna

Acknowledgements

Thank you to my advisor, Dr. Kerri Pratt, for always challenging me, for setting an example of excellence and integrity, and for entrusting me with ownership of my work. Thank you for your mentorship and support of my scientific goals and professional goals, from Arctic field work to D.C. policy. You've helped make many amazing opportunities possible that have allowed me to grow as a scientist and as a person and have prepared me for what comes ahead. I would also like to thank my committee members, Dr. Andrew Ault, Dr. Zhan Chen, and Dr. Mark Flanner, for your support and guidance through this program. In particular, I would like to thank Dr. Ault for your mentorship and the encouragement to learn any new technique that might advance a project, from Raman and fluorescence to AFM-IR, STXM-NEXAFS, and beyond. Thank you for encouraging me to think creatively and to never give up on a project.

I would also like to thank all of my collaborators, who have not only helped make my research a success, but have also shown me a positive, supportive, scientific community. I've learned from all of you, most importantly, how to bring joy into research. For the MAIA team, I couldn't have asked for a more amazing group of women in science to work with and to laugh with. I've learned so much from you and appreciate your support and encouragement. Dr. Paty Matrai, thank you for your valuable mentorship, and for always reminding me to pause and enjoy my Arctic adventure. For the entire MOCCHA expedition team, I couldn't have asked for a better group to spend ten weeks on a ship in the Arctic with - thank you for the great science and friendship. For Dr. Caroline Leck, from whom I learned a great deal, thank you for the mentorship and for sharing your stories. Thank you also to the crew of the *Oden*, for always lending a hand, attempting to teach me Swedish, and throwing some great parties. I would also like to thank the scientists and staff at PNNL EMSL, particularly Dr. Alex Laskin and Dr. Swarup China, who made each of my many trips to the national lab successful and enjoyable.

To the members of the Pratt and Ault labs, past and present, thank you for the last five years. I truly couldn't have asked for better colleagues or greater friends. We've been through so much together, from field work prep to taco tours to paint and pour, and for your friendship and support, I'm truly grateful. Becky, the Thelma to my Louise, thanks for always being there to help

fix the APS, roll a cart of equipment across campus, take a walk in the Arb, relax with a glass of rosé, buy way too many plants at the farmer's market, and make me pancakes when I just couldn't. Stephen, we've been in this together since the beginning. Thanks for being both the youngest and oldest student in the lab with me, always being willing to chat, for all the airport rides, and quests to find the best beer at AGU. Matt, thanks for always being willing to take my crazy projects to the machine shop, and when in doubt, visit our friends at ACE Hardware. I appreciate all the memes and our shared love of the Mayor. Amy, thanks for teaching me microscopy when I was brand new and making it fun by jamming to 90s boy bands in the SEM room. Nate, I'll always appreciate your Taylor Swift karaoke to convince me to come to Michigan. Thanks for always answering my questions about marine aerosol, bubbles, and hipster trends. Peter, thanks for the MATLAB tips, commentary, both genuine and sarcastic, and lab happy hour. Jun and Qianjie, thanks for answering all my MATLAB questions since Peter's been gone. Ryan, thank you for teaching me about fantasy football and for joining in the original taco tour. Siyuan and Ryan, thanks for sharing my love of dark beer. Jeff, I've truly enjoyed all our conversations about pedagogy, policy, faith, and Casey's pizza. Jess, thanks for your friendship and mentorship, and for trying to teach me how to knit that one time. Thanks for sharing my love of science, gardening, and wine. Nancy, thank you for all of your help with the AFM, it always behaved better when you were around. I'll miss our hot pot parties. Nicole, I've appreciated all the snapchats from MC^2, and our shared complaints about the lack of coffee in the NCRC. Jamy and Kathryn, thanks for the Bachelor fantasy leagues and watch parties, and for carrying on Pratt Lab traditions.

For all my friends in Ann Arbor and beyond, thank you for seeing me through this, understanding when I was busy, and checking in if you hadn't heard from me in a while. For the SMSP Grad/YP group, I'm so grateful to have been a part of this community in Ann Arbor. Thank you for sharing in my successes and struggles and reminding me there's a world outside of lab. Adrian at Chela's, for the wonderful food and genuine friendship, I'll always be grateful. For Kaitlin and Justin, who completed our ISU Chemistry trio, thank you for being great lab partners and the most accomplished study group – we're now a D.D.S., J.D., and Ph.D. Sarah, Andrea, Holly, Rachel, and Hannah, some of my greatest and oldest friends, thank you for your love and support and for always believing in me. Wherever we get together, Costa Rica, Oregon, Des Moines, or Ann Arbor, we always have a great time.

For all my past teachers and mentors, you've played a valuable role in my growth and development as a scientist, and for your support and encouragement, I thank you. Mrs. Barry, thank you for inspiring my love of science at such a young age. For your continued encouragement, from kindergarten through graduate school, and celebration of the person I've become, I'm grateful. For Mr. Hutcheson and Mrs. Blakely, who shared your love of science, inspired my pursuit of chemistry, and challenged me to rise to my potential, I'll always cherish your classes and appreciate your mentorship. For Dr. Emily Smith, who inspired my love of analytical chemistry, introduced me to Raman spectroscopy, and encouraged me in research, thank you for taking in a freshman and allowing me to run with my own project for the next three years. Dr. Brian Hornbuckle, thank you for your valuable advice and mentorship and active investment in my career. Without your encouragement, I would not have experienced field work, pursued a NASA internship, or discovered a passion for atmospheric chemistry. Thank you for always challenging me, strongly encouraging me to learn MATLAB, and helping me along the way. I'll always appreciate your excitement when I decided on Michigan, following in your footsteps, to pursue my Ph.D. For NASA SARP, thank you for creating an amazing opportunity and taking an interest in your students' success beyond the program. Dr. Emily Schaller, Dr. Don Blake, Dr. Josette Marrero, and Dr. Laura Judd, thank you for your mentorship and encouragement, for inspiring an interest in atmospheric chemistry, and demonstrating the breadth of career paths available.

Finally, thank you to my family, who have always supported me. Thank you for sharing your love of science and the environment and always inspiring me. Mom and Dad, you've always believed in me, even when I doubted myself, and have always been proud of me, even when I did not recognize my own accomplishments. Thank you for always supporting my dreams, and for letting me know that wherever I live, you'll come visit. For my brothers, Michael and Charles, thank you for always being there for me and encouraging my pursuit of science. Aunt Martha, thank you for showing me it was possible to get a Ph.D., and for celebrating me following in your footsteps here at Michigan. For my grandparents, thank you for your love and support; you've always been proud of all my accomplishments, even those so different than your own experiences. Thank you for teaching me how to find common ground when sharing my passions. For my family's constant love and support, I owe everything.

Table of Contents

List of Tables

List of Figures

List of Equations

Abstract

Atmospheric aerosol particles impact climate through scattering or absorbing solar radiation, altering surface albedo upon deposition, and aiding in cloud formation. These climate effects depend on the physical and chemical properties of individual particles, including chemical composition, size, phase, and morphology (physicochemical mixing state). In the Arctic, atmospheric particles play a key role in climate processes in the drastically changing region, but Arctic aerosol physicochemical mixing state is not well constrained. Large knowledge gaps remain in understanding the sources and composition of Arctic aerosol, as there is a lack of single particle measurements, particularly across seasons (including fall – winter) and throughout the region (especially the high Arctic). In this dissertation, the physicochemical properties of individual particles were examined at multiple Arctic locations (Bering Strait, Chukchi Sea, coastal Beaufort Sea, and high Arctic Ocean) and during different seasons (winter – spring and summer). The results of this work will increase understanding of Arctic aerosol sources and composition across scales, which is critical to predicting aerosol composition and climate-relevant properties in a New Arctic.

Sea spray aerosol (SSA) contributes the largest global flux of particles to the atmosphere, and is therefore an important climate driver, particularly in remote regions, including the Arctic. Laboratory-based sea spray aerosol generation experiments were conducted to evaluate the impacts of seawater temperature, salinity, and marine biology on SSA production and composition in cold environments. These results showed that temperature was as important as biology for controlling SSA production, and organic enrichment was observed in individual SSA particles, indicative of marine organics being transferred to the particle phase.

To investigate the role of SSA in the ambient Arctic environment, atmospheric particles were collected during wintertime in the Alaskan Arctic. SSA was a major fraction of the observed aerosol number, demonstrating that sea ice fractures are a source of wintertime aerosol. Further analysis of the wintertime SSA showed a major organic component in the SSA particles, with organic carbon coatings consisting of saccharides, amino acids, and fatty acids. These compounds are derived from exopolymeric substances (EPS) associated with biologically productive sea ice.

Greater SSA organic enrichment was observed in winter than in summer, suggesting a unique, previously unidentified source of SSA organics from sea ice algae EPS during winter. Motivated by this work in the wintertime Alaskan Arctic, both ambient and laboratory-generated SSA particles were collected during summer in the high Arctic. SSA production from open leads was observed under high wind conditions, and organic enrichment was observed in both lab-generated and ambient individual SSA particles. Saccharides and fatty acids were identified as the dominant organic compounds present in SSA particles, derived from EPS and marine organics.

Atmospheric particle samples were collected in the summertime Alaskan Arctic to investigate the impacts of sea ice loss and increasing development. Samples in the Bering Strait demonstrated great anthropogenic influence. Within the Chukchi Sea, samples were mainly influenced by marine biogenic sources. On the North Slope of Alaska during summer, ammonium sulfate particles demonstrating unique phase and morphology were observed. Organic coatings observed on the particles may play a role in inducing phase changes not previously predicted in the ambient atmosphere. Through these studies, we have gained a greater understanding of the climate-relevant complex atmospheric chemistry and aerosol physicochemical mixing state in the Arctic occurring under changing conditions and with evolving aerosol sources.

Chapter 1.   Introduction

1.1 Characteristics and Impacts of Atmospheric Aerosols

An aerosol is a suspension of a liquid or solid particle in a gas (e.g. air) (Pöschl, 2005). Aerosol particles, or particulate matter, can range in size from ~1 nm to ~100 μm in diameter, comprising a nucleation mode (<10 nm), Aitken mode (~10 – 100 nm), accumulation mode (~100 – 1000 nm), and coarse mode (> 1 μm) (Seinfeld and Pandis, 2012). Aerosol particles come from a diversity of natural and anthropogenic sources, with complex chemical composition (Pöschl, 2005). Aerosol particles can be primary, directly emitted to the atmosphere as solid or liquid particles, or secondary particles, formed by the oxidation and condensation of atmospheric gases (Pöschl, 2005). These particles impact air quality, human health, and climate, with the magnitude of these impacts dependent on particle size and chemical composition (Pöschl, 2005). These properties also determine particle atmospheric lifetime and the likelihood of particles to participate in atmospheric chemical reactions (Seinfeld and Pandis, 2012).

1.1.1 Aerosol Impacts on Climate

Aerosol particles impact climate directly by scattering or absorbing solar radiation, and indirectly by modifying cloud formation, properties, and lifetime, and altering snow albedo (Pöschl, 2005). Total aerosol particle contributions to radiative forcing comprise both the direct and indirect effects, but these contributions represent the largest source of uncertainty in global radiative forcing predictions, due to the complex and dynamic nature of aerosol composition, sources and atmospheric fluxes, spatial variability, and transformations in the atmosphere (Boucher et al., 2013). Through the direct effect, aerosol particles either absorb or scatter incident solar radiation, dependent on chemical composition (Pöschl, 2005). For example, soot absorbs solar radiation, leading to a warming effect, while sulfate particles scatter radiation, leading to a cooling effect (Pöschl, 2005). Through the indirect effect, particles impact cloud formation by acting as cloud condensation nuclei (CCN) or ice nucleating particles (INP), in turn impacting cloud brightness and lifetime (Andreae and Rosenfeld, 2008; Pöschl, 2005). Aerosol indirect

effects depend on particle concentration, size, and chemical composition. Typically, >100 nm diameter particles will be efficient CCN at lower water vapor saturation than <100 nm particles (Andreae and Rosenfeld, 2008). With higher particle number concentrations, a greater number of smaller cloud droplets are formed, resulting in higher albedo, more reflective clouds, and increased cloud lifetime due to decreased precipitation efficiency (Lohmann and Leck, 2005; Pöschl, 2005). Particle impacts on clouds are also dependent on chemical composition, with hygroscopic sea salt particles readily taking up water and acting as efficient CCN, while particles comprised of less hygroscopic material, such as organic carbon, will not efficiently form cloud droplets (Seinfeld and Pandis, 2012). Ice nucleation, through deposition nucleation, immersion freezing, condensation freezing, contact freezing, or inside-out evaporation freezing, is also dependent on particle morphology (porous or nonporous, crystalline or amorphous), phase (soluble or insoluble) and composition (Kanji et al., 2017). Particles that can readily act as INP include mineral dust and primary biological particles (e.g. pollen, spores, and bacteria), and in some cases, soot (Kanji et al., 2017; Murray et al., 2012). Generally, organic carbon and sulfate impede INP activity (Andreae and Rosenfeld, 2008).

1.1.2 Aerosol Mixing State

Many physical properties of particles relevant for climate impacts, including viscosity, phase, reactivity, hygroscopicity, and optical properties, depend on the chemical composition of the particles. The diversity of aerosol sources, in addition to atmospheric processing, can result in complex particle composition with hundreds to thousands of different compounds present (Prather et al., 2008; Riemer et al., 2019). Aerosol mixing state describes the distribution of chemical species within an aerosol population, considering both inter- and intraparticle variability (Riemer et al., 2019). An aerosol population is externally mixed if each particle only contains one chemical species (e.g. ammonium sulfate, soot, or organic carbon), while a fully internally mixed aerosol population would have the same chemical species present in the same relative abundance in all particles (e.g. all particles contain the same amounts of organic carbon and soot) (Fig. 1.1) (Ault and Axson, 2017; Riemer et al., 2019). In reality, ambient aerosol populations have more complex mixing states, varying with particle size, altitude, and atmospheric lifetime, with more internal mixing observed under stagnant conditions, during pollution events, and with transport away from aerosol sources (Riemer et al., 2019). The physical properties of ambient particles also vary throughout an aerosol population, which can be described by considering the physicochemical

mixing state (Ault and Axson, 2017; Riemer et al., 2019). For example, freshly emitted sea spray aerosol is a complex mixture of inorganic salts coated with marine organics (Quinn et al., 2015), and atmospheric reactions with nitrogen- and sulfur-containing gases contribute secondary species to the particles (Gard et al., 1998), demonstrating a complex, dynamic mixing state. Secondary organic aerosol, formed by the oxidation and condensation of volatile organic compounds, may be a complex mixture of different organic compounds, and become internally mixed with ammonium sulfate particles, resulting in particles with complex morphology, phase, and composition (Shiraiwa et al., 2013). Despite the important implications of mixing state for aerosol impacts on climate, few direct measurements of aerosol mixing state exist, since this requires the measurement of individual particles, which is not commonplace. In particular, Arctic aerosol mixing state variability with season and region is not well understood (Willis et al., 2018), particularly in the high Arctic (Leck and Svensson, 2015; Sierau et al., 2014) and during winter-spring in the coastal Arctic (Hara, 2003; Hara et al., 2002b; Weinbruch et al., 2012).
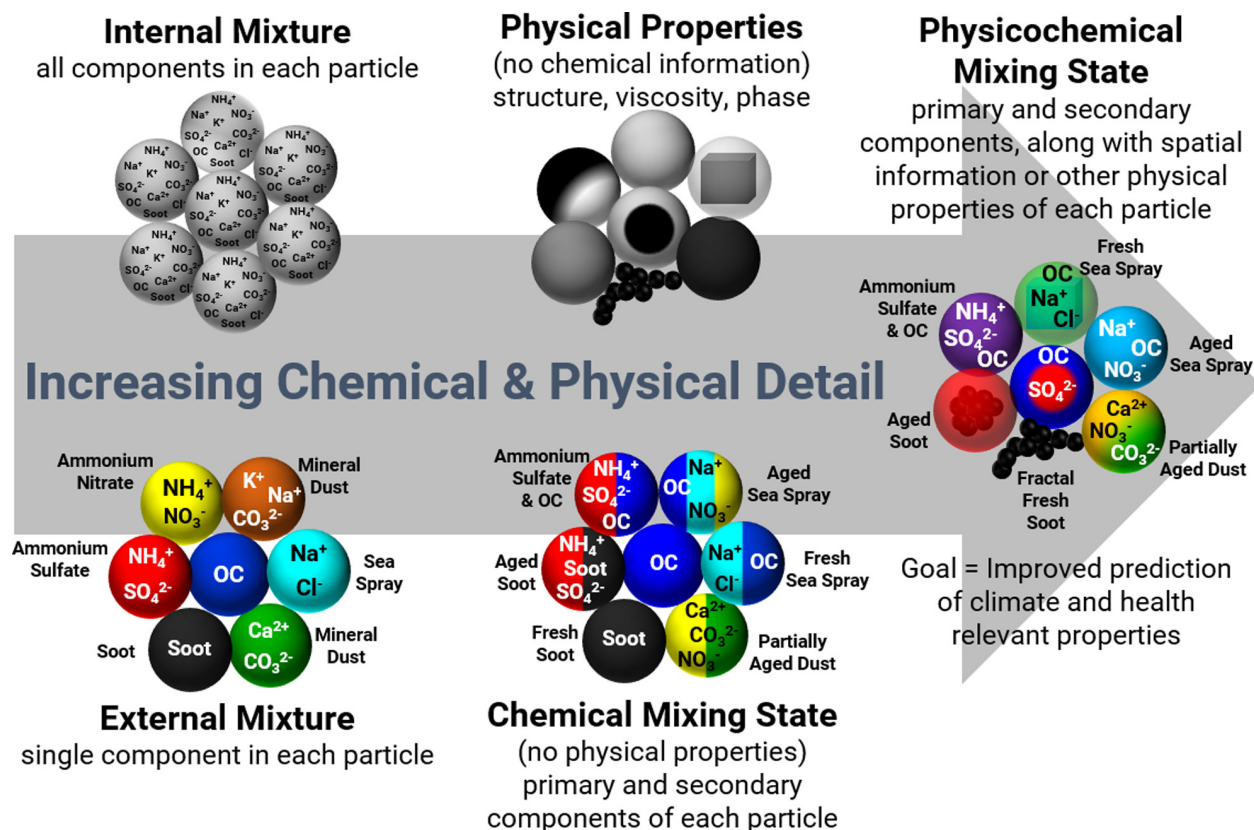
Figure 1.1 Representations of particle composition with increasing complexity and detail. Chemical mixing state provides information on primary versus secondary components, but does not provide spatial information or other physical properties. Physicochemical mixing state provides both chemical detail and spatial information or physical properties. Note that the locations of the colors in the chemical mixing state particles are not meant to convey spatial distribution, only the presence of both primary and secondary components. Reprinted with permission from Ault, A. P.; Axson, J. L. Atmospheric Aerosol Chemistry: Spectroscopic and Microscopic Advances. Analytical Chemistry 2017, 89 (1), 430–452. https://doi.org/10.1021/acs.analchem.6b04670. Copyright (2017) American Chemical Society.

1.2 The Changing Arctic Environment

The Arctic region is experiencing drastic transformations as a result of climate change. The Arctic is currently warming at twice the average global rate (Holland and Bitz, 2003; Serreze and Barry, 2011), with dramatic changes to tundra permafrost, sea ice, and atmospheric conditions. Sea ice is rapidly declining across the region, with the 10 lowest years of sea ice extent occurring within the last 12 years (Gautier, 2018). Based on current trends, completely ice-free summers are predicted by 2050, with some models predicting a lack of summer sea ice as early as 2030 (Overland and Wang, 2013). In addition to declining summer sea ice extent, many regions of the Arctic are experiencing delayed fall freeze-up (Beitler, 2017). This delay has been particularly

pronounced in coastal regions of the Bering, Chukchi, and Beaufort Seas in the Alaskan Arctic, in addition to the Greenland Sea and European Arctic Ocean, with these regions experiencing greater than 40 days delayed freeze-up in the most recent years, compared to the 1979 – 2017 average (Vizcarra, 2018). Declining summer ice extent and delayed fall freeze results in less sea ice surviving each year to transition from first year ice to multiyear ice (Stroeve et al., 2014). Multiyear sea ice is stronger and thicker, with the oldest ice several meters thick (Maslanik et al., 2011). The relative fraction of multiyear sea ice has rapidly decreased, previously comprising the majority of sea ice in the Arctic (Maslanik et al., 2011), but reduced to less than 10 – 15 % of the sea ice extent this year (Meier, 2019). This multiyear ice has been replaced with first year ice, which is thinner (less than 1 m thick) and more prone to fracturing (Stroeve et al., 2012). Fracturing of sea ice forms open leads, or areas of open water surrounded by sea ice (Stroeve et al., 2012). These open leads can range in width from <500 m to >20 km (Wernecke and Kaleschke, 2015), with large leads or polynyas persistent in many coastal areas, including off the coast of Utqiaġvik, Alaska (Hirano et al., 2018; Jones et al., 2016). Not only do increasing open leads change the landscape of the Arctic Ocean, these areas of open water change the surface albedo (Serreze and Barry, 2011; Stroeve et al., 2014). Open water is relatively darker than the bright sea ice surface, and therefore absorbs more incident sunlight, warming and melting the surrounding sea ice.

Declining Arctic sea ice and increasing open water is also contributing to the increasing development in the Arctic region. Shipping activity is expected to continue to increase in the region as sea ice declines and Arctic sea routes become available (Dalsøren et al., 2007; Roiger et al., 2015). The Bering Strait is one of the busiest shipping lanes in the world and is the entry to the Northern Sea Route and the Northwest Passage (Huntington et al., 2015). In addition, the Arctic is a region of increasing oil and gas development, as the Arctic shelf holds 13% of the world's undiscovered oil and 30% of natural gas reserves (Gautier et al., 2009). Coastal oil and gas activity is already prominent in the Alaskan Arctic, Norwegian Arctic, and Russian Arctic, and offshore exploration and resource extraction is predicted to continue to increase as sea ice decline provides access to new areas (Dalsøren et al., 2007; Ødemark et al., 2012; Peters et al., 2011; Roiger et al., 2015).

1.3 Sources and Characteristics of Arctic Aerosols

1.3.1 Seasonal Changes in Aerosol Sources and Composition

In the Arctic region, aerosol sources and composition vary with a seasonal cycle driven by sea ice and meteorological conditions. The greatest aerosol concentrations occur in the late winter and springtime, with influence of long-range transported pollution resulting in Arctic haze, comprised of sulfate, organic carbon, ammonium, nitrate, soot, dust, and trace metals (Myhre et al., 2007; Quinn et al., 2002). Springtime Arctic haze season occurs due to stronger transport from the midlatitudes during late winter – spring and weaker wet deposition, in addition to increased photochemistry after polar sunrise (Willis et al., 2018). During the summer and fall, with decreased sea ice extent and greater open ocean, sea spray aerosol and biogenic marine sources dominate (Quinn et al., 2002). The aerosol size distribution also changes seasonally, with a prevalent accumulation mode present in the spring, while <100 nm particles dominate in the summertime (Willis et al., 2018). Springtime Arctic haze dramatically reduces visibility, impacts the radiative budget in the Arctic, and is a large source of pollution to the region; therefore, the phenomenon has been an area of focused study (Law and Stohl, 2007; Myhre et al., 2007). However, Arctic aerosol composition in other seasons, particularly fall – winter, has not been well characterized, despite importance for cloud formation and longwave radiative forcing (Willis et al., 2018).

1.3.2 Sea Spray Aerosol

Sea spray aerosol (SSA) contributes the largest global aerosol flux to the troposphere (De Leeuw et al., 2011). In open water, SSA is produced by wavebreaking, which entrains air and forms bubbles that rise to the ocean surface and burst, producing jet drops and film drops (Quinn et al., 2015). These drops then evaporate to form aerosol, with film drops contributing to a ~100 nm SSA mode and jet drops contributing to a ~1-2 µm SSA mode (Quinn et al., 2015). Recent work has shown jet drops from smaller bubbles also contribute to the submicron SSA mode (Wang et al., 2017b). SSA production is influenced by factors including seawater temperature (Forestieri et al., 2018; Hultin et al., 2010; Salter et al., 2014; Schwier et al., 2017; Zábori et al., 2012), salinity (Hultin et al., 2010; Zábori et al., 2012), and biological activity (Alpert et al., 2015; Fuentes et al., 2010b; Hultin et al., 2010; Keene et al., 2017), but the magnitude and direction of these effects remains uncertain. SSA particles are primarily comprised of inorganic salts reflecting the composition of seawater, but can also contain organics that are enriched in the surface microlayer

(SML) or scavenged as bubbles rise through the water column (Quinn et al., 2015). Particle composition is size dependent, with greater organic enrichment in submicron film drop – derived particles, while supermicron particles contain primarily inorganic salts. Therefore, SSA organic composition is influenced by marine biology and the organic carbon pool (Quinn et al., 2014). Marine microorganisms also contribute to atmospheric chemistry by emitting dimethyl sulfide (DMS) and biogenic volatile organic compounds (BVOCs) (Engel et al., 2017). These trace gases can undergo oxidation reactions in the atmosphere to form secondary aerosol, including DMS oxidation to sulfuric acid and methanesulfonic acid (MSA).

In the Arctic, SSA is produced from open leads under high wind conditions (Leck et al., 2002; Nilsson et al., 2001), with a flux ~10 times smaller than from open water due to the reduced fetch, the distance over open water over which the wind blows (Nilsson et al., 2001). The size and number of open leads across the Arctic Ocean is uncertain (Wernecke and Kaleschke, 2015), but in some coastal regions, large leads or polynyas are persistent year-round (Hirano et al., 2018; Jones et al., 2016). In the Alaskan Arctic, SSA from open leads has been shown to be a significant aerosol source in all seasons (May et al., 2016b). Arctic sea ice leads are also greatly influenced by sea ice algae and bacteria (Vancoppenolle et al., 2013). These microorganisms can form massive algal blooms underneath and at the edges of ice (Assmy et al., 2017; Leu et al., 2015), contributing to organic enrichment in the SML (Galgani et al., 2016a; Gao et al., 2012), and producing DMS (Matrai et al., 2008; Vancoppenolle et al., 2013). SSA may be a particularly important aerosol source in the high Arctic, a CCN-limited regime with few local aerosol sources (Mauritsen et al., 2011). SSA, comprised of hygroscopic salts, are typically efficient CCN (Quinn et al., 2015), though organic material may reduce SSA hygroscopicity and CCN activity (Cochran et al., 2016; Collins et al., 2013). As a warming Arctic with declining sea ice results in greater open water and increasing SSA production (Struthers et al., 2011), as well as increasing biological productivity (Arrigo and van Dijken, 2015; Yool et al., 2015), there may be complex sea ice – aerosol – cloud feedbacks, impacting the rapidly changing climate in the region.

1.3.3 Local Anthropogenic Aerosol Sources

Increasing development in the Arctic region is leading to greater influence of anthropogenic aerosol sources from oil and gas activity and shipping emissions. Arctic oil and gas development is prevalent in Russia, Alaska, Norway, and Canada (Peters et al., 2011). Oil and gas extraction contribute soot and organic carbon aerosol to the Arctic atmosphere (Peters et al., 2011).

Greenhouse gases (CO_2, CH_4, N_2O) and gaseous aerosol and ozone precursors including SO_2, NO_x, and volatile organic compounds (VOCs) are also emitted from oil and gas activity (Peters et al., 2011). The Alaskan Arctic is influenced by emissions from Prudhoe Bay, the third largest oilfield in North America (U.S. Energy Information Administration, 2015). Large concentrations of CO have been observed from Prudhoe Bay production facilities (Brooks et al., 1997), in addition to increased concentrations of CCN and soot (Maahn et al., 2017). Enhanced levels of alkanes, including ethane, ethyne, propane, and *n*-butane, have been observed in the boundary layer within a radius of 300 km from Prudhoe Bay (Blake et al., 1992). Influence of Prudhoe Bay emissions has been observed across the Alaskan North Slope, with increased concentrations of CH_4, CO_2, and NO_y observed at Utqiaġvik during air mass influence from Prudhoe Bay (Jaffe et al., 1991, 1995). Prudhoe Bay emissions have been observed to contribute to regional ultrafine particle growth events (Creamean et al., 2018b; Kolesar et al., 2017) and impact local cloud properties by leading to smaller cloud droplets (Maahn et al., 2017). Combustion-derived particles (organic carbon, soot) and aged sea spray particles containing sulfate and nitrate have also been observed at Utqiaġvik, Alaska for Prudhoe Bay influenced air masses (Gunsch et al., 2017).

Natural resource extraction, cargo transportation, and tourism are increasing shipping activity in the Arctic region as sea ice decline enables access (Dalsøren et al., 2007; Roiger et al., 2015). In the Canadian Arctic, increased shipping activity has impacted air quality, with increased ozone and particulate matter concentrations observed from ship traffic, as well as NO_x, SO_2, and soot (Aliabadi et al., 2015; Gong et al., 2018). In the Alaskan Arctic, the Bering Strait has experienced record low sea ice extent in recent years (Stroeve et al., 2014). Already one of the busiest shipping lanes in the Arctic, ship traffic through the Bering Strait is predicted to increase with continued sea ice loss (Huntington et al., 2015), contributing to greater anthropogenic emissions in the region. Ship emissions of soot, VOCs, SO_2, NO_x, and trace metals, including vanadium, have been observed at elevated concentrations in the Bering Strait (Kim et al., 2015b; Laimin et al., 2008). Local sources of soot from oil and gas activity and shipping activity may particularly impact the Arctic climate, as deposition of the absorbing aerosol on bright snow and ice surfaces changes the surface albedo (Bond et al., 2013; Flanner et al., 2007).

1.3.4 Heterogeneous and Multiphase Reactions in the Atmosphere

During atmospheric transport, particles undergo "aging" by atmospheric reactions forming secondary species. These heterogeneous reactions (on solid surfaces) and multiphase reactions

(within aqueous droplets) result in a complex, dynamic aerosol mixing state as particles are transported from their emission source (Riemer et al., 2019). For example, SSA particles undergo reactions with sulfur- and nitrogen-containing gases (HNO_3, N_2O_5, H_2SO_4, MSA) to form particle-phase sodium sulfate or sodium nitrate, liberating chloride from the particle as HCl (Gard et al., 1998). These heterogeneous and multiphase reactions can impact atmospheric oxidizing capacity, atmospheric lifetimes of particles and trace gases, and aerosol climate properties (Seinfeld and Pandis, 2012). Characterizing individual particle mixing state can determine the extent of aerosol aging and inform particle age, transport, and potential sources (Riemer et al., 2019).

1.4 Chemical Characterization of Individual Aerosol Particles

Single particle analysis methods, including microscopic and spectroscopic methods, can be applied to characterize aerosol physicochemical mixing state (Ault and Axson, 2017). These microspectroscopic methods are offline, nondestructive techniques, allowing for analysis of the same sample by multiple methods. This multimodal approach provides a more complete picture of the physicochemical mixing state, as each technique has limits regarding the particles sizes and compositions that can be analyzed, due to requirements for sample preparation or instrumental limitations. An aerosol impactor, such as a micro-orifice uniform deposit impactor (MOUDI, MSP Corp.) or a microanalysis particle sampler (MPS, California Instruments) with size-resolved stages collects individual particles onto substrates for offline analysis.

1.4.1 Electron Microscopy

Electron microscopy has become a popular method for analyzing physical and chemical properties of individual aerosol particles (Ault and Axson, 2017; Laskin et al., 2016). Scanning electron microscopy (SEM) can collect detailed images of individual particles, providing information on morphology and size of particles >30 nm diameter, with a practical limit of >100 nm for very thin samples, including ambient particles (Laskin et al., 2006). The detection of different electron interactions with the sample can provide information regarding the surface features (back scattered electrons and secondary electrons) or internal structure (transmitted electrons) (Ault and Axson, 2017). Tilted SEM imaging can provide information about the three-dimensional particle shape (Laskin et al., 2016; Wang et al., 2016). Energy dispersive X-ray spectroscopy (EDX) coupled with SEM provides semi-quantitative chemical information for individual particles, by detecting element-specific X-rays emitted from the particle during

interaction with the electron beam (Ault and Axson, 2017). Spatially-resolved (<10 nm) intraparticle elemental composition can be determined by SEM-EDX by rastering across the entire particle (elemental mapping). A computer-controlled SEM-EDX method (CCSEM-EDX) allows for automated particle detection and facile analysis of thousands of particles per sample (Laskin et al., 2006), enabling data collection on a statistically representative subsample of the ambient aerosol population (Willis et al., 2002). Cluster analysis methods, including k-means clustering, have been employed to assist with the subsequent analysis of large CCSEM-EDX data sets in several previous studies (Ault et al., 2012; Axson et al., 2016a, 2016b; Bondy et al., 2018; Gunsch et al., 2017; Kirpes et al., 2018). The k-means clustering method, adapted from single particle mass spectrometry analysis methods (Anderson et al., 2005; Rebotier and Prather, 2007; Song et al., 1999), groups particles based on similarity of elemental composition, determined by the EDX spectra, resulting in clusters representing different particle types and sources (Ault et al., 2012). Transmission electron microscopy (TEM) provides greater spatial resolution than SEM, allowing for analysis of individual particles as small as 10 nm, and can also be coupled with EDX; however this method has not yet been automated (Ault and Axson, 2017; Pósfai and Buseck, 2010). SEM and TEM analyses have previously been applied to determine the chemical composition and infer sources of Arctic aerosols (Anderson et al., 1992; Bigg and Leck, 2001a; Chi et al., 2015; Creamean et al., 2018a; Geng et al., 2010; Gunsch et al., 2017; Hamacher-Barth et al., 2016; Hara et al., 2002b, 2002a; Hara, 2003; Hara et al., 1999, 2002c; Hiranuma et al., 2013; Karl et al., 2013; Leck et al., 2002; Leck and Svensson, 2015; Lohmann and Leck, 2005; Shaw, 1983; Weinbruch et al., 2012, 2018; Xie et al., 2007; Young et al., 2016).

1.4.2 Raman Microspectroscopy

Raman microspectroscopy combines optical microscopy with vibrational spectroscopy to provide information on the functional groups present in individual particles >1 μm (Ault and Axson, 2017). This method provides detailed characterization of covalently bonded species, including inorganic and organic functional groups, and some crystal lattice vibrations, present in individual particles. Additionally, specific peak positions provide information on local bonding environments (Ault and Axson, 2017). For example, $NO_3^-{}_{(aq)}$ and $NO_3^-{}_{(s)}$ have been differentiated in reacted SSA particles (Zangmeister and Pemberton, 2001), and the specific $v_s(SO_4^{2-})$ peak position between 975 – 1000 cm^{-1} can distinguish free sulfate, ammonium sulfate, sodium sulfate, magnesium sulfate, potassium sulfate, or calcium sulfate hydrates (Ault et al., 2013b; Mabrouk et

al., 2013). While Raman spectra of ambient particles can be complex due to the great number of specific compounds present, particularly organic species, comparison to spectra of standard compounds through methods such as χ^2 analysis enables characterization of the molecular classes present in individual particles (Cochran et al., 2017). Recently, a computer-controlled Raman microspectroscopy method was developed for the analysis of atmospheric particles, enabling analysis of hundreds of particles per sample (Craig et al., 2017). Several recent studies have applied Raman microspectroscopy to the characterization of ambient aerosol particles (Baustian et al., 2012; Bondy et al., 2017b; Chi et al., 2015; Craig et al., 2017; Creamean et al., 2016; Deng et al., 2014; Sobanska et al., 2012).

1.4.3 Atomic Force Microscopy – Infrared Spectroscopy

Atomic force microscopy with infrared spectroscopy (AFM-IR) was recently developed as a method to probe the vibrational modes of <1 µm atmospheric particles (Bondy et al., 2017a; Or et al., 2018). The photothermal expansion of a sample when irradiated with an infrared laser is detected by an AFM probe, enabling IR detection below the optical diffraction limit, with ~100 nm spatial resolution in individual particles (Dazzi et al., 2012). AFM imaging provides high spatial resolution information on particle morphology and phase, coupled with the chemical functional group information from IR absorption spectra. The ability to characterize molecular composition in individual submicron particles, in addition to morphology and phase, will allow greater understanding of the processes controlling aerosol mixing state and potential climate impacts.

1.4.4 Scanning Transmission X-ray Microscopy with Near Edge X-ray Absorption Fine Structure Spectroscopy

Scanning transmission X-ray microscopy with near edge X-ray absorption fine structure spectroscopy (STXM-NEXAFS) can distinguish chemical bonding and oxidation states of certain elements present in individual particles (Ault and Axson, 2017; Moffet et al., 2010a). Using highly monochromatic X-rays, STXM-NEXAFS detects the transmitted X-rays through a particle sample and creates a map (~25 nm spatial resolution) at each tightly packed energy across the region of interest (Ault and Axson, 2017). These maps can then be combined to provide a spectrum at each pixel of the image. By scanning across the K-edge of carbon, oxygen, or nitrogen, or the L-edge of sulfur or chlorine, detailed molecular speciation of these elements can be determined within

individual particles. In addition to determining chemical oxidation states present (e.g. sp^2 or COOH carbon; S(V) or S(VI)), the optical depth can be determined using Beer-Lambert's Law (Moffet et al., 2010a) to enable quantification.

Equation 1.1 $OD = -ln(I/I0) = \mu(E)\rho t$

where ρ is the mass density of the material, t is the sample thickness, and μ is the mass absorption coefficient. Using the optical depth, the ratio of inorganic to organic components can be determined at each pixel of the image using the pre-edge and post-edge absorption, and the organic volume fraction for each individual particle can be calculated (Moffet et al., 2010a). With this detailed chemical speciation of specific elements, STXM-NEXAFS is complementary to SEM-EDX. STXM-NEXAFS has been used to probe the chemical composition of ambient particles over the carbon K-edge (Bondy et al., 2018; Frossard et al., 2014; Laskin et al., 2012; Moffet et al., 2010a; O'Brien et al., 2015a, 2014, 2015b; Pham et al., 2017; Wang et al., 2016) and sulfur L-edge (Ault et al., 2013c; Hopkins et al., 2008), including for Arctic particles (Hawkins and Russell, 2010; Hiranuma et al., 2013).

1.5 Goals of Dissertation

This dissertation focuses on characterizing individual atmospheric particle chemistry, to advance understanding of aerosol physicochemical mixing state and address knowledge gaps concerning the complex processes influencing the changing Arctic climate. Microspectroscopic methods, including SEM-EDX, Raman microspectroscopy, STXM-NEXAFS, and AFM-IR, are applied to study the size, morphology, and chemical composition of individual atmospheric particles in order to answer climate-relevant questions. Chapter 2 describes a laboratory study to determine the impacts of seawater temperature, salinity, and biology on North Atlantic SSA production and characterize individual SSA composition in cold regions, relevant to dynamic environments including estuaries, river outflows, and areas of sea ice melt. Chapters 3 and 4 characterize ambient aerosol in the wintertime Alaskan Arctic, a season previously understudied. In Chapter 3, the composition and mixing state of particle types present was determined. Chapter 4 investigates the influence of marine biology on wintertime SSA chemistry. As part of the Microbiological – Ocean – Cloud Coupling in the High Arctic (MOCCHA) campaign, Chapter 5 characterizes aerosol mixing state and the influence of locally produced SSA on the summertime high Arctic atmosphere. In comparison to the high Arctic pack ice, Chapter 6 focuses on the Bering

Strait and Chukchi Sea to determine the influences of anthropogenic and marine emissions on summertime aerosol mixing state. Chapter 7 describes a unique particle type observed during summer on the North Slope of Alaska, demonstrating the importance of considering aerosol phase in determining climate impacts. Finally, Chapter 8 concludes the dissertation and discusses the future directions of on-going projects.

Chapter 2.   Factors Controlling the Chemical Composition and Mixing State of Wintertime Coastal Sea Spray Aerosol

2.1 Introduction

Sea spray aerosol (SSA) contributes the largest global flux of aerosol to the troposphere (De Leeuw et al., 2011). SSA is produced via seawater wave breaking, which entrains air to form bubbles that rise to the water surface and burst to form droplets (Quinn et al., 2015). Bubble bursting creates both film and jet drops that evaporate to form SSA, with diameter modes near 100 nm and 1-2 µm, respectively (Quinn et al., 2015; Wang et al., 2017b). SSA particles are largely inorganic sea salts, but also contain organic matter enriched in the water surface microlayer (SML) and/or seawater (Matrai et al., 2008) which is scavenged as bubbles rise through the water column (Quinn et al., 2015). SSA composition is generally size dependent, with larger particles containing primarily sodium chloride and smaller particles primarily organics (Ault et al., 2013c; Facchini et al., 2008; Quinn et al., 2015). However, recent studies have demonstrated the complexity of SSA composition, observing supermicron particles enriched in organics and the persistence of salts in sub-100 nm particles (Wang et al., 2017b). The diversity of seawater biology is reflected in the organic compounds observed in the SML and in SSA particles, including marine colloids or gels (Bigg and Leck, 2008; Chin et al., 1998; Decho and Gutierrez, 2017), aliphatic compounds including fatty acids (Bikkina et al., 2019; Cochran et al., 2017; Kanakidou et al., 2005; Kawamura and Bikkina, 2016), carbohydrates including monosaccharides and polysaccharides (Cochran et al., 2017; Frossard et al., 2014; Fu et al., 2013; Jayarathne et al., 2016; Russell et al., 2010), amino acids (Fu et al., 2015; Hawkins and Russell, 2010; Scalabrin et al., 2012), proteinaceous material (Fu et al., 2015; Hawkins and Russell, 2010; Scalabrin et al., 2012), and siliceous material, such as diatom fragments (Bigg and Leck, 2001b; Cochran et al., 2017; Wilson et al., 2015).

SSA impacts climate both directly, by scattering incident radiation, and indirectly, by aiding cloud formation and influencing cloud properties (Quinn et al., 2015). SSA effects on clouds are particularly important for climate in remote marine regions (Carslaw et al., 2010, 2013; Lohmann and Leck, 2005) with few other aerosol sources, as SSA are efficient cloud condensation

nuclei (CCN) (Collins et al., 2013; Quinn et al., 2014) and can serve as ice nucleating particles (INP) (DeMott et al., 2016; Wilson et al., 2015). These climate impacts not only depend on atmospheric SSA number concentrations, but also on individual particle composition (Riemer et al., 2019). Therefore, to determine SSA effects on climate, the many factors controlling SSA production and individual particle composition, including seawater temperature, salinity, and biological activity, must be considered.

Seawater temperature and salinity influence bubble distributions and therefore SSA production (Callaghan et al., 2014; Forestieri et al., 2018; Hultin et al., 2010; Salter et al., 2015; Schwier et al., 2017; Sellegri et al., 2006; Zábori et al., 2012). Previous studies have probed the influence of seawater temperature on SSA production from 0 ˚C to > 30 ˚C with differing results, and suggest a nonlinear relationship between seawater temperature, bubble production, and SSA size distributions and number concentrations (Forestieri et al., 2018; Hultin et al., 2010; Salter et al., 2014, 2015; Schwier et al., 2017; Sellegri et al., 2006; Zábori et al., 2012). Previous studies have also identified differing trends of SSA production with salinity, with increased SSA production observed for decreased salinity in the North Atlantic Ocean (Hultin et al., 2010) and decreased SSA production observed for decreased salinity in glacier melt-influenced seawater (Zábori et al., 2012). The complex relationship between seawater parameters and SSA production is further demonstrated by the different bubble plume characteristics observed for freshwater and seawater, including lower bubble densities and decreased surface foam accumulation observed for freshwater (Callaghan et al., 2014; May et al., 2016a; Zábori et al., 2012), leading to less aerosol production (May et al., 2016a).

The abundance and composition of seawater organic material can impact SSA production by influencing particle size distributions and number concentrations, with increased biological activity resulting in increasing number concentrations of submicron SSA particles (Alpert et al., 2015; Collins et al., 2013; Fuentes et al., 2010a; Hultin et al., 2010; Keene et al., 2017; Prather et al., 2013; Schwier et al., 2017; Sellegri et al., 2006). Through laboratory mesocosm studies, the influence of algal blooms on SSA organic content, particle hygroscopicity, and SSA CCN and INP activity have been examined, observing a size-dependent increase in SSA organic fractions and reduction of particle hygroscopicity during blooms (Ault et al., 2013c; Cochran et al., 2016; Collins et al., 2013, 2016; McCluskey et al., 2016; Schill et al., 2015; Wang et al., 2017b). Ambient SSA studies have also identified a complex relationship between seawater biology and SSA

chemistry, demonstrating the influences of marine dissolved organic material and biological productivity on SSA composition (Decesari et al., 2011; Eom et al., 2016; Miyazaki et al., 2018; Quinn et al., 2014). However, the dynamic relationship between seawater biological activity and SSA chemistry, particularly the molecular composition of seawater organics and transfer into the aerosol phase, is not well understood.

Concurrent changes in water temperature, salinity, and/or biology complicate the relationship between seawater characteristics and SSA production. Additionally, SSA properties, including reactivity and water uptake, are dependent on the chemical mixing state, or how components are distributed within each particle and throughout the aerosol population (Fierce et al., 2016; Prather et al., 2008; Riemer et al., 2019). In particular, the abundance and composition of SSA organics present will influence particle reactivity, optical properties, CCN efficiency, and INP activity (Collins et al., 2013, 2016; Prather et al., 2008; Wilson et al., 2015). The complex interactions of these different factors controlling SSA production may be particularly important for coastal marine environments, including estuaries and river outflows, and areas of snow or ice melt, but uncertainties remain regarding the influence of these many factors on SSA production. In the study described herein, we present a laboratory case study of wintertime SSA produced from Gulf of Maine seawater, and probe the influence of water temperature, salinity, and biogenic organic material on SSA production and individual particle chemical composition. These results have important implications for SSA impacts on climate in cold coastal and estuarial environments, including the Gulf of Maine and marine environments influenced by river outflows or snow and ice melt.

2.2 Methods

Four SSA generation experiments (Table 2.1) were conducted in January 2018 using a marine aerosol reference tank (MART) (Stokes et al., 2013) at the Bigelow Laboratory for Ocean Sciences in East Boothbay, Maine (43°51'35.0"N, 69°34'47.1"W). The MART bubble plume was optimized with a waterfall cycle of 4 s on, 4 s off with a total 4.5 min on and 0.5 min off cycle. For each experiment, the 210 L MART was filled with 100 L of filtered seawater (0.2μm Whatman high flow filter cartridge) from the laboratory seawater intake sampling from the Gulf of Maine. New seawater was collected for each experiment. For Experiment 1, the MART was located inside the laboratory building, at 20 °C room temperature, while Experiments 2-4 were conducted with the MART located outside, at average ambient temperatures between -5 and 10 °C (Table 2.1). To

probe the influence of dissolved organic material (DOM) on SSA production, filtrate (0.2μm Whatman high flow filter cartridge) of a *Haematococcus* microalgal culture, representative of local freshwater inputs, was added to the MART for Experiments 3 and 4, comprising 50% and 66%, respectively, of the total 100 L water volume for each experiment (Table 2.1). The addition of the microalgal filtrate also changed the salinity for Experiments 3 and 4, listed in Table 2.1.

Seawater samples were collected from the MART prior to and immediately after each experiment for measurements of dissolved organic carbon (DOC) and total dissolved organic nitrogen (TDN). DOC + TDN were analyzed using a Shimadzu TOC-L system equipped with TNM-L for N detection, located at the University of Miami, following the method described by Dickson et al. (2007), with reference material used for equipment calibration provided by the Hansell CRM program (Hansell, 2005). Water temperature was monitored over the course of each experiment using a temperature logger (HOBO Water Temperature Pro v2, Onset) deployed inside the MART tank. The average water temperature for each experiment (Table 2.1) was calculated for the period over which the temperature and aerosol size distributions were stable. Aerosol particles were sampled from the 110 L headspace in the MART, through two diffusion driers to maintain an aerosol flow relative humidity of ~15%, with a total air flow of 6.3 lpm from the MART to the aerosol instrumentation. The sampled air flow was balanced by an inflow of 7.0 lpm of particle-free air (1.2 μm pore size HEPA capsule filter, Pall Life Sciences) to maintain positive pressure within the MART and eliminate the possibility of sampling room air. The short residence time (~15 min) within the MART provided sampling of nascent SSA without atmospheric processing. Before starting the MART waterfall, the tank was purged with particle-free air to ensure aerosol number concentrations < 20 particles/cm^3.

Table 2.1 Summary of MART experiments and measured seawater parameters, including dissolved organic carbon (DOC) and total dissolved nitrogen (TDN). Experiments 3 and 4 included added microalgal dissolved organic material (DOM), which altered the salinity, initial DOC, and TDN. Average air and water temperatures are provided with standard deviations.

Experiment (Date)	Location	Average Air Temperature	Average Water Temperature	Salinity	Initial DOC	TDN
1 (01/05/18)	Inside (room temperature)	20 ± 1 °C	20 ± 3 °C	29 g/kg	not measured	not measured
2 (01/08/18)	Outside (cold)	-5 ± 2 °C	11.3 ± 0.3 °C	29 g/kg	95.5 μM	14.6 μM
3 (01/12/18)	Outside (cold)	10 ± 1 °C	18 ± 2 °C	19.5 g/kg	376.6 μM	761.4 μM
4 (01/16/18)	Outside (cold)	-5 ± 1 °C	16 ± 1 °C	16.2 g/kg	433.1 μM	929.8 μM

Prior to the SSA experiments, in December 2017, bubble spectra were measured within the MART for both Gulf of Maine seawater and freshwater (filtered tap water), and optimized to spectra previously determined for wave breaking in seawater (Brooks et al., 2009; Deane and Stokes, 1999; Norris et al., 2011; Phelps et al., 2002; Phelps and Leighton, 1998) and freshwater (Carey et al., 1993; Cartmill and Yang Su, 1993; May et al., 2016a; Monahan, 2001; Wang and Monahan, 1995), especially in cold regions (Brooks et al., 2009; Norris et al., 2011) (Fig. 2.1). The Gulf of Maine seawater bubble spectrum was consistent with previous open ocean observations (Brooks et al., 2009; de Leeuw et al., 2002; Norris et al., 2011; Phelps and Leighton, 1998). Freshwater bubble densities of three to six orders of magnitude lower than seawater bubble densities; in comparison, previous laboratory studies observed freshwater bubble density one to three orders of magnitude higher than seawater bubble densities (Callaghan et al., 2014; May et al., 2016a).
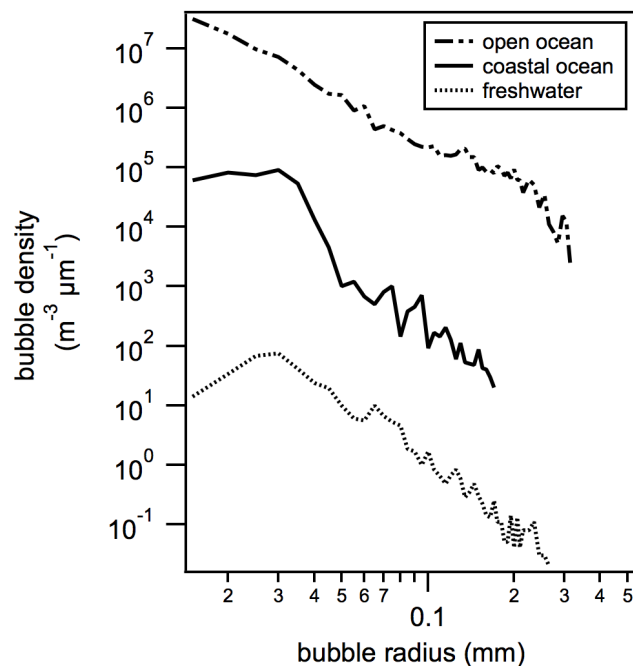
Figure 2.1 Mean lab-based bubble spectra for the MART filled with Gulf of Maine seawater optimized for the cold coastal and open ocean, compared to freshwater.

To measure SSA size distributions and number concentrations, a scanning mobility particle sizer (SMPS, Model 3938, TSI Inc.) and optical particle sizer (OPS, Model 3330, TSI Inc.) sampled from the MART at 0.3 and 1.0 lpm, respectively. For each MART experiment, the SMPS and OPS measured aerosol size distributions (5 min scans each) for particles $14 - 760$ nm (mobility diameter, d_m) and $337 - 10,000$ nm (optical diameter, d_{op}), respectively. Size distributions from the SMPS and OPS were combined following a previously established method (Khlystov et al., 2004; Taylor et al., 2012) to determine the total number concentration and particle size modes for each experiment. The OPS distributions were converted to mobility diameter, assuming a shape factor of 1 and a density of 2.0 g/cm^3 (representative of sodium chloride) (Pilson, 2013). Then the SMPS and OPS data were combined, using the SMPS size range from $14 - 737$ nm (d_m) and the OPS data from $1.25 - 10.0$ μm (d_{op}) (omitting the first six bins which overlapped with the SMPS), for a total distribution from $14 - 6,375$ nm d_m. Comparisons of particle size distributions for each experiment through statistical analysis were conducted with a Kolmogorov-Smirov test (K–S test) (Lilliefors, 1967; Massey Jr, 1951). A two-sample K–S test is a non-parametric test to determine if two data sets are drawn from the same underlying continuous distribution (null hypothesis)

(Lilliefors, 1967; Massey Jr, 1951). For this study, two size distributions were considered statistically different if the null hypothesis was rejected at the 5% significance level.

A 10-stage rotating micro-orifice uniform deposit impactor (MOUDI 110R, MSP Corp.) sampled from the MART at 5 lpm, with an additional 25 lpm of particle-free air (1.2 μm pore size HEPA capsule filter, Pall Life Sciences) for a total flow rate of 30 lpm. The SMPS, OPS, and MOUDI sampled simultaneously for 6 h. The MOUDI collected SSA particles onto silicon wafers and quartz substrates (Ted Pella, Inc.) for offline single particle analysis, described below. MOUDI substrates were stored in the dark at ambient temperature prior to analysis (Laskina et al., 2015).

Computer-controlled scanning electron microscopy with energy dispersive X-ray spectroscopy (CCSEM-EDX) was conducted for SSA particles collected on silicon from three MOUDI stages (1.0 – 1.8 μm aerodynamic diameter, d_a, 0.32 – 0.56 μm d_a, and 0.10 – 0.18 μm d_a). Analysis was conducted using a FEI Helios Nanolab SEM/FIB instrument equipped with a field emission gun operating at 20 kV accelerating voltage and an Everhart-Thornley secondary electron detector for SEM imaging. X-ray spectra from elements C, N, O, Na, Mg, S, Cl, K, Ca, Ti, Fe, Ni, and Zn were detected with an EDX detector (EDAX, Inc). CCSEM-EDX analyses of ~100 SSA particles per substrate provided the size, morphology, and relative abundance of the identified elements in individual SSA particles. EDX has previously been shown to quantitatively reproduce SSA and freshwater (lake spray aerosol) elemental ratios (Ault et al., 2013c, 2014; Axson et al., 2016a; May et al., 2016a, 2018b, 2018a). K-means clustering of the individual particle EDX spectra for ~1500 total analyzed particles grouped the particles into 20 clusters based on similarity of elemental composition (Ault et al., 2012; Bondy et al., 2018; Kirpes et al., 2018; Shen et al., 2016). These clusters were then combined into four main particle types (SSA, SSA+organic carbon (SSA+OC), organic, and Fe- or Ca-containing), based on comparison of the EDX spectra to previous studies of ambient and lab-generated SSA.

Individual SSA particles on quartz substrates were analyzed by Raman microspectroscopy using a Horiba LabRAM HR Evolution spectrometer coupled with a confocal optical microscope (100x N.A. 0.9 Olympus objective), Nd:YAG laser (50 mW, 532 nm), and CCD detector using a 600 groove/mm diffraction grating. Spectra were collected over the 500 – 4000 cm^{-1} range with spectral resolution of ~1.8 cm^{-1}. Spectra were compared to prior Raman studies of nascent SSA based on functional group peak assignments (Ault et al., 2013b; Cochran et al., 2017; Ebben et al., 2013). For each experiment, Raman spectra were collected for ~15 – 20 individual particles each

from two MOUDI stages (1.0 – 1.8 μm d_a and 0.32 – 0.56 μm d_a,), for a total of 150 particles analyzed.

2.3 Results and Discussion

2.3.1 Factors Influencing SSA Concentrations and Size Distributions

To investigate the effects of seawater temperature on SSA production, SSA generation experiments (Table 2.1) were conducted in January, 2018 using Gulf of Maine seawater inside the laboratory at room temperature (20 ˚C, Experiment 1) and outside, with low water temperature (11 ˚C, Experiment 2). Experiments 3 and 4 were also conducted outside at lower temperatures (18 ˚C and 16 ˚C, respectively) and with added DOM. Overall, all four experiments were characterized by similarly shaped aerosol size distributions, with a smaller mode at ~120 – 150 nm and an additional 1.2 μm mode (Fig. 2.2). Between the room temperature (20 °C, Experiment 1) and cold experiments (11 – 18 °C, Experiments 2-4), the submicron mode shifted from 155 ± 5 nm to 122 – 131 ± 5 nm (Fig. 2.2). A shift in the size distribution with temperature has also been observed in some previous studies, with a similar magnitude shift to smaller sizes with decreasing temperature (Salter et al., 2014; Sellegri et al., 2006) as with our observations. Additionally, the number concentration at the submicron mode increased by ~50% for the cold experiments, while the supermicron mode decreased by ~50%, consistent with previous laboratory studies of temperature-dependent SSA production (-1 to 30 ˚C) (Salter et al., 2015). The increased number concentration and decrease in mode diameter from Experiment 1 (1000 ± 100 particles/cm^3) to Experiment 2 (1300 ± 200 particles/cm^3) corresponded to a decrease in average water temperature from 20 ˚C to 11 ˚C, with no other variables changed, demonstrating a temperature-dependent response in SSA production. Previously published studies have shown differing trends in the direction of temperature effects on SSA production. Consistent with our observations, some previous studies have observed an increase in submicron SSA number concentration and decrease in supermicron SSA (Hultin et al., 2010; Salter et al., 2014, 2015; Zábori et al., 2012), including observations at similar temperature ranges (12.7 – 16.7 °C) and DOC concentrations (290 – 1095 μg/L) in the North Atlantic Ocean (Hultin et al., 2010).
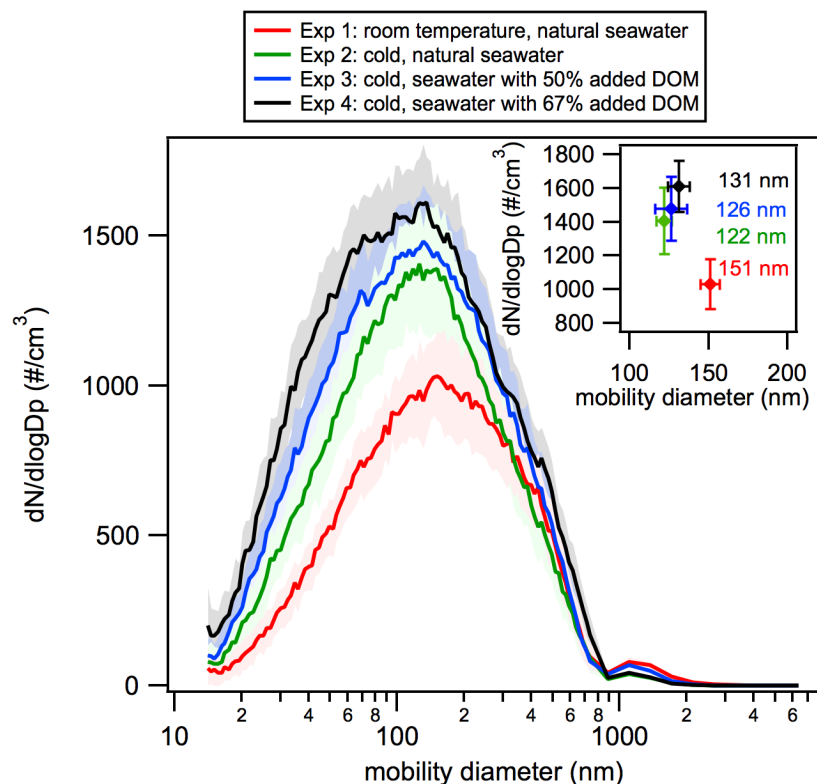
Figure 2.2 Average aerosol size distributions for each experiment. Shaded regions indicate standard deviations. The inset plot shows the size mode and associated standard deviation for each experiment.

While average water temperature increased between Experiments 2 (11 ˚C) and 3 (18 ˚C) due to changes in the outside ambient temperature, Experiment 3 also had increased DOC (376.6 μM, compared to 95.5 μM for Experiment 2) and lower salinity (19.5 g/kg) due to the addition of the *Haematococcus* microalgal culture. The size distributions and modes were consistent between Experiments 2 (122 ± 5 nm) and 3 (126 ± 9 nm), and the slightly increased total number concentration for Experiment 3 (1500 ± 200 particles/cm^3) was not statistically significant compared to Experiment 2 (1300 ± 200 particles/cm^3) (K–S test). When even more microalgal culture was added for Experiment 4 (DOC 433.1 μM), statistically greater (K–S test) particle number concentrations were observed for Experiment 4 (1700 ± 200 particles/cm^3), compared to Experiment 3 (1500 ± 200 particles/cm^3). However, in addition to the DOC increase from Experiment 3 to Experiment 4 (376.6 μM and 433.1 μM, respectively), the temperatures and salinities between Experiment 3 (18 ˚C, 19.5 g/kg) and 4 (16 ˚C, 16.2 g/kg) (Table 2.1) also changed; therefore the decreased temperature and increased DOC may both have contributed to the observed increased number concentrations. The impact of salinity is uncertain in previous

work, with differing observations of both increasing and decreasing SSA production with increasing salinity (Hultin et al., 2010; May et al., 2016a; Zábori et al., 2012). Therefore, the combination of these factors likely resulted in little overall impact on SSA production observed between Experiments 3 and 4.

In addition to confounding factors of seawater temperature and salinity, biological activity contributes to complex relationships between seawater properties and SSA production. Previous studies have observed increased SSA organic content with elevated DOC content and during algal blooms (Forestieri et al., 2016; Schwier et al., 2015, 2017); however, other studies have observed consistent SSA organic content despite changing biological productivity (Keene et al., 2017). In addition, previous work has shown increased DOM content leading to increased SSA number concentrations (Alpert et al., 2015; Fuentes et al., 2010b; Hultin et al., 2010; Keene et al., 2017). Based on these previous studies, we predicted increased temperature in Experiment 3 would result in a decrease in number concentration (Hultin et al., 2010; Salter et al., 2014, 2015; Zábori et al., 2012), while an increase in DOM would increase SSA production (Alpert et al., 2015; Fuentes et al., 2010b; Hultin et al., 2010; Keene et al., 2017), resulting in little overall change compared to Experiment 2, as was observed. Additionally, some studies have observed changes in SSA size distributions with shifts to smaller sizes (Alpert et al., 2015; Fuentes et al., 2010b) or increased concentrations of smaller particles (Prather et al., 2013; Sellegri et al., 2006) due to biological drivers. However, during our experiments, the size distribution mode did not change with added DOC, consistent with other previous studies (Collins et al., 2013; Hultin et al., 2010; Schwier et al., 2017), but the particle number concentration increased at the highest DOC concentration. Overall, in comparing the changes between each of the four experiments, our results suggest that temperature had a greater impact on SSA production than DOC for our Gulf of Maine seawater, consistent with previous Mediterranean seawater studies, which showed SSA production to be correlated with temperature rather than chlorophyll-a concentrations (Schwier et al., 2017). The influence of temperature on SSA production has not previously been investigated for the coastal North Atlantic.

2.3.2 SSA Chemical Composition

To further probe the influence of marine organic material on nascent SSA, the chemical composition of individual particles generated in each experiment was characterized using CCSEM-EDX. Four main particle types were identified, including SSA (primarily salts), SSA

internally mixed with organic carbon (SSA+OC), organic carbon particles, and Fe- or Ca-containing particles (Fig. 2.3). SSA particles were characterized as containing primarily Na and Cl, at elemental ratios (0.94 – 1.16), similar to the seawater Cl/Na ratio of 1.16 (Laskin et al., 2012; Pilson, 2013; Quinn et al., 2015). SSA+OC were SSA particles enriched in C and O, with at least 2% C in the EDX spectra (Ault et al., 2013c; Eom et al., 2016). For the total observed sea salt-containing particles (SSA and SSA+OC), Cl/Na elemental ratios were determined for individual particles from their EDX spectra (Fig. 2.4) (Laskin et al., 2012). Overall, individual supermicron SSA (SSA and SSA+OC, 1.0 – 1.8 μm d_a) Cl/Na ratios were similar to the seawater ratio (1.16 for Experiments 1-3 and 1.15 for Experiment 4), consistent with fresh SSA production (Pilson, 2013; Quinn et al., 2015). Submicron (0.10 – 0.18 μm d_a) SSA Cl/Na ratios were slightly depleted relative to seawater, particularly for Experiment 3 (average Cl/Na ratio 0.94) and Experiment 4 (average Cl/Na ratio 0.95) with added DOM. Submicron SSA Cl depletion has been previously observed and related to increased biological content (Laskin et al., 2012; Schwier et al., 2017).

Organic particles were most prevalent at sizes smaller than 500 nm (d_a) and primarily comprised of C and O, with 23% of these particles, by number, also containing S (Ault et al., 2013c), and 5%, by number, containing N. EDX can be less sensitive to nitrogen, such that the number fraction of particles containing N represents a lower limit (Laskin et al., 2006). The circular morphology of these organic particles is indicative of non-viscous particles (Fig. 2.3), consistent with the transfer of marine organics from the SML to the particle phase via bubble bursting (Ault et al., 2013c; Pham et al., 2017; Wang et al., 2017b). Fe- or Ca-containing particles comprised less than 5 – 10% of the particle number across the observed size range, but were present in all experiments (Fig. 2.3). These particles contained Ca or Fe as the primary cation, with smaller amounts of Na and Cl, in addition to organics (Forestieri et al., 2016; Guasco et al., 2014). In comparison, SSA and SSA+OC particles only contained small amounts (< 5 relative atomic percent) of Ca and no detectable Fe. The presence and composition of these Ca-containing particles (Fig. 2.5) are consistent with previous observations of calcium enrichment in submicron SSA (Forestieri et al., 2016; Salter et al., 2016; Schwier et al., 2017). Increases in iron-containing particles and those containing divalent cations (Mg, Ca) mixed with organic content have also been observed after nutrient addition to mesocosm experiments (Forestieri et al., 2016; Jayarathne et al., 2016).
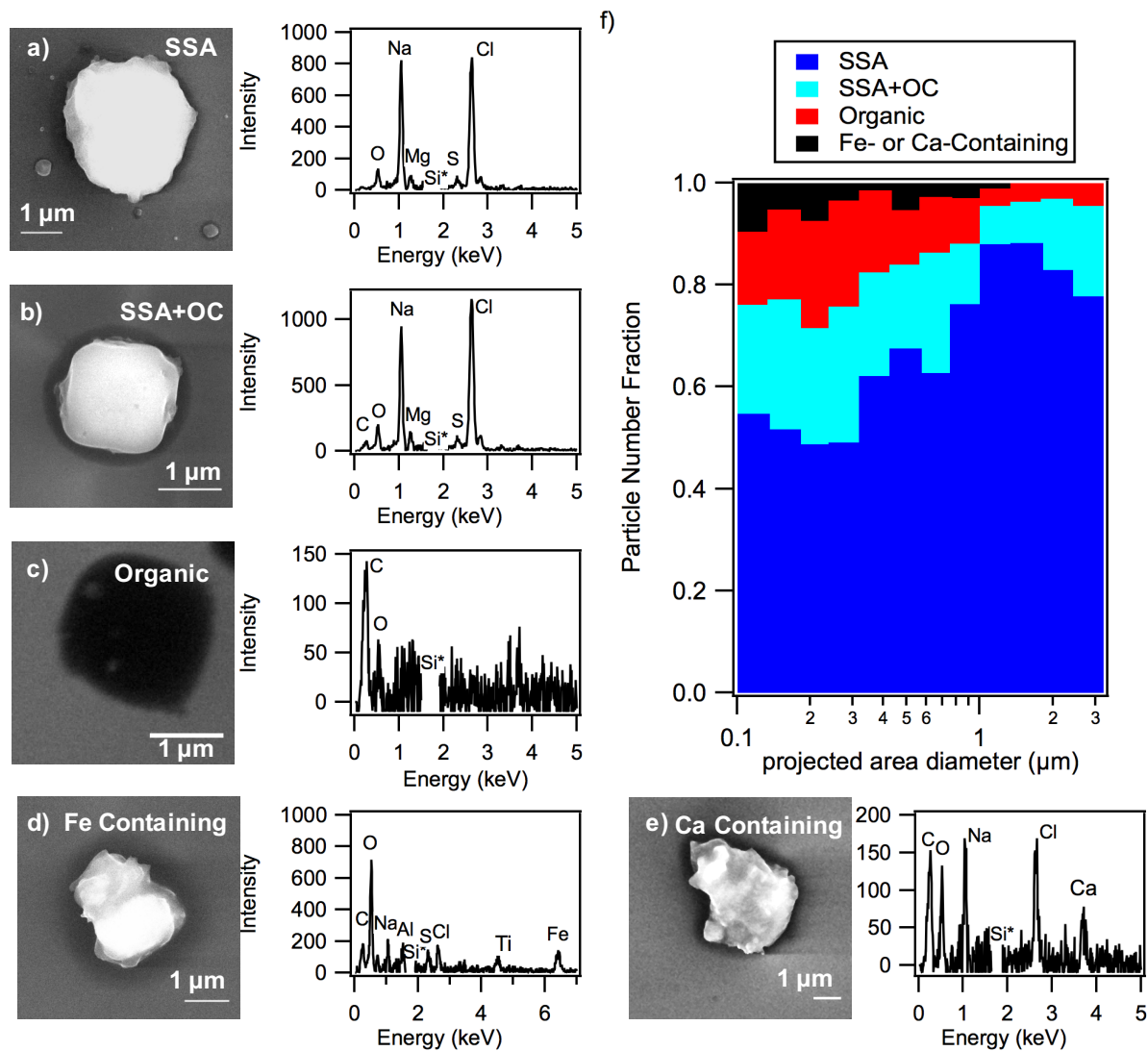
Figure 2.3 Representative SEM images and EDX spectra of observed particle types including a) sea spray aerosol (SSA), b) sea spray aerosol with organics (SSA+OC), c) organic aerosol, d) Fe-containing particle, and e) Ca-containing particle. *Spectra were background subtracted to remove signal from the silicon substrate, and the silicon peak was removed for clarity. f) Size-resolved CCSEM-EDX number fraction distributions of observed particle types.
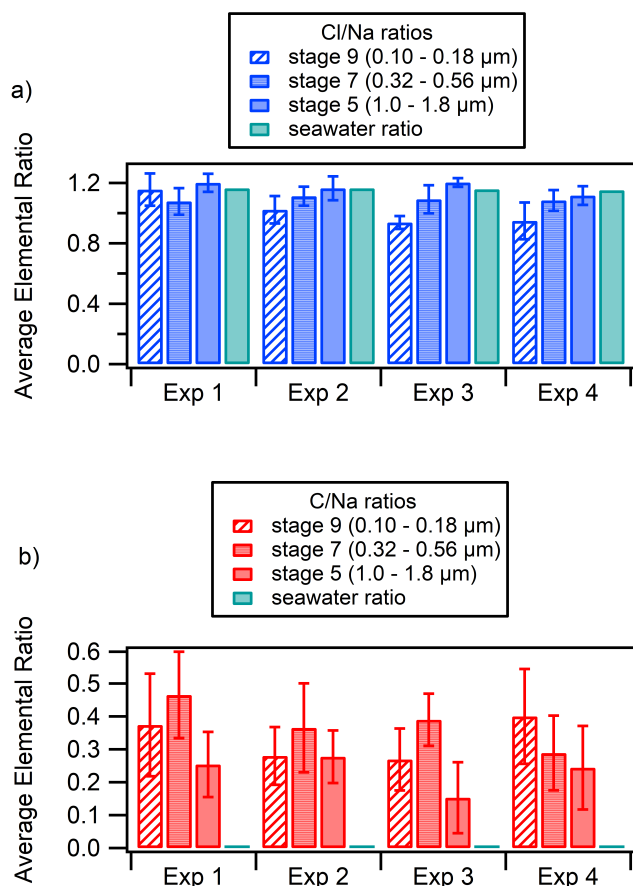
Figure 2.4 a) Average individual SSA and SSA+OC particle Cl/Na elemental ratios and b) median individual SSA+OC particle C/Na elemental ratios determined by EDX for each experiment and size range, compared to initial values measured for the water. Cl/Na ratios for the water were determined based on standard values and the ion concentrations for each experiment. C/Na ratios for the water were determined from initial DOC concentrations and salinity for Experiments 2-4. No DOC measurements were available for Experiment 1, so the ratio from Experiment 2 was used. Error bars show 95% confidence interval.
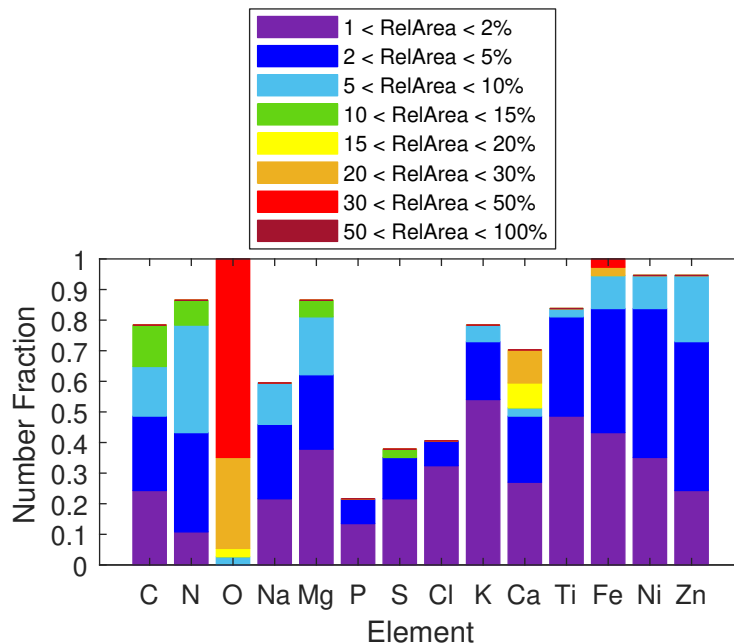
Figure 2.5 Digital color histograms showing the number fractions of spectra (particles) containing each element (bar height) at each EDX signal intensity range (color scale) for the Fe- and Ca-containing particle types.

2.3.3 Organic Enrichment in Individual SSA Particles

The relative number fractions of all four main particle types (SSA, SSA+OC, organic, and Fe- or Ca-containing) were similar across the four experiments (Fig. 2.6). At supermicron diameters (1.0 – 4.0 μm), SSA particles comprised most of the observed particles, ~ 80% by number, with number fractions of ~60% for submicron diameters (0.1 – 1.0 μm) (Fig. 2.3). At submicron diameters (0.1 – 1.0 μm), increased number fractions of SSA+OC and organic particles were observed, comprising ~15 – 20% and ~10 – 15% of particles, by number, respectively (Fig. 2.3). This size dependence of SSA organic content has been observed in previous studies in which SSA, SSA+OC, and organic particle types were observed (Ault et al., 2013c; Collins et al., 2013; Hultin et al., 2010; Lee et al., 2015; Prather et al., 2013; Wang et al., 2015a). The presence of SSA+OC and organic particles indicates influence of seawater biology through the transfer of SML and/or seawater column organic content to the particle phase. While this size dependence in organic content was observed, similar number fractions were observed for experiments with natural seawater (Experiments 1 and 2) and those with added microalgae (Experiments 3 and 4), suggesting that the amount of DOM present did not dramatically affect SSA mixing state. However, the observed number fractions of SSA and SSA+OC particle types do not reflect the

mass of organic material present in the individual SSA+OC particles; therefore, individual SSA particle carbon content was examined next.
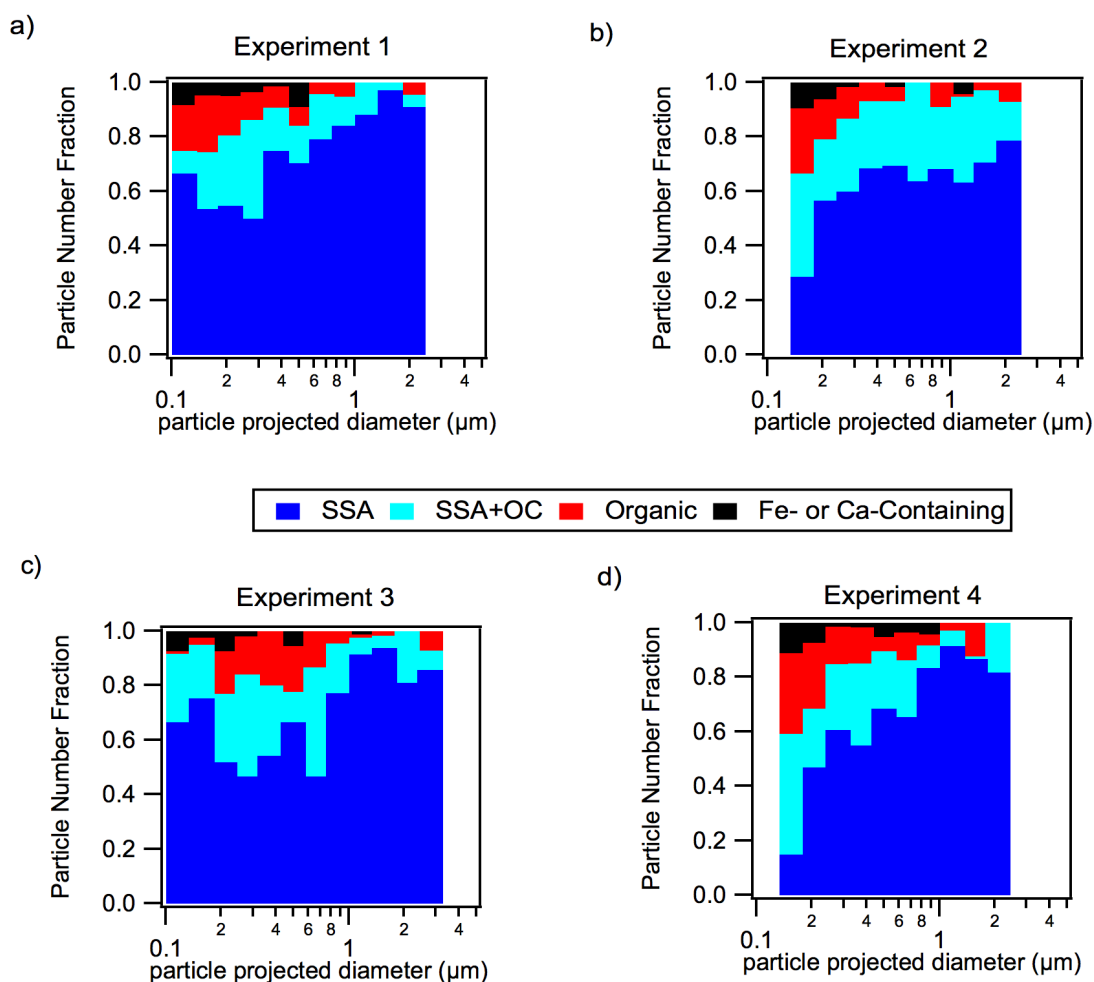
Figure 2.6 Size-resolved CCSEM-EDX number fractions of observed particle types for each experiment.

Organic enrichment in SSA+OC particles was present for all experiments and particle size ranges, with individual particle C/Na ratios (median ratios of 0.16 – 0.47) greatly enriched above the seawater ratio (0.0002 – 0.003), consistent with previous mesocosm studies observing organic enrichment in the particle phase (Collins et al., 2013; Forestieri et al., 2016; Schwier et al., 2015, 2017). The SSA+OC particle C/Na ratios were of similar magnitude for all experiments and size ranges. These results show no significant size-dependence in SSA composition, with submicron median C/Na ratios of 0.27 – 0.40 for 0.10 – 0.18 μm particles and median C/Na ratios of 0.29 – 0.47 for 0.32 – 0.56 μm particles, compared to supermicron median C/Na ratios of 0.15 – 0.28 for 1.0 – 1.8 μm particles. Notably, no significant differences were observed in the C/Na ratios

between experiments with natural seawater (Experiments 1 and 2) and experiments with added algal culture filtrate (Experiments 3 and 4), suggesting that increased DOC did not have a significant influence on SSA organic content at smaller particle diameters.

2.3.4 Molecular Characterization of SSA Organics

Raman microspectroscopy was used to characterize the chemical composition of the organics within the individual SSA+OC particles. Of the 150 particles analyzed, 28% fluoresced, masking the Raman signal. An additional 16% of particles exhibited fluorescence, but signals for organic functional groups could still be identified. Fluorescence is often indicative of conjugation within biological molecules present in particles (Fu et al., 2015; May et al., 2018a) and was observed in SSA particles from all experiments and across all sizes. The 72% of analyzed SSA+OC particles which had detectable Raman signal showed signatures characteristic of saccharides (Cochran et al., 2017), with no major differences in organic composition between experiments or across size ranges. Previous observations have identified a size dependence of SSA+OC composition, with submicron particles containing more aliphatic organics, while supermicron particles contained more oxidized organics (Wang et al., 2015a). Notably, SSA+OC particles from Experiments 3 and 4, with added microalgal culture filtrate, did not show distinct evidence of the added *Haematococcus*-derived DOM in the Raman spectra. The carotenoid astaxanthin is a major component of *Haematococcus* and is expected to have strong Raman modes at 1157 cm^{-1} for ν(C-C) and 1520 cm^{-1} for ν(C=C), which were not observed in the particle spectra (Kaczor and Baranska, 2011; Subramanian et al., 2014). Degradation of the astaxanthin molecule during filtration or through the water cycling process in the MART may result in similar free saccharide modes to those observed.

Figure 2.7 shows two representative Raman spectra of individual SSA+OC particles with free saccharide signatures. Characteristic free saccharide modes include δ(C-O-H), δ(C-C-H), and δ(O-C-H) side group deformations (870 - 871 cm^{-1}), ν(C-C) or ν(C-O) modes (1011, 1043, and 1100 cm^{-1}), δ(CH$_2$OH) deformations (1256 - 1258, 1316, 1367 - 1368, 1433 -1435, 1455 - 1457, and 1479 cm^{-1}), and ν(C=C) or ν(C=O) (1644 cm^{-1}) (Table 2.2) (Cochran et al., 2017). In the C-H stretching region, free saccharides have modes similar to those present at 2917 cm^{-1} for ν_a(CH), 2939 cm^{-1} for ν_a(CH$_2$), and 2985 – 2986 cm^{-1}. Modes in the ν(O-H) region also align with the free saccharide modes between 3386 - 3391 cm^{-1} (Table 2.2) (Cochran et al., 2017). A saccharide C-H

wagging mode at 1343 cm^{-1} was observed in 9%, by number, of analyzed SSA particles (Table 2.2) (Craig et al., 2017). The simultaneous presence of all of these modes (Fig. 2.7) are highly suggestive of the presence of saccharides. Modes characteristic of polysaccharides were also observed at 941 cm^{-1} for skeletal modes (Movasaghi et al., 2007) and 981 cm^{-1} for ν_a(C-O-C) (Cochran et al., 2017). Saccharides have previously been identified in the seawater SML and in the particle phase (Hawkins and Russell, 2010; Jayarathne et al., 2016; Kawamura et al., 2017; Pakulski and Benner, 1994; Russell et al., 2010). The prevalence of these modes suggests saccharides are abundant in Gulf of Maine seawater and may preferentially transfer into the aerosol phase.

Raman modes characteristic of other classes of organic compounds were also present in the SSA+OC particle spectra. Modes at 1128 - 1132 cm^{-1} for ν_s(C-C), 2850 cm^{-1} for aliphatic ν_s(CH$_2$), 2894 cm^{-1} for aliphatic ν_s(CH$_3$), 2907 cm^{-1} for aliphatic ν_a(CH$_2$), and 2998 - 3000 cm^{-1} for ν_s(=C-H) modes are indicative of fatty acids or aliphatic compounds (Ault et al., 2013b; Cochran et al., 2017; Deng et al., 2014). In particular, the aliphatic ν_a(CH$_2$) mode at 2907 cm^{-1} was present in 21%, by number, of observed SSA+OC particles. When present, the aliphatic ν_a(CH$_2$) mode was as intense as the saccharide ν_a(CH$_2$) mode, with an average 2907 cm^{-1}/2940 cm^{-1} peak intensity ratio of 1.05, indicating influence of both fatty acids and saccharides in the SSA particles. Fatty acids have previously been observed in SSA, demonstrating influence of SML organics transferred to the particle phase (Bikkina et al., 2019; Cochran et al., 2017; Ovadnevaite et al., 2014; Tervahattu et al., 2002). Additionally, 61%, by number, of SSA+OC particle spectra also contained a ν(N-H) stretch around 3100 cm^{-1}; the simultaneous presence of a broad C=C peak at 1603 cm^{-1} (Fig. 2.7) suggests the presence of amino acids (Movasaghi et al., 2007; Tang et al., 2016), compounds which have been identified in SSA particles in previous studies (Cochran et al., 2017; Leck and Keith Bigg, 2008; Scalabrin et al., 2012). Finally, modes at 709 & 776 cm^{-1} corresponding to ν_a(Si-C), and 1411 cm^{-1} and 2966 cm^{-1} corresponding to polydimethylsiloxane δ_a(CH$_3$) and ν_a(CH$_3$) modes, respectively, are likely characteristic of siliceous organics (Cochran et al., 2017). While the presence of siliceous material in the analyzed particles could not be determined by CCSEM-EDX due to the silicon substrate background, these Raman modes indicate that diatomaceous organics may be present, consistent with previous SSA studies (Bigg and Leck,

2001b; Cochran et al., 2017; Patterson et al., 2016) and the seawater source (Kane, 2011; Thompson et al., 2006).
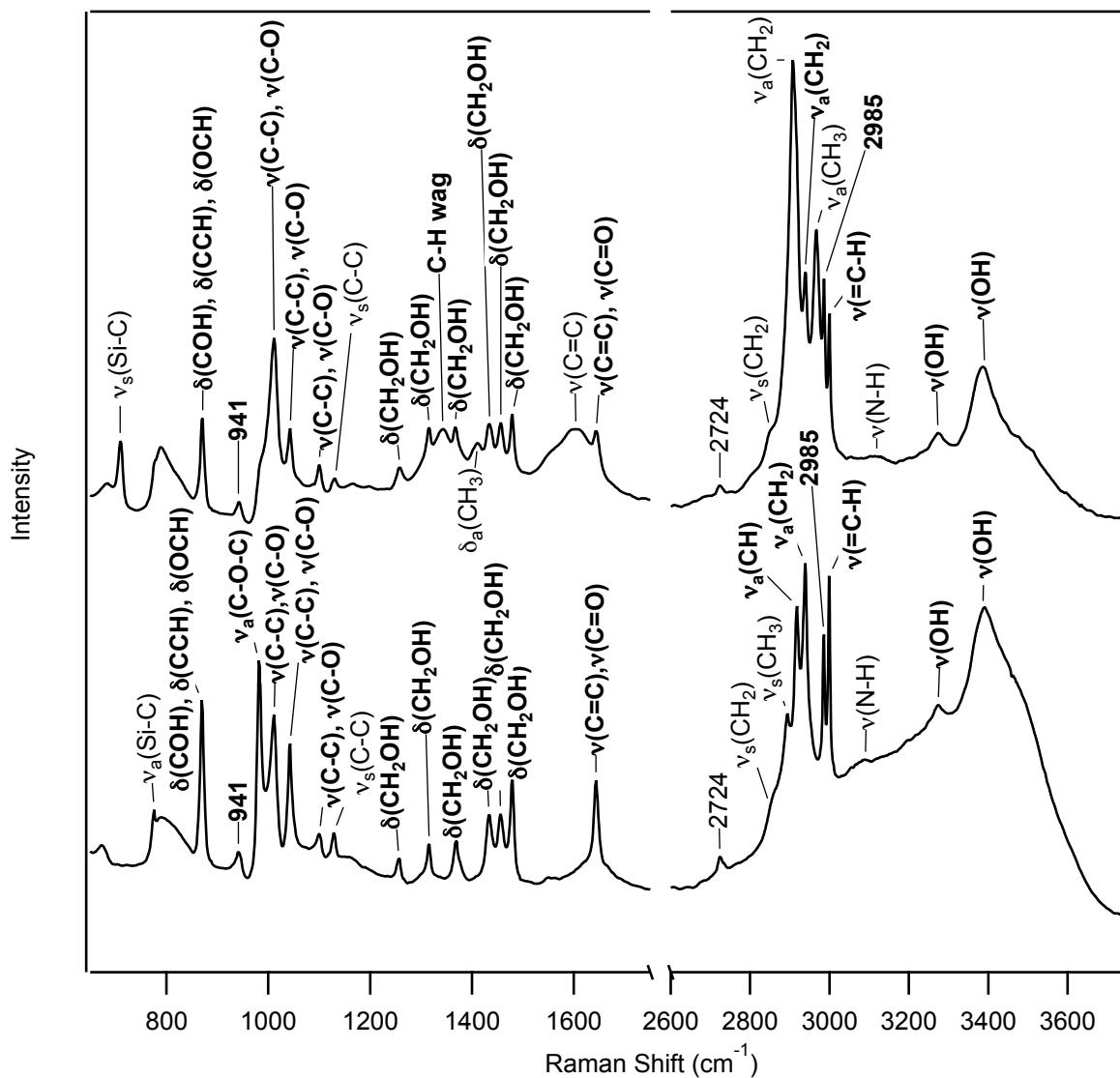
Figure 2.7 Representative Raman spectra of two individual SSA+OC particles, from Experiments 3 and 4, exhibiting the organic signatures of free saccharides (Cochran et al., 2017). Modes specific to free saccharides are labeled in bold.

Table 2.2 Peak assignments for vibrational modes observed in individual SSA particle Raman spectra.

Peak Position (cm⁻¹)	Mode Assignment	Literature Value (cm⁻¹)	Reference
709	ν_s(Si-C) (polydimethylsiloxane)	710	Cochran et al. (2017)
776	ν_a(Si-C) (polydimethylsiloxane)	791	Cochran et al. (2017)
870, 871	δ(C-O-H), δ(C-C-H), δ(O-C-H) side group deformations (saccharides)	861	Cochran et al. (2017)
941	skeletal modes (polysaccharides)	941	Movasaghi et al. (2007)
981	ν_a(C-O-C) (polysaccharides)	991	Cochran et al. (2017)
1011	ν(C-C), ν(C-O) (saccharides)	1009	Cochran et al. (2017)
1043	ν(C-C), ν(C-O) (saccharides)	1037	Cochran et al. (2017)
1100	ν(C-C), ν(C-O) (saccharides)	1097	Cochran et al. (2017)
1128, 1132	ν_s(C-C) (fatty acids)	1129	Cochran et al. (2017)
1256, 1258	δ(CH₂OH) deformations (saccharides)	1250	Cochran et al. (2017)
1316	δ(CH₂OH) deformations (saccharides)	1310	Cochran et al. (2017)
1343	C-H wag (saccharides)	1344	Craig et al. (2017), Movasaghi et al. (2007)
1367, 1368	δ(CH₂OH) deformations (saccharides)	1363	Cochran et al. (2017)
1411	δ_a(CH₃) (polydimethylsiloxane)	1408	Cochran et al. (2017)
1433, 1435	δ(CH₂OH) deformations (saccharides)	1428	Cochran et al. (2017)
1455, 1457	δ(CH₂OH) deformations (saccharides)	1452	Cochran et al. (2017)
1479	δ(CH₂OH) deformations (saccharides)	1475	Cochran et al. (2017)

1603	$\nu(C=C)$ (amino acids)	1603	Movasaghi et al. (2007)
1644	$\nu(C=C)$, $\nu(C=O)$ (saccharides)	1640	Cochran et al. (2017)
2724	overtone	2724	Cochran et al. (2017)
2850	$\nu_s(CH_2)$ (fatty acids)	2850	Cochran et al. (2017)
2894	$\nu_s(CH_3)$ (fatty acids)	2894	Movasaghi et al. (2007)
2907	$\nu_a(CH_2)$ (fatty acids)	2904	Cochran et al. (2017)
2917	$\nu_a(CH)$ (saccharides)	2915	Ault et al. (2013b) Cochran et al. (2017)
2939	$\nu_a(CH_2)$ (saccharides)	2935	Ault et al. (2013b)
2966	$\nu_a(CH_3)$ (polydimethylsiloxane)	2967	Cochran et al. (2017)
2985, 2986	(saccharides)	2980	Cochran et al. (2017)
2998, 3000	$\nu(=C-H)$ (fatty acids)	3005	Czamara et al. (2015)
3090	$\nu(N-H)$	3090	Shipp et al. (2017)
3119	$\nu(N-H)$	3134	Tang et al. (2016)
3274	$\nu(O-H)$	3275	Ault et al. (2013b)
3386, 3391	$\nu(O-H)$	3408	Cochran et al. (2017)

2.4 Conclusions

SSA impacts on climate are dependent on factors controlling SSA production and chemical composition. Four SSA generation experiments were conducted using a MART with wintertime Gulf of Maine seawater and added DOM from a *Haematococcus* microalgal culture. The influences of seawater temperature, biology, and salinity on aerosol production were investigated. For the conditions probed herein, temperature played a greater role than DOC concentration in changing SSA number concentrations and size distributions, with increased production of submicron (0.1 – 1.0 µm) SSA and decreased production of supermicron (1.0 – 4.0 µm) SSA for the cold, outdoor experiments compared to the inside, room temperature experiment. For all experiments, the particles produced were primarily inorganic SSA particles (60% of submicron

and 80% of supermicron particles, by number). SSA+OC and organic particles were observed at greater number fractions in the submicron size range (20% and 10 – 15% of submicron particles, respectively). The small fraction of Ca and Fe metal-containing particles observed (5 – 10%, by number) were most likely related to the seawater biological activity, as observed previously during algal blooms (Forestieri et al., 2018; Jayarathne et al., 2016; Salter et al., 2016). The observed individual SSA particle composition was influenced by seawater organics, with carbon enrichments relative to seawater (C/Na ratios of 0.005 – 0.36) observed across all particle sizes (Schwier et al., 2017). The molecular composition of the observed SSA organics was characterized primarily by free saccharides, with some contribution from aliphatic organics and siliceous material, as determined by individual particle analysis with Raman microspectroscopy.

The complex molecular composition of SSA organics, including the observed saccharides and fatty acids, influences individual particle chemical properties and climate impacts (Quinn et al., 2015). Saccharides are more hygroscopic than fatty acids and other aliphatic compounds, which will influence particle CCN efficiency (Cochran et al., 2017). Mesocosm studies have observed a decline in polysaccharides and increase of free saccharides and short chain fatty acids over the course of an algal bloom, suggesting a dynamic link between seawater biology and SSA hygroscopicity (Cochran et al., 2017). Additionally, the observed siliceous compounds, such as fragments of diatoms, may be active INP (Wang et al., 2011). Changes in SSA size distributions, number concentrations, and chemical composition due to factors including seawater temperature, salinity, and DOC are important to understand in order to predict SSA impacts on clouds. The shift to smaller sizes at lower temperatures indicates fewer SSA will be large enough to act as CCN. In addition, SSA organics may reduce particle hygroscopicity (Cochran et al., 2017; Collins et al., 2016) and CCN efficiency (Collins et al., 2013), and may contribute to INP activity (Wang et al., 2011; Wilson et al., 2015). The factors controlling SSA production are especially important to constrain in cold marine environments, areas of changing salinity, and regions of dynamic or enriched biological activity, including estuaries, river outflows, and areas of snow or ice melt. Determining the influence of temperature, salinity, and marine biology, and their combined impacts, on SSA size distributions and chemical composition, is crucial for predicting SSA production and climate impacts in dynamic marine environments, including temperate and polar regions of varying salinity and microbial activity.

2.5 Acknowledgments

Chapter 3.   Secondary Sulfate is Internally Mixed with Sea Spray Aerosol and Organic Aerosol in the Winter Arctic

3.1 Introduction

The Arctic region is experiencing warming at a greater rate than elsewhere on Earth (IPCC, 2014) and undergoing substantial transformations, including rapid loss of sea ice (Overland and Wang, 2013). This is leading to increased aerosol emissions, resulting in changes to atmospheric aerosol budgets and associated climate feedbacks (Struthers et al., 2011). Characterizing the chemical composition and morphology of individual Arctic aerosol particles is important for understanding the influence of local and transported aerosols on climate (Leck et al., 2002; Leck and Svensson, 2015), which remains one of the largest uncertainties in radiative forcing (Boucher et al., 2013). Aerosol mixing state, the distribution of chemical species across an aerosol population and within each individual particle, determines particle reactivity, hygroscopicity/cloud activation efficiency, and optical properties (Ault and Axson, 2017; Prather et al., 2008). However, the few studies that have used single particle analysis techniques to characterize the chemical mixing state of the Arctic aerosol population have been limited to Svalbard (Chi et al., 2015; Geng et al., 2010; Hara, 2003; Hara et al., 2002c; Weinbruch et al., 2012), Canadian archipelago (Köllner et al., 2017), and central Arctic (Sierau et al., 2014). Evaluating aerosol impacts on climate across the Arctic region is of particular importance given rapid changes in aerosol sources. Therefore, there is an urgent need to study the chemical composition of individual Arctic aerosol particles.

Aerosol influences on cloud formation and cloud-climate feedbacks in the Arctic are highly uncertain during winter, when there is little direct solar radiation and longwave radiative forcing dominates (Garrett and Zhao, 2006; Holland and Bitz, 2003; Letterly et al., 2016; Pithan and Mauritsen, 2014). Few studies have characterized Arctic aerosols, particularly those that may act

as cloud condensation nuclei (CCN) and ice nucleating particles (INP), during this period. Most studies in the winter-spring have focused on the components of Arctic haze, long-range transported pollution from the mid-latitudes present in the Arctic after polar sunrise, including non-sea salt sulfate, soot, organics, and metals (e.g. Fisher et al., 2011; Hara et al., 2002a; Norman et al., 1999; Polissar et al., 1999; Quinn et al., 2002; Sirois and Barrie, 1999; Sturges and Barrie, 1988). Notably, particulate sulfate concentrations in the Alaskan Arctic during haze season are 0.1-0.4 µg m^{-3} on average, and much higher than average nitrate concentrations of 0.01-0.03 µg m^{-3} (Quinn et al., 2007). SSA has also been identified as a significant contributor to the winter-spring aerosol budget by mass (10-30 %) in the Canadian Arctic (Norman et al., 1999; Quinn et al., 2002; Sirois and Barrie, 1999) and by number (55-85 %) in the Norwegian Arctic (Weinbruch et al., 2012). SSA are efficient CCN (Collins et al., 2013; Quinn et al., 2014) and can act as INP (DeMott et al., 2016), resulting in complex sea ice-aerosol-cloud interactions in the Arctic (Browse et al., 2014). Gaseous sulfuric acid or sulfur dioxide associated with Arctic haze has been shown to react with SSA, resulting in sulfate formation and internally mixed SSA-sulfate particles (Hara, 2003; Hara et al., 2002a). While less commonly observed in the Arctic, reactions between gaseous HNO_3 or N_2O_5 and SSA can also form mixed SSA-nitrate particles (Hara et al., 1999). These multiphase reactions result in chlorine (HCl, $ClNO_2$, Cl_2) liberation from SSA, contributing to atmospheric halogen chemistry (Barrie and Barrie, 1990; Hara et al., 2002c, 2002a; Sturges and Barrie, 1988) Given changing marine emissions coupled with transported pollution, it is important to understand aerosol chemical composition and heterogeneous processing to determine impacts on climate in the winter Arctic.

To improve our understanding of Arctic aerosol chemical mixing state under the changing radiation and sea ice conditions during the winter-spring transition (following polar sunrise), atmospheric particles were collected near Utqiaġvik (Barrow), Alaska during January and February 2014. Scanning electron microscopy with energy dispersive X-ray spectroscopy (SEM-EDX), Raman microspectroscopy, and scanning transmission X-ray microscopy with near-edge X-ray absorption fine structure spectroscopy (STXM-NEXAFS) were utilized to characterize individual particle chemical composition and mixing state. To our knowledge, these are the first measurements of individual particle chemical composition in the Alaskan Arctic during winter. The relative contributions of regional Arctic haze and SSA on the aerosol budget during this

winter-spring transition were examined, and the mixing states of individual aerosol particles were evaluated to examine atmospheric aging by multiphase reactions forming sulfate and nitrate.

3.2 Methods

Atmospheric particle sampling was conducted from January 23-28 and February 24-28, 2014 near Utqiaġvik (Barrow), Alaska at a tundra field site (71.28° N, 156.64° W) located ~5 km inland from the Arctic Ocean. Ozone concentrations and meteorological data, including wind speed, wind direction, and solar radiation, were obtained from the NOAA Barrow Observatory (71.32° N, 156.61° W), located 5 km to the northeast of the sampling site and separated only by flat tundra. Atmospheric particles were collected using a rotating micro-orifice uniform deposition impactor (MOUDI, MSP Corp., model 110) sampling at 30 LPM through a 10 μm cut-point cyclone (URG-2000-30EA) located ~2 m above the snow surface. 50 % particle collection efficiency size cuts for the six MOUDI stages used were 3.2, 1.8, 1.0, 0.56, 0.32, and 0.18 μm aerodynamic diameter (D_a). Particles were impacted on transmission electron microscopy grids (Carbon Type-B film copper grids, Ted Pella, Inc.) and silicon substrates (Ted Pella, Inc.) for SEM analysis, and quartz substrates (Ted Pella, Inc.) for Raman microspectroscopy analysis. Particle samples were stored frozen prior to analysis to keep near the ambient temperature at collection. Samples selected for analysis were collected for ~24 h on January 24-25 (10:15-10:00 AKST) and January 27-28 (11:00-10:30 AKST), ~18 h on January 26 (11:00-17:15 AKST), ~12 h on February 26 day (9:00-19:30 AKST), February 26 night (19:45-8:30 AKST), February 27 day (9:00-19:30 AKST), and February 27 night (20:00-7:30 AKST). These time periods were characterized by wind directions of 75-225° such that the town of Utqiaġvik was not upwind during sampling. Polar sunrise occurred at Utqiaġvik on January 22, 2014.

Computer-controlled SEM (CCSEM) analysis of individual atmospheric particles was completed using a FEI Quanta environmental SEM with a field emission gun operating at 20 keV with a high angle annular dark field (HAADF) detector (Laskin et al., 2006, 2012). An EDX spectrometer (EDAX, Inc.) collected X-ray spectra from elements with atomic numbers higher than Be (Z=4). 24,847 individual particles, typically ~1000 per sample, were analyzed by CCSEM-EDX. A size distribution showing the number of particles analyzed by CCSEM-EDX is shown in Fig. 3.1. Morphological data, including projected area diameter (D_{pa}) and perimeter, were collected for each particle, in addition to the relative abundance of the following elements quantified from

the EDX spectra: C, N, O, Na, Mg, Al, Si, P, S, Cl, K, Ca, Fe. Individual particle data were analyzed using K-means clustering of the EDX spectra (Ault et al., 2012; Axson et al., 2016b; Shen et al., 2016). K-means cluster analysis resulted in 50 clusters, which were then grouped into five particle classes (fresh SSA, partially aged SSA, organic+sulfate aerosol, fly ash aerosol, and mineral dust aerosol), based on comparisons of cluster EDX spectra with particle classes identified in previous studies. Prior ambient aerosol CCSEM-EDX studies have established EDX spectral signatures for fresh and aged SSA (Ault et al., 2013c; Hara, 2003; Hara et al., 2002c), organic+sulfate aerosol (Allen et al., 2015; Laskin et al., 2006; Moffet et al., 2010b), fly ash (Ault et al., 2012), and mineral dust (Axson et al., 2016b; Coz et al., 2009; Creamean et al., 2016; Sobanska et al., 2003).
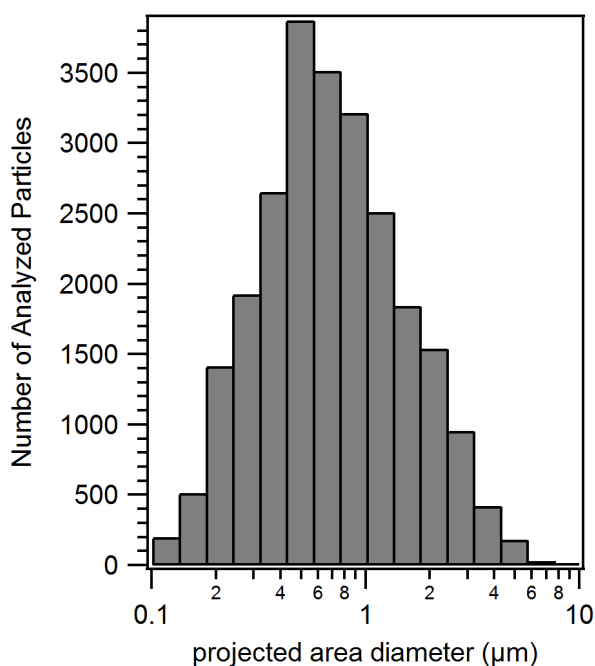
Figure 3.1 The number of individual particles analyzed by CCSEM-EDX for each of the 16 log size bins.

Individual particles from two MOUDI stages (1.0 – 1.8 and 0.56 – 1.0 μm aerodynamic diameter size ranges) for each of the seven samples were also analyzed by Raman microspectroscopy using a Horiba Scientific Labram HR Evolution spectrometer coupled with a confocal optical microscope (100x Olympus objective, 0.9 Numerical Aperture) equipped with a Nd:YAG laser source (50 mW, 532 nm) and CCD detector. A 600 groove/mm diffraction grating was used, yielding spectral resolution of 1.8 cm^{-1}. The laser power was adjusted between 25 – 100 % by varying a neutral density filter to prevent damage to the sample. Raman spectra were

obtained over the 500-4000 cm^{-1} range for ~300 particles. Spectra were compared with prior Raman studies of nascent and reacted sea spray aerosol (Ault et al., 2013b, 2014).

Beamline 5.3.2 on the Advanced Light Source at Lawrence Berkeley National Laboratory (Berkeley, CA) was used for STXM-NEXAFS analysis over the carbon k-edge (280-320 eV), as previously described by Moffet et al. (2010a). Briefly, X-rays from the synchrotron were energy-selected using a monochromator, focused on the sample, and raster scanned across a selected area. The sample was rescanned at closely spaced X-ray energies to complete a spectral image stack. After the X-ray spectra were converted to optical density using the Beer-Lambert law, STXM-NEXAFS maps were generated to show the distribution of organic carbon, soot, and inorganic components in individual aerosol particles, based on the X-ray absorptions at 288.5 eV, 285.4 eV, and 283 eV, respectively. 290 particles from the February 26 night sample (0.10 - 0.18 μm D_a) were analyzed for detection of organic carbon. D_{pa} was measured by CCSEM-EDX, Raman, and STXM-NEXAFS; therefore, is the parameter reported for all data herein. D_{pa} is often larger than geometric diameter due to particle deformation upon impaction (Hinds, 2012; O'Brien et al., 2014; Sobanska et al., 2014), indicating that particle size reported here is an upper bound and could represent smaller diameter in the atmosphere.

3.3 Results and Discussion

3.3.1 Chemical Composition and Size Distribution of Observed Particle Types

Five individual particle classes, including fresh sea spray aerosol (SSA), partially aged SSA, organic+sulfate particles, fly ash, and mineral dust particles, were identified from the CCSEM-EDX data (Fig. 3.2). SSA (both fresh and partially aged) and organic (with and without sulfate) particles were the most commonly observed types, indicating that mixing of sulfate with SSA and organic aerosol may be significant in the winter Arctic. Fresh and partially aged SSA comprised 99 %, by number, of the observed supermicron particles (1.0-7.5 μm D_{pa}) (Fig. 3.3). Across the submicron size range (0.1-1.0 μm D_{pa}), the majority of particles were also SSA (50-75 %, by number) (Fig. 3.3). The prevalence of SSA particles, even in the winter, may be a result of changing conditions in the Arctic, with previous work showing local SSA influence in Utqiaġvik, AK from nearby sea ice leads, even during winter (May et al., 2016b). Organic particles (with and without sulfate) were also a significant fraction (25 – 50 %, by number) of submicron particles. Only a limited fraction of particles (~ 1 % by number across the entire size range) were classified

as fly ash or mineral dust, characterized by silicon and oxygen, with trace amounts of aluminum, sodium, and iron (Coz et al., 2009; Sobanska et al., 2003).
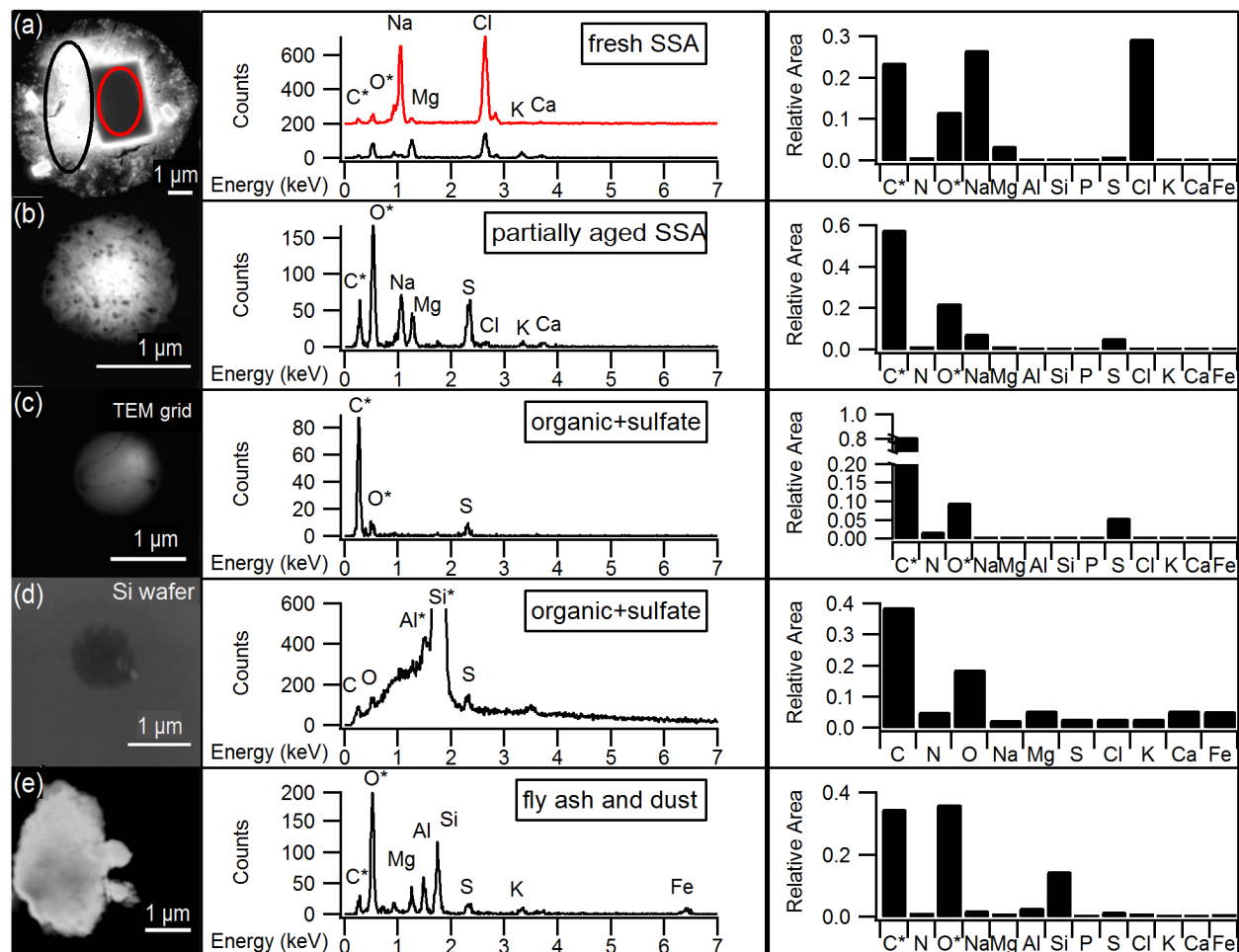
Figure 3.2 Representative SEM images and EDX spectra of individual particles corresponding to the main particle types observed by CCSEM-EDX, and the average EDX spectrum for each particle type. Average spectra show the relative peak areas of all elements analyzed by CCSEM-EDX. (a) Fresh SSA particle comprised of sodium chloride core (red) and magnesium chloride shell (black). The spectrum for the core is offset for clarity. (b) Partially aged SSA particle containing sodium and more sulfur than chlorine. (c) Organic+sulfate particle. (d) Organic+sulfate particle on silicon substrate. (e) Aluminum- and silicon- containing dust particle. *Carbon and oxygen peaks include some signal from TEM grid substrate background for particles a, b, c, and e. Aluminum and silicon peaks are due to sample holder and silicon substrate background, respectively, for particle d.
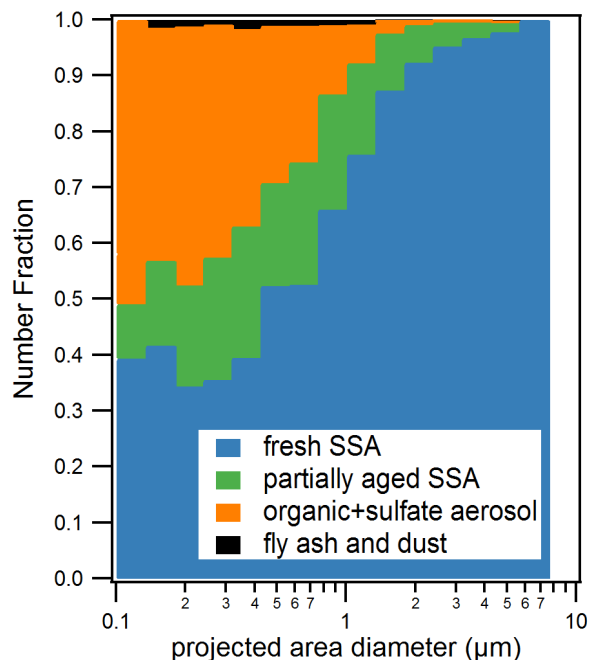
Figure 3.3 Size-resolved CCSEM-EDX number fraction distributions of observed particle types for all samples. Particles were sorted into 16 bins (logarithmic) from 0.1 to 10.0 μm projected area diameter (8 bins per decade). Organic+sulfate class includes a small fraction of internally mixed soot.

Particles classified as fresh SSA, based on grouping by chemical composition by K-means analysis, contained sodium, magnesium, sulfur, and chlorine in similar mole ratios (Table 3.1) to those found in seawater (Cl/Na = 1.2, Mg/Na = 0.11, S/Na = 0.06) (Pilson, 2013; Quinn et al., 2015), indicating these particles had not undergone chemical aging processes during atmospheric transport. Some SSA particles were observed with a sodium chloride core and magnesium chloride outer coating (Fig. 3.2), which is likely due to the particle undergoing efflorescence after collection (Ault et al., 2013a); this morphology has been previously observed for Arctic SSA particles (Chi et al., 2015). The partially aged SSA particles contained sulfur and/or nitrogen and were characterized by Cl/(Na+0.5Mg) ratios of less than 1 (Laskin et al., 2012). This indicates that multi-phase reactions had occurred releasing chlorine-containing trace gases, primarily hydrochloric acid (Gard et al., 1998; Laskin, 2003; Laskin et al., 2002), resulting in the formation of sulfate and nitrate in the particles. SSA chemical mixing state information is further discussed in Sec. 3.3.2. SSA aging was observed for few 1.0-7.5 μm particles (7 %, by number, aged SSA and 90 % fresh SSA), with a greater fraction of submicron 0.1-1.0 μm SSA particles having undergone aging (18 %, by number, aged SSA and 42 % fresh SSA) (Fig. 3.3). Compared to

supermicron particles, submicron particles have longer atmospheric lifetimes, a smaller Cl reservoir, and greater surface area to volume ratios, which are conducive to increased atmospheric processing (Ault et al., 2014; Hara et al., 2002c; Leck et al., 2002; Williams et al., 2002). While concentrations of sulfur- and nitrogen-containing gases are lower in the Arctic winter compared to the peak of spring haze season, allowing for SSA particles to remain chemically fresh further from the emission point, aged SSA particles have also been observed during winter at Svalbard (Hara et al., 1999, 2002c). Overall, fresh and aged SSA were significant contributors to the winter Arctic aerosol budget (Fig. 3.3). This observation is consistent with studies of annual Arctic aerosol trends that have shown a large influence of SSA in the winter by mass: constituting up to 40 % of supermicron mass at Barrow (Quinn et al., 2002) and 60-90 % of 0.5-10 µm particles, by number, for winter samples at Svalbard (Weinbruch et al., 2012).

Organic particles, classified by K-means analysis, were characterized by spherical morphology and carbon and oxygen in the single particle EDX spectra. Since there is background C and O EDX signal from the TEM grid substrate film, the contribution of C and O to this particle class was confirmed by CCSEM-EDX analysis of 110 particles that had been collected simultaneously on silicon substrates that do not have these interferences. Figure 3.2 shows the representative EDX spectra of organic particles analyzed on TEM grids and silicon substrates for comparison. Sulfur was present in 47 %, by number, of organic particles, at levels of at least 2% atomic content in the EDX spectrum; therefore, these organic particles will be discussed together as an organic+sulfate particle class (Laskin et al., 2006; Moffet et al., 2010b). Example organic+sulfate particles are shown in Fig. 3.2c and d. Organic+sulfate particles were primarily observed in the submicron size range (Fig. 2). Overall, 40-50 % of the particles 0.1 - 0.5 µm in diameter and 15 - 25 % of the particles 0.5 – 1.0 µm, by number, were classified as organic+sulfate (Fig. 3.3). The detailed chemical mixing states of these organic+sulfate particles will be discussed in Sect. 3.3.3. The presence of a large number fraction of submicron organic+sulfate particles is consistent with previous winter-spring Arctic studies, which have observed organic particles contributing up to 30 % of submicron aerosol by mass and greater than 80 %, by number, at Barrow (Hiranuma et al., 2013; Shaw et al., 2010) and greater than 80 %, by number, of 0.1-0.5 µm (aerodynamic diameter) particles at Svalbard (Weinbruch et al., 2012). Internal mixing of organic and sulfate aerosol has previously been observed in the Arctic winter-spring at Svalbard, with most 0.2-2.0 µm (aerodynamic diameter) organic particles containing sulfate (Hara et al., 2002b).

Internally mixed organic+sulfate aerosol is now being observed across the Arctic during the winter, highlighting the importance of considering sulfate mixing states during this period.

3.3.2 Internal Mixing of SSA with Sulfate and Nitrate

Raman microspectroscopic analysis of individual aged SSA particles confirmed that the sulfur and nitrogen detected by EDX in SSA were in the forms of sulfate and nitrate, respectively, based on the presence of sharp peaks corresponding to characteristic symmetric stretches at ~1000 cm^{-1} for $\nu_s(SO_4^{2-})$ and ~1050 cm^{-1} for $\nu_s(NO_3^-)$ (Fig. 3.4) (Ault et al., 2014; Deng et al., 2014; Eom et al., 2016). In addition, these particles were characterized by broad peaks in the 3000-3500 cm^{-1} range (Fig. 3.4), corresponding to O–H stretching, likely due to particle-phase water (Ault et al., 2014), confirmed by the frequency of the $\nu_s(NO_3^-)_{(aq)}$ mode at ~1050 cm^{-1}. Raman C-H stretching peaks in the 2800-3000 cm^{-1} range indicated that organic compounds were present in both fresh and aged SSA (Ault et al., 2013b; Baustian et al., 2012; Eom et al., 2016); the organic functional groups are discussed further in Chapter 4.
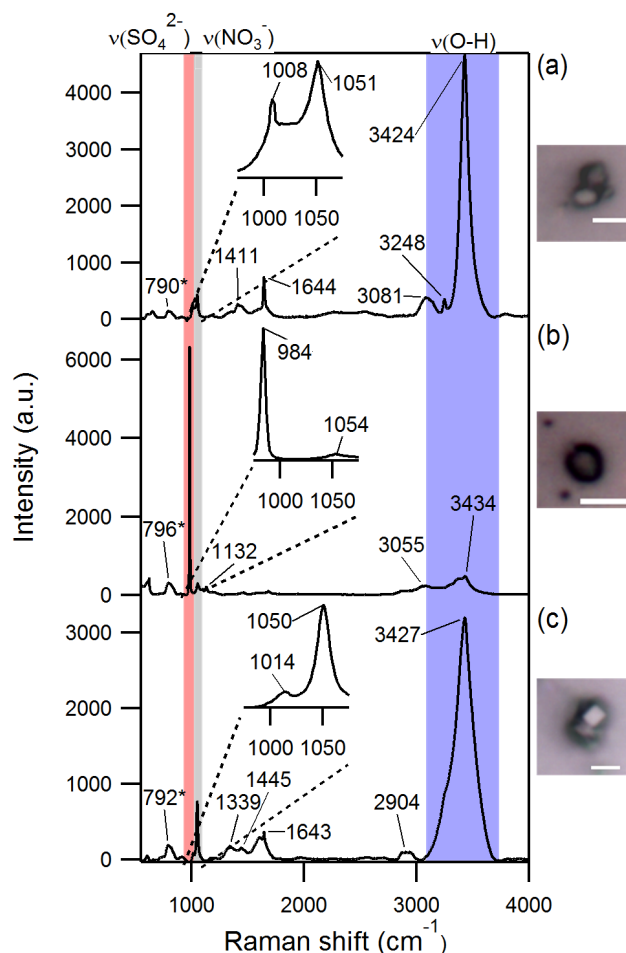
Figure 3.4 Optical images and Raman spectra of three representative SSA particles containing nitrate and/or sulfate and hydroxyl groups. A total of ~300 individual particles were analyzed by Raman microspectroscopy. *790-796 cm-1 peak is due to quartz substrate background. Scale bar for all images is 5 μm.

Based on the CCSEM-EDX analysis, SSA aging by sulfur species (e.g. sulfuric acid) was more prevalent than aging by nitrogen species (e.g. nitric acid) in the submicron size range, consistent with previous measurements of SSA during Arctic haze periods in the Norwegian Arctic (Hara et al., 2002c). 73 % of partially aged SSA, by number, in the 0.1-1.0 μm size range contained secondary sulfate. This was determined by a S/Na ratio at least 25 % greater than the seawater molar ratio 0.06 (Pilson, 2013), with these particles having an average S/Na ratio of 1.07 (Table 3.1). In comparison, only 22 % of 0.1-1.0 μm particles contained nitrate (Table 3.1). The diffusion limited uptake of SO_2 in submicron particles is favored over the thermodynamically controlled uptake of HNO_3, resulting in a preference for sulfate in submicron aged SSA (Kerminen et al., 1998; Liu et al., 2007; Zhuang et al., 1999). However, sulfate was also more prevalent than nitrate

in supermicron SSA (Table 3.1), where kinetically favorable uptake of HNO_3 would be expected to dominate, suggesting higher concentrations of H_2SO_4, compared to HNO_3, influenced particle aging. The prevalence of SSA aging by sulfur species near Utqiaġvik is consistent with the appearance of springtime Arctic haze, as 30 % of submicron particle mass corresponds to sulfate during haze season (January to May) (Quinn et al., 2002, 2007). Sulfate mass concentrations peak in winter-spring near Utqiaġvik, while methanesulfonic acid mass is greatest in the summer and has not been observed during winter months (Quinn et al., 2007). Therefore, the prevalence of mixed SSA-sulfate suggests that reactions with sulfuric acid from Arctic haze are an important source of SSA sulfate (Barrie and Barrie, 1990; Hara et al., 2002c). SSA aging through sulfate addition was likely also due to influence from Prudhoe Bay SO_2 emissions (Gunsch et al., 2017; Peters et al., 2011), discussed further in Sec. 3.3.4.

Table 3.1 Size resolved number fractions of individual fresh SSA, partially aged SSA, and organic+sulfate particles containing Cl, S, and N, in addition to average atomic (mole) ratios of Cl/Na, S/Na, and N/Na for individual fresh and partially aged SSA.

Particle class and size range	Number fraction containing Cl	Number fraction containing S	Number fraction containing N	Average Cl/Na	Average S/Na	Average N/Na
Fresh SSA (0.1 – 1.0 μm)	1.0	0.15	0.15	0.98	0.05	0.04
Fresh SSA (1.0 – 10 μm)	1.0	0.18	0.10	1.26	0.05	0.04
Partially aged SSA (0.1 – 1.0 μm)	0.07	0.73	0.22	0.04	1.07	0.25
Partially aged SSA (1.0 – 10 μm)	0.38	0.81	0.52	0.24	1.53	0.95
Organic+sulfate (0.1 – 1.0 μm)	---	0.46	0.13	---	---	---
Organic+sulfate (1.0 – 10 μm)	---	0.87	0.60	---	---	---

3.3.3 Organic Particle Mixing States

Organic particles and internally mixed organic+sulfate particles composed a significant number fraction of submicron particles, which is consistent with the presence of organic aerosol, sulfuric acid, and ammonium sulfate in Arctic haze (Hara et al., 2002b; Hirdman et al., 2010).

STXM-NEXAFS indicated the presence of organic carbon in these particles, based on X-ray absorption at 288.5 eV, characteristic of carboxylic acids (Moffet et al., 2010a). Additionally, STXM-NEXAFS analysis confirmed that organic and inorganic (likely sulfate, based on sulfur detected during CCSEM-EDX analyses) components were internally mixed within individual particles (Fig. 3.5), with particles showing an internal mix of both inorganic dominant (> 50 %) and organic dominant regions. The pre-post edge ratio of inorganic to organic components also indicated that most analyzed particles contained both inorganic and organic species (Fig. 3.5). Raman analysis confirmed sulfur was present in the form of sulfate. Nitrogen (nitrate, according to Raman analysis) was also present in 15 % of 0.1 – 1.0 µm organic+sulfate particles, by number.
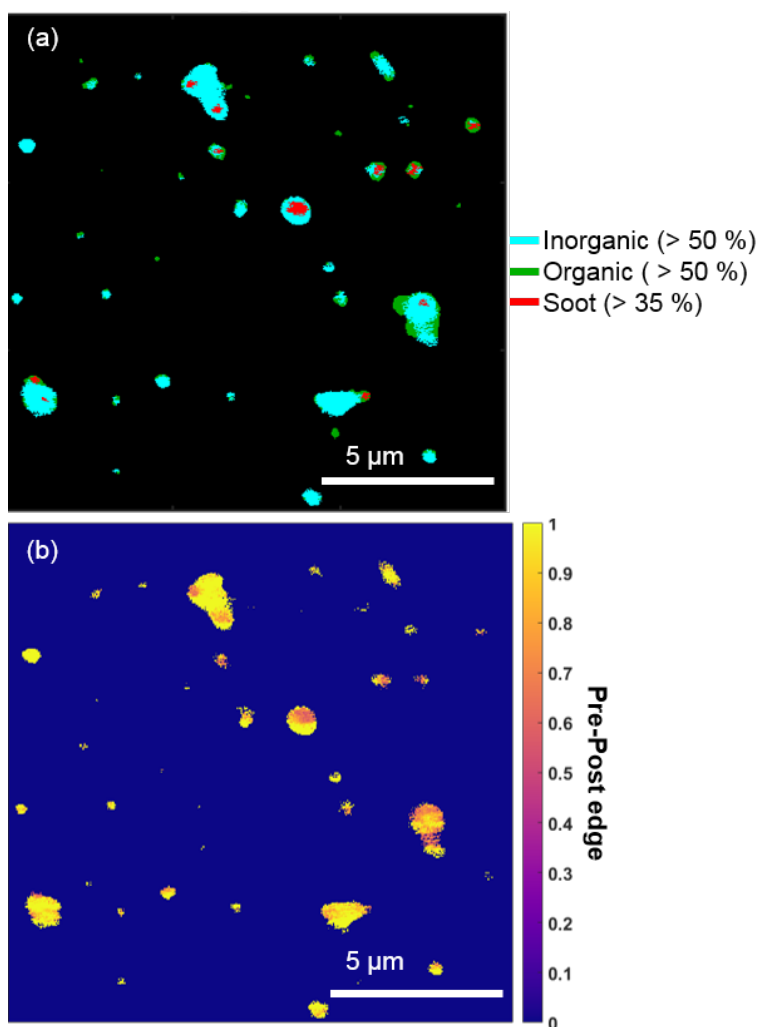
Figure 3.5 Representative STXM/NEXAFS map from February 26 night showing a) the distributions of inorganic dominant (blue, > 50 % by mass), organic carbon dominant (green, > 50 % by mass), and soot (red, sp2 > 35 %) and b) the ratio of inorganic (pre-) and organic (post-edge) components between populations of individual particles sampled during a period with a high fraction of organic+sulfate particles.

Chemical mixing state analysis determined that a small fraction of particles classified as organic+sulfate (7 % of this particle class, by number) by CCSEM-EDX were primarily carbon-containing particles with less than 5 % oxygen and sulfur. For the February 26 night sample analyzed by STXM-NEXAFS, elevated levels of sp^2 carbon, indicative of soot, were observed in some particles (Fig. 3.5) (Moffet et al., 2010a). These small soot particles observed by STXM-NEXAFS were likely members of the "primarily carbon" group identified by CCSEM-EDX and were internally mixed with organic carbon and inorganic species (likely sulfate, based on sulfur detected during CCSEM-EDX analyses). Therefore, these particles were included in the organic+sulfate class. Externally mixed soot particles, comprised solely of elemental carbon with no organic or sulfate component, were not observed in any sample, indicating that all soot was internally mixed with organic+sulfate particles. Soot present in Arctic haze (Law and Stohl, 2007; Quinn et al., 2007) has previously been observed to be internally mixed with sulfate for winter-spring Arctic aerosol, with soot-sulfate particles contributing ~ 10-20 % of observed particles sampled (<2.0 μm), by number, at Svalbard (Hara, 2003).

3.3.4 Influence of Marine- and Prudhoe Bay-Influenced Air Masses on Particle Composition

There was no clear dependence or trend with wind speed or month (Jan. vs. Feb.) for SSA S/Na or Cl/Na ratios, with average wind speeds ranging from 5 – 12 m/s for the selected sampling periods, but some variability in particle composition between samples could be attributed to the influence of different air masses. Though all samples experienced some degree of Arctic Ocean air mass influence due to the sampling location and prevailing wind direction from the north over the Beaufort Sea to the sampling site, using NOAA HYSPLIT 48 h backward air mass trajectory analysis two main air mass source regions (Arctic Ocean and Prudhoe Bay influence) were determined for the seven analyzed sample periods. Most notably, the February 26 day sample was influenced by air from the north and east over the Arctic Ocean within the boundary layer for the 6-7 h prior to arrival at the sampling site, whereas the January 27 sample had prolonged surface influence (18 h) along the air mass trajectory from the east/southeast, during which the air mass passed over Prudhoe Bay, the third largest oilfield in North America (U.S. Energy Information Administration, 2015) (Fig. 3.6). Prudhoe Bay influence was determined by HYSPLIT trajectories that passed within 1 degree (~50 km) of the Prudhoe Bay emissions box, described in Kolesar et al. (2017) as the area significantly influenced by combustion emissions from the oilfields. The air mass trajectories for the remaining samples (January 24, January 26 day, February 26 night,

February 27 day, February 27 night) fell in between the two regions (Arctic Ocean and Prudhoe Bay influence).
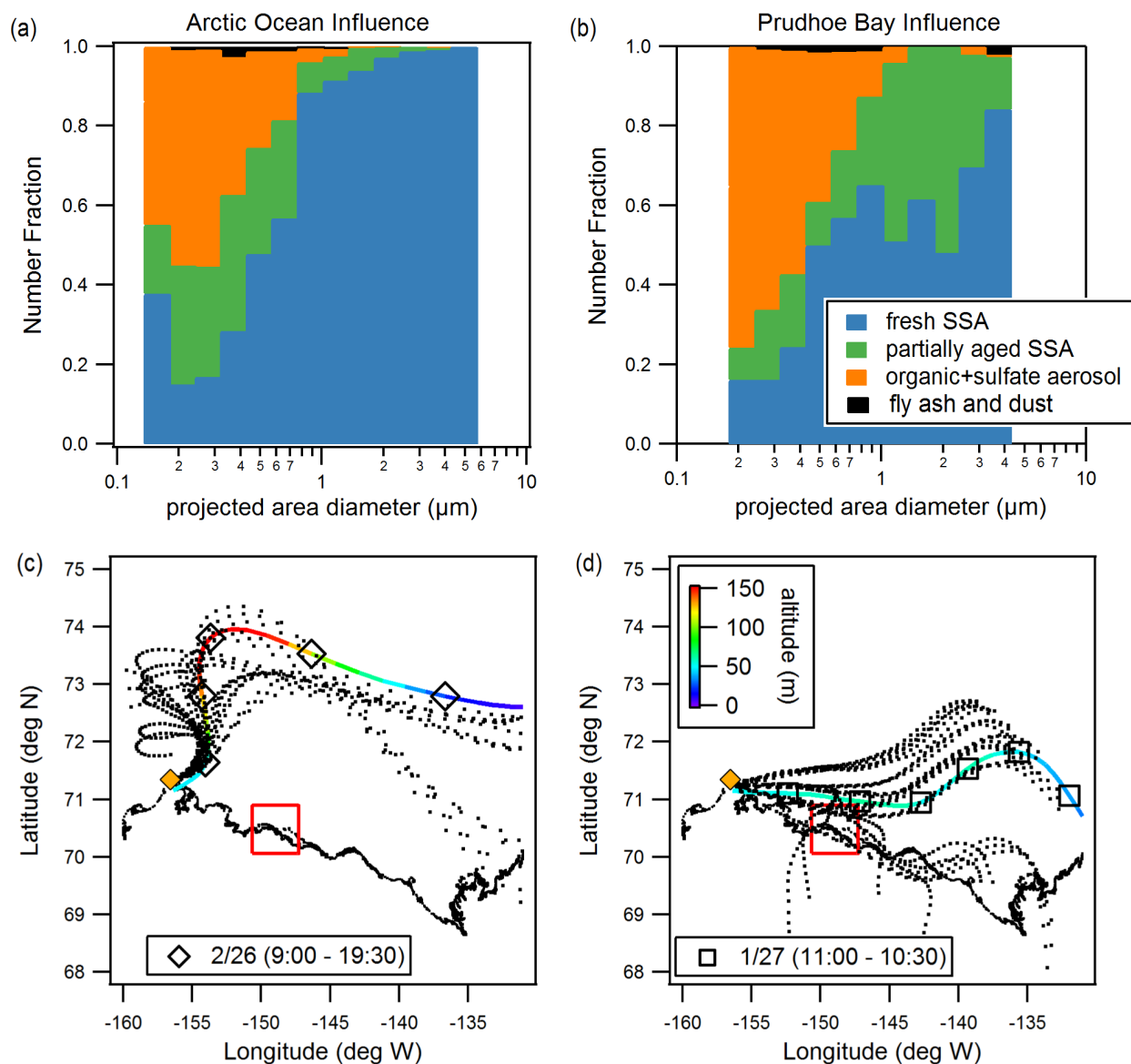
Figure 3.6 Size-resolved number fractions of observed particle types (CCSEM-EDX) for example a) Arctic Ocean (February 26 day, 4490 particles) and b) Prudhoe Bay (January 27, 1475 particles) influenced sample periods. Air mass influence is shown for c) February 26 day and d) January 27 as determined by NOAA HYSPLIT 48 h backward air mass trajectories. Both ensemble (dotted line) and single representative trajectories are shown. Color scale indicates air mass altitude, and markers are placed at 6 h intervals. Red line shows extent of Prudhoe Bay emissions influence box (Kolesar et al., 2017). Yellow diamond indicates sampling site near Utqiaġvik.

Comparison of particle type contributions as a function of size for the representative Arctic Ocean influenced (February 26 day) and Prudhoe Bay influenced (January 27) samples are shown in Fig. 3.6 (with results of additional samples shown in Fig. 3.7). The Arctic Ocean influenced sample was characterized by a large fraction (95 %) of fresh SSA in the 1.0 – 7.5 μm size range. In comparison, the Prudhoe Bay influenced sample was characterized by 55 % fresh SSA and 40 - 45 % partially aged SSA, by number, in the supermicron range. This is indicative of multiphase reactions between SSA and gaseous emissions from combustion at the oilfields (e.g. SO_2, NO_x) (Gunsch et al., 2017; Jaffe et al., 1991; Peters et al., 2011), contributing to a greater number fraction of aged SSA during Prudhoe Bay influenced periods. The Prudhoe Bay influenced sample also had a greater number fraction of organic+sulfate particles in the 0.1-0.5 μm range (60 - 70 %) compared to the Arctic Ocean influenced sample (40 – 50 %). Given that organic+sulfate particles were a significant fraction of submicron particles in all samples, including ocean-influenced periods, these samples were likely influenced by long-range transported pollution from the mid latitudes, consistent with regional background haze (Quinn et al., 2007). However, it is likely that gas-particle partitioning of oxidation products from Prudhoe Bay oilfield combustion emissions, including volatile organic compounds and SO_2 (Gunsch et al., 2017; Jaffe et al., 1991; Peters et al., 2011), also results in the formation of organic+sulfate particles, including particles internally mixed with soot (Sect. 3.3), contributing to the increased number fraction of organic+sulfate particles observed during Prudhoe Bay influenced periods.
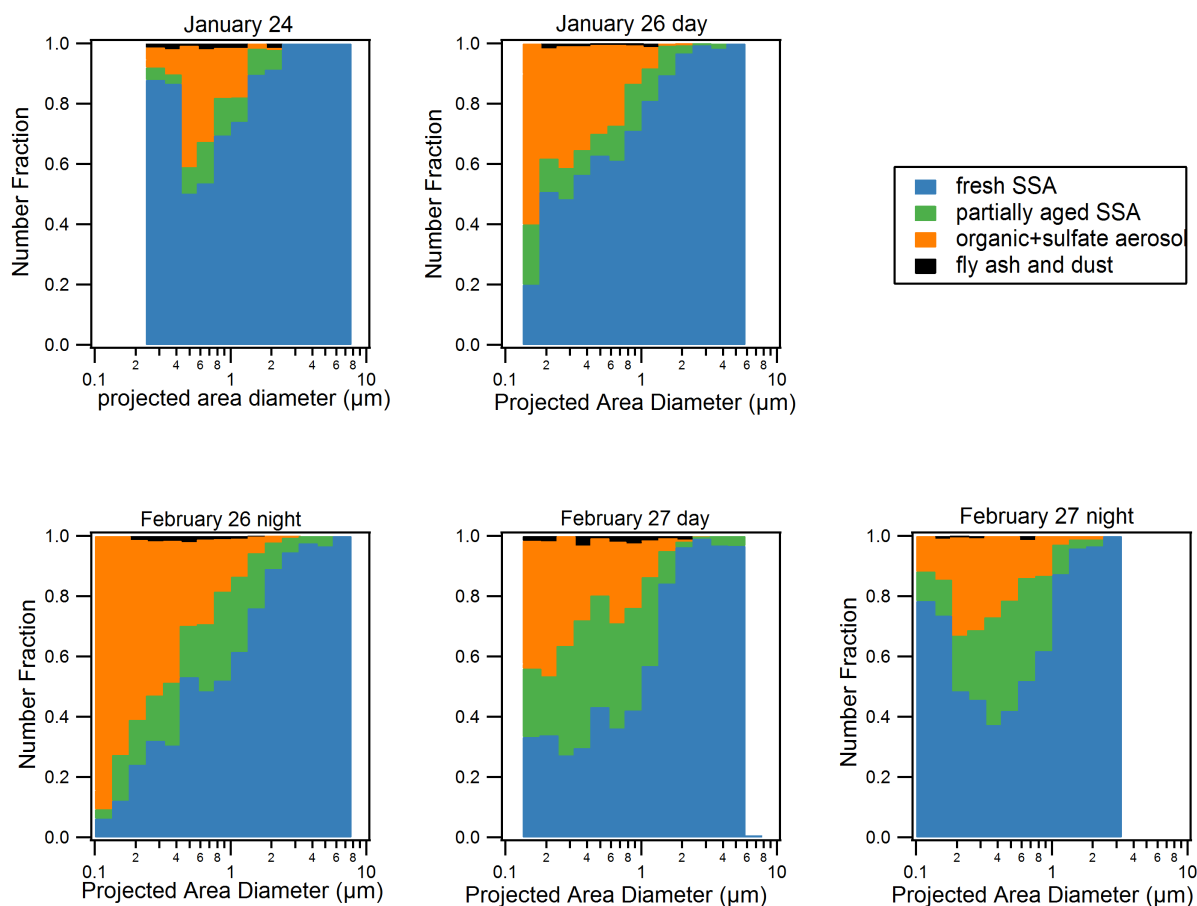
Figure 3.7 Size-resolved number fractions of particle types for additional sample periods not shown in Figure 3.6. Particles were sorted into 16 log size bins.

3.4 Conclusions

For atmospheric particles collected in January and February 2014 near Utqiaġvik, Alaska, SSA was observed to be the most prevalent particle type, composing 50-75 % and 99 %, by number, of particles in the 0.1-1.0 µm and 1.0-7.5 µm projected area diameter ranges, respectively. Internal mixing of sulfate and nitrate with SSA particles was observed in all samples, regardless of air mass influence, suggesting prevalent regional pollution, such as Arctic haze influence, for secondary inorganic aerosol formation. Prudhoe Bay influenced air masses were characterized by higher number fractions of partially aged SSA, however, suggesting that oilfield emissions also contribute significantly to multiphase reactions with SSA. Most global and regional climate models assume that Arctic haze components (sulfate, organic aerosol, black carbon) and natural aerosols are externally mixed and do not predict climate impacts of internally mixed species (Alterskjr et al., 2010; Eckhardt et al., 2015; Korhonen et al., 2008). However, no externally mixed

sulfate or sulfuric acid particles were observed during January or February sampling in Utqiaġvik, Alaska; all sulfate was internally mixed with organic aerosol particles or with SSA. Internal mixing of SSA and sulfate reduces CCN efficiencies compared to externally mixed sulfate aerosol or SSA, as sodium sulfate is less hygroscopic than sodium chloride or sulfuric acid (Gong and Barrie, 2003; Petters and Kreidenweis, 2008). The prevalence of SSA internally mixed with sulfate should be considered in the interpretation of elevated sulfate concentrations in the winter-spring Arctic atmosphere (Hara et al., 2002a; Sirois and Barrie, 1999; Sturges and Barrie, 1988).

While SSA comprised 50-60 % of 0.1 – 0.5 µm particles, by number, organic+sulfate particles made up 40-50 %, by number, in this particle diameter range and were present in similar number fractions in all samples, suggesting the importance of Arctic haze as a source of submicron particles in January and February in Utqiaġvik, Alaska. Internal mixing of sulfate and nitrate with organic aerosol is consistent with previous single particle measurements at Svalbard, where organic aerosol mixed with sulfate and nitrate was observed to be the dominant particle type in the submicron size range in the winter and spring (Weinbruch et al., 2012). Weinbruch et al. (2012) also observed soot particles internally mixed with organics, sulfate, and nitrate, consistent with the small fraction of internally mixed organic+sulfate and soot particles (~2 – 3 % of total observed particles, by number) observed in this study. The internal mixing of sulfate with organic aerosol is important to consider in climate predictions, as the CCN activity of internally mixed organic+sulfate aerosol is reduced relative to externally mixed sulfate, due to the lower hygroscopicity of the organic fraction (Petters and Petters, 2016; Wang et al., 2015b). Continuing oil and gas development in the Arctic region will influence both SSA and organic aerosol composition (Peters et al., 2011), as well as mixing state, due to secondary inorganic aerosol formation.

3.5 Acknowledgments

Chapter 4. Wintertime Arctic Sea Spray Aerosol Composition Controlled by Sea Ice Lead Microbiology

4.1 Introduction

With rapidly declining Arctic sea ice extent and increasing open water (Haine and Martin, 2017), SSA emissions are predicted to be increasing (Struthers et al., 2011). Notably, even wintertime coastal sea ice in the Arctic is drastically decreasing as a result of sea ice freeze-up delays in the Bering, Chukchi, Barents, and East Greenland Seas (Beitler, 2017). Thick multi-year sea ice is being replaced by thinner first-year ice, which is more susceptible to fracturing and forming leads, open areas of water surrounded by ice (Richter-Menge and Farrell, 2013). During Arctic winter, fresh (nascent) SSA comprises a significant aerosol fraction: up to 40 % and 25 % of supermicron and submicron aerosol mass (Quinn et al., 2002), and up to 90 % and 50 % of supermicron and submicron aerosol number, respectively (Kirpes et al., 2018). While wintertime SSA was previously thought to primarily be transported long distances to the Arctic (Quinn et al., 2002), recent work showed that leads contribute to local Arctic SSA emissions year-round (May et al., 2016b).

SSA composition reflects the seawater surface microlayer (SML) (Ault et al., 2013c; Quinn et al., 2014), which is expected to be altered by changing marine productivity in the warming Arctic (Ardyna et al., 2014). In the open ocean, SSA are primarily generated by wave breaking processes resulting in bubble bursting at the ocean surface, creating film and jet drops that form SSA (Quinn et al., 2015). Wind-driven wave breaking processes also produce SSA in leads, at lower concentrations than in open water due to the reduced fetch (Leck et al., 2002; May et al., 2016b; Nilsson et al., 2001; Scott and Levin, 1972). Supermicron SSA particles (> 1 μm, 2 μm mode) are primarily inorganic salts, but can also contain organic matter (Quinn et al., 2015). These inorganic salts are hygroscopic, with high efficiency of forming cloud droplets (Quinn et al., 2015). Submicron SSA particles (< 1 μm, ~200 nm mode) can be significantly enriched in organic matter (>50 %, by mass) that are in excess in the SML (Ault et al., 2013c; Facchini et al., 2008). SSA organic coatings can inhibit heterogeneous reactions of trace gases, inhibiting particulate chloride

depletion, and impacting trace gas budgets and atmospheric composition (Ault et al., 2014). Laboratory studies with ambient seawater show also suppression of SSA hygroscopicity and cloud condensation nuclei (CCN) activity by certain organics (Cochran et al., 2017; Collins et al., 2013), yet likely contribute to cloud ice nucleation (Wilson et al., 2015). Despite important climate implications for cloud formation and phase, and associated longwave radiative forcing (Graham et al., 2017), limited knowledge exists regarding ambient SSA organic coatings and the transfer of marine biogenic organics to the particle phase (Quinn et al., 2014), particularly for Arctic winter.

While previous studies have primarily focused on marine biological activity during the Arctic summer, recent work has shown microalgal growth is initiated prior to the spring phytoplankton bloom period and under extremely low light conditions under sea ice (Assmy et al., 2017; Hancke et al., 2018), including during sea ice covered periods (Arrigo et al., 2012; Mayot et al., 2018). The sea ice algae and bacteria present produce exopolymeric substances (EPS) as a cryoprotectant (Boetius et al., 2015; Krembs et al., 2002), with phytoplankton releasing it extensively (Vernet et al., 1998). Production of EPS is critical to sea ice algae survival through the winter (Krembs et al., 2011; Leu et al., 2015). Indeed, EPS have been observed in winter in both sea ice (Mayot et al., 2018; Niemi et al., 2011) and seawater (Niemi et al., 2011). In the high Arctic, aerosols produced from laboratory bubbling experiments in the summer pack ice showed enrichment of EPS-derived polysaccharides relative to the SML (Gao et al., 2012), with microgels and EPS-derived compounds also observed in the ambient aerosols (Leck et al., 2013). However, there is a critical knowledge gap in our understanding of wintertime aerosol sources and composition in the changing Arctic (Kirpes et al., 2018), particularly with increasing open water (Beitler, 2017). Therefore, atmospheric aerosols were collected near Utqiaġvik, Alaska in January and February 2014 for individual particle measurements of morphology, elemental composition, spatial distribution and quantity of organic material, and organic functional groups associated with marine biogenic compounds. This novel detailed characterization of individual SSA, and associated organic material, significantly improves our knowledge of Arctic SSA and connections to sea ice microbiology at a time of year when few aerosol measurements exist.

4.2 Methods

Atmospheric particles were collected near Utqiaġvik (Barrow), AK during January 24-27 and February 26-27, 2014, at a tundra site ~5 km inland (71.17° N, 156.38° W), at a sampling height ~ 1.5 m above ground level. Sample collection times and meteorological parameters,

measured at the NOAA Barrow Observatory located 5 km upwind across flat tundra, are provided in Table 4.1. Particles were collected using a 10-stage rotating micro-orifice uniform deposit impactor (MOUDI, model 110, MSP Corp.) sampling at 30 L min^{-1} through a 10 µm cut point cyclone (URG-2000-30EA). Particles were impacted on silicon substrates (Ted Pella, Inc.) and aluminum foil substrates (MSP Corp.) for analysis by SEM-EDX, quartz substrates (Ted Pella, Inc.) for analysis by Raman microspectroscopy, and transmission electron microscopy (TEM) grids (Carbon Type-B Formvar film copper grids, Ted Pella, Inc.) for analysis by STXM-NEXAFS. Samples were stored frozen at −15 °C prior to analysis. Particles collected on two MOUDI stages with 50 % size cuts of 1.8 and 0.56 µm d_a, respectively, were analyzed in this work.

Table 4.1 Aerosol sampling timing and meteorological conditions measured at the NOAA Barrow Observatory.

Sample name/date	Sample Time (AKST)	Sampling duration (h)	Average wind speed (m s-1)	Wind speed range (m s-1)
January 24-25	10:16-10:02	24	12	8.6-14.9
January 26 day	11:00-17:15	6.25	8	6.2-9.9
January 27-28	10:55-10:30	23.5	6	3.9-8.1
February 26-27	19:45-8:30	12.5	10	5.8-16.6
February 27	8:50-19:30	10.5	12	8.5-15.3
February 27-28	20:00-7:20	11.25	10	6.9-15.0

For comparison to the winter SSA SEM-EDX analysis, atmospheric particles were collected at the same location during September 15 – 16 and 23 – 24, 2015. Samples were collected for ~ 8 h each using a three-stage microanalysis particle sampler (MPS, California Measurements, Inc) with aluminum foil substrates (MSP Corp.) on stages 1 and 2 (2.8 – 5.0 µm and 0.50 – 2.8 µm, respectively) and TEM grids (Carbon Type-B Formvar film copper grids, Ted Pella, Inc.) on

stage 3 (0.07 – 0.40 µm). Additional sampling details are described by Gunsch et al. (2017). Similar size particles were analyzed for the winter and summer samples (Fig. 4.1).
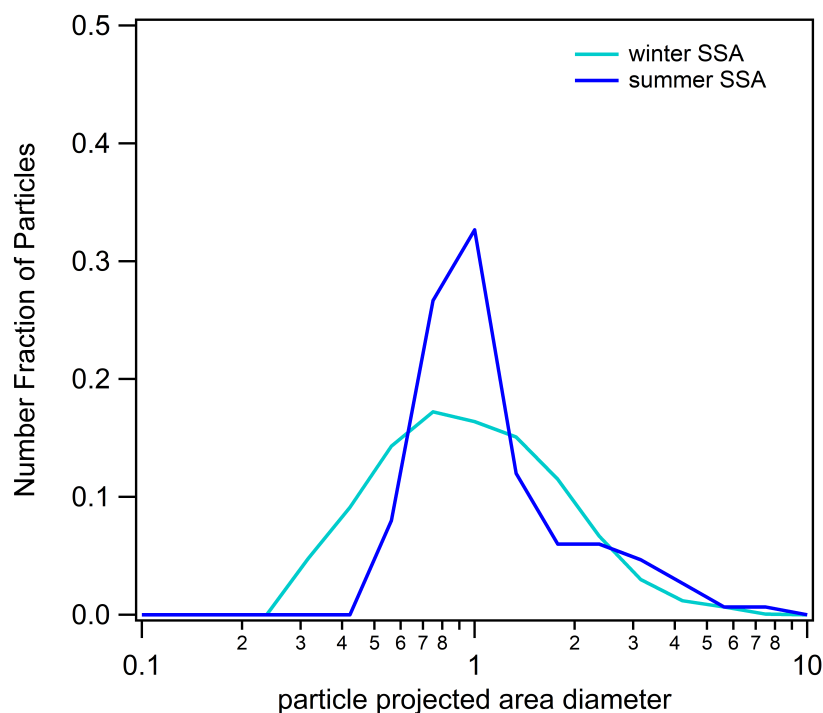
Figure 4.1 Size distributions for the individual particles analyzed by CCSEM-EDX to determine carbon to sodium ratios and organic coating to salt core ratios, for winter and summer SSA.

Individual particle analysis by computer-controlled SEM-EDX (CCSEM-EDX) was conducted using a FEI Nova 200 nanolab SEM/FIB operating at 15 kV accelerating voltage with a secondary electron detector. X-ray spectra from elements with atomic numbers greater than Be (Z>4) were detected with an EDX detector (EDAX, Inc.). For each substrate collected during the six winter sample periods, ~75-150 particles were analyzed by CCSEM-EDX to measure individual particle morphology (particle projected area, average diameter, and perimeter) and relative abundance of the following elements: C, N, O, Na, Mg, S, Cl, K, Ca, Ti, Fe, and Zn (Laskin et al., 2006). EDX has previously been shown to quantitatively reproduce SSA elemental ratios (Ault et al., 2013c). Carbon was below the detection limit on the Si wafer without particles, indicating that substrate contamination from C was not present in the particle spectra (Fig. 4.2). EDX can be slightly less sensitive to C, N, and O, compared to heavier elements, such that the C, N, and O percentages reported here represent lower limits (Laskin et al., 2006). Particle types present were determined by k-means clustering of the EDX spectra using a previously established method (Ault et al., 2012).
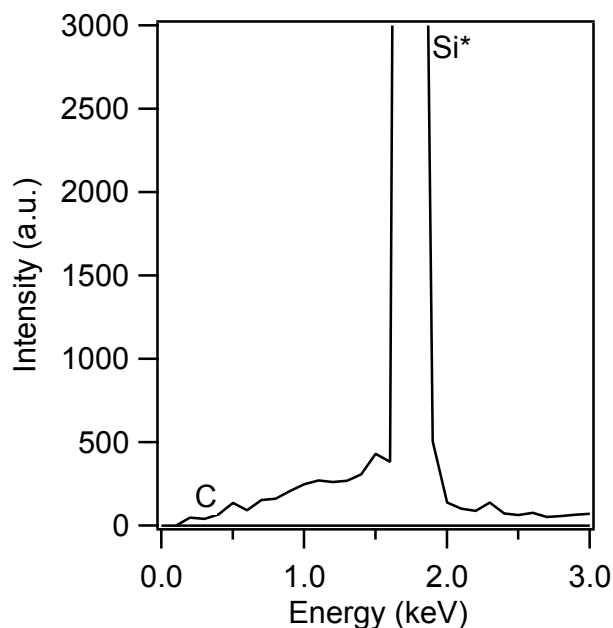
Figure 4.2 EDX spectrum of Si wafer background, showing no detectable contribution from carbon.

SEM images of particles collected on aluminum foil substrates were used to measure individual SSA particle coating to core ratios for 77 winter particles from January 24, 2014, as well as 82 summer SSA particles collected at the same sampling location on September 16, 2015 (Gunsch et al., 2017). SEM images of each sample were analyzed using ImageJ to determine the inorganic (bright core) and organic (dark coating) areas of each individual SSA particle (Fig. 4.3). The coating (primarily organic) to core (primarily inorganic) ratio was calculated by dividing the inorganic core area by the organic coating area.
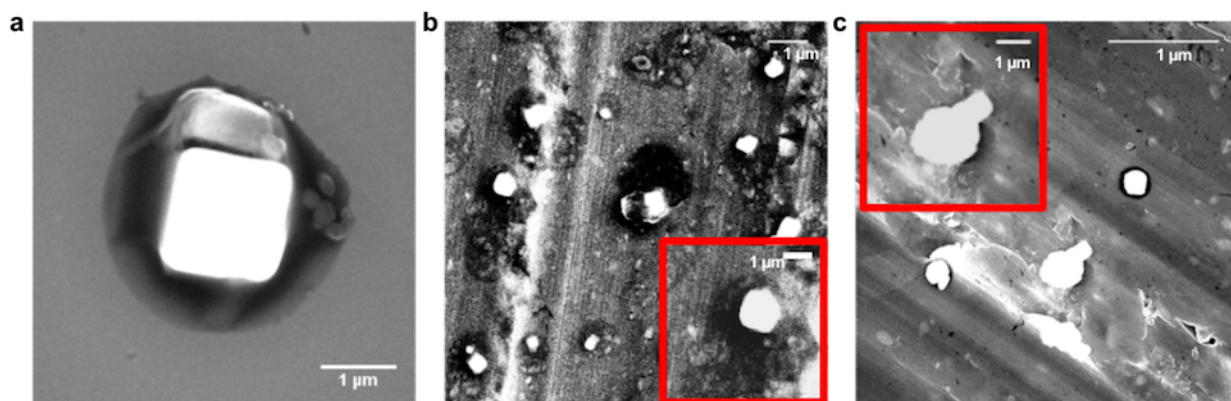
Figure 4.3 Representative SEM images of a) wintertime organic coated SSA particle on silicon, without outlines, and example b) wintertime, and c) summertime SSA particles on aluminum foil substrates, within insets highlighting representative particles.

Individual particles were analyzed by Raman microspectroscopy using a Horiba Scientific Labram HR Evolution spectrometer coupled with a confocal optical microscope (100x N.A. 0.9 Olympus objective), Nd:YAG laser (50 mW, 532 nm), and CCD detector using a 600 groove/mm diffraction grating. Individual particle Raman spectra were collected over the 550-4000 cm^{-1} range, with a spectral resolution of ~1.8 cm^{-1}, according to a previously established method (Craig et al., 2017). Raman spectra of 88 submicron (0.32-0.56 μm d_a stage) and 212 supermicron (1.0-1.8 μm d_a stage) sampled SSA particles, identified based on morphology using the optical microscope, were compared to Raman spectra of ~50 standard organic compounds (Table 4.2), including saccharides, short chain fatty acids, long chain fatty acids, and amino acids representative of species present in the marine SML (Cochran et al., 2017). Linear combinations of up to two model Raman spectra (e.g., 69 % galactose + 31 % succinic acid) were fit to ambient SSA Raman spectra following the method of Cochran et al. (2017). Therefore, each particle spectrum could match to up to two organic compound types, for example, sucrose + fucose (saccharide + saccharide) or galactose + succinic acid (saccharide + short-chain fatty acid). Model linear combinations and ambient SSA spectra were compared by calculating χ^2 values over the 800-1800 and 2600-3600 cm^{-1} ranges. This analysis provides a value between zero (spectra are identical) and one (spectra have no correlation). Particle spectra matching each organic compound type were characterized by unique peaks corresponding to specific organic functional groups in the 850-1650 and 2700-3500 cm^{-1} regions (Eom et al., 2016). Further discussion of peak assignments and χ^2 best fit analysis is included in Section 4.3.3. The organic compounds corresponding to the best χ^2 fit (smallest value) between model linear combinations and the ambient SSA spectrum are reported.

Table 4.2 List of standard compounds available for matching in the Raman spectra reference library (Cochran et al.).

Saccharides	Short chain fatty acids	Long chain fatty acids	Amino acids
Acetylnearuaminic acid	Adipic acid	Avanti Lipid A	Bovine Serum Albumin
Arabinose	Butyric acid	DPPA	Ethanolamine
Arabitol	Caproic acid	DPPC	Serine
Dextrin	Citric acid	Myristic acid	
Fucose	Malic acid	Hexadecanol	
Galactose	Decanoic acid	Hydroxymyristic acid	
Glucose	Docosanol	Lauric acid	
Inulin	Enanthic acid	Oleic acid	
Laminarin	Glutaric acid	Palmitic acid	
LPS	Hexanoic acid	Stearic acid	
Mannitol	Hydroxyhexanoic acid	Tridecanoic acid	
Rhamnose	Malonic acid	Triolein triglyceride	
Sialic acid	Nonanoic acid	Tripalmitin triglyceride	
Sucrose	Octanoic acid		
	Oxalic acid		
	Succinic acid		
	Valeric acid		

Individual particles from January 26 and February 26 – 27 samples were analyzed with the same Raman instrument for fluorescence analysis. Fluorescence spectra were collected from 540 – 600 nm with 0.1 s acquisitions over a 50 x 50 µm area with 0.5 step size to create fluorescence intensity maps of individual particles (May et al., 2018a).

STXM-NEXAFS analysis was conducted on approximately 150 particles total from the 1.0-1.8 and 0.32-0.56 µm size ranges from two periods (January 26 11:00-17:15 AKST and February 26-27 19:45-8:30 AKST). Beamline 5.3.2.2 at the Advanced Light Source at Lawrence

Berkeley National Laboratory (Berkeley, CA) was used for STXM-NEXAFS analysis in a He filled chamber (~200 torr) of individual particles over the carbon K-edge (278-320 eV), following the method of Moffet et al. (2010). The pre- and post-edge optical densities at the carbon K-edge were used to determine the inorganic and organic portions of particles (Moffet et al., 2010a). X-ray absorption at 288.6 eV, corresponding to the –COOH functional group, served as an indicator of organic carbon (Moffet et al., 2010a). The thickness of inorganic (NaCl) and organic portions were determined using the optical densities, calculated atomic cross sections for organic (adipic acid) and inorganic (sodium chloride) components, and assumed densities (ρ_{OC}=1.35 g/cm^3, ρ_{NaCl}=2.16 g/cm^3) (Collins et al., 2013). The organic volume fraction for each particle was calculated as the thickness of the organic portion over the total thickness of organic and inorganic portions (Collins et al., 2013; Pham et al., 2017).

Organic coating thicknesses for submicron and supermicron particles were determined using average organic volume fractions of 0.45 based on STXM-NEXAFS analysis. The median aerodynamic diameter for the submicron (440 nm) and supermicron (1400 nm) particle size ranges collected were used to determine the total volume of a representative submicron and supermicron particle, assuming the particles (both core and shell) to be spherical. The inorganic volume was then determined, in order to calculate the organic coating thickness (difference between total volume and inorganic volume). A coating thickness of 9 %, or 130 nm for a supermicron (1400 nm d_a) particle and 40 nm for a submicron (440 nm d_a) particle, was determined for particles with 0.45 organic volume fractions. Atomic force microscopy was used to measure the degree of spreading for the winter SSA and showed an average spreading ratio (height/radius) of 2.3 ± 0.6. However, both the inorganic and organic components spread similarly, with spreading ratios for just the inorganic cores averaging 2.7 ± 0.6. Estimating the coating thickness with AFM using these measurements gave similar results to the estimations using STXM-NEXAFS organic volume fraction data.

Surface (top 6 cm) snow samples were collected near the aerosol sampling site at the beginning of each sample period and over first year sea ice (15 km from the sampling site, ~ 3 km from open leads) on February 27, 2014. Samples were double-bagged in Whirl-pak low-density polyethylene bags and kept frozen at -40 °C. Immediately prior to analysis by ion chromatography, samples were placed in a refrigerator at ~6 °C to melt. Snow melt water was sampled into 200 μL sample injection loops with 1 mL syringes equipped with 0.22 μM PVDF filters. The ICS-1100

and ICS-2100 ion chromatographs were each equipped with a guard column (ICS-1100: CG12A-5 µm (3 x 30 mm) IonPac; ICS-2100: AG18 4 mm (4 x 50 mm), Dionex), analytical column (ICS-1100: CS12A-5 µm (3 x 150 mm) IonPac; ICS-2100: AS18 4 mm (4 x 250 mm), IonPac), suppressor (ICS-110: CSRS 500 (4 mm), ICS-2100: AERS 500 (4 mm), Dionex), and a heated conductivity cell (DS6, Dionex). Methanesulfonic acid (20 mM) was used as eluent for the cation column, and a KOH gradient generated by an EGC III KOH system was used as eluent for the anion column. All samples were run in triplicate, with average values and standard deviations reported herein. Limits of detection for the measured inorganic ions were 2.35 µM (Na^+), 0.18 µM (NH_4^+), 0.15 µM (Ca^{2+}), 0.12 µM (Mg^{2+}), 0.087 µM (K^+), 0.94 µM (Cl^-), 0.25 µM (NO_2^-), 0.32 µM (SO_4^{2-}), 0.025 µM (Br^-), and 0.11 µM (NO_3^-).

4.3 Results and Discussion

4.3.1 SSA Production from Open Leads

A total of 1691 individual particles (0.32 – 0.56 and 1.0 – 1.8 µm aerodynamic diameter, d_a) from six sample periods (January 24 – 27 and February 26 – 27, 2014) were analyzed by computer-controlled scanning electron microscopy with energy dispersive X-ray spectroscopy (CCSEM-EDX) to determine individual particle morphology and elemental composition. Nearly all (86 % submicron and > 99 % supermicron particles, by number) of the collected particles were identified as SSA (Fig. 4.4), consistent with our previous measurements during this study (Kirpes et al., 2018). For the samples herein, 75 %, by number, of SSA were classified as nascent, based on the presence of Na and Cl in ratios similar to seawater (Kirpes et al., 2018). An additional 25 %, by number, of the SSA were classified as partially-aged based on the simultaneous enrichment of S and/or N and depletion of Cl, relative to seawater, and consistent with long-range transport (Kirpes et al., 2018). Given local Arctic production of nascent SSA (May et al., 2016b). the sources and composition of the nascent SSA are the focus of this study.
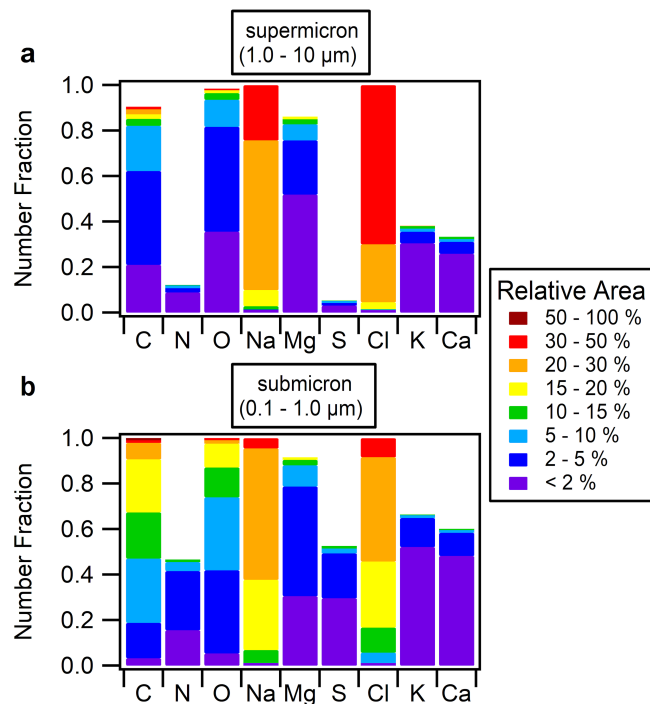
Figure 4.4 Digital color histograms showing the number fraction of spectra (particles) containing each element (bar height) at each EDX signal intensity range (color scale) for supermicron (a) and submicron (b) SSA particles. Al and Si are excluded due to interferences from the sample holder and substrate, respectively.

SSA production from open leads (Fig. 4.5) is supported by the presence of nearby open leads on all sampling days; the closest upwind leads were within 4 h of atmospheric transport time to the sampling site, according to satellite and local sea ice imagery, combined with backward air mass trajectories (Fig. 4.6, 4.7). In recent years, open leads have persisted throughout the winter near Utqiaġvik (Beitsch et al., 2014; Hirano et al., 2018; Johnson and Eicken, 2016; May et al., 2016b; Wernecke and Kaleschke, 2015). Consistent with lead-based SSA production at elevated wind speeds (> 4 m s^{-1}) (Leck et al., 2002; May et al., 2016b; Nilsson et al., 2001; Scott and Levin, 1972), all samples were collected during periods of wind speeds greater than or equal to 4 m s^{-1} (average wind speeds of 6 – 12 m s^{-1}), and four samples were collected during sustained periods of high wind speeds (6 – 17 m s^{-1}) (Table 4.1). While nascent SSA were observed in all samples, the samples with the greatest number fractions of nascent SSA relative to partially aged SSA had the greatest near-surface (< 70 m above sea level) air mass transport over the ice-fractured Arctic Ocean (Kirpes et al., 2018). All samples had air mass back trajectories influenced by the central Arctic Ocean, as shown in previous work (Kirpes et al., 2018). Average elemental mole ratios of Mg/Na, S/Na, and Cl/Na for individual SSA particles were similar to seawater ratios (Fig. 4.6,

Table 4.3) (Pilson, 2013). These elemental ratios have been observed previously for laboratory-generated SSA (Ault et al., 2013c) and are consistent with aerosol production from the nearby open leads (Leck et al., 2002; May et al., 2016b). Based on the low concentrations of sulfur- and nitrogen-containing trace gases in the winter Arctic (Sander and Bottenheim, 2012), nascent SSA in the sub- and supermicron size ranges could be transported from these leads with little influence from multiphase aging reactions altering particle chemical composition.
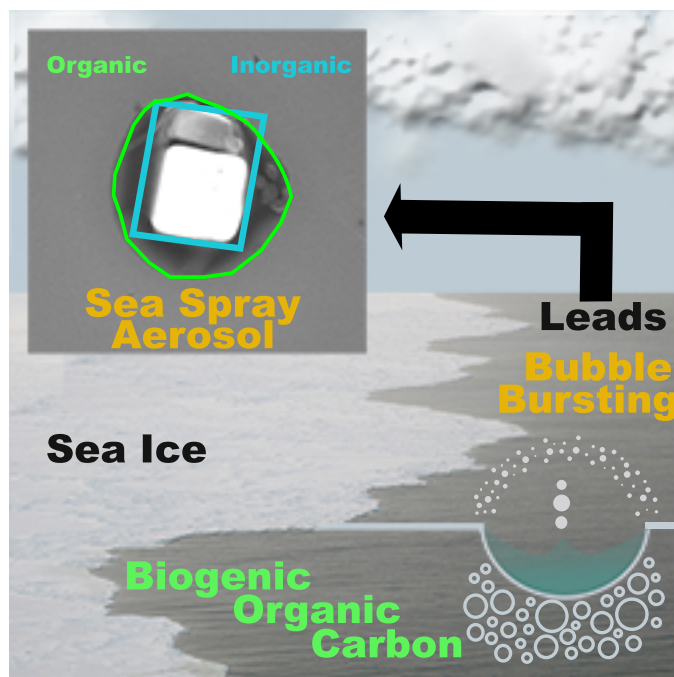
Figure 4.5 Sea spray aerosol generation from open sea ice leads. Sea spray aerosol is produced via bubble bursting from open leads, resulting in individual atmospheric particles containing inorganic salts coated by organic material originating from biogenic organic matter present in the seawater surface microlayer, likely from sea ice algae, bacteria, and phytoplankton.
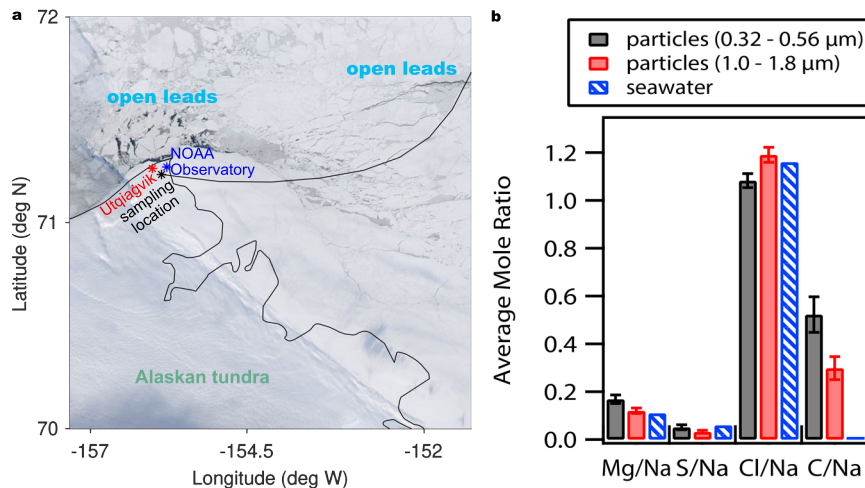
Figure 4.6 Observations of open leads and wintertime SSA composition. a) MODIS satellite imagery from February 26, 2014 (NASA Worldview) shows open leads near Utqiaġvik, Alaska. Locations of the town, NOAA Observatory, and aerosol sampling location are shown. The black line shows 8 h of a NOAA HYSPLIT backward air mass trajectory (February 26, 2014 20:00 AKST; 50 m altitude at the sampling site) passing over the closest open leads before arriving at the site. The air mass traveled ~ 60 km from open leads to the northeast. b) CCSEM-EDX average individual SSA particle elemental mole ratios compared to literature values for seawater (Pilson, 2013). Error bars denote 95 % confidence intervals.
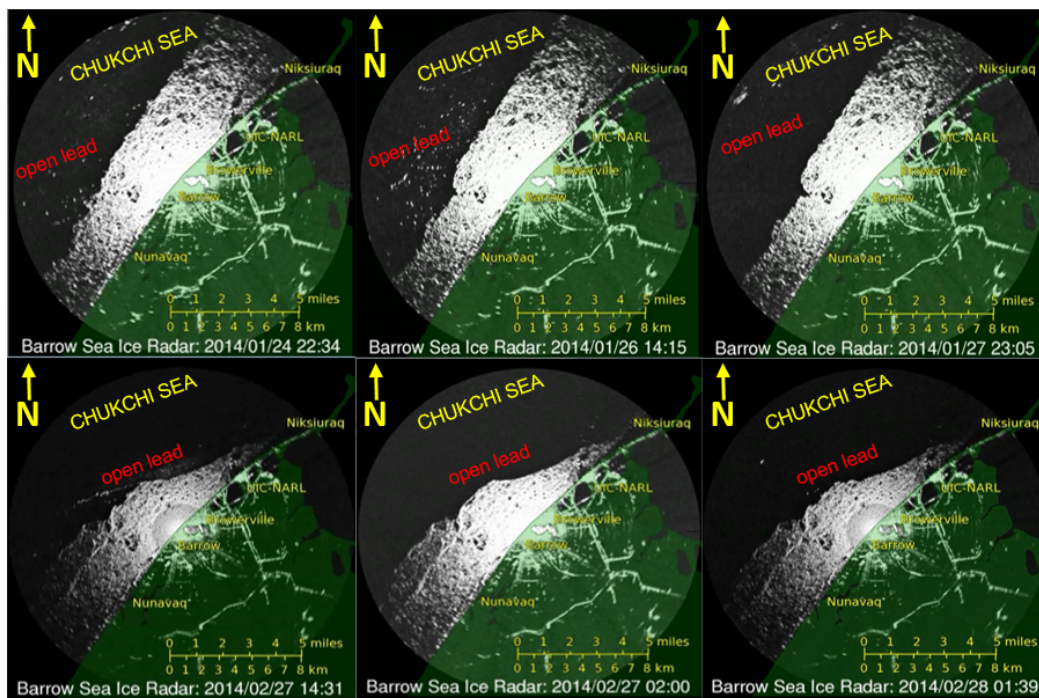
Figure 4.7 Representative Utqiaġvik (Barrow) coastal radar images showing the open lead present during each aerosol sampling period. The green region indicates land extent, and the white regions are sea ice. The lead was open for the duration of all samples. Images were obtained from the University of Alaska, Fairbanks Sea Ice group (http://seaice.alaska.edu/gi/data/barrow_radar).

At high wind speeds, blowing snow and frost flowers have also been hypothesized to result in lofted SSA (Douglas et al., 2012; Jacobi et al., 2012). However, particles produced by aerosolization of blowing snow or frost flowers can be distinguished from nascent SSA based on chemical composition, characterized by S/Na depletion (blowing snow and frost flowers) and Mg/Na enrichment (blowing snow) compared to seawater (Table 4.3) (Douglas et al., 2012; Jacobi et al., 2012). Notably, during this study, there was no dependence of individual SSA S/Na or Mg/Na mole ratios on wind speed (Fig. 4.8), a trend which would be expected for a wind-dependent blowing snow or frost flower source. Further, sub- and supermicron SSA elemental ratios are not consistent with simultaneously measured tundra and sea ice surface snow or previous measurements of blowing snow and frost flowers (Douglas et al., 2012; Jacobi et al., 2012), making them unlikely sources. Recent work has also determined frost flowers to be unlikely to produce aerosol under high wind conditions (Roscoe et al., 2011; Yang et al., 2017). While supermicron SSA Ca/Na and Mg/Na ratios were similar to seawater, submicron SSA were more enriched in calcium and magnesium than both seawater and surface snow, as shown in Fig. 4.6. Calcium and magnesium enrichment in submicron SSA is also suggestive of the presence of EPS as assembled gels bound by divalent cations (Ca^{2+}; Mg^{2+}) (Jayarathne et al., 2016; Orellana and Leck, 2014). Therefore, the nascent SSA observed is consistent with SSA production from local open sea ice leads, as we previously observed through multi-year bulk aerosol measurements at Utqiaġvik from fall – spring (May et al., 2016b). Our observation herein further highlights the year-round nature of SSA emissions in the Alaskan Arctic from open water, including leads.

In addition to the comparison of SSA particle average elemental ratios and seawater ratios shown in Fig. 4.6, CCSEM-EDX particle composition was also compared to ratios, determined by IC, for surface snow collected during the sampling study (Table 4.3). Comparisons were also made to blowing snow and frost flower composition, determined previously near Utqiaġvik (Douglas et al., 2012; Jacobi et al., 2012). Average mole ratios measured for surface snow (top 6 cm) collected on February 27 at 11:00 AKST for Mg^{2+}/Na^+ and SO_4^-/Na^+ were compared to seawater ratios (Pilson, 2013) (Table 4.3), as blowing snow near Utqiaġvik, AK has been previously characterized by sulfate depletion and magnesium enrichment compared to seawater (Jacobi et al., 2012). Similarly, frost flowers are also characterized by sulfate depletion compared to seawater (Douglas et al., 2012); however, recent studies have shown frost flowers are not a likely source of SSA (Yang et al., 2017). Previous studies of frost flower composition determined ion ratios for

Mg^{2+}/Na^+, SO_4^{2-}/Na^+, and Cl^-/Na^+ (Douglas et al., 2012). Supermicron SSA particles had composition close to seawater ratios (Table 4.3). These supermicron SSA particles were slightly depleted in S compared to seawater and surface snow composition, but not depleted to the levels previously observed for blowing snow or frost flowers (Douglas et al., 2012; Jacobi et al., 2012). Further, supermicron SSA had Mg/Na ratios most similar to seawater. While the submicron SSA showed slight Mg enrichment above the seawater ratio, submicron S/Na ratios were similar to seawater and did not show sulfate depletion expected for frost flowers or blowing snow (Douglas et al., 2012; Jacobi et al., 2012), or when compared to measured sea ice surface snow and tundra snow (Table 4.3). Average SSA Cl/Na ratios for both sub- and supermicron particles were also closer to seawater than frost flower composition and local tundra and sea ice surface snow composition (Table 4.3). Surface snow measured in this study was enriched in calcium. While submicron SSA particles showed enhancement in calcium, with an average, supermicron particles had an average Ca/Na ratio similar to the seawater ratio. The presence of mineral dust in snow could influence snow composition, however, mineral dust and fly ash comprised less than 1 % of the observed aerosol, by number, during this sampling period, and no supermicron dust was observed (Kirpes et al., 2018). Overall, SSA particle composition was close to seawater and did not consistently exhibit trends expected for blowing snow or frost flower sources for all elements or across size ranges. Therefore, the observed individual SSA composition is consistent with SSA production from open leads rather than production from blowing snow or frost flowers.

Table 4.3 SSA particle composition and snow composition. Snow, frost flower, and seawater ion ratios and aerosol particle elemental ratios and 95 % confidence intervals.

Sample Type	Mg^{2+}/Na^+ Or Mg/Na Mole Ratio	SO_4^{2-}/Na^+ Or S/Na Mole Ratio	Cl^-/Na^+ Or Cl/Na Mole Ratio	Ca^{2+}/Na^+ Or Ca/Na Mole Ratio	Reference
Submicron SSA (average)	0.17 ± 0.02	0.05 ± 0.01	1.08 ± 0.03	0.085 ± 0.007	
Supermicron SSA (average)	0.12 ± 0.01	0.0330 ± 0.0006	1.19 ± 0.03	0.031 ± 0.004	
Seawater	0.11	0.06	1.16	0.022	Pilson, 2013
Sea ice surface snow	0.12784 ± 0.00002	0.0360 ± 0.0001	1.223 ± 0.001	0.07030 ± 0.00004	
Tundra surface snow	0.13 ± 0.09	0.061 ± 0.05	1.1 ± 0.8	0.06 ± 0.05	
Frost flowers	0.135 ± 0.005	0.016 ± 0.003	1.30 ± 0.03	$0.0216 \pm .0009$	Douglas et al., 2012
Blowing snow	0.2 ± 0.1	0.02 ± 0.01	$1.2 \pm .9$	0.05 ± 0.03	Jacobi et al., 2012

Previous work hypothesized a frost flower source for carbohydrate signatures detected in bulk winter – spring ambient aerosol samples at Utqiaġvik, AK under high wind and oceanic influence (Shaw et al., 2010). However, more recent work has shown frost flowers do not fracture to produce aerosol (Roscoe et al., 2011; Yang et al., 2017). In addition, our previous multiyear study examining sea salt aerosol (bulk aerosol IC measurements) as a function of wind speed and sea ice conditions showed SSA production during elevated wind speeds and lead/open water influence, without the presence of fresh supermicron SSA when leads/open water were not present, consistent with a lead/open water-based SSA source, rather than blowing snow (May et al., 2016b). As described above, our individual SSA chemical composition results also support lead-based SSA production, rather than blowing snow or frost flower aerosol production.
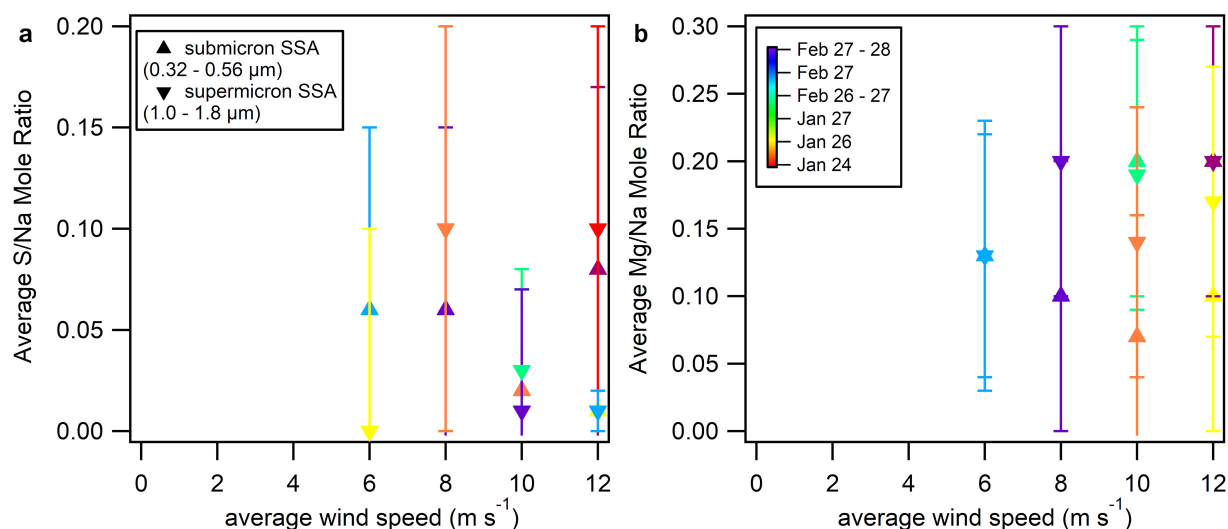
Figure 4.8 Average a) S/Na and b) Mg/Na mole ratios for submicron and supermicron SSA particles compared to wind speeds during each of the six winter sample periods. Error bars denote 95 % confidence intervals.

4.3.2 Abundance of Organic Material in SSA

Carbon was observed in over 98 % of the nascent SSA particles, by number, and was typically observed as a coating on the salt particles (Fig. 4.9). Individual SSA with similar morphology and organic coatings were previously observed during spring in the Norwegian Sea (Hawkins and Russell, 2010). Previous bulk aerosol measurements at Utqiaġvik also showed organic mass to be correlated with sea salt during winter (Shaw et al., 2010). We demonstrate through single-particle analyses that these organics are present as sea salt coatings. The individual

nascent SSA particles contained substantial amounts of carbon (average 15 ± 8 atomic % C and 6 ± 5 atomic % C for submicron and supermicron SSA, respectively), with significant carbon

enrichment relative to seawater (C/Na ratio 0.30 ± 0.05 and 0.52 ± 0.07 for submicron and supermicron SSA, respectively, compared to 0.01 for seawater) (Fig. 4.6) (Pilson, 2013). Significant supermicron SSA C/Na enrichments (0.83 ± 0.33) have also previously been observed in the Antarctic during winter (Eom et al., 2016). Analysis of 150 SSA particles by scanning transmission X-ray microscopy with near edge X-ray absorption fine structure spectroscopy (STXM-NEXAFS) showed over 90 %, by number, contained organic carbon (detected as the -COOH functional group), consistent with the CCSEM-EDX results (Table 4.4). Notably, no organic gel-like particles (Orellana et al., 2011) without inorganic salts were observed. For all particles measured here (>100 nm), all submicron organic carbon was either coating SSA particles (Fig. 4.4, 4.10), consistent with mid-latitude SSA studies (Ault et al., 2013c), or internally mixed with anthropogenic secondary sulfate (Kirpes et al., 2018). Given the calcium enrichment in the wintertime submicron SSA and thick organic coatings, these results are consistent with assembled gel coatings surrounding inorganic sea salt cores.

Table 4.4 STXM-NEXAFS number fractions of individual SSA particles containing organics, as well as individual SSA particle organic volume fractions, for the four analyzed samples.

Sample timing (AKST) and aerodynamic diameter range	Number Fraction of SSA containing organics	Average SSA organic volume fraction	# of particles analyzed
Jan 26 11:00-17:15 (1.0-1.8 µm)	0.88 ± 0.08	0.41 ± 0.04	16
Jan 26 11:00-17:15 (0.32-0.56 µm)	1.00	0.5 ± 0.1	13
Feb 26-27 19:45-8:30 (1.0-1.8 µm)	1.00	0.44 ± 0.08	21
Feb 26-27 19:45-8:30 (0.32-0.56 µm)	0.98 ± 0.01	0.4 ± 0.2	103
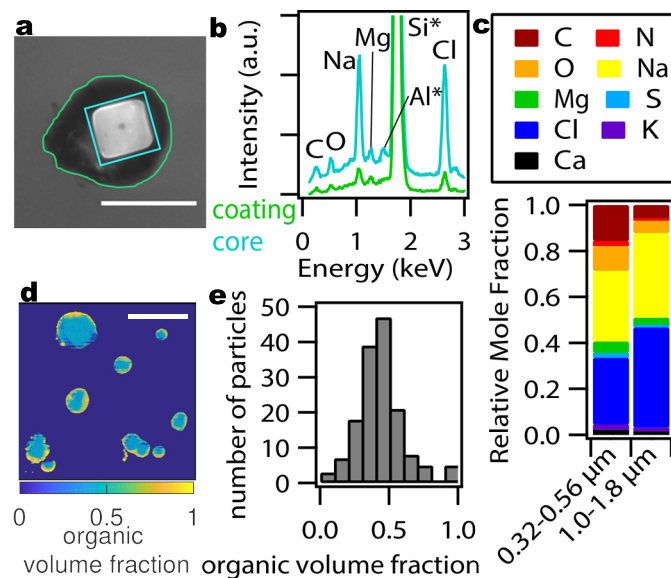
Figure 4.9 Organic coatings observed on wintertime sea spray aerosol (SSA) particles. a) SEM image with a 3 μm scale bar shown and b) EDX spectra of a representative SSA particle with a cubic salt core (blue) and organic coating (green). *Al and Si signal contributions are from the sample holder and substrate, respectively. c) Average relative elemental (mole) fractions for all submicron and supermicron nascent SSA particles (CCSEM-EDX). d) Representative STXM-NEXAFS image showing organic volume fraction spatial distribution within individual SSA particles, with a 5 μm scale bar shown. e) Histogram of 150 individual SSA particle organic volume fractions (STXM-NEXAFS).
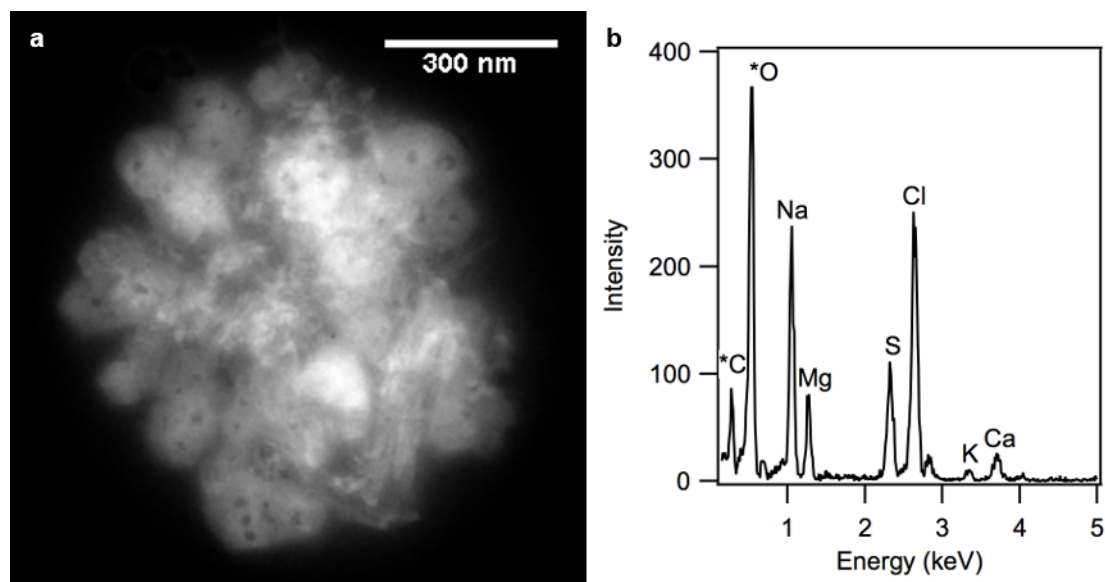
Figure 4.10 TEM image and EDX spectrum of a representative submicron wintertime SSA particle from January 26, containing both inorganic and organic components. *C and O signals include some influence from the TEM grid substrate film.

The average individual SSA organic volume fractions for each sample ranged from 0.41 – 0.47 (Table 4.4), with little variation across the time periods and particle size ranges analyzed. As shown in Fig. 4.9, the majority of SSA particles (71 %, by number) had organic volume fractions between 0.3 and 0.5, consistent with organic volume fractions (0.2– 0.5) observed for SSA produced in mid-latitude algal bloom mesocosm experiments (Collins et al., 2013; Pham et al., 2017). Notably, 26 % of the SSA particles analyzed by STXM-NEXAFS had organic volume fractions of 0.5 or greater. Particles with lower organic volume fractions (< 0.2) were inorganic salts with thin organic coatings; whereas particles with higher organic volume fractions (> 0.2) had thick organic coatings around inorganic salt cores (Fig. 4.9). Based on the average individual SSA particle measured organic volume fraction of 0.45, the average coating thickness was calculated to be ~0.04 μm and ~0.13 μm for the median submicron (0.44 μm) and supermicron (1.4 μm) particle aerodynamic diameters analyzed, respectively.

For comparison to the wintertime SSA described herein, SSA were also collected at the same site near Utqiaġvik during September 2015, when the nearest sea ice was > 400 km upwind. Meteorological conditions, including wind speeds, were similar during the winter (Table 4.1) and summer (Gunsch et al., 2017) studies. To compare the enrichment of organics in SSA between winter and summer, individual SSA particle carbon/sodium (C/Na) ratios were determined by SEM-EDX for ~150 particles. Overall, the winter SSA particles had statistically greater C/Na ratios (range 0.2 – 1.2; median 0.6) compared to the summer SSA particles (range 0.1 – 0.3; median 0.2) (Fig. 4.11). The higher carbon content observed in the winter SSA is consistent with the measured ratios of organic coating thickness relative to the salt core diameter, as determined by SEM-EDX, which showed statistically thicker coatings for winter compared to the summer SSA particles (Fig. 4.11). The coating thickness to salt core diameter analysis of the winter SSA is in agreement with the thick organic coatings observed by STXM-NEXAFS (Fig. 4.9). 78 %, of winter SSA particles had coating to core ratios greater than 0.4, compared to the summer SSA samples, which showed 57 %, by number, to have coating to core ratios of 0.1 or less (Fig. 4.11). Together these measurements show that the organic coatings of winter SSA particles sampled near Utqiaġvik, Alaska were much thicker than the organic coatings on the summer SSA particles, indicating an important unique source of SSA organic content during winter. This is consistent with previous work, showing through bulk measurements that organic mass was higher in the winter near Utqiaġvik and correlated with sea salt aerosol (Shaw et al., 2010). Given the lack of

nearby sea ice in the summer near Utqiaġvik, we suggest that sea ice algae, bacteria, and phytoplankton contribute to the thick SSA organic coatings observed in winter when these microorganisms use EPS in great quantities as a cryoprotectant (Boetius et al., 2015; Krembs et al., 2002; Leu et al., 2015; Mayot et al., 2018; Vernet et al., 1998). Therefore, the molecular composition of the winter SSA organic content was investigated to probe this hypothesis.
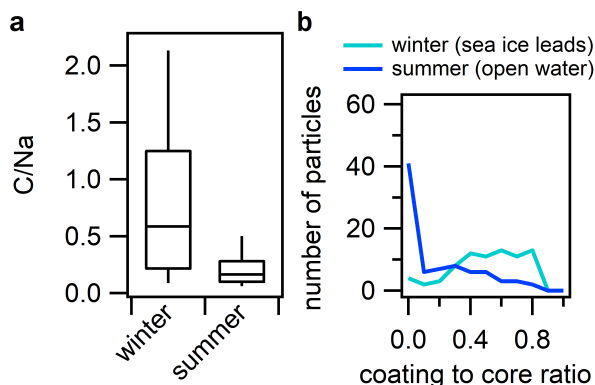
Figure 4.11 Comparison of SSA organic coatings observed in winter and summer. a) Box and whisker plot (90th/10th percentiles,75th/25th percentiles, and medians) of C/Na ratios determined for individual SSA particles in winter and summer. C/Na distributions for winter and summer SSA were significantly different (Kolmogorov-Smirnov test, $p = 2.0010 \times 10^{-27}$). b) Histogram of measured organic coating to salt core diameter ratios determined from SEM images for winter (77 particles) and summer (82 particles). SSA on aluminum foil substrates. A two-sample Kolmogorov-Smirnov test showed that the two distributions were not from the same underlying population ($p = 5.28 \times 10^{-14}$).

4.3.3 Molecular Characterization of SSA Organic Content

To determine the chemical composition of the SSA organic coatings, 88 submicron and 212 supermicron individual SSA particles were analyzed with Raman microspectroscopy. Similar organic composition was observed for the sub- and supermicron SSA particles. The organic compound classes present included saccharides (monosaccharides, polysaccharides, and lipopolysaccharides), short-chain fatty acids (and dicarboxylic acids), long-chain fatty acids (and lipids and phospholipids), and amino acids, with representative individual SSA spectra shown in Fig. 4.12. Raman peak assignments and χ^2 fitting with SML standards are given in Table 4.5 and Fig. 4.13 (Cochran et al., 2017). Fluorescence microscopy confirmed the presence of fluorescing biological organic material (Fu et al., 2015) in the individual wintertime SSA particles (Fig. 4.14).
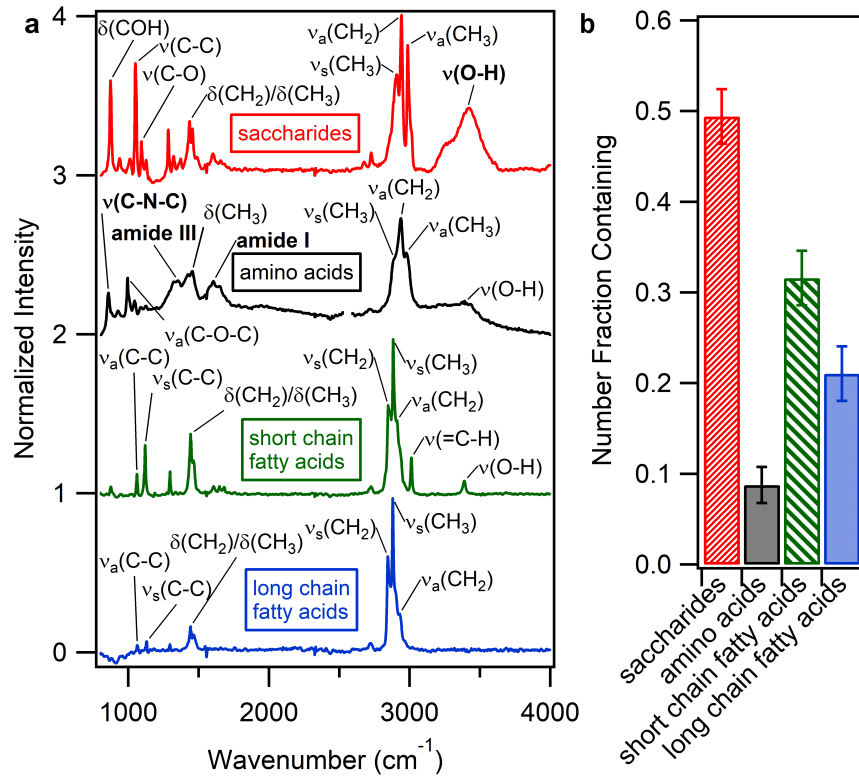
Figure 4.12 Marine-derived organic compound types observed in individual wintertime SSA particles. a) Raman spectra of four representative individual SSA particles matching marine-derived saccharides ($\chi^2 = 0.013$), amino acids ($\chi^2 = 0.011$), short chain fatty acids ($\chi^2 = 0.003$), and long chain fatty acids ($\chi^2 = 0.0005$), respectively. b) Number fractions (and associated standard errors) of 300 individual SSA particles containing saccharides, amino acids, short chain fatty acids, and/or long chain fatty acids. Each SSA particle Raman spectrum was allowed to be fit to up to two organic compound types, following the method of Cochran et al. (2017).

73
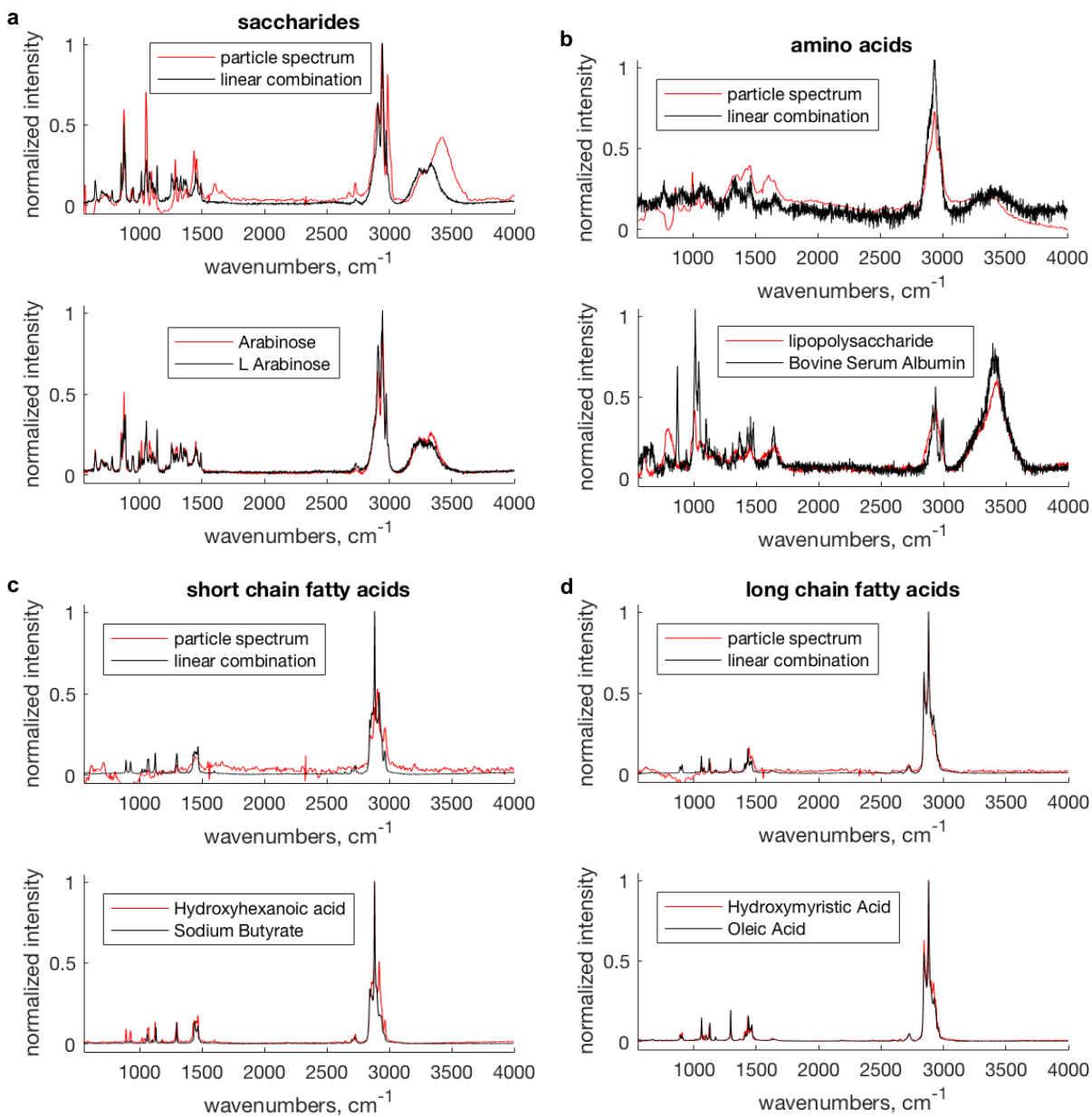
Figure 4.13 Linear combinations and χ^2 fits of representative SSA particle Raman spectra shown in Fig. 4.12.
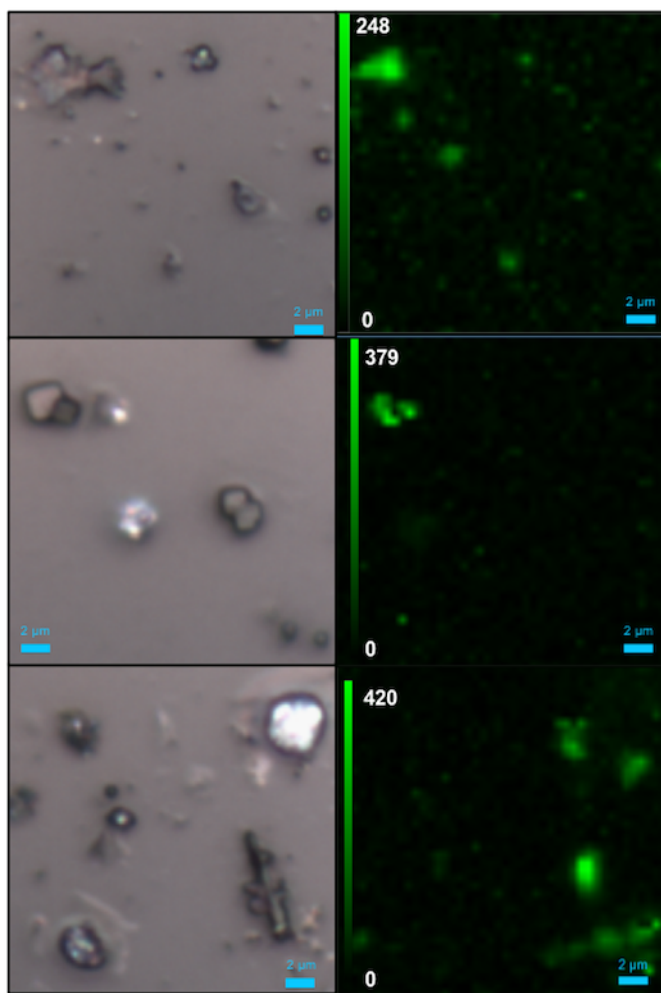
Figure 4.14 Representative optical images (left) and fluorescence maps (right), showing the fluorescence intensity counts (color scale) of individual SSA particles from February 26, 2014.

Figure 4.12 shows Raman spectra of representative individual particles for each organic class, based on comparisons to standard spectra (Table 4.2). The standard model spectra within each organic type (e.g. all saccharides) were similar, exhibiting Raman peaks for the same functional groups; therefore, ambient SSA spectra are classified by general organic types (saccharides, short chain fatty acids, long chain fatty acids, amino acids). The ambient SSA particle spectrum representative of saccharides (arabinose, $\chi^2 = 0.01$) had characteristic peaks at 1014, 1050, and 1095 cm^{-1}, corresponding to ν(C-C) and ν(C-O) and a peak at 1127 cm^{-1} corresponding to ν_s(C-C) (Cochran et al., 2017; De Gelder et al., 2007). A peak corresponding to δ(CH$_2$/CH$_3$) was observed at 1436 cm^{-1} (10, 11). ν_s(CH$_3$) and ν_a(CH$_2$) peaks were observed at 2906 and 2942 cm^{-1}, respectively (Ault et al., 2013b; Deng et al., 2014). ν(O-H) stretching peaks were observed at 3250 and 3410 cm^{-1}, likely due to particulate water (Fig. 4.12, Table 4.5) (Ault et al., 2013b;

Deng et al., 2014; Frost et al., 2005; Xiao et al., 2008). The SSA particle spectrum representative of short chain fatty acids (hydroxyhexanoic acid+butyric acid, $\chi^2 = 0.003$) had peaks at 1062 and 1121 cm^{-1} corresponding to ν_a(C-C) and ν_s(C-C), 1297 and 1444 cm^{-1} for δ(CH$_2$) and δ(CH$_3$) peaks, and 2847, 2883, and 2910 cm^{-1} characteristic of ν_s(CH$_2$), ν_s(CH$_3$), and ν_a(CH$_2$), respectively, in addition to a ν(O-H) stretching peak at 3389 cm^{-1} (Fig. 4.12, Table 4.5) (Ault et al., 2013b; Deng et al., 2014; De Gelder et al., 2007; Jentzsch et al., 2013; De Villepin et al., 1982). The particle spectrum representative of long chain fatty acids (hydroxymyristic acid+oleic acid, $\chi^2 = 0.0005$) had characteristic peaks at 1065 and 1130 cm^{-1} corresponding to ν_a(C-C) and ν_s(C-C and at 1296 cm^{-1} corresponding to δ(CH$_2$), in addition to δ(CH$_2$)/ δ(CH$_3$) modes at 1444 cm^{-1} (Ault et al., 2013b; Deng et al., 2014; Mertes et al., 2004). Peaks at 2844, 2880, and 2930 cm^{-1} correspond to ν_s(CH$_2$), ν_s(CH$_3$), and ν_a(CH$_2$), respectively (Fig.4.12, Table 4.5) (Ault et al., 2013b; Deng et al., 2014). The particle spectrum representative of amino acids and saccharides (lipopolysaccharide+bovine serum albumin, $\chi^2 = 0.016$) had characteristic peaks at 858 cm^{-1} corresponding to ν(C-N-C) amino, ν_a(C-O-C) and ν(C-C) peaks at 996 and 1045 cm^{-1}, respectively, 1353 cm^{-1} for an amide III peak, 1455 cm^{-1} corresponding to δ(CH$_3$) and 1606 cm^{-1} for an amide I peak (Cochran et al., 2017; De Gelder et al., 2007; Mertes et al., 2004). ν_s(CH$_3$) and ν_a(CH$_2$) peaks were observed at 2890 and 2938 cm^{-1}, respectively, in addition to a ν_a(CH$_3$) peak at 2976 cm^{-1} and ν(O-H) at 3391 cm^{-1} (Fig. 4.11, Table 4.5) (De Gelder et al., 2007; Jentzsch et al., 2013; McLaughlin et al., 2002; Xiao et al., 2008). There was no detectable ν(N-H) peak in the spectrum representative of amino acids and saccharides, likely due to the low abundance of amino acids and the weak polarizability of N-H moieties making identification by Raman difficult (Larkin, 2011). A fraction of particle Raman spectra (19 %, by number) did not match any standard organic compounds due to fluorescence, burning, or low organic signal during Raman analysis (χ^2 value < 0.05 and/or spectral signatures of fluorescence/burning).

Table 4.5 Peak assignments for vibrational modes and associated intensities (strong (s), medium (m), weak (w)) observed in individual SSA particle Raman spectra.

Observed Peak	Peak Intensity	Raman Mode	Literature Peak Position	Reference
858	m	ν(CNC) amino	853	De Gelder et al., 2007
873, 877	m	δ(COH)	861	Cochran et al., 2017
927, 939	w			
996	m	ν_a(C-O-C)	991	Cochran et al., 2017
1014	w	ν(C-C), ν(C-O)	1009	Cochran et al., 2017
1045, 1050	s	ν(C-C)	1044	Cochran et al., 2017
1062, 1065	w	ν_a(C-C)	1063	De Gelder et al., 2007
1095	m	ν(C-O)	1095	De Gelder et al., 2007
1121, 1127, 1130	m	ν_s(C-C)	1128	De Gelder et al., 2007
1285	m			
1296, 1297	w	δ(CH$_2$)	1296	De Gelder et al., 2007
1323	w			
1353	w	Amide III	1351	De Gelder et al., 2007
1372	w			
1436, 1444	m	δ(CH$_2$)/δ(CH$_3$)	1440	Ault et al., 2013b Mertes et al., 2004
1455	w	δ(CH$_3$)	1459	McLaughlin et al., 2002 Cochran et al., 2017
1601				
1606	w	Amide I	1596	De Gelder et al., 2007
2723, 2725, 2727	w	overtone	2723, 2724	Cochran et al., 2017

2844, 2847	s	$\nu_s(CH_2)$	2850	Ault et al., 2013b Deng et al., 2014
2880, 2883, 2890, 2906	s	$\nu_s(CH_3)$	2870	Ault et al., 2013b Deng et al., 2014
2910, 2930, 2938, 2942	w	$\nu_a(CH_2)$	2930	Ault et al., 2013b Deng et al., 2014
2976	m	$\nu_a(CH_3)$	2974	McLaughlin et al., 2002
2986	s	$\nu_a(CH_3)$	2986	Larkin, 2011
3013	m	$\nu(=C\text{-}H)$	3005	Czamara et al., 2015
3389, 3391	w	$\nu(O\text{-}H)$	3402	Jentzsch et al., 2015
3410	s	$\nu(O\text{-}H)$	3430	Xiao et al., 2008

Saccharides and short-chain fatty acids were the most commonly observed marine biogenic organic compound classes present in the SSA particles, with 49 % of individual SSA particle Raman spectra containing at least one saccharide (Fig. 4.12). Saccharides observed, particularly xylose, fucose, and glucose, are major components of EPS (Gao et al., 2012; Hawkins and Russell, 2010; Orellana et al., 2011). The monosaccharides observed are similar to that of the SML, as well as bulk ambient aerosol and aerosols produced from laboratory bubbling experiments in the summer high Arctic pack ice (Gao et al., 2012; Leck et al., 2013). In prior studies during spring over the Norwegian Sea, individual SSA with organic coatings were characterized by STXM-NEXAFS as having a prominent carboxylic acid peak (as observed here), which was attributed to polysaccharides from the SML (Hawkins and Russell, 2010). Saccharides have also previously been observed in bulk Arctic aerosol samples during spring over the Norwegian Sea (Frossard et al., 2014; Russell et al., 2010), summer in the Canadian (Fu et al., 2013) and high (Leck et al., 2013) Arctic, and winter near Utqiaġvik (Shaw et al., 2010).

Similar to saccharides, long-chain fatty acids and amino acids were also commonly observed in the winter SSA coatings. 32 % of individual SSA particle Raman spectra contained at least one short-chain fatty acid, while long-chain fatty acids and amino acids were present in 21 % and 9 % of SSA particles, by number, respectively (Fig. 4.12). Amino acids and fatty acids have previously been observed in the SML in the summer high Arctic (Mashayekhy Rad et al., 2018;

Matrai et al., 2008) and in bulk ambient aerosols during spring – summer in the Canadian Arctic (Fu et al., 2009, 2013) and during spring – fall at Svalbard (Mashayekhy Rad et al., 2019; Scalabrin et al., 2012). Notably, all SSA particles containing amino acids also contained saccharides, and most particles (75 %, by number) containing one short chain fatty acid also contained a saccharide signature. Since saccharides, amino acids, and fatty acids are EPS components (Gao et al., 2012; Hawkins and Russell, 2010; Orellana et al., 2011), the presence of these compounds together in the individual SSA organic coatings is consistent with incorporation during the bubble bursting aerosol formation process due to enrichment in the SML of sea ice leads.

4.4 Conclusions

In this study, we identified abundant wintertime SSA thickly coated by marine biogenic organic carbon, with signatures consistent with EPS produced as a cryoprotectant by sea ice algae and bacteria. This study was conducted soon after polar sunrise, in line with recent unexpected evidence of sea ice biological activity under low light conditions in the Arctic (Hancke et al., 2018; Krembs et al., 2011; Lovejoy et al., 2007). The measured SSA chemical composition is consistent with Arctic lead-based aerosol production, illustrating the connections between sea ice fracturing, marine biological activity, EPS, and SSA production in the winter Arctic. This finding further highlights the year-round nature of Arctic SSA emissions. Open sea ice leads are identified as leading to organic enrichment in wintertime SSA. The Arctic is currently changing at an unprecedented rate (Haine and Martin, 2017), with winter warming events rapidly increasing (Graham et al., 2017). Resulting sea ice loss is expanding first year sea ice (Haine and Martin, 2017), which is prone to fracturing and expected to result in increasing SSA emissions (Struthers et al., 2011). Notably, delayed sea ice freeze-up in the Bering, Chukchi, Barents, and East Greenland Seas is dramatically decreasing sea ice extent in the region (Beitler, 2017) and increasing marine biological activity (Ardyna et al., 2014; Assmy et al., 2017; Krembs et al., 2011), impacting SSA emissions and organic content. SSA organic coatings can reduce reactivity toward trace gases, such as nitric acid, thereby impacting atmospheric composition (Ault et al., 2014) and Arctic haze formation (Law and Stohl, 2007). Organic coatings can also reduce SSA hygroscopicity (Cochran et al., 2017) and CCN efficiency (Collins et al., 2013) and may contribute to cloud ice nucleation (Wilson et al., 2015), which impacts cloud formation in the often CCN-limited Arctic (Mauritsen et al., 2011). Cloud-aerosol feedbacks are especially important in the Arctic winter when there is little to no direct solar radiation; clouds trap longwave radiation near

the surface and contribute to warming, with increasing sensitivity to clouds projected for the fall – winter (Graham et al., 2017; Walden et al., 2015). Therefore, additional studies are critical to quantify and upscale the details of, and connections between, changing Arctic microbiology, EPS production, SSA production, atmospheric composition, and cloud feedbacks in the winter.

4.5 Acknowledgments

Chapter 5.   Local Production of Primary Marine Aerosol under High Winds in the Summertime High Arctic

5.1 Introduction

The Arctic is drastically transforming due to climate change and associated rapidly declining sea ice extent (Haine and Martin, 2017). In fact, the summer Arctic is predicted to be ice-free by 2050 (Overland and Wang, 2013). The sea ice has transitioned from thick multiyear ice to majority younger, thinner first year ice, which is more prone to fracturing (Richter-Menge and Farrell, 2013). Sea ice fracturing results in the formation of leads, or areas of open water surrounded by sea ice (Richter-Menge and Farrell, 2013). Open leads provide a source of sea spray aerosol (SSA) in the otherwise ice-covered Arctic, and SSA emissions are expected to be increasing with declining sea ice (Struthers et al., 2011).

In open water, SSA is produced via entrainment of air during wavebreaking, forming bubbles which rise to the water surface and burst to emit droplets, evaporating to form aerosol particles (Quinn et al., 2015). In open leads, a wavebreaking mechanism for SSA production has been observed under high wind conditions (Leck et al., 2002; Nilsson et al., 2001; Scott and Levin, 1972), although the SSA flux from open leads is approximately 10 times less than in open water, due to the reduced fetch (Nilsson et al., 2001). SSA production from open leads has been observed year-round in the coastal Arctic (May et al., 2016b) and may be an underappreciated source of aerosol to the high Arctic (Leck et al., 2002), a region with few local aerosol sources. As SSA contributes the largest global aerosol flux to the troposphere (De Leeuw et al., 2011), understanding open water and lead-based SSA production is critical to predicting climate in the New Arctic.

SSA is composed of inorganic salts and organic material that is enriched in the seawater surface microlayer (SML) and scavenged as bubbles rise through the water column (Quinn et al., 2015). Bubble bursting at the water surface produces jet drops and film drops, which evaporate to form SSA (Quinn et al., 2015). SSA composition is size dependent, with supermicron particles, mainly from jet drops, primarily comprised of inorganic salts, while submicron particles, mainly

from film drops, can be greatly enriched in organics present in the SML (Quinn et al., 2014, 2015; Wang et al., 2015a). SSA composition is driven by marine biology contributing organic material to the SML (Quinn et al., 2014).

In the Arctic, marine biology is greatly influenced by sea ice algae and bacteria, which can form massive algal blooms underneath and at the edges of sea ice (Arrigo et al., 2012; Assmy et al., 2017; Hancke et al., 2018). These algae and bacteria produce exopolymeric substances (EPS) as a cryoprotectant (Boetius et al., 2015; Krembs et al., 2002). Therefore, sea ice algae and EPS secretions may particularly influence the organic material present within sea ice leads (Gao et al., 2012). EPS has been observed in the high Arctic SML within leads and in ambient aerosol (e.g. Gao et al., 2012; Leck et al., 2013).

SSA impacts climate directly by scattering incident radiation, and indirectly by participating in cloud formation, altering cloud properties (Andreae and Rosenfeld, 2008). The bubble-bursting mechanism results in a bimodal SSA size distribution, with a supermicron $\sim 1 - 2$ μm diameter mode acting as efficient cloud condensation nuclei (CCN) (Quinn et al., 2015) and a submicron $\sim 100 - 200$ nm mode, for which CCN efficiency is dependent on individual particle composition, particularly the amount and molecular composition of organics present (Cochran et al., 2017; Collins et al., 2013). SSA, dependent on composition, may also act as ice nucleating particles (INP) (DeMott et al., 2016; Wilson et al., 2015). Thus, given particle diversity, measurements of individual SSA particle composition are critical for predicting SSA climate effects (Quinn et al., 2015). SSA impacts on clouds may be particularly important in the high Arctic, a high-albedo environment where clouds greatly influence the radiation budget (Holland and Bitz, 2003). With few local aerosol sources, the high Arctic is a CCN-limited regime (Heintzenberg et al., 2006; Mauritsen et al., 2011). SSA may be a particularly important driver of cloud formation in this environment; however, there remain large gaps in knowledge of high Arctic CCN and INP sources, composition, and cloud nucleation efficiencies.

Large uncertainties in high Arctic aerosol sources, composition, and cloud impacts persist due to the lack of measurements, particularly of individual particle composition (Leck and Svensson, 2015). In order to further our understanding of aerosol – cloud – climate connections in the high Arctic, atmospheric particle samples were collected aboard the icebreaker *Oden* during August – September 2018, as part of the Microbiological – Ocean – Cloud Coupling in the High Arctic (MOCCHA) campaign. Sea spray aerosol generation experiments were conducted aboard

the icebreaker with local seawater from leads. These experiments were compared to ambient particle composition to investigate the influence of sea ice leads on ambient aerosol production and composition. Offline microspectroscopic analysis provided information on individual particle composition and mixing state, and bulk aerosol analysis provided ambient sea salt aerosol concentrations. INP efficiency was determined for particles collected from the SSA generation experiments. Molecular characterization of the SSA organics identified EPS components. Detailed information on local and regional meteorology, sea ice conditions, seawater, and surface snow composition allowed examination of particle sources during high wind periods. These results will further understanding of the influence of local SSA production on the high Arctic aerosol population.

5.2 Methods

During the MOCCHA campaign, atmospheric measurements (meteorology, online and offline aerosol particle sampling) were conducted aboard the icebreaker *Oden* while moored to an ice floe, August 14 – September 15, 2018 (89.5 ˚N, 34.1 ˚E – 88.5 ˚N, 43.2 ˚E). Three aerosol particle sample periods are focused on herein (August 21-22, August 29-30, and September 02-03). Seawater and surface snow samples were collected from the ice floe. The collected seawater was used in aerosol generation experiments, to compare particle production and composition to the ambient aerosol. Details are provided below.

5.2.1 Meteorological and Sea Ice Conditions

Air temperature and wind speed were determined by ship measurements on the *Oden* 7th deck, ~27 m amsl. Precipitation events were determined based on personal observations and hourly webcam images from the *Oden.* 10-day backward air mass trajectories were calculated using the Lagrangian analysis tool LAGRANTO (Sprenger and Wernli, 2015) with wind fields from 3 h operational ECMWF analyses, interpolated to a regular grid with 0.5 deg horizontal resolution on the 137 model levels. AMSR2 sea ice concentration maps were obtained from the University of Bremen (https://www.seaice.uni-bremen.de/).

5.2.2 Sample Collection

5.2.2.1 Seawater Sampling

Surface water (0.6 m depth) was sampled from the ice edge at the open lead site located on the ice floe research station on August 26, 2018. 200 L of water were collected and stored at ambient temperature (~ -1 °C) for ~ 3 h prior to analysis and use in aerosol generation experiments. Initial water temperature was -0.9 °C, and salinity was 28.4 g/kg (Table 5.2). The collected seawater was subsampled prior to aerosol generation experiments for measurements of dissolved organic carbon (DOC), dissolved organic nitrogen (DON), particulate organic carbon (POC), particulate organic nitrogen (PON), and chlorophyll (Table 5.2).

5.2.2.2 Atmospheric Particle Sampling

Atmospheric particles were sampled through a PM_{10} inlet (particulate matter < 10 μm diameter) located on the *Oden* 4th deck. A pollution control system ensured samples were not influenced by local pollution, including occasional ship plume and helicopter emissions (Tjernström et al., 2014). Through the pollution control system, impactor pumps turned off for wind directions outside the previously determined "clean sector" (± 70˚ from the bow) or under stagnant wind conditions (< 2 m/s). The pollution control system also included an ozone monitor (model 202, 2B Technologies) and ultrafine particle counter (UCPC, model 3025, TSI Inc.) to turn off the impactor pumps under increased pollutant concentrations. A scanning mobility particle sizer (SMPS, model 3938, TSI Inc.) and aerodynamic particle sizer (APS, model 3321, TSI Inc.) measured ambient aerosol size distributions and number concentrations from the PM_{10} inlet. The APS measured size distributions from 0.523 – 19.81 μm aerodynamic diameter (d_a) (1 min scans), and the SMPS measured size distributions from 13.6 – 736.5 nm mobility diameter (d_m) (5 min scans).

A ten-stage rotating micro-orifice uniform deposit impactor (MOUDI, model 110R, MSP Corp.) sampled from the PM_{10} inlet at 30 lpm. The MOUDI collected ambient particles onto Formvar film copper transmission electron microscopy (TEM) grids, silicon wafers, and quartz substrates (Ted Pella, Inc) on four stages (< 0.056, 0.10 – 0.18, 0.32 – 0.56, and 1.0 – 1.8 μm d_a) for offline single particle analyses. MOUDI substrates were stored in the dark at room temperature prior to single particle analysis (Laskina et al., 2015).

5.2.3 Marine Aerosol Generation Experiments

A sea spray aerosol generation experiment was conducted using a Marine Aerosol Reference Tank (MART) (Stokes et al., 2013). The 210 L tank was filled with 100 L of seawater collected from the open lead site (Section 5.2.2.1). The MART bubble plume was optimized with a waterfall cycle of 4 s on, 4 s off with a total 4.5 min on and 0.5 min off cycle. To maintain the water temperature as close as possible to collection (-0.9 °C), the MART was placed outside on the deck of the ship under a tent, and the water in the tank was continuously cycled through chilling coils. Water temperature (average 1.1 ± 0.5 °C) was monitored over the course of each experiment using a temperature logger (HOBO Water Temperature Pro v2, Onset) deployed inside the MART tank, and the ambient air temperature (average 0.3 ± 0.6 °C) was monitored by a second temperature logger deployed inside the tent.

Aerosol particles were sampled from the 110 L MART headspace for a 6 h sampling duration, through two diffusion driers to maintain an aerosol flow relative humidity (RH) of ~15 %, monitored by a temperature and RH sensor (model EK-H5, Sensirion). All aerosol instrumentation and diffusion driers were housed inside a laboratory at ~20 °C, with a 0.5 m insulated sampling line between the tank and driers. The 6.3 lpm total sample air flow was balanced by an inflow of 7.0 lpm of particle-free air to maintain positive pressure within the MART and eliminate the possibility of sampling ambient air. The short residence time within the MART (~15 min) provided sampling of nascent SSA. Before starting the MART waterfall, the tank was purged with particle-free air until aerosol number concentrations were < 10 particles/cm^3.

To measure aerosol size distributions and number concentrations, a scanning mobility particle sizer (SMPS, model 3938, TSI Inc.) and aerodynamic particle sizer (APS, model 3321, TSI Inc.) sampled from the MART at 0.3 and 2.5 lpm, respectively. The total 5 lpm flow to the APS was made up with particle-free ambient air (1.2 μm pore size HEPA capsule filter, Pall Life Sciences). The SMPS and APS measured aerosol size distributions (5 min scans each) for particles 14.1 – 736.5 nm (d_m) and 0.523 – 19.81 μm (d_a), respectively. For both ambient and MART measurements, size distributions from the SMPS (14.1 – 615.3 nm, d_m) and APS (0.634 – 19.81 μm, d_a) were combined, following a previously established method (Khlystov et al., 2004). The APS distributions were converted to mobility diameter, assuming a shape factor of 1 and density of 2.0 g/cm^3 (representative of sodium chloride) (Pilson, 2013).

A 10-stage rotating micro-orifice uniform deposit impactor (MOUDI, model 120R, MSP Corp.) sampled from the MART at 3.5 lpm, with an additional 26.5 lpm of particle-free air (1.2 µm pore size HEPA capsule filter, Pall Life Sciences) for a total flow rate of 30 lpm. The MOUDI collected SSA particles on substrates for offline single particle analyses as described in section 2.2.2.

5.2.4 Single Particle Analysis

5.2.4.1 Electron Microscopy

Computer-controlled scanning electron microscopy with energy dispersive X-ray spectroscopy (CCSEM-EDX) (Laskin, 2003; Laskin et al., 2006) was to analyze ~ 1000 particles per substrate conducted (0.10 – 1.8, 0.32 – 0.56, and 1.0 – 1.8 µm d_a MOUDI stages) for ambient (6,826 particles total, August 21-22, August 29-30, and September 02-03) and MART-generated samples (2,272 particles total, August 26) on TEM grids, and ~100 particles per substrate for MART-generated samples on silicon (793 particles total, August 26). CCSEM-EDX analysis was conducted using a FEI Quanta environmental SEM with a field emission gun operating at 20 keV accelerating voltage with a scanning transmission electron microscopy high angle annular dark field (STEM HAADF) detector to collect SEM images and morphological information for individual particles on TEM grids and an Everhart-Thornley (ETD) secondary electron detector for particles on silicon. For the ambient samples, additional CCSEM-EDX was conducted for ~100 SSA particles per substrate (1,203 particles total, August 29-30 and September 02-03) collected on silicon (1.0 – 1.8, 0.32 – 0.56, and 0.10 – 0.18 µm d_a stages) using a FEI Helios nanolab SEM/FIB instrument equipped with a field emission gun operating at 20 kV accelerating voltage and an ETD secondary electron detector for SEM imaging. An EDX spectrometer (EDAX, Inc.) measured X-ray spectra and provide the relative atomic abundance of elements C, N, O, Na, Mg, Al, Si, P, S, Cl, K, Ca, Ti, V, Fe, Ni, and Zn for individual particles. Al and Si were omitted from EDX measurements for particles on silicon substrates due to significant background from the sample holder and substrate, respectively. For clean Si wafers not impacted with particles, carbon was below the detection limit, indicating that substrate contamination from carbon was not present in the particle spectra. EDX can be slightly less sensitive to C, N, and O, compared to heavier elements, such that the C, N, and O percentages reported here represent lower limits (Laskin et al., 2006).

K-means clustering of the individual particle EDX spectra was conducted to group the particles into clusters based on similarity of elemental composition (Ault et al., 2012; Shen et al., 2016). These clusters were then combined into four particle types (nascent SSA, aged SSA, organic and sulfate aerosol, and dust) for the ambient samples and two types (nascent SSA and organic aerosol) for the MART-generated samples, based on comparison of the EDX spectra to previous studies of ambient aerosol and lab-generated SSA (Ault et al., 2013c, 2014; Gunsch et al., 2017; Kirpes et al., 2018). Prior ambient aerosol CCSEM-EDX studies have established EDX spectral signatures for fresh SSA (Ault et al., 2013c; Hopkins et al., 2008; Prather et al., 2013), aged SSA (Bondy et al., 2017b; Laskin, 2003; Laskin et al., 2002, 2012), mineral dust (Axson et al., 2016b; Coz et al., 2009; Creamean et al., 2016; Sobanska et al., 2003), and organic aerosol (Gunsch et al., 2017; Kirpes et al., 2018; O'Brien et al., 2015b; Sobanska et al., 2003). EDX has previously been shown to quantitatively reproduce SSA elemental ratios (Ault et al., 2013c, 2014).

5.2.4.2 Raman Microspectroscopy

Individual SSA particles were analyzed by Raman microspectroscopy using a Horiba Scientific Labram HR Evolution spectrometer coupled with a confocal optical microscope (100x N.A. 0.9 Olympus objective), Nd:YAG laser (50 mW, 532 nm), and CCD detector using a 600 groove/mm diffraction grating. Individual particle Raman spectra were collected over the 500-4000 cm^{-1} range, with a spectral resolution of ~1.8 cm^{-1}, according to a previously established computer-controlled method (Craig et al., 2017). Raman spectra of ~100 SSA particles per substrate were collected for three MOUDI stages (0.10 – 1.8, 0.32 – 0.56, and 1.0 – 1.8 µm d_a) from two ambient samples (August 29-30 and September 02-03) and the MART experiment, for a total of 805 particles analyzed. SSA particles were identified based on morphology using the optical microscope, and were compared to Raman spectra of ~50 standard marine organic compounds, including saccharides, short chain fatty acids, long chain fatty acids, and amino acids, representative of compounds present in the SML (Cochran et al., 2017). Linear combinations of up to two standard Raman spectra (e.g., 53 % fucose + 47 % butyric acid) were fit to individual SSA Raman spectra following the method of Cochran et al. (2017). Particle spectra matching each organic compound type were characterized by unique peaks corresponding to specific organic functional groups in the 850-1650 and 2700-3500 cm^{-1} regions (Eom et al., 2016). Therefore, each particle spectrum could match up to two organic compound types, for example, fucose + xylose (saccharide + saccharide) or fucose + octanoic acid (saccharide + short-chain fatty acid). Model

linear combinations and ambient SSA spectra were compared by calculating χ^2 values over the 800-1800 and 2600-3600 cm^{-1} ranges. This analysis provides a value between zero (spectra are identical) and one (spectra have no correlation). The organic compounds corresponding to the best χ^2 fit (smallest value) between model linear combinations and the ambient SSA spectrum are reported.

Projected area diameter (d_{pa}) was measured by CCSEM-EDX, TEM, and Raman; therefore, it is the parameter reported herein. D_{pa} is often larger than geometric diameter due to particle deformation upon impaction (Hinds, 2012; Sobanska et al., 2014), indicating that particle size reported here is an upper bound and could represent smaller diameter in the atmosphere.

5.3 Results and Discussion

5.3.1 High Winds, Sea Ice, and Snow Conditions

Sustained periods of high winds occurred during the MOCCHA campaign from August 21 – September 04. Three aerosol sampling periods (24 h periods: August 21-22, August 29-30, and September 02-03) were identified for a case study of high winds and SSA production using individual particle analyses. These three days had average wind speeds of 7.2 m s^{-1}, 11.2 m s^{-1}, and 11.0 m s^{-1}, respectively, with maximum wind speeds of 12.4 – 18.5 m s^{-1} (Table 5.1). These high wind conditions facilitate wind-driven sea spray aerosol production (De Leeuw et al., 2011). During the period of sustained high winds on August 29, breaking waves were observed at the open lead site, located ~0.5 km from the ship. These conditions of sustained high wind speeds have been previously shown to produce nascent SSA from open leads (Leck et al., 2002; Nilsson et al., 2001). While the SSA flux from leads is much less than that from open water due to the reduced fetch (Nilsson et al., 2001), the presence of many open leads across the high Arctic may result in the accumulation of SSA resulting in open leads being a significant source of locally-produced nascent SSA during high wind periods.

Table 5.1 Meteorological parameters during ambient aerosol sampling periods of interest during the 2018 MOCCHA study.

Sample Start Time (UTC)	Sample End Time (UTC)	Average Temperature (°C)	Average Wind Speed (m/s)	Wind Speed Range (m/s)	Precipitation	Average total number concentration (particles/cm³)
August 21 2100	August 22 2100	-0.3 ± 0.3	7 ± 3	1.6 - 12.4	Freezing rain and snow overnight	8.5 ± 0.2
August 29 0700	August 30 0700	-1.6 ± 0.4	11 ± 2	6.1 - 18.5	Snow in morning	40 ± 10
September 02 1700	September 03 1700	-2 ± 1	11 ± 2	6.1 - 17.6	Clear to cloudy	50 ± 20

Sea ice concentration maps and backward air mass trajectories were used to determine the extent of regional open lead influence during the ambient aerosol sampling periods (Fig. 5.1). The distance from the ship to the sea ice edge was between 700 – 1500 km during the sample periods of interest. For August 21-22, August 29-30, and September 02-03, the marginal ice zone was within 24 – 30 h upwind, as determined by LAGRANTO backward air mass trajectories started at altitudes within the boundary layer at the ship position (Fig. 5.1). The August 29-30 and September 02-03 samples experienced air mass influence from regions of lower sea ice concentrations, within the pack ice region for the September 02-03 sample and near coastal Greenland and the Canadian archipelago for the August 29-30 and September 02-03 samples (Fig. 5.1). However, the August 21-22 sample air mass had spent more time over dense pack ice before reaching the East Siberian Sea (> 24 h). This suggests that the August 29-30 and September 02-03 samples were influenced by open leads present along the air mass trajectories, providing possible sources of local SSA production, in contrast to the August 21-22 sample.
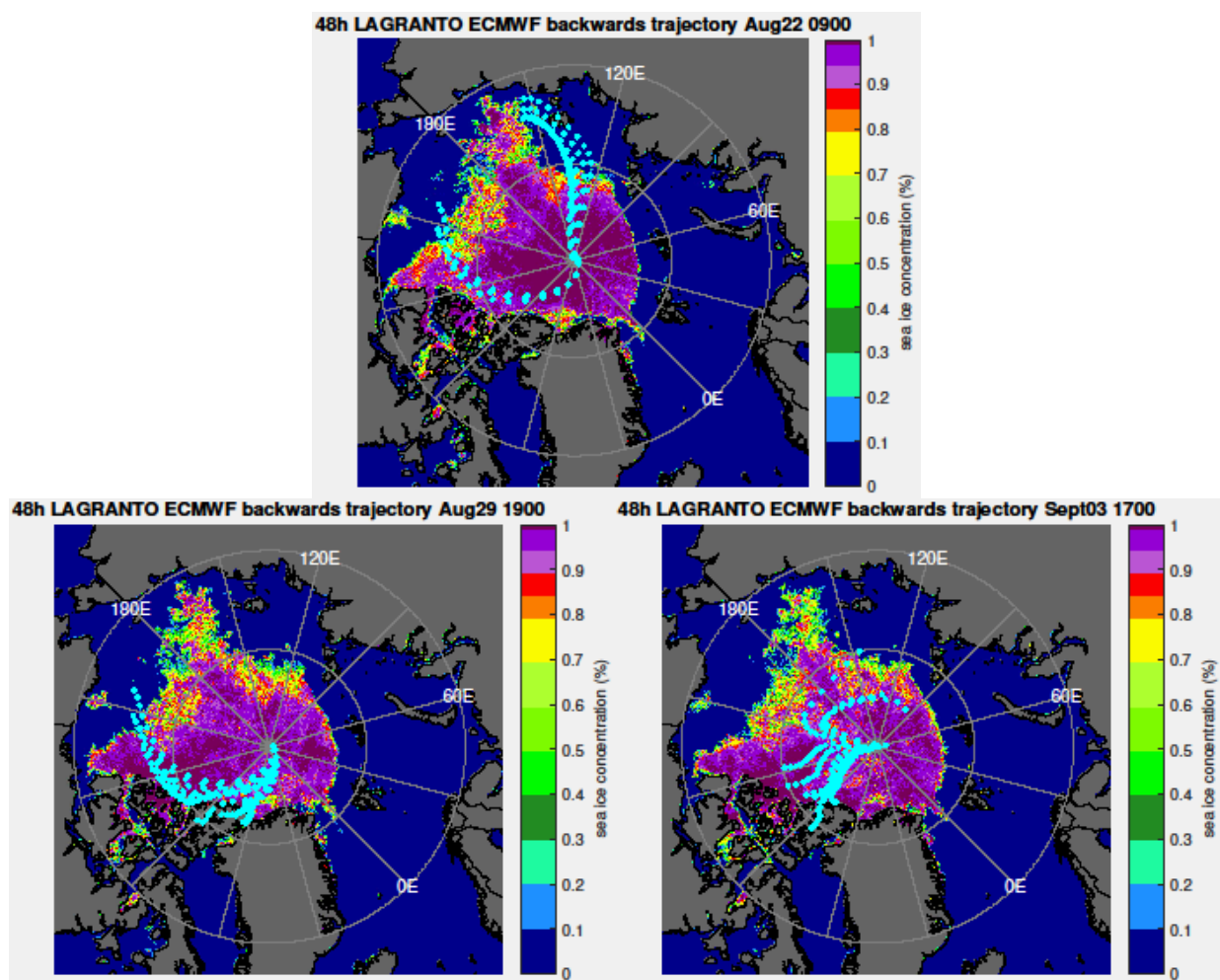
Figure 5.1 Sea ice concentration and backwards air mass trajectories for aerosol samples collected on August 21, August 24, August 29, and September 02, 2018. Trajectories starting at each sample midpoint time are shown for 48 h from sampling site at altitudes that were within the boundary layer at the initial ship position.

Total ambient aerosol concentrations during the open lead-influenced sample periods were much higher (40 ± 10 particles cm^{-3} for August 29-30 and 50 ± 20 particles cm^{-3} for September 02-03 periods) than the August 21-22 sample period (8.5 ± 0.2 particles cm^{-3}). Figure 5.2 shows average ambient aerosol size distributions for these sample periods. A much greater ~150 nm mode was observed for August 29-30 and September 02-03, consistent with a $\sim 100 - 200$ nm SSA mode (Quinn et al., 2015). This suggests lead-based SSA production may greatly influence both the total aerosol number and aerosol size distribution in the high Arctic, with few other aerosol sources present. As accumulation mode particles may be efficient CCN and act as INP, dependent on composition (Leck and Svensson, 2015; Martin et al., 2011), locally produced SSA may have a great influence on cloud formation and climate impacts in the high Arctic.
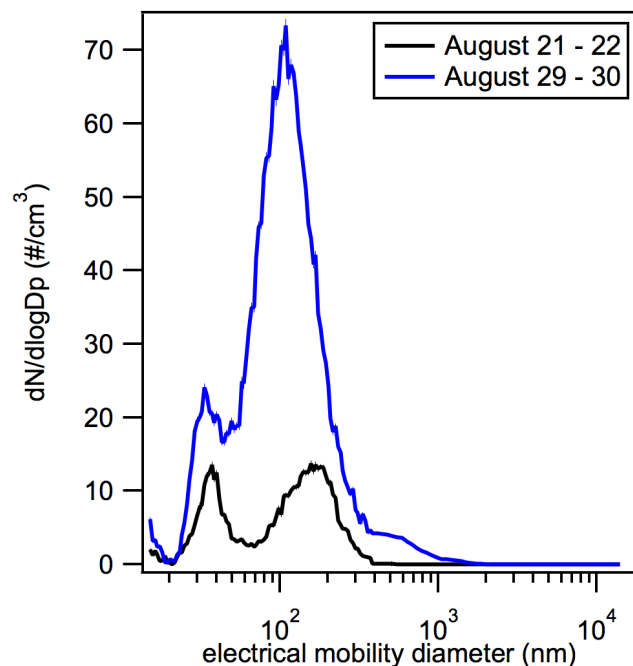
Figure 5.2 Average aerosol size distributions, measured by SMPS and APS, for the August 21-22 and August 29-30 sampling periods. Periods with local ship pollution influence (Section 5.2.2.2) were omitted from sample averages.

5.3.2 Observations of Locally-Produced Nascent SSA

An aerosol generation experiment was conducted aboard the icebreaker using seawater from the nearby open lead to study primary marine aerosol production and composition under high wind conditions. Analyses of the MART samples identified primary marine aerosol particle types, including nascent SSA, SSA enriched in organic carbon (SSA+OC), and organic particles. Nascent SSA was characterized by primarily Na and Cl in the EDX spectra, in addition to Mg, S, K, and Ca, in ratios similar to seawater (Fig. 5.3) (Ault et al., 2013c). A subset of nascent SSA particles were classified as SSA+OC, based on organic enrichment characterized by the presence of C and O in the EDX spectra (Ault et al., 2013c) and visible organic coatings observed by SEM analysis on silicon substrates (Fig. 5.3). Organic particles were primarily observed in the submicron size range (0.1 – 1.0 μm d_a) and were characterized by mainly C and O in the EDX spectra (Ault et al., 2013c).

For the ambient particles, four main particle types were identified by CCSEM-EDX analysis: nascent SSA, aged SSA, organic carbon and sulfate aerosol (OC+sulfate), and dust. The ambient nascent SSA particle type includes both SSA and SSA+OC, as in the MART samples.

Aged SSA particles were characterized by Cl depletion and S enrichment in the EDX spectra (Fig. 5.3) (Gunsch et al., 2017; Weinbruch et al., 2012), indicative of multiphase aging reactions occurring during atmospheric transport (Gard et al., 1998). SSA sources, composition, and aging processes are discussed further in section 5.3.3. OC+sulfate particles were primarily observed in the submicron (0.1 – 1.0 μm d_a) size range and were characterized by mainly C and O in the EDX spectra, with a fraction of these particles also containing S and/or N (Fig. 5.3) (Gunsch et al., 2017; Weinbruch et al., 2012). The OC+sulfate particle type likely contains both primary marine organics, as observed in the MART samples, including marine gels (Heintzenberg et al., 2006; Leck et al., 2013; Leck and Bigg, 2005a), and secondary organic aerosol, but the sources of the organics cannot be distinguished by CCSEM-EDX. Previous studies have observed sulfate coating primary marine organic particles in the high Arctic (Hamacher-Barth et al., 2016; Leck et al., 2002). Dust particles were characterized by Al and/or Si and trace metals including Fe, Ni, and Zn in the EDX spectra (Coz et al., 2009; Creamean et al., 2018a; Kirpes et al., 2018), and were a small fraction of the observed ambient particles (< 1 %, by number, across the analyzed size range from 0.1 – 4.0 μm).
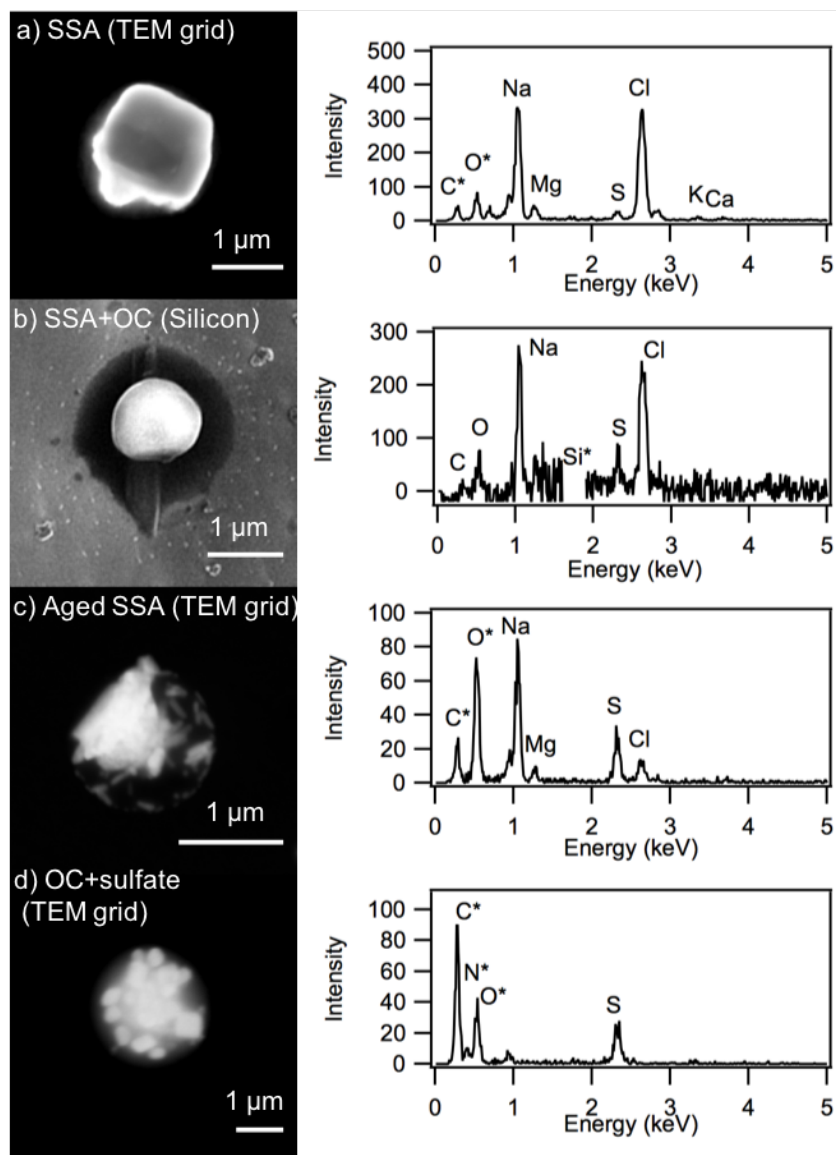
Figure 5.3 Representative individual particle SEM images and EDX spectra for the ambient particle types observed, including a) fresh SSA, b) SSA+OC, c) aged SSA, and d) OC+sulfate particles, with the substrate used noted. *C and O peaks include some signal from the TEM grid substrate film. *Si background peak from the silicon substrate has been subtracted from the EDX spectrum in panel b for clarity.

Previous studies have observed primary marine gel particles produced from leads (e.g. Bigg and Leck, 2001a; Leck et al., 2013; Leck and Bigg, 1999; Leck and Svensson, 2015; Matrai et al., 2008). Organic-rich marine gels would be distinguished by secondary OC+sulfate particles based on particle morphology and chemical composition, specifically the presence of divalent cations, including Mg^{2+} and Ca^{2+} (Orellana and Leck, 2014). However, no distinct marine gel particle type (Orellana et al., 2011) was identified by CCSEM-EDX analysis. CCSEM-EDX

analysis of the MART-generated samples showed 12 % of the observed organic particles, by number, contained magnesium, 0.6 % contained calcium, and 2 % contained sulfur, suggesting minimal contribution from solely marine gel particles. For the ambient OC+sulfate particles, 33 %, by number, contained sulfur, likely secondary sulfate, while 2 % of the particles contained magnesium and 1 % contained calcium. Marine gels were either classified with OC+sulfate particles or observed internally mixed with sea salt and classified as SSA+OC particles. This is likely as manual SEM-EDX analysis identified a small number of organic particles exhibiting a gel-like morphology (Orellana et al., 2011) in the MART-generated and ambient samples, with examples shown in Fig. 5.4, suggesting marine gels may contribute to a small fraction of the observed organic particle number, while the majority of ambient organic particles are likely from secondary sources (Barrett and Sheesley, 2017; Croft et al., 2019; Fu et al., 2013; Mungall et al., 2017; Richard Leaitch et al., 2018; Willis et al., 2017). Detailed characterization of SSA and SSA+OC composition is discussed in section 5.3.3.
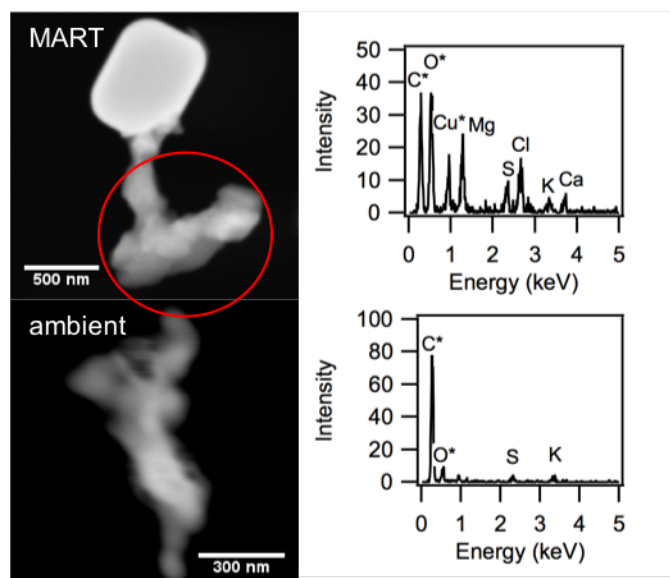
Figure 5.4 SEM-EDX images and spectra of organic gel-like particles (circled) for the MART sample and ambient August 29-30 sample. *Cu signal is from TEM grid substrate, and C and O peaks contain some signal from the substrate background.

Size-resolved number fractions of the observed CCSEM-EDX particle types were compared for the MART-generated particles and the ambient case study days (Fig. 5.5). Primary marine particle types were observed in both the MART-generated and ambient samples across the entire size range analyzed ($0.1 - 5.0$ μm d_{pa}). The MART-generated sample was composed of ~70 – 90 % nascent SSA, by number, and ~10 – 30 % organic particles in the submicron size range

(Fig. 5.5). The supermicron size range (1.0 – 5.0 μm d_{pa}) was composed of greater than 90 % nascent SSA, by number, and <10% organic particles (Fig. 5.5). Consistent with the MART-generated sample, the ambient August 29-30 and September 02-03 samples, both influenced by air masses over fractured sea ice, contained 90 – 100 %, by number, nascent SSA in the supermicron size range (1.0 – 3.2 μm d_{pa}), with only a small fraction (< 5 %, by number), of aged SSA observed. (Fig. 5.5). In comparison, the August 21-22 sample, with air mass influence from areas of higher sea ice concentration (less fracturing), showed negligible supermicron aerosol number concentrations and did not show influence of nascent SSA (Fig. 5.6). The August 29-30 and September 02-03 samples also contained large fractions of submicron nascent SSA, ~ 40 – 80 %, by number, for 0.5 – 1.0 μm d_{pa} (Fig. 5.5), as observed for the MART sample, and consistent with wind-driven SSA production from open leads.
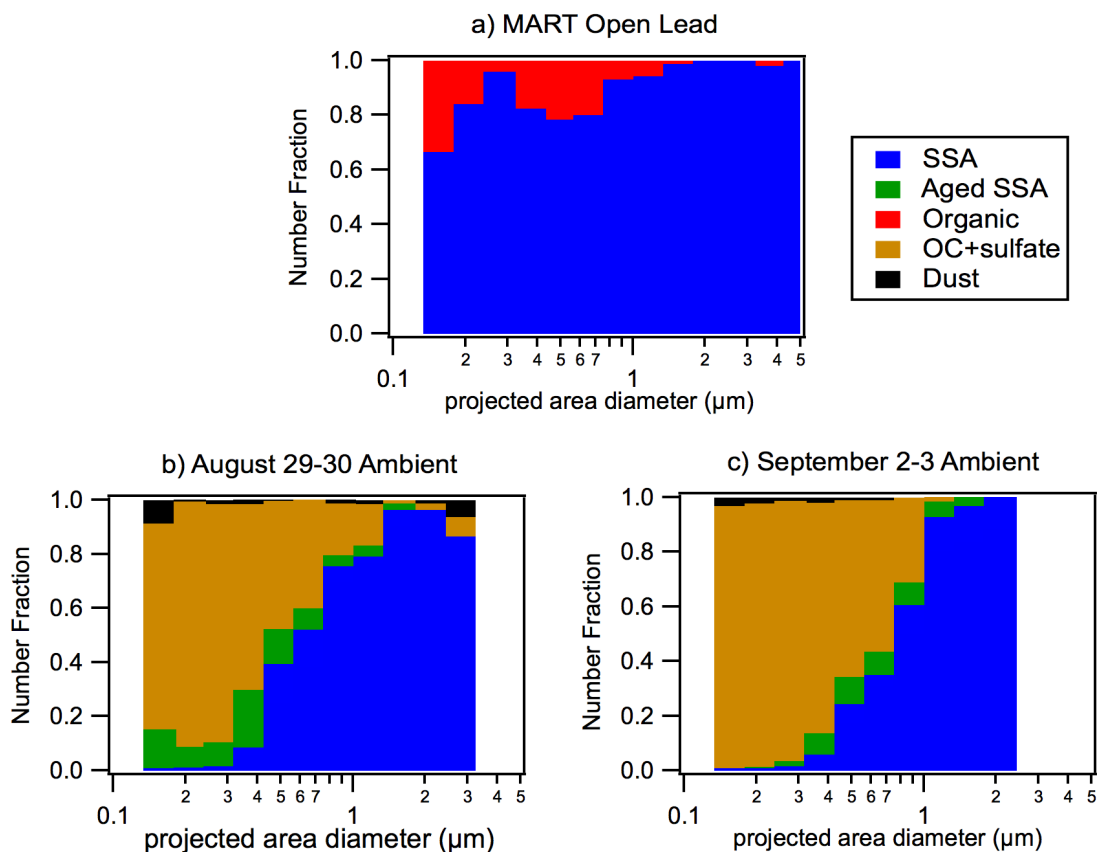
Figure 5.5 Size-resolved number fractions of particle types observed by CCSEM-EDX for the a) MART-generated SSA sample, using seawater collected from the open lead, compared to the ambient b) August 29-30, and c) September 02-03 samples.
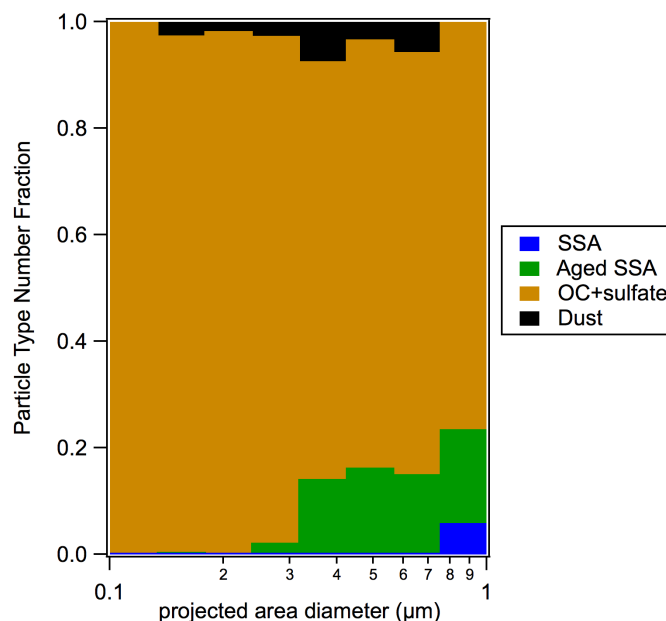
Figure 5.6 Size-resolved number fractions of particle types observed by CCSEM-EDX for the August 21-22 sampling period.

Influences of additional particle types, beyond nascent SSA, were observed in the submicron size range for the ambient samples. The ambient samples contained large fractions of OC+sulfate particles (25 – 85 %, by number, from 0.1 – 1.0 μm d_{pa}), particularly smaller than 0.5 μm d_{pa} (75 – 85 %, by number) (Fig. 5.5 and 5.6). This OC+sulfate fraction likely contains primary marine organics, as observed in the MART sample, which could become coated with sulfate (Hamacher-Barth et al., 2016), in addition to secondary organic and sulfate particles (Burkart et al., 2017; Mungall et al., 2017), demonstrating influence of both local aerosol sources and long-range transport. Aged SSA was also observed in the submicron size range (0.1 – 1.0 μm d_{pa}), comprising ~ 5 – 15 %, by number, on August 29 and September 02, and ~ 15 – 20 %, by number, on August 21, indicative of influence of atmospheric processing during long-range transport. While a supermicron (1 μm diameter) SSA particle could be transported from the ice edge without exhibiting significant aging, a submicron (100 nm diameter) SSA particle could be expected to exhibit complete chloride depletion within the transport time (24 – 48 h) from the ice edge to the sampling location, consistent with a long-range transported source of the submicron aged SSA particles.

The reaction rate of sulfuric acid with sodium chloride was determined using

Equation 5.1 $\frac{d[H_2SO_4]}{dT} = \frac{\gamma c A}{4} [H_2SO_4]$

according to the method of Jacob (2000), where c is the mean free velocity and A is the particle surface area. The value of the uptake coefficient γ was assumed to be 1.0 as an upper limit (Ten Brink, 1998). The sulfuric acid concentration used was 1.32×10^6 cm^{-3}, as measured during summertime at Summit, Greenland (Sander and Bottenheim, 2012; Ziemba et al., 2010). Particles were assumed to be aqueous NaCl, with densities of 1.5 g cm^{-3} and salinity of 35 g kg^{-1}. Under these conditions, a 100 nm diameter particle would experience complete chloride displacement in 21 h. Under these same conditions, a 1 µm diameter particle would be less than 10 % aged in 21 h, with 25 % aging in 48 h, and 100 % chloride displacement only with an atmospheric lifetime of nine days.

5.3.3 SSA Composition and Sources

5.3.3.1 Size-Dependent SSA Composition

To further characterize the observed SSA composition, individual particle elemental mole ratios were calculated from the CCSEM-EDX spectra for all SSA (nascent SSA, SSA+OC, and aged SSA) from the August 29-30 and September 02-03 ambient samples and MART-generated sample (Fig. 5.7 and 5.8). SSA Mg/Na, Ca/Na, K/Na, and N/Na ratios were similar to the seawater ratios across all size ranges for the ambient and MART-generated SSA (Fig. 5.7 and 5.8), consistent with locally-produced nascent SSA. Previous studies have observed submicron SSA enriched in Mg and Ca (~20 % of particles, by number), related to seawater biological activity (Forestieri et al., 2016; Jayarathne et al., 2016) and the presence of marine gels (Gao et al., 2012; Orellana et al., 2011), no enrichment of Mg or Ca was observed for these ambient or MART samples. Overall, the observed ambient SSA composition is consistent with locally-produced nascent SSA and suggest a wind-driven open lead source on the high wind days.

By comparing size-resolved median ratios to standard seawater ratios, a size dependence in individual SSA particle composition was observed. SSA undergoes multiphase reactions resulting in chloride displacement, for example atmospheric sulfuric acid reacts with particle-phase sodium chloride to form sodium sulfate in the particle, releasing HCl gas (Gard et al., 1998; Laskin et al., 2003). Submicron ambient SSA ranging from 0.1 – 0.5 µm (d$_{pa}$) were nearly fully depleted in chloride (median Cl/Na ratios of 0 – 0.3), compared to the MART SSA (median Cl/Na ratios of 0.5 – 0.9) and the standard seawater ratio (1.16) (Fig. 5.7). Further evidence of multiphase aging of submicron SSA was also demonstrated by sulfur enrichment (median S/Na ratios 0.07 –

0.2) compared to the MART SSA (median S/Na ratios 0 – 0.05) and seawater ratio (0.06) (Fig. 5.7). Larger ambient SSA ranging from 0.5 – 3.2 µm (d_{pa}) showed Cl/Na (median ratios 0.8 – 1.1) and S/Na (0.07 – 0.09) ratios very similar to the MART SSA (median Cl/Na 0.9 – 1.1 and S/Na 0.5 – 0.7) (Fig. 5.7), indicative of locally-produced nascent SSA. Notably, Cl/Na ratios for MART-generated and ambient SSA from 0.5 – 3.2 µm (d_{pa}), though similar, were slightly depleted (0.8 – 0.9) compared to the seawater ratio. Minor chloride depletion in nascent SSA has previously been observed with increased biological activity during algal blooms (Schwier et al., 2017), and consistent with marine organics influencing the observed SSA composition, discussed in section 5.3.3.2.
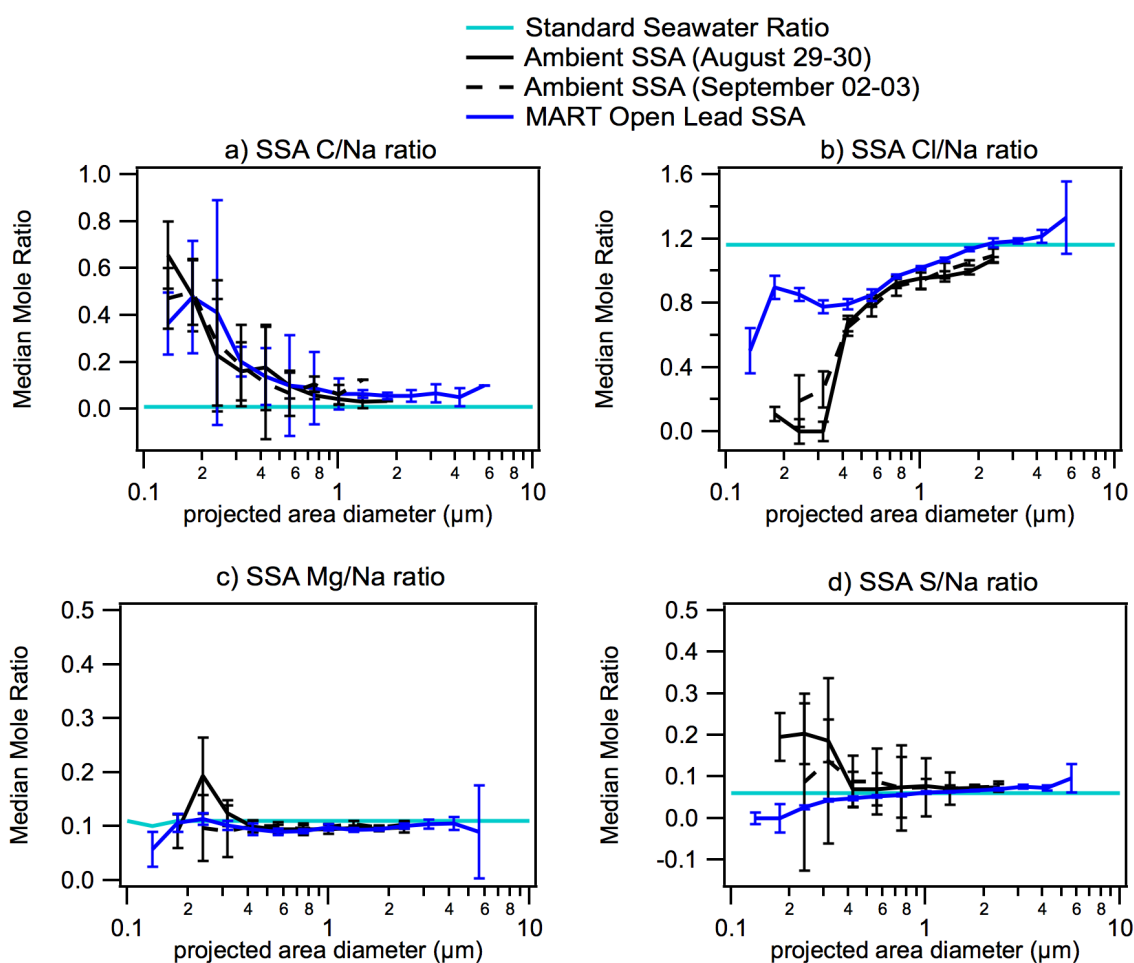
Figure 5.7 Size-resolved median individual SSA particle mole ratios including a) C/Na, b) Cl/Na, c) Mg/Na, and d) S/Na, for ambient August 29-30 and September 02-03 samples, and the MART-generated SSA sample, compared to standard seawater ratios (Pilson, 2013). Particles were sorted into 14 logarithmic size bins. Error bars denote 95% confidence intervals.
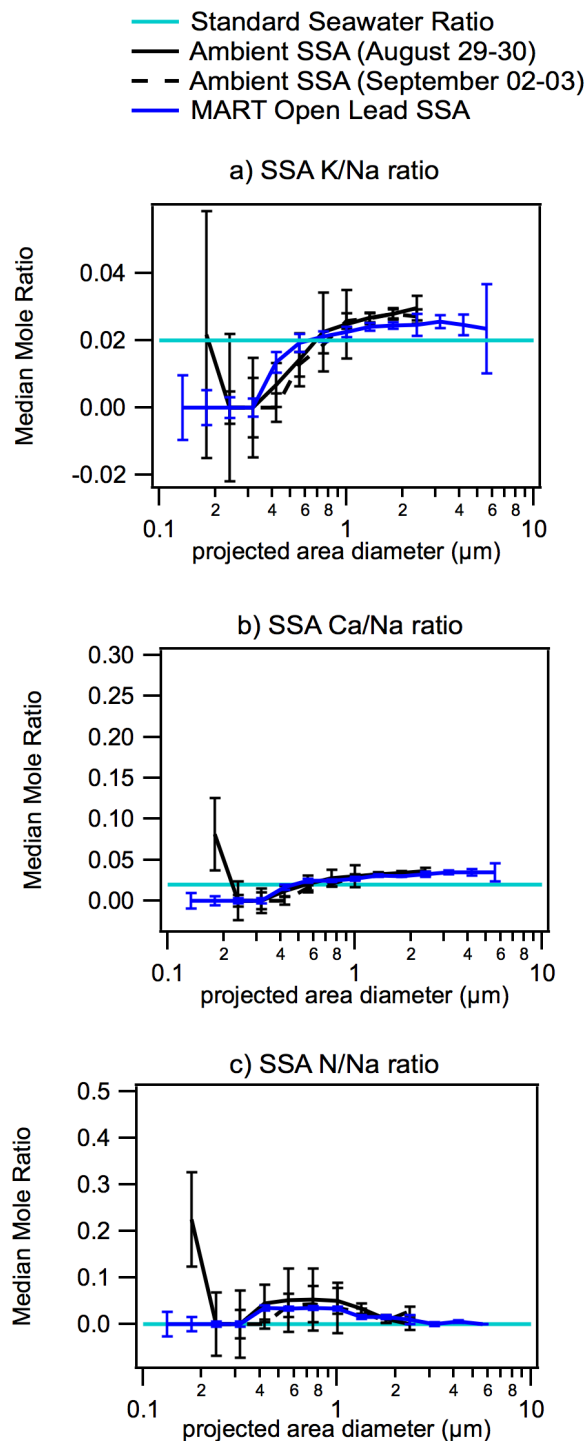
Figure 5.8 Size-resolved median individual SSA particle mole ratios, including a) K/Na, b) Ca/Na, and c) N/Na, for ambient August 29-30 and September 02-03 samples, and MART-generated SSA sample, compared to standard seawater ratios (Pilson, 2013). Particles were sorted into 14 logarithmic size bins. Error bars denote 95% confidence intervals.

5.3.3.2 Characterization of SSA Organics

The influence of marine biology was demonstrated by the organic enrichment observed in the SSA, present as organic coatings on the salt particles. Individual particle C/Na ratios were enriched compared to the standard seawater ratio (0.01, Pilson, 2013), for all size ranges (Fig. 5.7). The greatest organic enrichment was observed in the submicron size range (C/Na ratios of 0.07 – 0.7 for particles from 0.1 – 0.5 μm (d_{pa}), compared to ratios of ~0.01 – 0.03 for 0.5 – 3.2 μm particles). Statistically similar C/Na ratios and size-dependent trends were observed for the ambient and MART SSA, suggesting that the ambient SSA organic coatings were from the SML. These results are consistent with previous observations of submicron SSA C/Na enrichment (0.8 – 1.1) in the Southern Ocean (Eom et al., 2016), demonstrating transfer of SML organics to the aerosol phase (Quinn et al., 2014). For the MART experiment, the open lead seawater dissolved organic carbon concentration was 107 ± 1 μM (Table 5.2), similar to some previous midlatitude seawater mesocosm studies (Alpert et al., 2015; Fuentes et al., 2010a; Hultin et al., 2010; Keene et al., 2017; Schwier et al., 2015) and previous Arctic lead observations (Gao et al., 2012; Orellana et al., 2011), indicative of high levels of organic content in the seawater and/or SML.

Table 5.2 Open lead seawater physical, chemical, and biological parameters.

MART Open Lead (August 26, 2018)	
Seawater sample depth (m)	0.6
Chlorophyll (μg/L)	0.73 ± 0.02
Dissolved organic carbon (μM)	107 ± 1
Dissolved organic nitrogen (μM)	7.4 ± 0.9
Particulate organic carbon (μg/L)	0.15 ± 0.03
Particulate organic nitrogen (μg/L)	0.022 ± 0.006
Open lead seawater temperature (°C)	-0.9
MART seawater temperature (°C)	0.08
Salinity (g/kg)	28.4

To further characterize the observed SSA organics and examine the influence of marine biology on SSA chemistry, individual SSA particles were analyzed by Raman microspectroscopy. Of the 805 particles analyzed, 26 % were classified into organic types. Marine organic compounds, including saccharides, short chain fatty acids, long chain fatty acids, and amino acids, were identified in the SSA particles, based on comparison to standard marine organic compound Raman spectra (Cochran et al., 2017). The remaining particles either did not provide sufficient Raman signal for analysis or fluoresced, masking the Raman signal. Fluorescence is also indicative of biological organic material (Fu et al., 2015). A fraction of the particle Raman spectra had observable organic modes but too little intensity for organic type characterization and were therefore categorized as "trace organics"; these comprised ~40 – 60 %, by number, of all particles analyzed for each sample (Fig. 5.9).

Figure 5.9 shows representative Raman spectra of individual ambient and MART SSA with signatures of saccharides, saccharides+short chain fatty acids, and saccharides+amino acids. Raman peak assignments are shown in Table 5.3. Similar number fractions of classified organic types were present in ambient and MART SSA (Fig. 5.9), and similar organic signatures were observed for both sub- and supermicron SSA and between the ambient and MART-generated SSA particles, although MART SSA generally demonstrated more intense Raman spectra. The most dominant observed organic types were saccharides and saccharides+short chain fatty acids, comprising ~30 – 40 %, by number, of each sample. Additional observed organic types included saccharides+long chain fatty acids and saccharides+amino acids. Overall, less than 5% of the SSA, by number, only contained short chain and long chain fatty acids without a saccharide signature (Fig. 5.9). Saccharides, fatty acids, and amino acids are commonly found in the SML and transferred to the aerosol phase (Bikkina et al., 2019; Cochran et al., 2016, 2017; Falk-Petersen et al., 1998; Fu et al., 2013; Galgani et al., 2016b; Gantt and Meskhidze, 2013; Jayarathne et al., 2016; Mashayekhy Rad et al., 2019; Russell et al., 2010; Scalabrin et al., 2012). Saccharides have previously been observed in the high Arctic SML and aerosol (Gao et al., 2012; Leck et al., 2013). Fatty acids and amino acids have also previously been observed in high Arctic SML and aerosol (Mashayekhy Rad et al., 2019; Matrai et al., 2008). These compounds are also components of EPS secreted by sea ice algae and bacteria and enriched in the SML in open leads (Gao et al., 2012; Hawkins and Russell, 2010; Orellana et al., 2011), consistent with the influence of the open lead

biology on SSA composition (Bigg and Leck, 2008; Leck et al., 2013; Leck and Bigg, 2005a; Orellana et al., 2011).
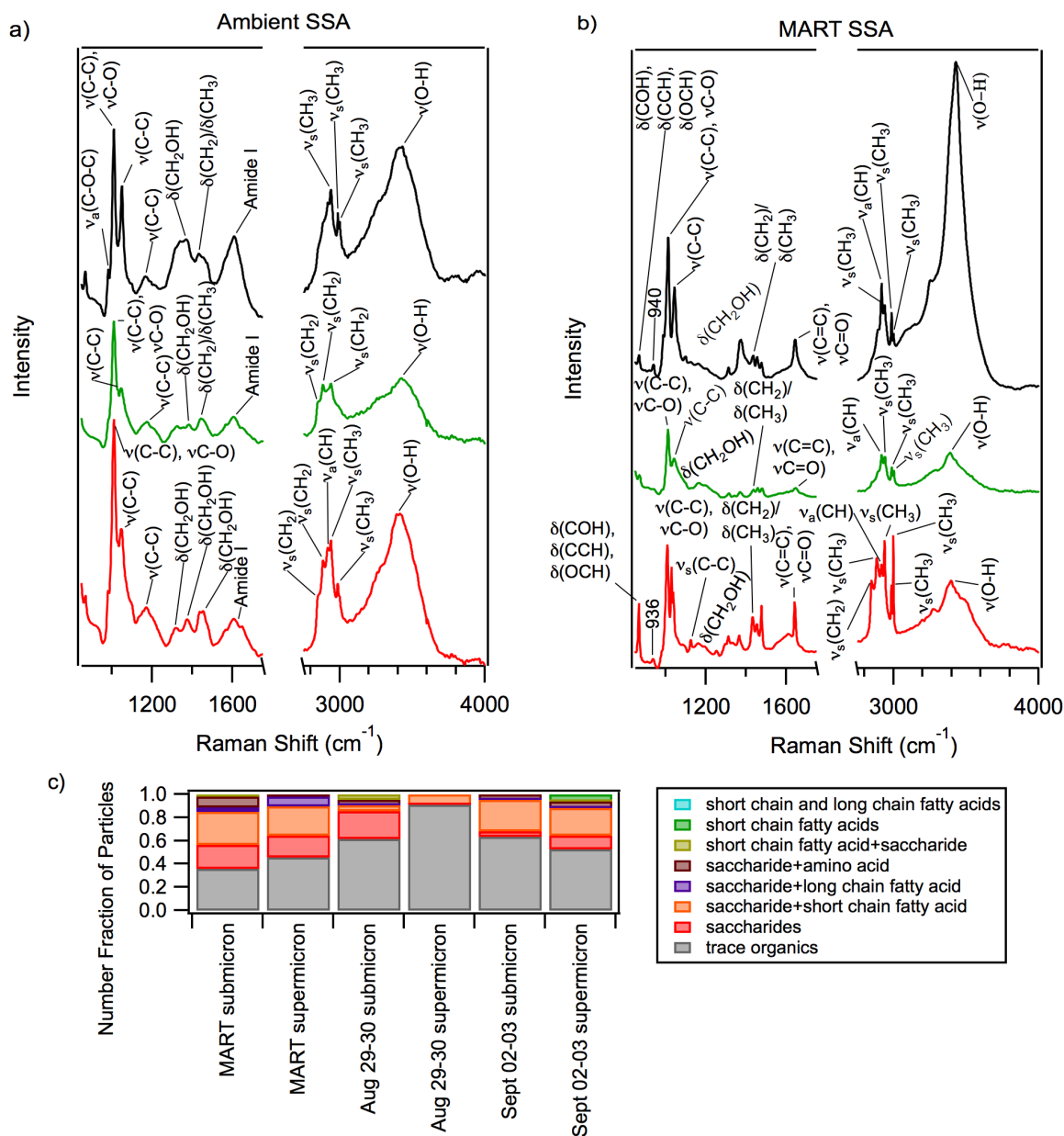
Figure 5.9 Representative individual particle Raman spectra with signatures of (top to bottom) saccharides+amino acids, saccharides+short chain fatty acids, and saccharides, for a) ambient SSA from the August 29-30 sample and b) MART-generated SSA. c) Number fractions of SSA particle Raman spectra best matching standard marine organic compound classes for each sample. Trace organics spectra could not be matched to a specific organic compound due to low intensity Raman signal.

Table 5.3 Observed SSA Raman modes and peak assignments based on literature references.

Observed Peak	Raman Mode	Literature Peak Position	Reference
868	δ(COH), δ(CCH), δ(OCH) side group deformations	861	Cochran et al, 2017
936 940	skeletal modes (polysaccharides)	941	Movasaghi et al, 2007
985	ν_a(C-O-C)	991	Cochran et al, 2017
1010 1011 1013 1015	ν(C-C), ν(C-O)	1009	Cochran et al, 2017
1030 1038	ν(C-C), ν(C-O)	1037	Cochran et al, 2017
1043 1045 1046 1049 1051	ν(C-C)	1044	Cochran et al, 2017
1127	ν_s(C-C)	1129	Cochran et al, 2017
1167 1176	ν(C-C)	1167	Czamara et al, 2015
1311 1313 1314	δ(CH2OH) deformations	1310	Cochran et al, 2017
1365 1370 1372 1373 1383	δ(CH2OH) deformations	1363	Cochran et al, 2017
1432 1435 1441	δ(CH$_2$)/δ(CH$_3$)	1440	Ault et al, 2013 Mertes et all, 2004
1452 1454 1456 1457	δ(CH2OH) deformations	1452	Cochran et al, 2017
1476 1479	δ(CH2OH) deformations	1475	Cochran et al, 2017
1605 1606 1622	Amide I	1596	De Gelder et al, 2007

1641 1644 1647	ν(C=C), ν(C=O)	1640	Cochran et al, 2017
2848	ν_s(CH$_2$)	2850	Ault et al, 2013 Deng et al. 2013
2883 2885	ν_s(CH$_2$)	2880	Ault et al, 2013
2918 2919	ν_a(CH)	2915	Cochran et al, 2017
2937 2939 2941	ν_s(CH$_3$)	2935	Cochran et al, 2017
2984 2985 2987	ν_s(CH$_3$)	2985	Cochran et al, 2017
2997 2998 3000 3001	ν_s(CH$_3$)	2998	Cochran et al, 2017
3388 3392 3397 3424 3429 3430	ν(O-H)	3402 3430	Vargas Jentzsch et al, 2013 Xiao et al, 2008

5.4 Conclusions

Locally produced SSA was observed to be an important contributor to the high Arctic aerosol number and mass, with increasing accumulation mode aerosol concentrations observed on high wind days with open leads upwind. Local SSA production was observed in the summertime high Arctic, with a significant contribution to the accumulation and coarse mode aerosol number under high wind conditions and air mass influence over open leads. The chemical composition of the observed SSA was similar to that of particles generated from local seawater, consistent with lead-based production of nascent SSA (Leck et al., 2002; Nilsson et al., 2001; Scott and Levin, 1972). The accumulation and coarse mode SSA (~0.1 – 2.0 μm d$_a$) were identified as internally mixed inorganic salts and marine organics, with few externally mixed marine gels observed in this size range. The individual SSA particles were enriched in marine organics, present as organic coatings on salt particles, across the observed particle size range (0.1 – 5.0 μm d$_{pa}$). Significant

C/Na enrichment (0.2 – 0.6) above the seawater ratio (0.01) was observed in the submicron range. The marine organic content within the open lead was similar to previous high Arctic observations (Gao et al., 2012) but indicative of relatively low chlorophyll-a productivity compared to midlatitude studies (Fuentes et al., 2010b; Hultin et al., 2010; Keene et al., 2017; Schwier et al., 2015). The SSA organic coatings were composed of marine-derived saccharides and fatty acids, including fucose and xylose, consistent with EPS secreted by sea ice algae and bacteria (Orellana et al., 2011). These results further demonstrate the influence of sea ice lead biology on accumulation mode and coarse mode SSA through the incorporation of organic coatings on SSA particles produced via wind-driven wavebreaking in open leads.

This local SSA source may be an important climate driver in the high Arctic, with few other aerosol sources, as SSA can be efficient CCN (Quinn et al., 2015) and act as INP (DeMott et al., 2016). The Arctic environment is often CCN-limited, with aerosol-cloud-precipitation interactions leading to low aerosol concentrations (Mauritsen et al., 2011). Previously in the high Arctic, CCN concentrations averaging $15 – 30$ cm^{-3} and ranging from $1 – 100$ cm^{-3} have been observed, with distinct local sources in Aitken mode aerosol attributed to primary marine organics (Leck and Bigg, 2005b; Leck and Svensson, 2015) and a wind-dependent sea salt source in the accumulation mode (Leck et al., 2002). The observed SSA may therefore be an important source of accumulation mode CCN in the high Arctic. The composition and mixing state of individual SSA particles determines CCN efficiency and INP activity, as organics may decrease SSA hygroscopicity and suppress CCN efficiency (Collins et al., 2013, 2016), while primary organic particles have been identified as active INP (Creamean et al., 2019; Irish et al., 2017; Wilson et al., 2015). Arctic clouds have been shown to be particularly sensitive to INP concentrations (Harrington et al., 2002; Jiang et al., 2002). For the particles generated from local open lead seawater, composed of sea salt and saccharide-rich organic coatings, the INP activity was low. There have been few previous studies of INP composition in the high Arctic (Bigg and Leck, 2001a). Further consideration of cloud-active particle composition and mixing state is needed to understand and predict the complex aerosol – cloud – climate interactions in the high Arctic.

5.5 Acknowledgements

Chapter 6.   Influence of Marine Emissions and Atmospheric Processing on Individual Particle Composition of Summertime Arctic Aerosol in the Bering Strait and Chukchi Sea

6.1 Introduction

The Arctic region is currently warming at twice the rate of the global average (Pithan and Mauritsen, 2014; Serreze and Barry, 2011). In the Arctic summertime, atmospheric particles directly affect climate by scattering or absorbing incoming solar radiation, both in the atmosphere and on snow and ice-covered surfaces following deposition, contributing to the Arctic amplification (Alvarado et al., 2016; Flanner, 2013; Goldenson et al., 2012; Law and Stohl, 2007; Quinn et al., 2002, 2008; Willis et al., 2018). Additionally, atmospheric particles impact the Arctic climate by participating in cloud formation and altering cloud properties, including cloud brightness and lifetime (Martin et al., 2011; Mauritsen et al., 2011; Quinn et al., 2008). Particle composition is influenced by condensation of lower volatility species and multiphase reactions in the atmosphere with both natural marine and anthropogenic trace gases (Gunsch et al., 2017; Hara, 2003; Hara et al., 1999; Kirpes et al., 2018). The resulting complex and evolving aerosol composition affects subsequent climate-relevant properties, including cloud condensation nuclei (CCN) efficiency and ice nucleating particle (INP) activity (Andreae and Rosenfeld, 2008; Baustian et al., 2012; Wang et al., 2010).

The summertime Arctic is primarily influenced by local and regional aerosol sources (Gunsch et al., 2017; Quinn et al., 2002; Willis et al., 2018), which are changing as the Arctic is experiencing increasing sea ice loss (Notz and Stroeve, 2016; Overland and Wang, 2013). This sea ice loss is particularly extreme in coastal regions, including the Bering and Chukchi Seas in the Alaskan Arctic and the Greenland Sea (Stroeve et al., 2014). With declining sea ice, production of primary sea spray aerosol and secondary aerosol precursors, including trace gases dimethyl sulfide (DMS) and biogenic volatile organic compounds (VOCs), are expected to be increasing (Mungall et al., 2017; Sharma et al., 2012; Struthers et al., 2011). Increasing development, including oil and gas activity, in the Alaskan, Russian, and Norwegian Arctic also contribute to local anthropogenic aerosol and precursor emissions (Dalsøren et al., 2007; Ødemark et al., 2012; Peters et al., 2011).

Decreasing sea ice is also expected to facilitate increased shipping activity and associated emissions, particularly in the Alaskan Arctic (Dalsøren et al., 2007; Ødemark et al., 2012; Peters et al., 2011), since the Bering Strait is a critical point of entry to the Arctic and the Northern Sea route (Huntington et al., 2015). Projected increases in ship traffic (by more than 50% by 2050) and continued oil and gas activity will contribute to emissions of primary aerosol, including soot (Ault et al., 2009, 2010; Murphy et al., 2009), and aerosol precursors including trace gases NO_x, SO_2, and VOCs (Aliabadi et al., 2015; Browse et al., 2013; Dalsøren et al., 2007; Gunsch et al., 2017; Kolesar et al., 2017; Peters et al., 2011; Roiger et al., 2015).

Aerosol mixing state describes the distribution of chemical species across an aerosol population and within each individual particle (Riemer et al., 2019). The direction and magnitude of aerosol impacts on radiative forcing and clouds are dependent on individual particle composition and mixing state. For example, soot absorbs radiation, resulting in warming, and sulfate scatters radiation, resulting in cooling, and the hygroscopicity of sea salt can be reduced by an organic coating (Willis et al., 2018). Aerosol composition and mixing state are determined by aerosol sources and subsequent atmospheric processing through reactions and condensation of secondary materials (Ault and Axson, 2017; Prather et al., 2008). Single particle measurements are well-suited to determine aerosol mixing state, by measuring the distribution of chemical species within individual particles (Ault and Axson, 2017; Laskin et al., 2016; Prather et al., 2008). However, few single particle studies have been conducted in the Arctic (Willis et al., 2018). Therefore, significant gaps remain in understanding Arctic aerosol mixing state to inform prediction of subsequent climate impacts (Willis et al., 2018).

Ship-based studies in the Bering Strait and Chukchi Sea have observed influences of both natural and anthropogenic sources on aerosol composition, using bulk measurements to determine contributions of sea salt, mineral dust, metals, organic compounds, and soot (Kim et al., 2015b; Laimin et al., 2008; Laimin and Liqi, 2008; Sakerin et al., 2015; Taketani et al., 2016; Xie et al., 2006). However, despite the climate implications of this complex aerosol chemistry in the summertime Arctic, there have been few single particle measurements in the Bering Strait or Chukchi Sea (Kim et al., 2015b; Tian et al., 2019; Xie et al., 2007). In this study, atmospheric particles were collected aboard the R/V *Araon* during August, 2016 within the Bering Strait and eastern Chukchi Sea. Subsequent measurements of individual particle chemical composition and

morphology were conducted to determine the influences of marine and anthropogenic sources on atmospheric composition and mixing state in the Alaskan Arctic.

6.2 Methods

Atmospheric aerosol particles were collected aboard the R/V *Araon* from August 1 – August 20, 2016 during a research cruise in the Alaskan Arctic. Particles were collected using a microanalysis particle sampler (MPS-3, California Measurements) with aluminum foil substrates (MPS Corp.) on stage 2 (0.40 – 2.8 μm aerodynamic diameter, d_a) and transmission electron microscopy (TEM) grid substrates (carbon Type-B Formvar film copper grids, Ted Pella Inc.) on stage 3 (0.07 – 0.40 μm d_a). Samples were sealed and stored in the dark at room temperature (~20 °C) until analysis. This study focuses on eight sampling periods during the cruise in the Bering Strait and Chukchi Sea (Table 6.1, Fig. 6.1). Samples were collected for 12 h durations during clean periods, which were determined by establishing a clean sector void of ship emissions, defined by the relative wind direction to the bow of the ship. The August 02 sample was collected during a port stop at Nome, Alaska, during stagnant air (wind speeds < 2 m/s). For these samples, less than 1 % of measured particles, by number, were soot, indicating that the particle samples were not influenced by the ship's emissions.

Table 6.1 Summary of atmospheric particle samples collected aboard the R/V Araon during August, 2016.

Sample	Sample Time (UTC)	Start Location	Average Wind Speed	Average Temperature	Weather
August 01 AM	0418 - 1624	61.67° N, 171.79° W		11 °C	clear
August 01 PM	1639 - 0443	62.97° N, 167.42° W	stagnant	11 °C	foggy, cloudy
August 02	0449 - 1625	64.48° N, 165.32° W	stagnant	10 °C	cloudy
August 06	0412 - 1603	65.15° N, 168.65° W	5.5 m/s	10 °C	foggy, cloudy
August 10	1845 - 0416	75.12° N, 175.26° W	13 m/s	-4 °C	cloudy
August 12	1952 - 0618	77.01° N, 176.62° W		-4 °C	cloudy, foggy
August 14	0623 - 1903	77.99° N, 177.00 °W		-3 °C	foggy, cloudy
August 20	0615 - 1840	76.01° N, 162.30° W	5.5 m/s	-1 °C	cloudy
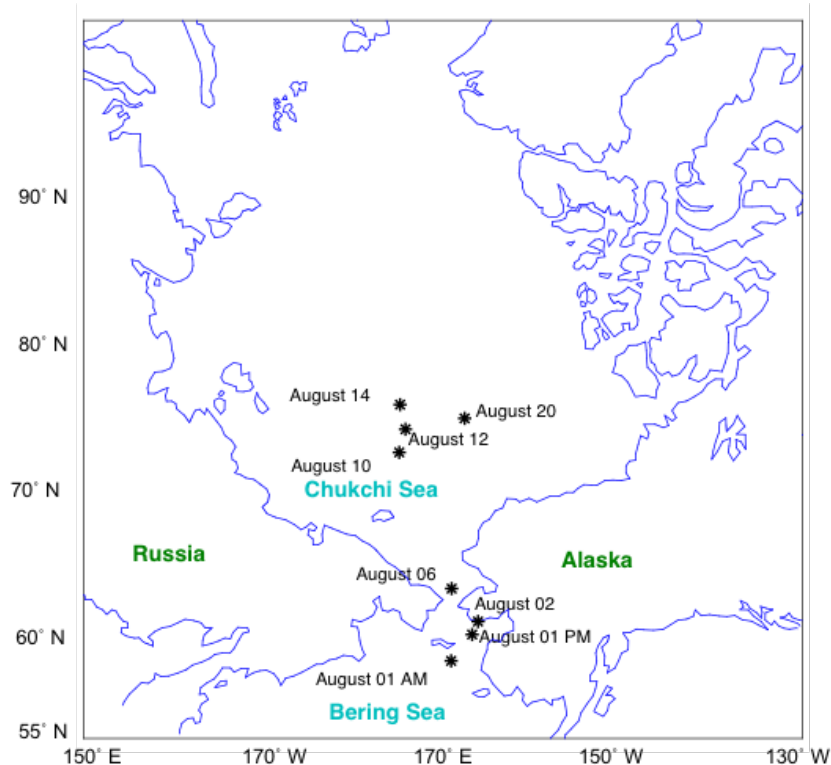
Figure 6.1 Locations of atmospheric aerosol particle samples collected aboard the R/V Araon during August, 2016.

Computer-controlled scanning electron microscopy with energy dispersive X-ray spectroscopy (CCSEM-EDX) was conducted, with analysis of ~ 1000 particles per sample. Samples on stage 3 TEM grid substrates were analyzed using a FEI Quanta environmental SEM with a field emission gun (FEG) operating at 20 keV accelerating voltage with a scanning transmission electron microscopy high angle annular dark field (STEM HAADF) detector to collect SEM images, providing morphological information. An EDX spectrometer (EDAX, Inc.) measured individual particle X-ray spectra and provided the relative atomic abundance of elements C, N, O, Na, Mg, Al, Si, P, S, Cl, K, Ca, Ti, V, Fe, Ni, and Zn. Additional CCSEM-EDX analysis of stage 2 samples on aluminum foil were conducted using a FEI Helios SEM/FIB with FEG operating at 20 keV with a secondary electron Everhart-Thornley detector to collect SEM images. An EDX spectrometer (EDAX, Inc.) measured X-ray spectra and provide the relative atomic abundance of elements C, N, O, Na, Mg, P, S, Cl, K, Ca, Ti, V, Fe, Ni, and Zn; Al and Si were omitted from stage 2 EDX measurements due to significant background from the substrate and detector, respectively (Gunsch et al., 2017). K-means clustering of the individual particle EDX spectra resulted in 50 clusters each for all stage 2 particle data and stage 3 particle data, which

were then all grouped together into six particle classes (fresh SSA, aged SSA, mineral dust, ammonium sulfate, organic aerosol (OA), and soot) based on comparisons of the EDX spectra to particle classes determined by previous studies (Ault et al., 2012; Gunsch et al., 2017; Shen et al., 2016). Prior CCSEM-EDX studies have established EDX spectral signatures for fresh SSA (Ault et al., 2013a; Kirpes et al., 2018), aged SSA (Gunsch et al., 2017; Kirpes et al., 2018), mineral dust (Axson et al., 2016b; Creamean et al., 2016; Kirpes et al., 2018), ammonium sulfate (Bondy et al., 2018), OA (Gunsch et al., 2017; Kirpes et al., 2018), and soot (Gunsch et al., 2017; Jiang et al., 2011). While a small number of particles with morphology indicative of primary biological aerosol were observed during manual SEM imaging, no biological particle cluster was identified by k-means clustering. These particles were likely included in the OA class based on similarity of chemical composition (Bondy et al., 2018) and the low abundance of biological particles.

Individual particle morphology, phase, and infrared spectra were obtained by atomic force microscopy with photothermal infrared spectroscopy (AFM-PTIR) using a nanoIR2 instrument (Anasys Instruments), following a method previously established for atmospheric particles (Bondy et al., 2017a; Kwon et al., 2018; Or et al., 2018). August 2 (12 particles) and August 12 (15 particles) stage 3 samples ($0.07 – 0.40$ μm d_a) were analyzed by AFM-IR. AFM images were collected in contact mode at a 1.0 Hz scan rate over a 5 μm x 5 μm area on the copper grid bar of the TEM grid substrates. IR spectra were collected over the $900 – 3600$ cm^{-1} range at 4 cm^{-1} resolution.

6.3 Results and Discussion

6.3.1 Observed Particle Types

For atmospheric particles collected within the Bering Strait and Chukchi Sea during August 2016, six individual particle classes were identified by CCSEM-EDX analysis: fresh SSA, aged SSA, organic aerosol (OA), ammonium sulfate, dust, and soot (Fig. 6.2). Fresh SSA particles were characterized by Na and Cl with ratios (average Cl/Na = 0.98 ± 0.01, 95% confidence interval) similar to seawater (1.16) (Pilson, 2013), indicative of local production (Ault et al., 2013c; Kirpes et al., 2018). Aged SSA particles exhibited partial or full Cl depletion (average Cl/Na = 0.2 ± 0.4), with replacement by sulfate and/or nitrate (identified by S and/or N in the EDX spectra) (Bondy et al., 2017b; Gunsch et al., 2017; Kirpes et al., 2018; May et al., 2018b). SSA aging is a result of multiphase reactions during atmospheric transport between sodium chloride and nitrogen- and

sulfur-containing gases, resulting in the formation of sodium nitrate and sodium sulfate in the particle phase, with Cl liberation in the form of gaseous HCl (Gard et al., 1998; Ravishankara, 1997). Ammonium sulfate particles were identified based on the predominance of N and S in the EDX spectra (Bondy et al., 2018), in addition to their distinct morphology and behavior, as these particles are semi-volatile and sensitive to the electron beam during SEM imaging (Even et al., 1998; Veghte et al., 2014). Since EDX is not particularly sensitive to detection of N (Laskin et al., 2006), the detection of N and S dominant particles is indicative of an ammonium sulfate rich particle type, formed by the reaction of ammonia with sulfuric acid. The ammonium sulfate particles likely also contained some organic material. OA particles were characterized by C and O, with a fraction of the particles containing S and/or N, indicative of internal mixing of organic compounds with sulfate and/or nitrate (Gunsch et al., 2017; Kirpes et al., 2018). Based on their morphology, these OA particles are likely secondary aerosol formed from the condensation of semivolatile anthropogenic or biogenic trace gases.

Minor particle types (in total < 5% of the particle number) included dust and soot. Dust particles were characterized by Ca, Al, and/or Si; a fraction of particles also contained trace metals including Mg and Zn, suggesting influence from both terrestrial and industrial sources (Axson et al., 2016b; Creamean et al., 2016, 2018a; Kirpes et al., 2018). Dust particles were overall a small fraction of the observed aerosol number (< 3 %), but were present in all samples, likely transported from regional sources in Alaska or from long range transport from the Asian continent (Fitzgerald et al., 2015). A small fraction of observed particles were also identified as soot, characterized by C-rich EDX spectra and distinct morphology (Fig. 6.2) (Creamean et al., 2018a; Gunsch et al., 2017; Jiang et al., 2011). This fresh soot was a very small fraction of the observed particles (< 2%, by number, from 0.1 – 1.0 μm), indicating that these samples were not contaminated by direct emissions from the ship itself. Some aged soot may have been present, internally mixed with OA and/or sulfate as a result of atmospheric aging during transport from pollution sources, and these particles would be classified as part of the OA type (Gunsch et al., 2017; Kirpes et al., 2018).
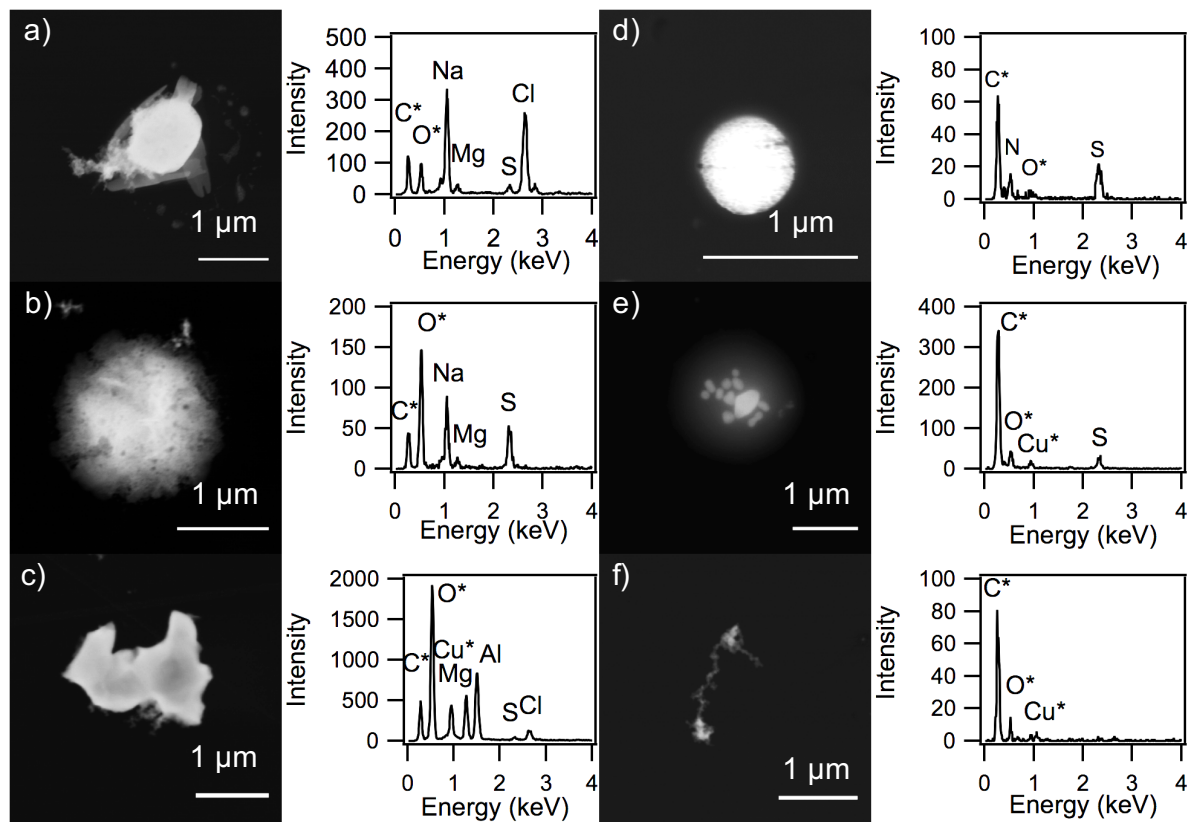
Figure 6.2 Representative SEM images and EDX spectra of individual particles corresponding to the six types, identified by CCSEM-EDX, including: a) fresh SSA, characterized by Na and Cl, b) aged SSA, characterized by Na and S, c) aluminum and magnesium dust particle, d) ammonium sulfate particle, e) OA particle with sulfur, and f) fresh soot. *Copper, carbon, and oxygen peaks include some signal from the TEM grid and substrate background.

6.3.2 Air Mass Influences and Particle Sources

Distinct differences in the size-resolved number fractions of the particle classes were observed for particles collected in the Bering Strait compared to the Chukchi Sea, indicative of different air mass and source influences (Fig. 6.3 and 6.4). No sea ice was present in the Bering Sea during August, 2016, but the region is biologically productive (Hill et al., 2018; Lin et al., 2014), indicated by high chlorophyll-a concentrations within the Bering Strait (Fig. 6.3). There was also minimal sea ice present in the Chukchi Sea during this period, with samples collected from open water or the marginal ice zone (Fig. 6.4). With this great extent of open water, marine influences were present in the Bering Strait and Chukchi Sea. However, the Bering Strait also experienced terrestrial dust influence from Alaska and eastern Russia, and anthropogenic influence from oil and gas activity and shipping activity.

Bering Strait samples included August 01 AM (morning) and PM (evening), August 02, and August 06. Backward air mass trajectories showed influence of marine coastal regions within the Bering Strait for August 01 AM and PM and August 02, and terrestrial influence from inland Alaska on August 06 (Fig. 6.3). All Bering Strait samples showed coastal marine and anthropogenic influence. Fresh SSA was the dominant particle type in the supermicron range (55 - 65 % of particles, by number), and was present in the submicron range as well (20 – 30 %, by number), with aged SSA comprising only ~20 %, by number, of particles in the submicron size range (0.1 – 1.0 μm d_{pa}) (Bondy et al., 2017b) (Fig. 6.3). Consistent with this observation, previous bulk aerosol studies have observed influence of sodium and chloride in the Bering Strait (Kim et al., 2015b; Laimin et al., 2008; Sakerin et al., 2015).

Dust was also present in all Bering Strait samples (~3 %, by number, from 0.5 – 5.0 μm), from terrestrial and industrial sources (Creamean et al., 2018a; Gunsch et al., 2017; Laimin et al., 2008; Xie et al., 2006). Increased number fractions of dust were present in both the sub- and supermicron ranges on August 01 (Fig. 6.3), with air masses from eastern Russia. These August 01 dust particles contained aluminum and zinc, likely from Russian industrial sources (de Velde et al., 2000), while calcium-containing dust was present in all samples (< 5 %, by number), likely from crustal weathering dust (Creamean et al., 2016; Fitzgerald et al., 2015; Laimin et al., 2008).

In all Bering Strait samples, OA particles dominated the submicron size range (40 - 50 %, by number) (Fig. 6.3). Previous studies have attributed OA observed in the Bering Strait to marine biogenic gaseous precursors (Bikkina et al., 2015; Kim et al., 2015b), wildfires (Atkinson et al., 2013), and anthropogenic sources (e.g. shipping emissions) (Kim et al., 2015b; Xie et al., 2007). Vanadium, a tracer for shipping emissions, was present in 7% of the Bering Strait OA particles, with similar number fractions of vanadium-containing particles observed in all samples. In addition to OA, ammonium sulfate (likely also containing organics) contributed a significant fraction to the aerosol number (~15 – 25 %) in both the submicron (0.1 – 1.0 μm d_{pa}) and supermicron (1.0 – 5.0 μm d_{pa}) size ranges (Fig. 6.3). Sources of ammonia, a precursor to ammonium sulfate aerosol, in the Arctic include continental sources (e.g. wildfires), microbial oxidation of marine dissolved organic nitrogen, and seabirds (Croft et al., 2016; Eom et al., 2016; Fisher et al., 2011; Vancoppenolle et al., 2013; Wentworth et al., 2016). On August 01 and 02, there were wildfires present upwind in eastern Russia (Fig. 6.5). There are also large seabird colonies present in the Bering Strait during summer (Croft et al., 2016; Wentworth et al., 2016),

likely a large contributor to atmospheric ammonia and subsequent ammonium sulfate formation (Croft et al., 2016; Giamarelou et al., 2016; Köllner et al., 2017; Wentworth et al., 2016; Willis et al., 2017). The August 02 sample had a greater number fraction of ammonium sulfate particles in both the submicron (0.1 – 1.0 µm d_{pa}, 25 %, by number) and supermicron (1.0 – 5.0 µm d_{pa}, 65 %, by number) size ranges, compared to the other samples (Fig. 6.3). It was also characterized by an increased number fraction of supermicron aged SSA (10 %, by number) (Fig. 6.3), indicative of more polluted air mass influence, including local sources at Nome.

Only a small fraction of soot was observed in the Bering Strait samples (<5 %, by number, from 0.1 – 0.5 µm). No significant soot fraction was observed on August 02 (< 1%) during the stop at Nome, consistent with other samples. Low background levels of soot, averaging 1.0 ng/m^3, have been previously observed in this region (Taketani et al., 2016). Local combustion emissions from Nome are expected to be below the measured size range (< 0.1 µm d_{pa}) (Moffet and Prather, 2009). The August 06 sample showed an increased fraction of submicron (0.1 – 1.0 d_{pa}) soot, likely from inland pollution sources near Fairbanks (Browse et al., 2012; Gunsch et al., 2017; Taketani et al., 2016), consistent with aging timescales for soot in remote environments (Fig. 6.3) (China et al., 2015; Shen et al., 2014).
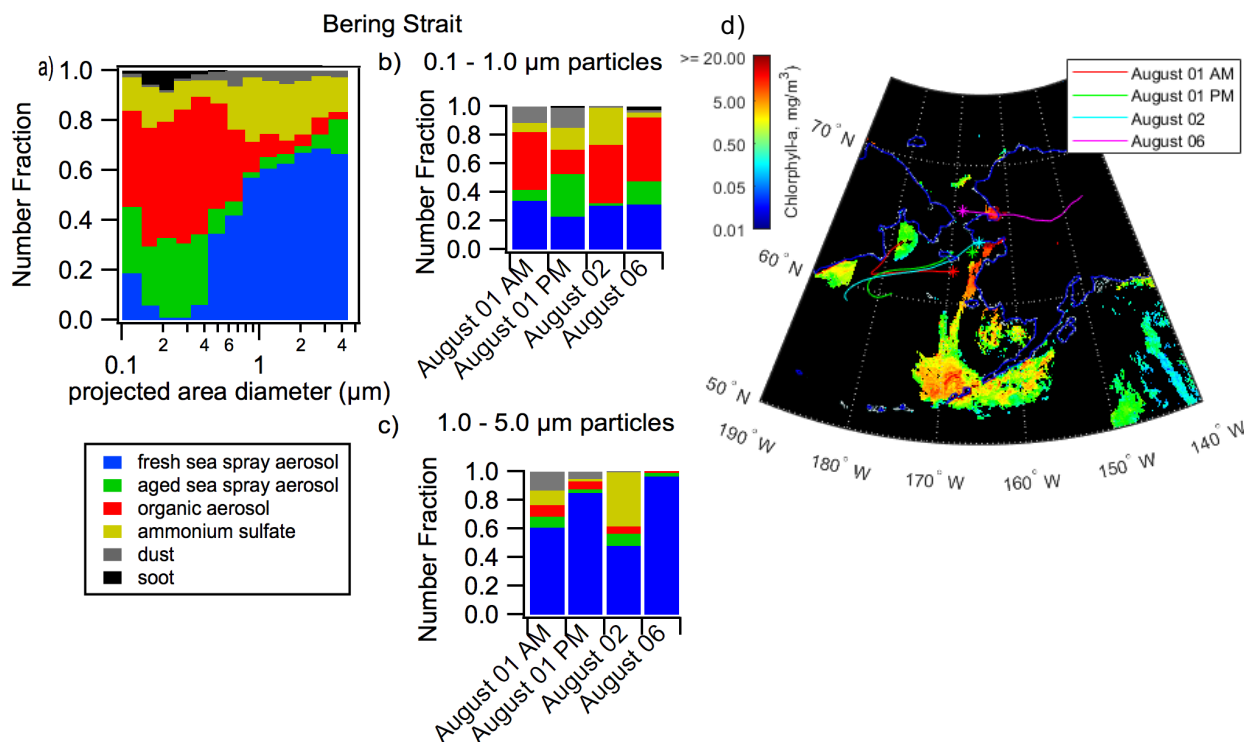
Figure 6.3 a) Average size-resolved CCSEM-EDX number fraction distributions of observed particle types from 0.1 to 5.0 µm projected area diameter for all Bering Strait samples. Number fractions of particle types observed for each Bering Strait sample in the b) submicron and c) supermicron size ranges. d) Air mass influence of each Bering Strait sample as determined by NOAA HYPSLIT 48 h backward air mass trajectories. Stars denote particle sampling locations. MODIS ocean chlorophyll-a concentrations (NASA Worldview) across the sampling region on August 1, 2016 are shown.
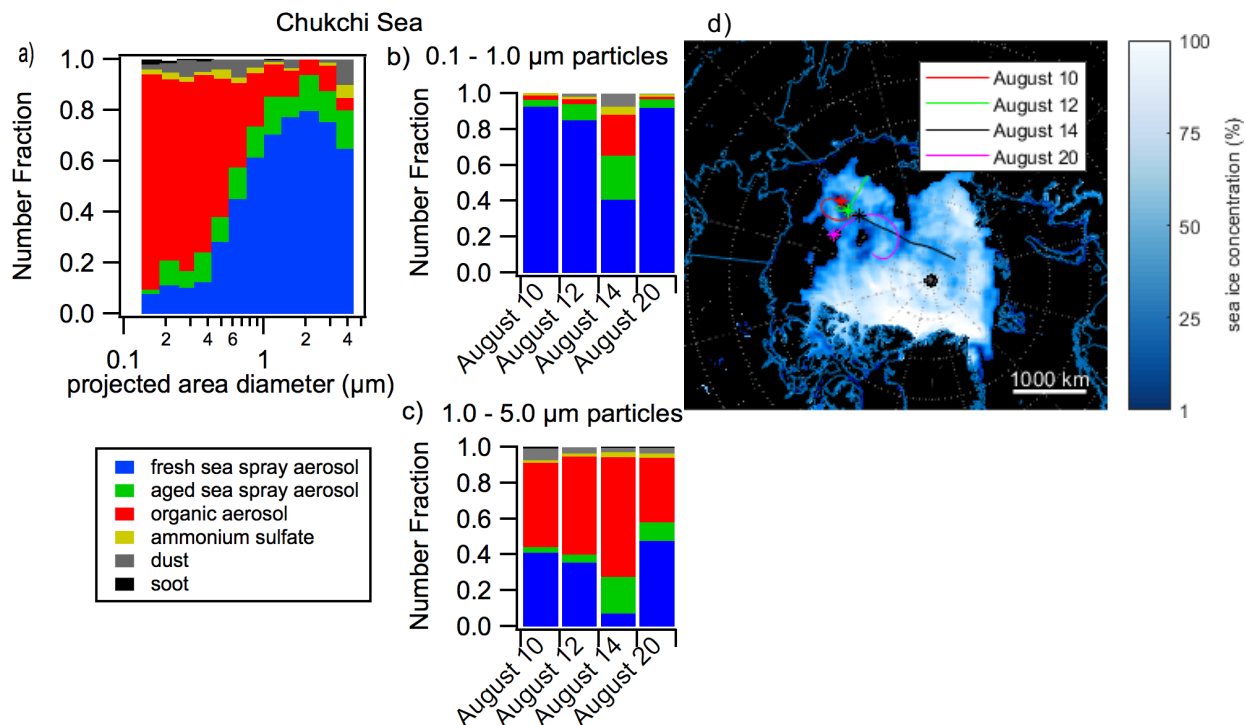
Figure 6.4 a) Average size-resolved CCSEM-EDX number fraction distributions of observed particle types from 0.1 to 5.0 µm projected area diameter for all Chukchi Sea samples. Number fractions of particle types observed for each Chukchi Sea sample in the b) submicron and c) supermicron size ranges. d) Air mass influence of each Chukchi Sea sample as determined by NOAA HYPSLIT 48 h backward air mass trajectories. Stars denote particle sampling locations. Nimbus-7 SMMR and SSM/I-SSMIS sea ice concentration map (NASA Worldview) of the sampling region on August 14, 2016 is shown.

Figure 6.5 Suomi NPP/VIIRS fires and thermal anomalies (NASA Worldview) on August 01, 2016 in eastern Russian and Alaska, shown as red dots.

In contrast to the Bering Strait samples showing influence of anthropogenic pollution and terrestrial emissions, the Chukchi Sea samples, collected on August 10, 12, 14, and 20, showed primarily marine influence. These samples were all influenced by air mass trajectories coming from within the Chukchi Sea and across the Arctic Ocean, through the marginal ice zone and pack ice (Fig. 6.4). Consistent with this marine influence, supermicron ($1.0 - 5.0$ µm d_{pa}) particles were mainly fresh SSA ($60 - 80$ %, by number), and submicron particles were mainly OA (50 %, by number, from $0.5 - 1.0$ µm and 85 %, by number, from $0.1 - 0.5$ µm) (Fig. 6.4). Previous studies in the Chukchi Sea have identified sea spray aerosol and marine biogenic aerosol (OA) as major sources (Kim et al., 2015b; Laimin et al., 2008; Tian et al., 2019; Xie et al., 2006; Ye et al., 2015). Aged SSA comprised only ~10 % of the particle number across both the sub- and supermicron size ranges (Fig. 6.4), consistent with limited pollution influence. Ammonium sulfate and dust particles each contributed less than ~ 5 % of the overall particle number, and soot was negligible, suggesting minor influence of anthropogenic and terrestrial sources. All Chukchi Sea samples, like the Bering Strait samples, contained a small fraction (< 1%) of calcium-containing dust. However, silicon-containing dust was observed only in the Chukchi Sea samples, and the aluminum- or zinc-containing dust was unique to the Bering Strait samples. Silicon-containing dust is likely from soil or coastal beach sand sources, indicating a small amount of terrestrial influence (Gunsch et al., 2017; Laimin et al., 2008).

Notably, the August 14 Chukchi Sea sample was influenced by an air mass that had traveled from across the pack ice in the central Arctic Ocean (Fig. 6.4). Compared to the other Chukchi Sea samples, this sample had increased number fractions of aged SSA (~25% of submicron and ~20% of supermicron particles, by number) and OA (~70% of submicron and ~20% of supermicron particles, by number) (Fig. 6.4). This sample also had a smaller number fraction of fresh SSA (40%) compared to the other Chukchi Sea samples (85 - 95%), indicative of longer atmospheric transport over the pack ice. Additionally, a greater number fraction of the OA particles observed on August 14 contained sulfate (48% of supermicron OA particles and 88% of submicron OA particles, by number), compared to the other Chukchi Sea samples (15% of supermicron OA particles and 45% of submicron OA particles, by number) (Fig. 6.4). The increased fraction of aerosol containing secondary sulfate is consistent with an aged air mass transported further from aerosol sources over a region with greater ice concentration in the central Arctic Ocean (Heintzenberg et al., 2015; Kirpes et al., 2018; May et al., 2016b).

6.3.3 Aerosol Mixing State

To further investigate the degree of atmospheric aging of the observed SSA, average individual particle S/Na, N/Na, and Cl/Na ratios were determined for the SSA (fresh and aged) for the Bering Strait and Chukchi Sea samples (Fig. 6.6). For the Bering Strait SSA particles, individual particle Cl/Na ratios were depleted relative to seawater (1.16) (Pilson, 2013), with greater depletion observed for submicron SSA (Cl/Na of 0.40 ± 0.02, 95% confidence interval) than supermicron SSA (0.98 ± 0.04) (Fig. 6.6), consistent with the greater fraction of submicron aged SSA (Fig. 6.3). Additionally, S/Na (0.165 ± 0.007 for submicron and 0.139 ± 0.006 for supermicron SSA) and N/Na ratios (0.035 ± 0.002 for submicron and 0.081 ± 0.004 for supermicron SSA) were enhanced relative to seawater (0.06 and 0.0002, respectively) (Pilson, 2013), with greater N/Na enrichment observed for supermicron SSA (Fig. 6.6). SSA aging by reactions with SO_2 or H_2SO_4 is commonly observed in the Arctic (Gunsch et al., 2017; Hara, 2003; Hara et al., 2002c; Kirpes et al., 2018), and is consistent with the anthropogenic air mass influences observed for the Bering Strait samples. In comparison, Chukchi Sea SSA particles were more similar in composition to seawater, indicative of fresh SSA (Ault et al., 2013c; Gunsch et al., 2017; Kirpes et al., 2018), with supermicron Cl/Na ratios (1.02 ± 0.05) close to the seawater ratio (1.16). Slight chloride depletion was observed for submicron Cl/Na (0.75 ± 0.04), with slight S/Na and

N/Na enrichment for both sub- (0.154 ± 0.008 S/Na and 0.039 ± 0.002 N/Na) and supermicron particles (0.139 ± 0.007 S/Na and 0.070 ± 0.004 N/Na) (Fig. 6.6), consistent with the small fraction of aged SSA observed in addition to fresh SSA (Fig. 6.4).

High concentrations of chlorophyll-a ($0.5 – 20$ mg/m^3) were observed along the sampling track (Fig. 6.3), as the Bering Strait is a region of biologically productive water (Arrigo and van Dijken, 2015; Huntington et al., 2015), enriched in organic material that has been observed in the aerosol phase (Bikkina et al., 2015; Li et al., 2017). Enrichment of marine organics in Arctic SSA has been previously observed as an organic coating on the salt particles (Russell et al., 2010), and previous observations in Antarctica have shown increased SSA C/Na ratios in more productive waters (Eom et al., 2016). For supermicron SSA particles (collected on foil substrates), C/Na ratios were compared to seawater to determine carbon enrichment. For the Bering Strait samples, 39 %, by number, of the SSA particles contained carbon, with C/Na ratios between 0.05 and 0.2 (Fig 6.6), compared to the seawater ratio of 0.01 (Pilson, 2013). For the Chukchi Sea samples, 60 % of the SSA particles from the Chukchi Sea samples contained carbon, with C/Na ratios between 0.05 and 0.5 (Fig. 6.6). A higher number fraction of Chukchi Sea SSA particles had C/Na ratios greater than 0.1 (20 %), compared to the Bering Strait SSA (5 %). This may be indicative of increased productivity near the ice edge in the Chukchi Sea (Gosselin et al., 1997; Hill et al., 2018; Kim et al., 2015a), providing additional organic material that is transferred to the aerosol phase. This is consistent with previous observations of SSA organic enrichment present as an organic coating on the inorganic salt core, which may alter CCN efficiency (Collins et al., 2013; Forestieri et al., 2016; Moore et al., 2011; Schill et al., 2015; Wex et al., 2010).
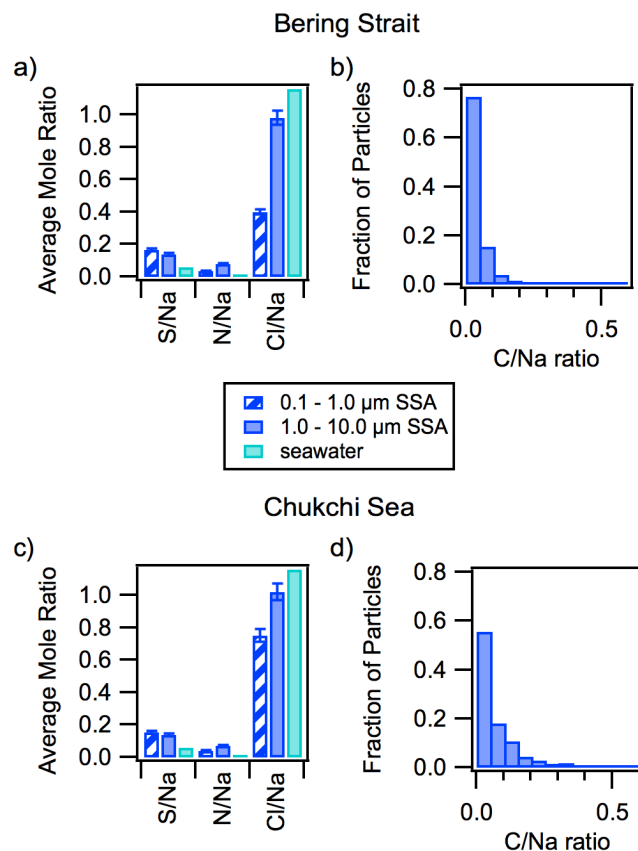
Figure 6.6 Average S/Na, N/Na, and Cl/Na mole ratios for individual sea spray aerosol (SSA) particles for a) Bering Strait and c) Chukchi Sea samples, compared to standard seawater ratios (Pilson, 2013). Error bars denote 95% confidence intervals. Histograms of C/Na mole ratios for individual supermicron SSA particles on foil substrates for b) Bering Strait and d) Chukchi Sea samples.

The mixing state of OA was also investigated by examining the number fractions of individual particles containing sulfur (sulfate) and/or nitrogen (nitrate). Internal mixing of organics and sulfate in submicron OA particles was confirmed by AFM-IR analysis (Fig. 6.7). For both the Bering Strait and Chukchi Sea samples, greater number fractions, determined by CCSEM-EDX, of supermicron OA particles contained sulfate and nitrate (60 – 70 % of supermicron particles, compared to 15 % of submicron particles, by number), possibly due to challenges in detecting S and N by EDX in the submicron particles (Laskin et al., 2006). Overall, a greater number fraction of Bering Strait OA particles contained sulfate and/or nitrate, determined by CCSEM-EDX. For supermicron Bering Strait OA particles, 50 %, by number, contained both sulfate and nitrate, with 16 % only containing sulfate, and 3 % only containing nitrate (Fig 6.8). For submicron Bering

Strait OA, 8 %, by number contained only sulfate, 2 %, by number, contained only nitrate, and 5 %, by number, contained both sulfate and nitrate (Fig. 6.8). Previous summertime studies have measured non-sea salt sulfate within the north Bering Sea, with higher concentrations observed with more pollution influence (Aranami et al., 2002). The Bering Strait is a busy shipping lane, providing NO_x and SO_2 combustion emissions for nitrate and sulfate formation (Aliabadi et al., 2015; Ødemark et al., 2012; Peters et al., 2011; Roiger et al., 2015). In addition, in the summer, a fraction of the OA particulate sulfate likely originates from marine DMS oxidation (Ghahremaninezhad et al., 2016; Kerminen and Leck, 2001; Lundén et al., 2007; Mungall et al., 2016). Elevated DMS levels have been observed in the Bering and Chukchi Seas and correlated with phytoplankton chlorophyll (Barnard et al., 1984; Jodwalis et al., 2000; Li et al., 2019; Sharma et al., 1999), with high chlorophyll levels observed in the region (Fig. 6.3), suggesting both marine and anthropogenic sources influence the OA mixing state.
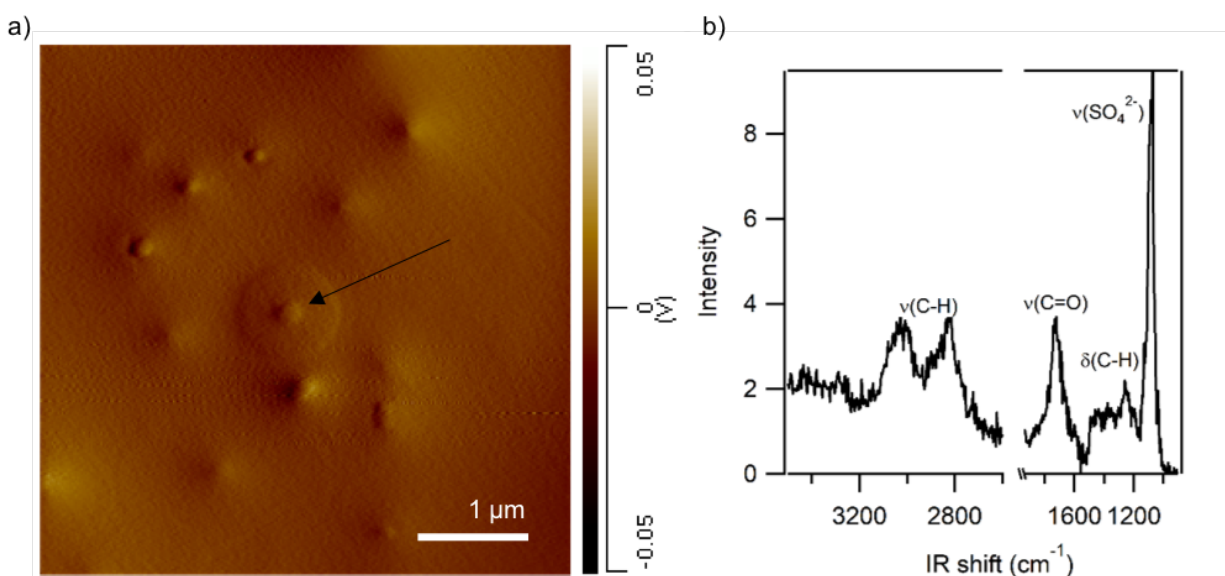
Figure 6.7 a) AFM deflection image and b) corresponding IR spectrum of a representative organic particle (indicated by the arrow) containing sulfate and organics.
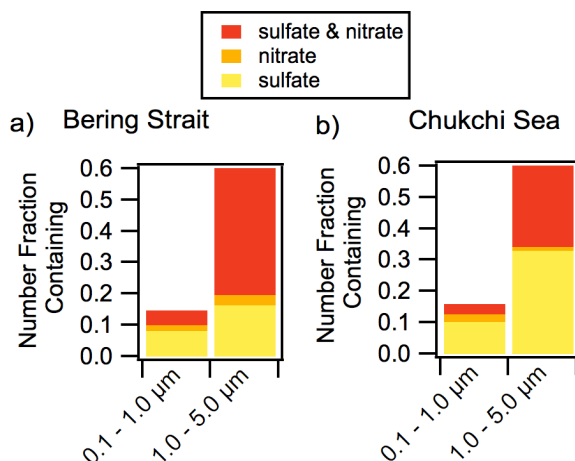
Figure 6.8 Number fractions, determined by CCSEM-EDX, of individual organic aerosol (OA) particles containing sulfate (S), nitrate (N), or sulfate and nitrate (S & N) for a) Bering Strait and b) Chukchi Sea samples.

Chukchi Sea samples had smaller number fractions of OA particles containing both sulfate and nitrate compared to Bering Strait samples. In the submicron size range (0.1 – 1.0 µm), 10 % of the OA particles, by number, contained only sulfate, 2 % contained only nitrate, and 3 % contained both sulfate and nitrate (Fig. 6.8). For supermicron OA (1.0 – 5.0 µm), 28 % contained sulfate and nitrate, 33 % contained only sulfate, and 1 % contained only nitrate (Fig. 6.8). Given the sampling locations and limited nitrate contributions, these are likely marine-derived OA particles with sulfate from DMS oxidation, rather than anthropogenic SO_2 oxidation (Barrett and Sheesley, 2017; Kim et al., 2015b; Shaw et al., 2010). Elevated levels of MSA (average 12 ng/m^3) have been previously observed during summer near the ice edge in the Chukchi Sea (Ye et al., 2015). Additionally, marine VOCs have recently been observed to be involved in Arctic secondary OA formation (Croft et al., 2019; Mungall et al., 2017; Willis et al., 2017). Primary OA from marine sources have also been previously observed in the summer Arctic, with organic compounds including saccharides, fatty acids, and amino acids identified in aerosols, further supporting the origin of the Chukchi Sea OA particles as marine (Fu et al., 2013; Kawamura et al., 2012; Kim et al., 2015a).

6.4 Conclusions

Characterization of aerosol mixing state in the summertime Alaskan Arctic is important for determining particle CCN efficiency and INP activity, influence on surface albedo, and resulting

climate effects in the region with declining sea ice. Previous studies in the region have observed influence of marine biogenic and anthropogenic sources on the aerosol composition (Kim et al., 2015b; Laimin et al., 2008; Laimin and Liqi, 2008; Sakerin et al., 2015; Taketani et al., 2016; Xie et al., 2006), but there have been few single particle studies to determine the aerosol mixing state (Kim et al., 2015b; Xie et al., 2007). Individual atmospheric particles collected in the summertime Alaskan Arctic within the Bering Strait and Chukchi Sea were comprised primarily of fresh and aged sea spray aerosol, organic aerosol, and ammonium sulfate particles. Chukchi Sea samples were primarily marine influenced, with fresh SSA and OA. In contrast, Bering Strait samples contained more aged SSA, ammonium sulfate, soot, and internally mixed sulfate with OA, indicating anthropogenic and terrestrial influence on the aerosol mixing state. In a changing Arctic with decreasing sea ice, increasing emissions of SSA are expected (Struthers et al., 2011), as well as greater anthropogenic influence from increasing shipping activity (Dalsøren et al., 2007; Ødemark et al., 2012; Peters et al., 2011), particularly in the Bering Strait (Huntington et al., 2015). These evolving aerosol and precursor gas sources will likely impact regional atmospheric chemistry and climate effects, including cloud formation and properties (Creamean et al., 2018b; Maahn et al., 2017).

Further studies are needed for improved predictions of atmospheric composition and climate impacts in the changing Arctic. Continued studies are needed to determine the impacts of sea ice loss on both natural and anthropogenic emissions, as increasing open water will result in greater marine aerosol and trace gas emissions, as well as increasing combustion emissions from development and shipping activity. Additionally, a more detailed molecular characterization of OA composition is necessary to further investigate OA sources, formation mechanisms, and potential climate impacts. Within the Bering Strait and Chukchi Sea, measurements across seasons are needed to characterize aerosol sources, concentrations, and mixing state with increasing sea ice loss, particularly during autumn freeze up and with springtime algal blooms. In order to determine aerosol-cloud-climate impacts in the Bering Strait and Chukchi Sea region, measurements of concurrent cloud and aerosol properties are needed, including CCN and INP measurements. Observations of aerosol and cloud properties across seasons are necessary to understand the seasonality of aerosol-cloud impacts in the Alaskan Arctic, given rapidly changing sea ice conditions.

6.5 Acknowledgments

Chapter 7.   Solid Ammonium Sulfate Aerosol in the Cold, Humid Summertime Arctic

7.1 Introduction

In the atmosphere, aerosols impact climate by directly scattering or absorbing solar radiation and taking up water to act as cloud condensation nuclei (CCN) or ice nucleating particles (INP), modifying cloud properties. Water uptake is intrinsically a single-particle process governed by an individual particle's physicochemical properties, such as size, composition, phase, and morphology (Farmer et al., 2015; Riemer et al., 2019). Aerosol phase impacts particle reactivity (Riva et al., 2016; Zhang et al., 2018), water uptake (Berkemeier et al., 2014), gas partitioning (Riva et al., 2016; Zhang et al., 2018), optical properties (Moffet and Prather, 2009), and CCN activity (Farmer et al., 2015). Particles with high viscosity impact heterogeneous chemistry by inhibiting diffusion into particles (Koop et al., 2011; Renbaum-Wolff et al., 2013; Zhou et al., 2019). Thus, it is critical to understand the water phase behavior of a particle to be able to predict aerosol impacts on climate. Water uptake calculations are typically driven by thermodynamic predictions incorporated into global climate models. However, recent laboratory and field evidence, as well as modeling predictions, have suggested that organic particles are more often in a solid or viscous state than previously assumed.

Despite the evidence for frequent solid or glassy organic particles (Lienhard et al., 2015; Reid et al., 2018), ubiquitous hygroscopic inorganic components, such as ammonium sulfate, are presumed to be primarily present as ions dissolved in aqueous particles in the marine boundary layer due to the high RH. When considering the phase of ammonium sulfate there is a well-known hysteresis effect where solid ammonium sulfate will undergo a phase transition to an aqueous particle at 78% RH when RH is increasing, while a liquid particle will not crystallize when drying until 34% RH. Thus, since the presumed formation mechanism for SO_4^{2-} (aq) in the Arctic troposphere is aqueous phase oxidation of SO_2 and the RH over the Arctic Ocean does not go below 34%, it is commonly assumed that ammonium sulfate is present as ions in aqueous particles in the summertime Arctic. Even at temperatures approaching 0 °C, the phase transition to a solid for pure ammonium sulfate is not predicted at ambient RH values by the ammonium sulfate phase diagram (Xu et al., 2002).

In this study we report the surprising observation of solid ammonium sulfate particles with thin organic coatings collected in the summertime Arctic at temperatures and RH values (77 – 94%) where ammonium sulfate is predicted to be present in aqueous particles. These particles were characterized using a multimodal microspectroscopic approach to determine their chemical composition, phase, and morphology. A combination of laboratory studies, thermodynamic modeling, and attribution of sources and formation processes are used to explain these unexpected results and their potential implications for atmospheric chemistry in cold, humid environments, such as the summertime Arctic marine boundary layer.

7.2 Methods

7.2.1 Sample Collection

Atmospheric particles were sampled at a tundra field site (71°16'30" N, 156°38'26" W), near Utqiaġvik, Alaska during August – September, 2015. Individual particles (70 – 400 nm aerodynamic diameter) were collected using a microanalysis particle sampler (MPS-3, California Measurements Inc.) with TEM grid substrates (carbon Type-B Formvar film copper grids, Ted Pella Inc.). Samples were collected for ~8 h, with 22 samples containing significant number fractions of the ammonium sulfate particle type discussed herein (Table 7.1). Complete sampling details can be found in Gunsch *et al.* (Gunsch et al., 2017). PM_{10} samples were collected onto prebaked quartz filters using a high-volume sampler over a duration of 7 days. Samples were collected at the Utqiaġvik site. Samples were stored in baked aluminum foil packets at -10° C until analysis.

Table 7.1 Atmospheric aerosol sampling periods containing significant number fractions of ammonium sulfate particles.

Sample start time (AKDT)	Sample end time (AKDT)
082415 1600	082515 0000
082515 0000	082515 0800
082715 0000	082715 0800
082715 0800	082715 1600
082715 1600	082715 1600
082915 0000	082915 0800
082915 0800	082915 1600
082915 0800	082915 1600
082915 1600	083015 0000
090515 0000	090515 0800
090515 0800	090515 1600
090515 1600	090615 0000
090715 0000	090715 0800
090715 0800	090715 1600
090715 1600	090815 0000
090815 0000	090815 0800
090815 0800	090815 1600
090915 0000	090915 0800
091515 0000	091515 0800
091615 0000	091615 0800
092315 0800	092315 1600
092315 1600	092415 0000

7.2.2 Particle Generation

Ammonium sulfate aerosol particles were generated using an atomizer from a 10 µM solution (Fisher Scientific, 99.7 % ammonium sulfate). Particles 200 nm in diameter were selected using a differential mobility analyzer (DMA, TSI Inc., model 3082) to be representative of the

observed ambient particle size mode. The relative humidity within the DMA was controlled using a humidified air flow or diffusion driers upstream to generate aqueous and solid particles at 50 % and 15 % RH, respectively. Particles were impacted onto TEM grids for offline analysis using a MPS.

7.2.3 Single Particle Microscopy Measurements

The TEM grid substrates were analyzed by computer-controlled SEM-EDX using a FEI Quanta scanning electron microscope with field emission gun operating at 20 keV accelerating voltage. The instrument is equipped with a high angle annular dark field detector and energy-dispersive X-ray detector (EDAX, Inc) to provide information on the size, morphology, and elemental composition of individual particles. K-means clustering of the EDX data identified unique particle classes, as described by Gunsch et al. (2017) and references therein. Additional SEM images were collected using a secondary electron detector with the sample tilted 75° to provide additional information on particle three-dimensional morphology.

AFM-IR was used to further probe the morphology and chemical composition of individual particles using a nanoIR2 (Anasys Instruments). AFM images were collected in contact mode at a 0.75 Hz scan rate over a 5 μm x 5 μm area on the copper grid bar of the TEM grid substrate in order to measure the diameter and height of individual particles, according to a method for AFM-IR application to aerosol particles (Bondy et al., 2017a; Kwon et al., 2018). IR spectra were collected over the $900 - 3600$ cm^{-1} range at 4 cm^{-1}/point resolution. Additional AFM images were collected in tapping mode to provide information on phase (Schmitz et al., 1997).

STXM-NEXAFS was conducted over the carbon K-absorption edge and sulfur L-absorption edge to distinguish carbon and sulfur oxidation states present in the individual particles, using a previously described method (Hopkins et al., 2008; Moffet et al., 2010a). Briefly, X-ray energies are selected with a monochromator and raster scanned across the sample. Images at closely spaced X-ray energies are combined to create an image stack, and X-ray spectra are converted to optical density using the Beer-Lambert law. Pre-edge/post-edge ratios of X-ray absorption over the carbon K-absorption edge ($280 - 320$ eV) were used to create a map showing the relative contribution of organic and inorganic components in individual particles. Sulfur L-absorption edge spectra were collected over the $168 - 176$ eV range. The ratio of peaks at 1702.9 and 170.9 eV was used to assess the relative contribution of different sulfur oxidation states (S(V) and S(VI)).

7.2.4 Bulk Particle Filter Analysis

Small portions of the quartz filters were extracted in 25 ml Milli-Q (Ω 18.2) water and sonicated for 30 min before analysis by ion chromatography. Extract was sampled into 200 µL injection loops using a 1 ml syringe with 0.22 µM PVDF filter. Dionex ICS-1100 and ICS-2100 ion chromatographs were used to analyze inorganic ions in solution, including Na^+ (LOD 2.35 µM) and SO_4^{2-} (LOD 0.32 µM). The ion chromatographs were each equipped with a guard column (ICS-1100: AG18 RFIC, 4 x 50 mm, IonPac; ICS-2100: UTAC-ULP1 RFIC, 5x23 mm, Dionex), analytical column (ICS-1100: CS12A-5µm, RFIC; ICS-2100: AS18 RFIC, 4 x 50 mm, IonPac), suppressor (ICS-110: CERS-4 mm 500 RFIC, ICS-2100: AERS500 4 mm, Dionex), and a heated conductivity cell (DS6, Dionex). Methanesulfonic acid (20 mM) was used as eluent for the cation column, and a KOH gradient generated by an EGC III KOH system was used as eluent for the anion column. All samples were run in triplicate, with average values and standard deviations reported herein. Additional ion chromatography analysis was conducted using the same extraction procedure and sampled onto a column equipped to measure methanesulfonic acid (MSA). Portions of the quartz filter were also combusted and analyzed for sulfur elemental and isotope analysis using a ThermoFinnigan MAT 253/Eurovector EA.

7.3 Results and Discussion

7.3.1 Solid Particles Observed at Low Temperature and High Relative Humidity

Ambient particles were collected at a coastal Arctic location during August – September 2015, at ambient temperatures between –3˚ – 10 ˚C and relative humidities between 77 – 94%. Microscopic analysis revealed a unique ammonium sulfate particle type exhibiting an unexpected solid phase and complex morphology (Fig. 7.1). The physical properties of these particles were investigated using atomic force microscopy (AFM), which demonstrated the tall nature of the particles, with heights of 150 – 200 nm measured for 200 – 500 nm d_{pa} particles (Fig 7.1). These heights are ~3 – 4 times larger than for an aqueous ammonium sulfate particle (Bondy et al., 2017a) which spread out nearly flat upon impaction (Koop et al., 2011), indicative of a solid or viscous phase present in the ambient particles. AFM phase images revealed heterogeneity within the particles, showing a difference in particle phase (Schmitz et al., 1997), particularly between the particle core and edge protrusions (Fig. 7.1), indicative of a core-shell structure. Scanning transmission electron microscopy imaging showed that most of these round particles contained

small cubic edge protrusions that were brighter than the particle core (Fig. 7.1), indicating different phases between the core and shell components (Yamashita et al., 2018). Scanning electron microscopy (SEM) images collected at a 75° tilt further demonstrated the tall, hemispherical nature of these particles (Fig. 7.1), indicative of a solid or viscous phase (Wang et al., 2016), in comparison to other flat, liquid particle types (Fig. 7.2). This morphology has not been previously observed for ambient particles in the Arctic or beyond, suggesting it is unique to the observed atmospheric conditions and particle's history since its formation. Based on the ambient conditions during sampling, ammonium sulfate particles would be expected to be in a liquid phase, particularly for small submicron particles (Laskina et al., 2015), as particle phase transitions and phase separation may depend on particle size (Cheng et al., 2015; Veghte et al., 2013). These particles were frequently observed in the submicron size range, comprising 15 – 20 % of the total particle number fraction from 100 - 500 nm (projected area diameter, d_{pa}) (Fig. 7.1), indicating a significant fraction of the observed particle number exhibited a solid phase in a key size range for CCN activation (Gunsch et al., 2017).

The physical properties of these particles determined by AFM analysis were compared to the morphology of standard laboratory-generated liquid (deliquesced) and solid (effloresced) ammonium sulfate particles (Fig. 7.3). Particle phase can be inferred by the extent of spreading when inertially impacted onto a substrate at ambient pressure, determined by the particle diameter and height. AFM height traces of each particle type at similar diameters showed that the tall ambient particles were similar to solid ammonium sulfate particles, while the liquid particles were shorter (Fig. 7.3). Three-dimensional AFM height images further demonstrated the similar morphology of the tall ambient and solid ammonium sulfate particles, compared to the liquid ammonium sulfate particles (Fig. 7.3), indicating the ambient particles exhibited a solid phase (Lee et al., 2017).
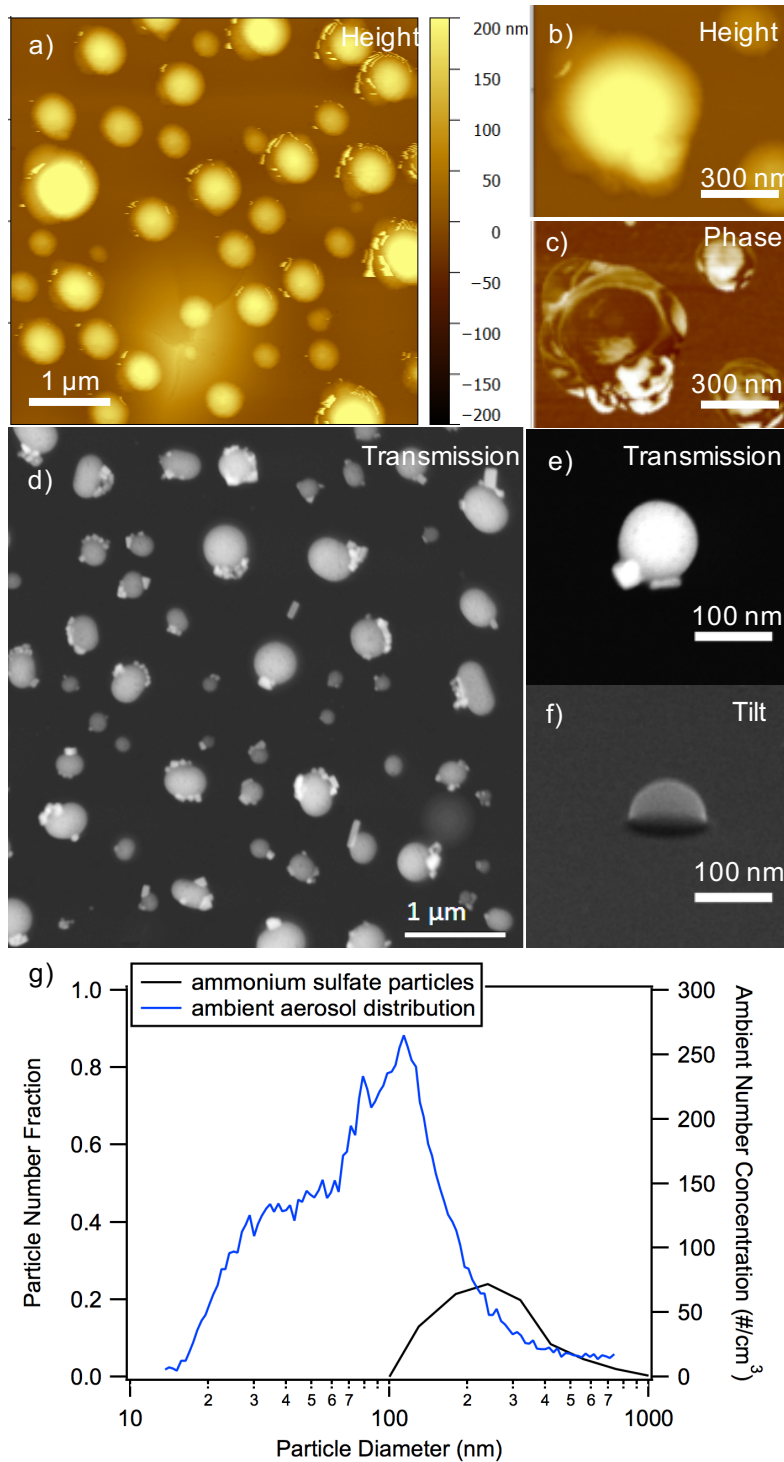
Figure 7.1 AFM a-b) height and c) phase images demonstrating the unique morphology of the observed ammonium sulfate particles. SEM d-e) STEM images and f) 75 ˚ tilted image further demonstrating the morphology of these particles. g) size-resolved relative number fraction of the ammonium sulfate particle type, compared to a representative ambient aerosol size distribution from September 07, 2015.
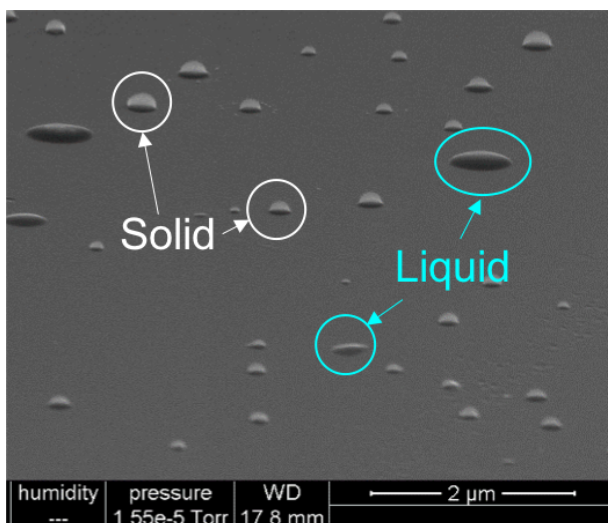
Figure 7.2 75˚ tilted SEM image demonstrating the presence of the solid particle type, circled in white, and other liquid particle types, circled in cyan.
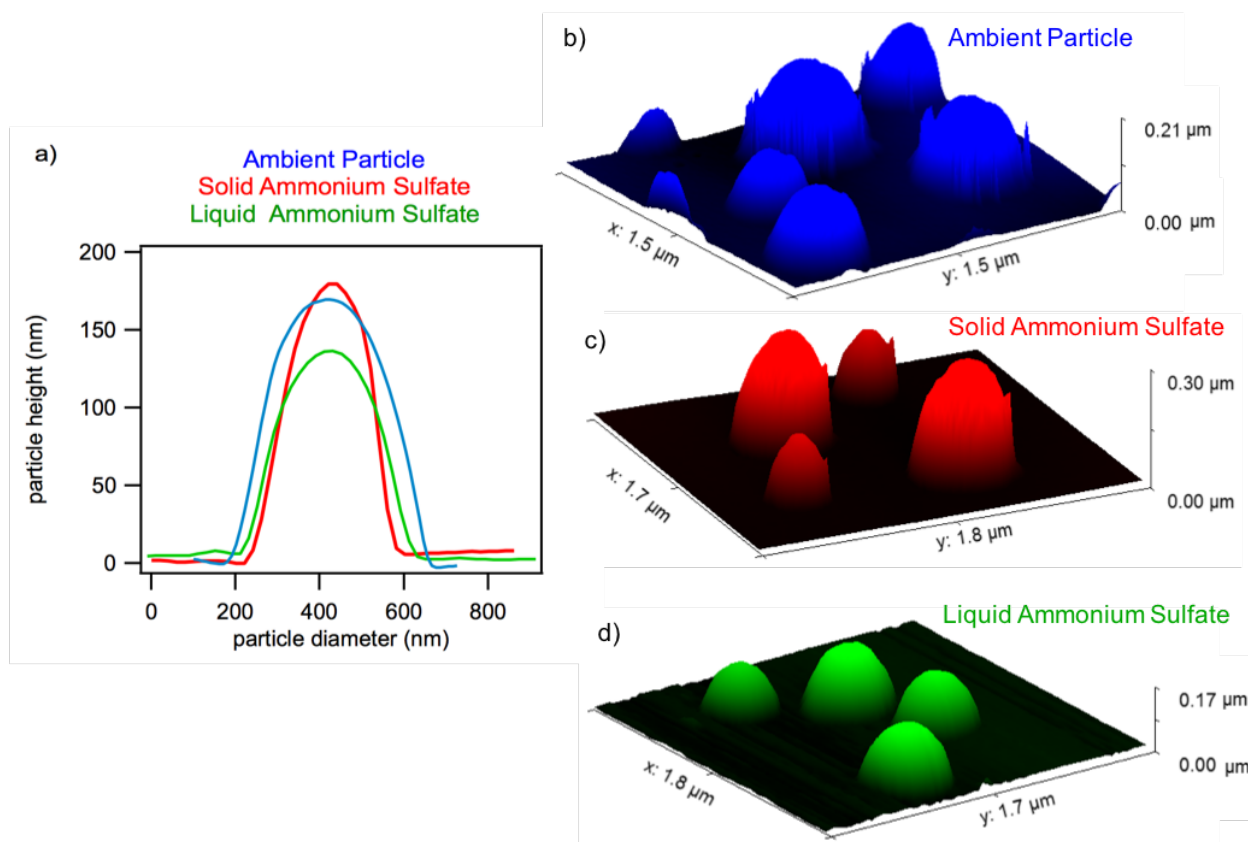
Figure 7.3 a) average AFM height traces for ambient particles, solid ammonium sulfate, and liquid ammonium sulfate particles. AFM three-dimensional height profiles for b) ambient particles, c) solid ammonium sulfate, and e) liquid ammonium sulfate particles.

7.3.2 Chemical Composition and Phase Separation

In order to understand the possible factors contributing to the observed morphology and phase, the chemical composition of the individual particles was determined. SEM coupled with energy dispersive X-ray spectroscopy (SEM-EDX) identified carbon, oxygen, and sulfur in the individual particles (Fig. 7.4, Fig. 7.5), indicative of sulfate and organics. Notably, these particles were extremely sensitive to the electron beam, characteristic of ammonium sulfate (Veghte et al., 2014). Scanning transmission X-ray microscopy with near-edge X-ray absorption fine structure (STXM-NEXAFS) spectra of individual particles over the sulfur L-edge confirmed the presence of sulfate (S(VI)) in the particles (Fig. 7.6) (Hopkins et al., 2008). In order to further characterize the chemical composition of the individual particles, AFM coupled with photothermal infrared spectroscopy (AFM-IR) was used to identify functional groups present in particles smaller than the optical diffraction limit (Bondy et al., 2017a; Dazzi et al., 2012). AFM-IR analysis of individual particles identified ammonium sulfate, with characteristic $\nu(SO_4^{2-})$ and $\partial(NH_4^+)$ modes at 1082 cm^{-1} and 1420 cm^{-1}, respectively (Bondy et al., 2017a; Cziczo and Abbatt, 1999), and a $\partial(OH)$ mode at 1726 cm^{-1} (Cziczo and Abbatt, 1999) (Fig. 7.4). Notably, the location of an ammonium $\partial(NH_4^+)$ mode at 1420 cm^{-1} is consistent with solid ammonium sulfate (Cziczo and Abbatt, 1999), from studies of efflorescence. AFM-IR analysis also indicated trace organic species were present in the particles, with peaks at 1098 cm^{-1} and 1260 cm^{-1} corresponding to $\nu(CO)$ modes (Larkin, 2011) (Fig. 7.4).
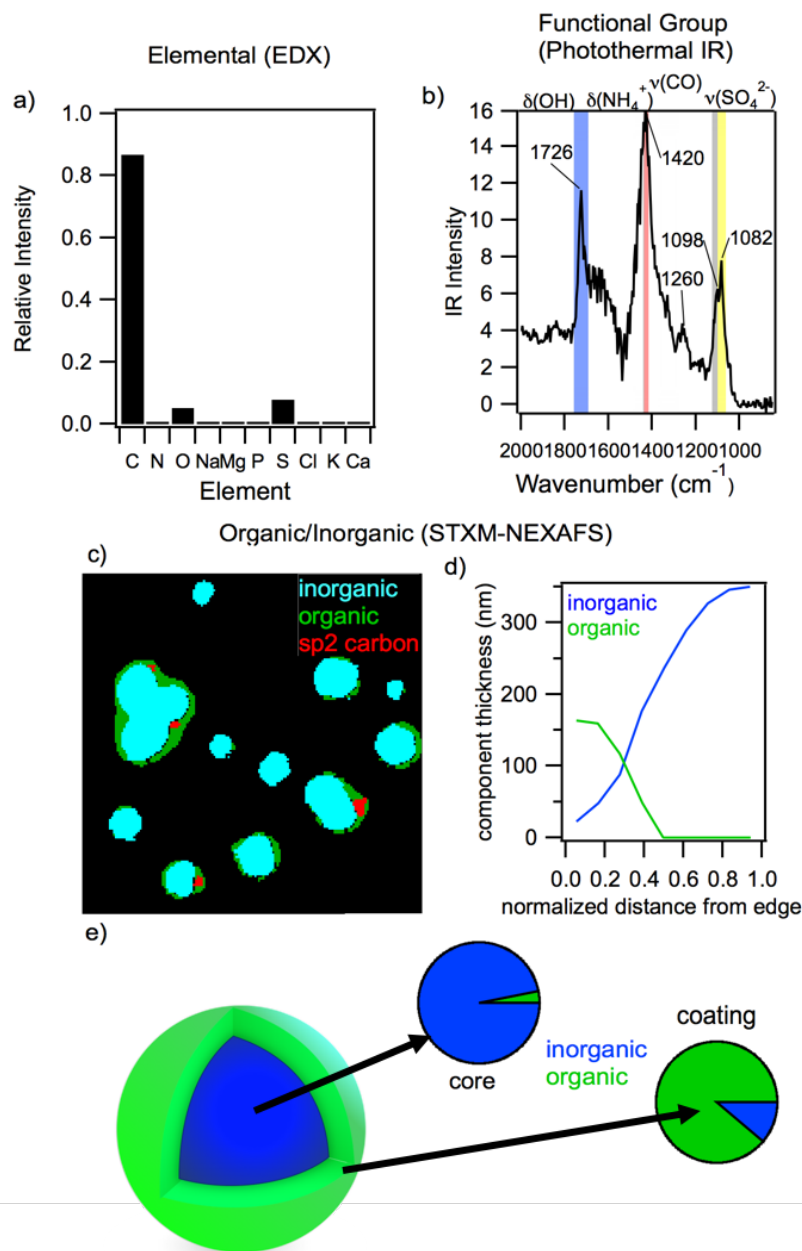
Figure 7.4 a) average EDX spectrum for the ammonium sulfate particle type b) representative AFM-IR spectrum of an ammonium sulfate particle. c) STXM-NEXAFS map showing the distribution of inorganic (blue), organic (green), and sp2 carbon (red) within individual sulfur-rich particles. d) average organic and inorganic fractions for the coating and core regions of sulfur-rich particles determined by STXM-NEXAFs. e) Distribution of inorganic and organic thickness from coating to core of a representative ammonium sulfate particle, determined by STXM-NEXAFS.
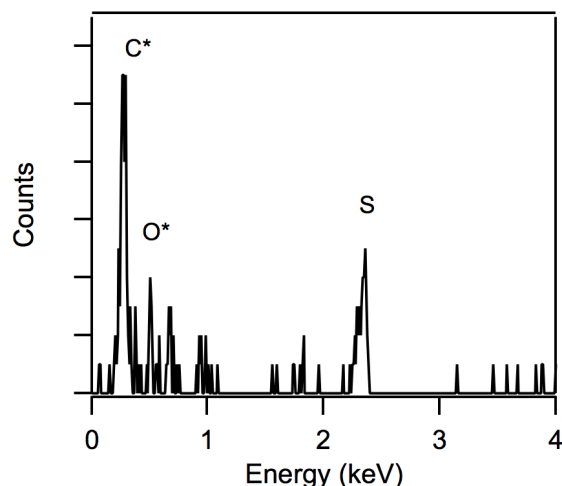
Figure 7.5 Raw EDX spectrum of a solid particle containing carbon, oxygen, and sulfur. *C and O peaks contain some signal from the substrate background.
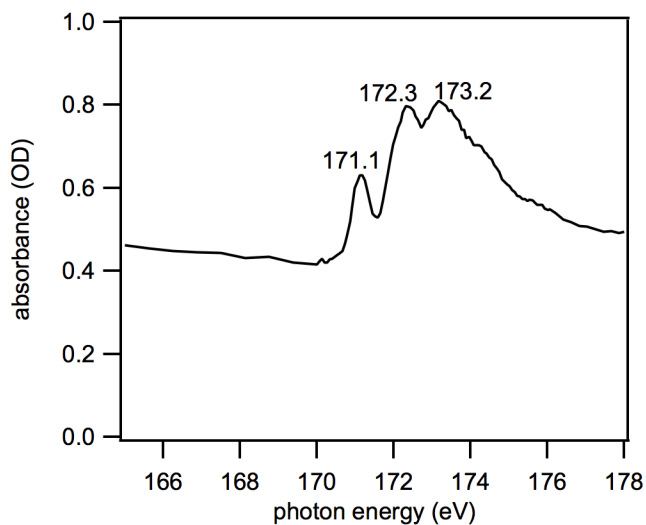
Figure 7.6 Representative STXM-NEXAFS spectrum collected over the sulfur L-absorption edge of an individual solid ammonium sulfate particle. Peaks at 171.1, 172.3, and 173.2 eV are characteristic of sulfate (S(VI)) (Hopkins et al., 2008).

Trace organic compounds will impact particle phase (Dong and Yu, 2003) and physical properties of the ammonium sulfate particles, including deliquescence, efflorescence, and crystallization (Baustian et al., 2010; Nie et al., 2017; Pearson and Beyer, 2015; Wang et al., 2017a; Van Wyngarden et al., 2015; Xu et al., 2002; Zawadowicz et al., 2015). The presence of organics in the ambient particles was confirmed by STXM-NEXAFS mapping over the carbon K-edge, which showed organic components coating the primarily inorganic particles (Fig. 7.4). sp^2 carbon inclusions were also observed on the organic/inorganic interface (Fig. 7.4), indicative of material

not soluble in the organic phase and further demonstrating the complex multiphase nature of these particles. Organic volume fractions within the individual particles were determined based on the STXM-NEXAFS data, and by partitioning the particle area into < 50 % and > 50 % organic volume fraction regions, two distinct phases were defined, an organic coating (89 % organic, 11 % inorganic) and an inorganic core (3 % organic, 97 % inorganic) (Fig. 7.4). The thickness of the inorganic and organic component from the edge to center of each particle was determined based on the organic volume fraction, further demonstrating the presence of an organic dominant coating (100 – 150 nm thickness) and inorganic dominant core (Fig. 7.4).

The observed relative humidity during ambient sampling (77 – 94 %) is within the range where ammonium sulfate is expected to deliquesce (Xu et al., 2002), but the ambient temperature was near 0 ˚C for the duration of aerosol sampling (Fig. 7.7). The solubility of organic components decreases with temperature (Brooks et al., 2002), therefore the observed organic coatings may inhibit water uptake at the observed temperatures (–3˚ – 10 ˚C). The liquid water content of these particles was estimated using ISORROPIA to be on the order of $0.1\,\mu g\ m^{-3}$, which is ~5 – 50 times lower than observations in midlatitude and tropical coastal locations (Deetz et al., 2018; Fajardo et al., 2016; Kuang et al., 2018; Nguyen et al., 2016). Recent work by Slade et al. (2019) suggests temperature may be more important than relative humidity or aerosol liquid water content in predicting aerosol phase, with glassy aerosol more likely to exist at colder ambient temperatures, consistent with the observed sampling conditions during this study (Fig. 7.7). The organic component likely has a higher glass transition temperature than the inorganic component (Dette and Koop, 2015). The viscous particles observed in Slade et al also had greater organic fractions compared to sulfate and were observed under "cleaner" air mass conditions, which may be comparable to Arctic aerosol concentrations. Oligomerization of less hygroscopic species in the organic coatings would increase the glass transition temperature (Slade et al.). The observed organic coatings may play a role in the particle morphology by providing structure. A viscous organic shell may enable salt inclusions by inhibiting salt diffusion through the organic layer (Ciobanu et al., 2009), causing salt inclusions to remain in the organic phase after separation (Bertram et al., 2011; Ciobanu et al., 2009; Gorkowski et al., 2017), and allowing crystals to form at the particle edge. Similar irregular morphologies have been observed in the laboratory for mixed ammonium sulfate and low solubility organic particles (Veghte et al., 2014).
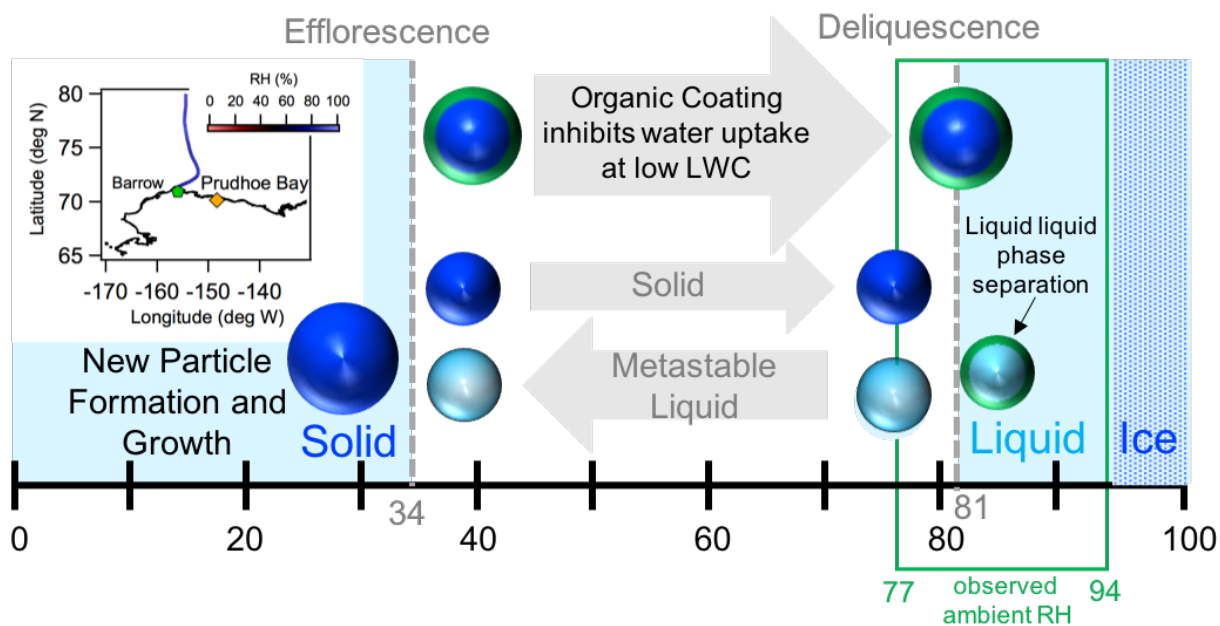
Figure 7.7 Ammonium sulfate phase diagram for the observed ambient temperatures (near 0 ˚C), with a representative backwards air mass trajectory for the September 07, 2015 sample, showing marine influence. At the observed ambient relative humidities (RH) at the sampling location and along the air mass trajectory, particles would be expected to be in a liquid or metastable liquid phase. At higher RH (> 95 %), an ice phase may be present. Particles are not expected to be solid above 81% RH without influence of the organic coating inhibiting water uptake.

7.3.3 Proposed Sources and Formation Mechanisms

The ammonium sulfate particles are expected to be secondary aerosol formed by the reaction of atmospheric ammonia with sulfuric acid. Large regional growth events were observed during this summer sampling period at Eureka and Alert in the Canadian Arctic (Tremblay et al., 2019), suggesting a particle formation and growth mechanism for these particles, though local growth events were not common during this study. Particle growth events are common in the summer Alaskan Arctic from both marine and anthropogenic sources (Kolesar et al., 2017) and ammonium sulfate is a key component of new particles (Giamarelou et al., 2016). Previous work has shown ammonia emissions from sea birds contribute to Arctic new particle formation (Croft et al., 2016), which could be driven by neutralization reactions with ammonium sulfate (Tremblay et al., 2019). Cloud processing is also a possible formation pathway for ammonium sulfate via SO_2 aqueous oxidation and NH_3 at low concentrations (Boone et al., 2015; Easter and Hobbs, 2002) and ammonium enhancement has been observed in cloud residuals (Schneider et al., 2017) with higher concentrations at lower temperatures. While the region was cloudy or mostly cloudy throughout the duration of study, according to MODIS satellite imagery, the cloud base height was

typically quite high; only eight sample periods had a cloud base lower than 1.5 km, and five samples occurred when clouds were lower than 1.1 km, unlikely to have influenced the observed particles. The lack of cloud processing influence further supports these solid particles forming due to new particle formation and growth of secondary aerosol, rather than aqueous oxidation producing liquid droplets. The observed morphology and phase could be also due to transformations during transport to the sampling location. Previous studies have proposed mechanisms for humidity-induced phase transitions during updraft and adiabatic cooling (Berkemeier et al., 2014). The ambient relative humidity for air mass influences $0 - 120$ hours backwards from the sampling site was determined using the HYSPLIT model (Fig. 7.8). Within 120 hours, the particles never experienced RH values near or below the efflorescence point (34 % RH). In fact, the RH was nearly always greater than 60 % and all samples experienced periods of greater than 80 % RH, above the deliquescence point (Fig. 7.8). This suggests phase transition due to RH cycling during transport was unlikely. The prevalence of regional scale growth events and the formation of solid ammonium sulfate particles during these processes, acquiring organic coatings, and persisting in the ambient atmosphere, should be explored further.

The greatest abundance, by number fraction, of the sulfur-rich particle type was observed under marine air mass influence from the Arctic Ocean, which was the dominant air mass type during the study (Gunsch et al., 2017). Methanesulfonic acid was present in the submicron range but contributed only $5 - 15$ % of total submicron sulfur species. Ammonium concentrations were not above the limit of detection for supermicron PM_{10} samples but were present in submicron PM_1 samples. Quinn et al. (2002) shows ammonium contributes < 1 % on average of supermicron aerosol mass. Chloride to sodium ratios were very close to the seawater ratio of 1.12 (Pilson, 2013), indicating that submicron sulfate was mixed with ammonium or other species rather than sea salt, consistent with Gunsch et al. (2017) for marine air masses. Sulfur isotope mass spectrometry showed that the non-sea salt sulfate fraction, after accounting for MSA, had a $\partial^{34}S$ value between $8 - 12$ ‰, suggesting a mix of sources, such as mineral dust or fossil fuel combustion, for the remaining sulfate fraction (Calhoun et al., 1991; Harris et al., 2012b, 2012c, 2012a, 2013; Norman et al., 1999). This suggests that while the observed ammonium sulfate particles are likely of marine origin, they are not a result of dimethylsulfide oxidation to methanesulfonic acid.
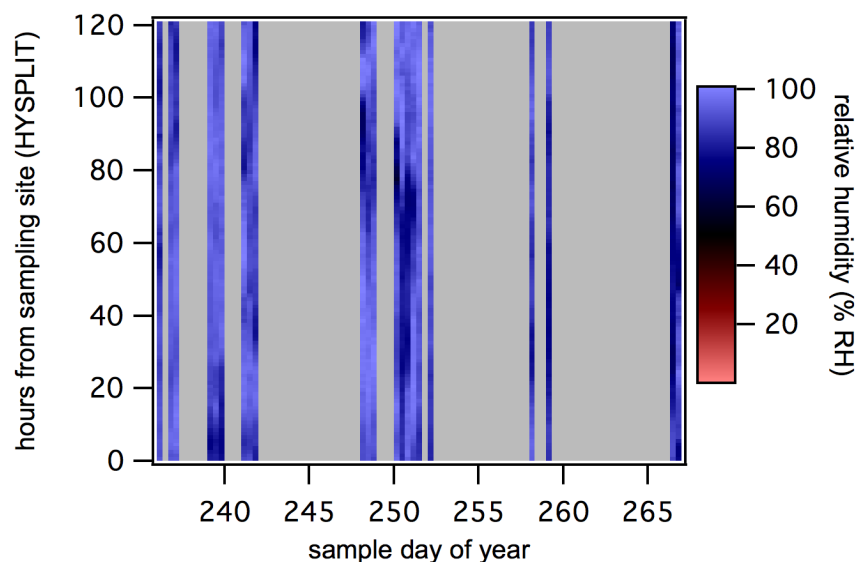
Figure 7.8 Ambient relative humidity, determined by HYSPLIT, from 0 – 120 hours backwards from the sampling site for each aerosol sampling period.

7.4 Conclusions

The observation of ammonium sulfate particles with complex composition and phase in the Arctic boundary layer has significant implications for regional atmospheric chemistry, cloud formation, and climate processes. The unexpected phase of these solid, organic-coated particles will affect climate-relevant particle properties, including water uptake, CCN efficiency and INP activity, gas partitioning, reactivity, and optical properties (Ruehl and Wilson, 2014; Schill and Tolbert, 2013). Sources, formation mechanisms, and particle history of solid and phase separated particles in the ambient atmosphere are not well understood or constrained in climate models. Recent incorporation of SOA viscosity into climate models has shown SOA is mostly liquid or semisolid in the boundary layer, and glassy particles mostly exist in the upper troposphere (Shiraiwa et al., 2017), while we demonstrate organic species contribute to solid particles found lower in the boundary layer under summertime Arctic conditions with low temperature and high relative humidity. While the observed particles may be formed through new particle formation and growth, the chemical mechanisms driving these processes in the summertime marine Arctic are not well characterized, despite playing an important role in atmospheric chemistry and climate feedbacks. Further understanding of the importance of temperature, relative humidity, liquid water content, and chemical composition on aerosol phase is necessary to constrain aerosol – cloud – climate feedbacks, particularly in the Arctic boundary layer.

7.5 Acknowledgements

Chapter 8. Conclusions and Future Directions

8.1 Conclusions

Aerosol impacts on climate are dependent on the chemical composition and properties of individual particles. In the high albedo Arctic environment, aerosol impacts on clouds can greatly influence the radiative budget; therefore, it is important to determine CCN and INP sources and composition. However, the physicochemical mixing state of atmospheric particles has not been well characterized, particularly in the Arctic, due to analytical challenges of measuring individual particle composition and logistical challenges of measurements in cold, dark, and remote environments. This dissertation focused on applying a multimodal microspectroscopic approach to characterization of Arctic aerosol mixing state under different conditions to better understand climate-relevant aerosol properties. These findings improved our understanding of Arctic aerosol processes and provide motivation for future studies.

SSA, as the largest aerosol flux to the troposphere, is an important climate driver in remote regions, including the Arctic. In Chapter 2, the factors controlling SSA production under cold conditions were investigated using a laboratory seawater generation experiment, demonstrating complex interactions of seawater temperature, salinity, and biological activity on SSA production and composition. Previous studies have not converged regarding the magnitude or direction of temperature, salinity, and biological effects on SSA production. For cold seawater collected from the Gulf of Maine, we observed temperature to be more important than dissolved organic carbon content for driving SSA production, with increased SSA concentrations observed at colder temperatures. The influence of seawater biology was observed in individual SSA composition, with enrichment of saccharides and aliphatic organics in the SSA particles.

In Chapter 3, aerosol composition and mixing state in the wintertime coastal Arctic was characterized, observing SSA to be the dominant particle type present and that all observed sulfate was internally mixed with SSA or organic aerosol, demonstrating influence of Arctic haze and Prudhoe Bay oil field emissions and interactions with natural aerosol. In Chapter 4, the source of the wintertime SSA was determined to be open sea ice leads present in January – February in the Alaskan Arctic, based on the chemical composition of these SSA particles and air mass influence.

143

Wintertime SSA from open leads were greatly enriched in organics compared to summertime SSA from the same location with open water nearby. These organic coatings were comprised of saccharides, fatty acids, and amino acids, consistent with EPS produced by sea ice algae and bacteria, suggesting a unique wintertime marine organic source in sea ice leads.

In Chapter 5, the influence of sea ice microbiology on nascent SSA composition was investigated for locally-produced SSA from open leads in the summertime high Arctic, suggesting local aerosol sources may contribute to summer high Arctic cloud formation. Increased SSA concentrations were observed under high wind conditions and air mass influence from over open leads, compared to high wind conditions with air mass influence only over pack ice. SSA were enriched in organic compound classes consistent with EPS from sea ice algae and bacteria present in the open leads. While previous studies have observed the influence of EPS and marine gels on <100 nm particles, these observations demonstrate the influence of sea ice microbiology on accumulation mode and coarse mode SSA, with implications for CCN and INP activity in the high Arctic.

Chapter 6 describes summertime aerosol mixing state in the Alaskan Arctic, demonstrating the influence of marine biogenic, anthropogenic, and terrestrial emissions. Greater organic enrichment of SSA was observed in the biologically productive Bering Strait, compared to the Chukchi Sea marginal ice zone. Organic aerosol, ammonium sulfate, and soot particles were observed in the Bering Strait, due to terrestrial and anthropogenic influences. In Chapter 7, organic-coated ammonium sulfate particles, collected in the summertime coastal Alaskan Arctic, exhibited unique physical properties that were further examined using AFM and AFM-IR analyses. The viscous phase and organic coatings on the ammonium sulfate particles likely impact reactivity and water uptake. Particle phase affects climate relevant properties including CCN efficiency, INP activity, and optical properties. Further studies are needed to determine the formation mechanisms of these complex particles.

Overall, the work presented in this dissertation provides a significant advancement in our understanding of aerosol composition in the changing Arctic. Two major themes are present throughout the research presented: 1) increasing marine emissions and anthropogenic development are impacting Arctic aerosol composition, and 2) temperature, salinity, and marine biology are driving sea spray aerosol production and composition in cold environments, specifically the Arctic. The changing sources influencing aerosol physicochemical mixing state and particle properties

were investigated for the wintertime (Chapter 3) and summertime (Chapters 6 and 7) Alaskan Arctic. The influence of both marine biogenic and anthropogenic aerosol sources were observed in both seasons, and notable findings included the observation of internally mixed organic+sulfate particles in the winter and summer, with some summertime organic coated ammonium sulfate particles demonstrating unexpected physical properties. The factors driving SSA production and composition in cold environments were investigated in Chapters 2, 4, and 5, for the wintertime North Atlantic, wintertime coastal Arctic, and summertime high Arctic, respectively. For laboratory SSA generation experiments conducted with Gulf of Maine seawater, temperature was determined to be as important as marine biology for impacting SSA production. However, the composition of individual SSA particles were influenced by marine organics, observed as organic coatings, for all three environments. The composition of these organic coatings was dominated by saccharides for both North Atlantic and Arctic SSA, and both wintertime and summertime SSA organics showed signatures of sea ice algae and bacteria EPS, demonstrating a unique source of marine organics transferred to the particle phase.

Understanding the processes driving aerosol chemistry and climate impacts is critical for predicting atmospheric chemistry and climate feedbacks in the New Arctic. The response of natural and anthropogenic trace gas and aerosol emissions to sea ice decline remains uncertain. Marine biogenic emissions are expected to increase in an ice-free Arctic and increasing development may have a great impact on the Arctic climate. Additionally, aerosol production from snow and ice surfaces remains unconstrained, leading to uncertainties in predicting the influence of these sources with declining sea ice. Uncertainties also remain regarding aerosol-cloud-climate feedbacks, as the sources and composition of Arctic CCN and INP are not well understood. This dissertation contributes further understanding of Arctic aerosol sources, composition, and mixing state in multiple seasons and regions. However, further studies are needed in order to characterize climate-relevant aerosol properties across the Arctic, incorporating seasonal and spatial variability. These aerosol processes must be constrained in climate models for better prediction of future Arctic conditions.

8.2 Selection of Substrates for Multimodal Microspectroscopic Analyses

With a multimodal analysis approach, inevitably each technique is best suited for analysis from a specific substrate. However, it is often the case with ambient aerosol data that the desired analysis techniques are not determined until after sample collection and initial analysis. Through

the work described in this dissertation, many different substrates were tested in order to maximize versatility of use with different aerosol impactors, compatibility with multiple analysis techniques, and best data quality. The key traits of each analysis technique discussed herein have been described elsewhere (Ault and Axson, 2017); therefore, this summary focuses on the substrates themselves and the data that can be collected from them. Table 8.1 lists the substrates used in this dissertation and recommendations for use with the considered analysis techniques, including compatible, usable with caveats, or usable but not recommended, and incompatible substrates. In Fig. 8.1, example SEM images of SSA particles are shown collected on silicon, aluminum foil, and TEM grid substrates.

Table 8.1 Substrates for microspectroscopic analysis of individual particles.

Substrate	Compatible with						Best for
	SEM-EDX	CCSEM	TEM-EDX STXM-NEXAFS	Raman	AFM	AFM-IR	
TEM grid	(Compatible)	(Compatible)	(Compatible)	(incompatible)	(With caveats)	(Not recommended)	CCSEM, TEM-EDX (best contrast)
Silicon wafer	(Compatible)	(With caveats)	(incompatible)	(Not recommended)	(Compatible)	(Compatible)	SEM-EDX for carbon, AFM-IR
Quartz chip	(incompatible)	(incompatible)	(incompatible)	(Compatible)	(incompatible)	(incompatible)	Raman
Aluminum foil	(Compatible)	(With caveats)	(incompatible)	(With caveats)	(incompatible)	(incompatible)	Versatility, cost conscious
Metal tapes	(Compatible)	(With caveats)	(incompatible)	(With caveats)	(incompatible)	(incompatible)	Versatility, use with DRUM impactor

Legend: Compatible (green) | With caveats (yellow) | Not recommended (orange) | incompatible (red)

Copper TEM grids, with very thin carbonate polymer Formvar films, provide the best contrast for SEM-EDX, TEM-EDX, and CCSEM analysis of all particle types, including organic particles, with minimal background interference (Fig. 8.1c). However, there is carbon and oxygen background signal from the films in the EDX spectra, making chemical characterization of organic particles challenging and non-quantitative. TEM grids are the only substrate that can be used for TEM-EDX and STXM-NEXAFS analyses. Due to interference from the Formvar film, and

difficulties for mounting and focusing, TEM grids cannot be used for Raman analysis. Handled with care, AFM imaging can be conducted off a TEM grid mounted on a metal puck, but the Formvar film overwhelms AFM-IR signal. AFM-IR spectra can be collected from the copper grid bars, but this irregular surface does not provide good AFM imaging. TEM grids are extremely delicate, and the more they are handled the greater the risk of bending, tearing, or otherwise damaging the grid. Due to how fragile these substrates are, use with the DRUM impactor is not recommended due to damage that can occur during drum rotation. An advantage of these thin copper Formvar grids is reference grid numbers to identify locations on the substrate, but thicker copper or nickel Formvar grids could be considered in the future for a more robust substrate. Lacey TEM grids, rather than a whole film, could also be considered to reduce EDX signal from the substrate film. However, impaction onto lacey grids will alter the morphology of liquid particles.
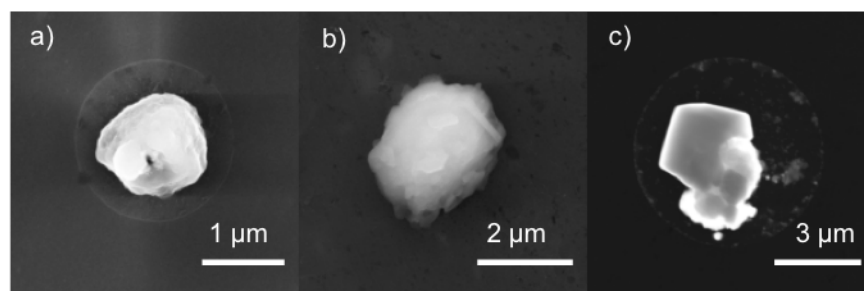
Figure 8.1 Representative SEM images of SSA particles collected on a) silicon (MOCCHA 2018), b) aluminum foil (Utqiaġvik, summer 2015), and c) TEM grid (Oliktok, summer 2016).

For quantification of carbon in particles and characterization of organic particles, silicon substrates can be used for SEM-EDX and CCSEM. Silicon does not provide as good of contrast for CCSEM analysis as TEM grids. The silicon substrate is "gray", so when selecting brightness/contrast thresholds for CCSEM, only particles brighter than the substrate (e.g. SSA, dust) or darker (e.g. organic particles) can be detected at one time. This likely means that organic particles will be undercounted or not detected when setting thresholds for an ambient sample. However, organic coatings around salt particles can be more visible on silicon that TEM grids (Fig. 8.1b). Silicon is also an ideal flat surface for AFM imaging and provides no interference for AFM-IR analysis. Silicon is a very versatile substrate, providing a compatible surface for ToF-SIMS and nano-SIMS analysis as well, for example. Silicon has peaks in relevant regions for Raman analysis, however, including a flat peak at $\sim 900 - 1000$ cm^{-1} in the sulfate stretching region, so Raman analysis from silicon substrates is not recommended.

147

While quartz is not a very versatile substrate, it is best suited for Raman analysis. Quartz is "transparent" to Raman and therefore does not give any background signal in the regions of interest. Collection of fluorescence spectra and fluorescence mapping can also be conducted with the Raman microscope, however, this also requires quartz, as a non-fluorescing substrate. A sample on quartz could be spin coated with gold to provide a conductive surface for SEM analysis; however, this would permanently alter the sample and interfere with EDX analysis, so is not recommended. Quartz is not a sufficiently flat surface for AFM analysis.

Aluminum foil is a cheap, versatile substrate that can be used for SEM-EDX analysis (Fig. 8.1a). However, aluminum foil has the same contrast issues as silicon, has many surface features, and is difficult to keep flat, making CCSEM analysis challenging. Surface features are often detected as particles, meaning a large amount of background or "junk" data must be thrown out. Raman analysis can be conducted from aluminum foil, if the substrate is mounted sufficiently to remain stable. However, fluorescence can be much worse from aluminum foil substrates, making Raman analysis very challenging, if not impossible, for some samples. Due to the rough surface and flimsy nature of foil, it cannot be used for AFM imaging. Metal tapes, including aluminum tape and copper tape, have similar traits to aluminum foil, but are well-suited for use with the DRUM impactor. These tapes are cheap, easy to mount, and microscopy-grade tapes provide a much smoother, feature-free surface for imaging than aluminum foil. However, these tapes can be degraded by acidic particles.

Regardless of the substrate chosen, different particle types are better detected by manual or CCSEM analyses, so care must be taken when setting up CCSEM to reduce these biases. For example, CCSEM cannot determine physicochemical mixing state or complex morphologies, while this information is extremely valuable during manual analysis to characterize particle types and sources (e.g. aged soot or biological particles), particularly for less common particle classes (Eriksen Hammer et al., 2019). However, the greater statistics collected by CCSEM provide a more representative characterization of the prevalent particle types in the sample (Willis et al., 2002). For CCSEM, brightness/contrast thresholds must be carefully chosen to ensure accurate detection of particle size and morphology, including not grouping multiple particles together or omitting particle protrusions or halos (Eriksen Hammer et al., 2019).

When selecting substrates, compromises may be made based on the impactor used. The MPS can only collect particles on one substrate per stage, therefore, versatile substrates including silicon

or aluminum foil may be chosen. The MOUDI, miniMOUDI, and DRUM impactors can collect on multiple substrate per stage, allowing for more versatility. The rotating MOUDI ensures even particle distribution across all substrates without overloading the sample; however, a non-rotating MOUDI or miniMOUDI will still distribute particles evenly on different substrates based on the multiple orifice, uniform deposition design. The DRUM impactor also has rotating stages, but this rotation is temporal, rather than spatial, so multiple substrates must be aligned along the length of the slit to simultaneously collect particles. The DRUM impactor provides automated collection of temporally resolved particle samples, while the other impactors provide samples collected over discrete time periods.

Sample storage and analysis conditions can also inherently change the particle composition and morphology. SEM and TEM analyses are conducted under vacuum, so the particles are imaged "dry" and some volatile components may be lost (Laskina et al., 2015). AFM and Raman analyses are conducted at ambient temperature and pressure, so particles may be imaged at closer to their atmospheric state, but particle phase and morphology is dependent on the ambient RH during analysis (Laskina et al., 2015). Samples stored frozen will reduce risk of compositional change, degradation, or loss of volatile components prior to analysis. However, freezing and thawing samples has been shown to change particle phase and morphology, and lead to water condensation (Laskina et al., 2015). Therefore, the preferred method is to store samples sealed, in the dark, and at a relative humidity and temperature similar to that in which they were collected (Laskina et al., 2015). Since impactors are typically located indoors during sampling, the recommendation is to store samples at room temperature, even if collecting in the wintertime. Samples have been shown to remain stable for several months stored in this manner, though particles will degrade with time, so prompt analysis is recommended whenever possible.

8.3 Future Directions

8.3.1 High Arctic Aerosol Mixing State and Climate Impacts across Seasons

Large knowledge gaps remain in our understanding of high Arctic aerosol sources, composition, and climate properties, particularly across seasons. There have been very few measurements of particle composition in the fall – spring high Arctic due to logistical challenges. However, understanding the seasonality of single particle composition, mixing state, and aerosol – cloud – climate interactions in the high Arctic is critical for understanding climate processes in

the rapidly changing region. During 2019 – 2020, particle samples will be collected aboard the icebreaker *Polarstern* as part of the yearlong Multidisciplinary drifting Observatory for the Study of Arctic Climate (MOSAiC) research expedition in the high Arctic. These samples will provide valuable information about high Arctic aerosol, including the seasonality of lead-based SSA production and marine biology influences on aerosol chemistry in the high Arctic.

Further analysis of samples collected during the 2018 MOCCHA campaign will build upon the findings shown in Chapter 5 and advance knowledge of marine biogenic influences on summertime high Arctic aerosol. Several MART experiments were conducted to investigate the impacts of seawater temperature, biology, and salinity on high Arctic SSA production. In addition to single particle analysis for particle composition and mixing state, samples were collected for INP analysis in order to understand the climate-relevant properties of high Arctic nascent SSA. Comparison of these experiments to ambient aerosol observations will improve understanding of the role of local SSA production in driving Arctic aerosol – cloud – climate processes, as well as the contribution of sea ice microbiology to SSA composition. Ambient particle samples were also collected behind a counterflow virtual flow inlet to sample cloud droplet and fog residues. Characterizing the composition of particles found in cloud and fog will improve understanding of CCN sources in the high Arctic.

Analysis of additional ambient particle samples from MOCCHA will also determine the sources and composition of high Arctic aerosol under different meteorological conditions (high winds, stagnant conditions, clear skies, cloudy, foggy, during freeze up) throughout the campaign. In particular, the processes driving new particle formation (NPF) and growth events in the high Arctic are not well understood, but observations from MOCCHA suggest sea ice freeze up to be associated with NPF. During a large NPF and growth event, ammonium sulfate particles with similar morphology to those described in Chapter 7 were observed. Detailed analysis of the composition, morphology, and phase of these particles may advance understanding of the processes driving these NPF and growth events and connections to freeze up events. As the particles observed in Chapter 7 exhibited unique phase and morphology considering the ambient conditions at collection, laboratory studies of the phase of organic coated ammonium sulfate particles as a function of relative humidity and temperature may also improve understanding of the processes driving the formation of these particles and the ambient conditions under which particles with these unique properties may occur.

The potential role of sea ice melt ponds, pools of melted water on top of sea ice, in ocean – atmosphere interactions is not understood. In a rapidly warming Arctic, the frequency of melt ponds may increase. As a potential wind-driven aerosol source, these melt ponds are a unique environment, with low salinity but potentially distinct biological activity (Zhang et al., 2019). Ambient aerosol samples and aerosol generation experiments were conducted with melt pond water from the Alaskan Arctic during a research expedition aboard the icebreaker *Araon* in 2017, and a MART experiment was conducted with high Arctic melt pond water during the 2018 MOCCHA campaign. Analysis of particle samples collected from these experiments, in comparison to the ambient particles, may provide unique insights into the influence of melt pond biology on particle composition and climate relevant properties of aerosol produced from a potential melt pond source. Additionally, field measurements are needed to determine the potential aerosol flux from melt ponds, by monitoring bubble production and eddy covariance fluxes as has been done for open leads (Held et al., 2011; Nilsson et al., 2001; Norris et al., 2011).

8.3.2 Alaskan Arctic Aerosol Mixing State Across Seasons

Many previous studies have focused on aerosol composition in the spring Arctic during Arctic haze season. However, few single particle studies have been conducted in the past 20 years to determine aerosol mixing state during this season. In this time, conditions have drastically changed, with rapidly declining sea ice and changing midlatitude pollution sources, in addition to increased Arctic development. Bulk aerosol studies have shown concentrations of non-seasalt sulfate have decreased 30 – 70% during this time, and an increase in light scattering aerosol has been observed (Quinn et al., 2007). Particles were collected during March – May, 2016 at Utqiaġvik, Alaska for offline analysis of single particle composition and mixing state. Analysis of these samples will provide characterization of current springtime Arctic aerosol chemical composition, mixing state, sources, and processes.

To investigate the influence of increasing Arctic development on aerosol composition, samples were also collected at Oliktok Point, within the Prudhoe Bay oilfields, in August – September 2016 and March – May 2017. Influence of marine, terrestrial, and anthropogenic aerosol sources were observed in spring 2017, with marine and terrestrial particles contributing to INP, despite the highly polluted environment (Creamean et al., 2018a). Further single particle analysis of the spring and summer samples for aerosol composition and mixing state in this

polluted environment would determine the relative importance of anthropogenic, marine, and terrestrial sources for aerosol composition and climate-relevant properties.

Particle samples were also collected during the Aerosols in the Polar Utqiaġvik Night (APUN) study during November – December, 2018 at Utqiaġvik, Alaska. Few studies have characterized aerosol composition in the fall-winter, despite the potential importance of aerosol-cloud interactions on longwave radiation during this period, with no direct sunlight. As this period covers the fall freeze-up, it is important to understand the relative contribution of SSA, in addition to local-regional anthropogenic aerosol sources. By characterizing individual particle composition and mixing state during spring and fall, we will have a near-full picture of the seasonal trends in aerosol sources and composition on the Alaskan North Slope. Understanding these seasonal trends will allow for better predictions of aerosol – climate impacts in the changing Arctic environment.

Upon aging, soot becomes internally mixed with organics and sulfate (Raatikainen et al., 2015; Weinbruch et al., 2012, 2018; Xie et al., 2007), and the characteristic chainlike soot agglomerates often collapse within an organic/sulfate shell (Demirdjian et al., 2007; Jiang et al., 2011; Köllensperger et al., 1999; Lehmpuhl et al., 1999; Unga et al., 2018). This aged soot becomes difficult to distinguish from organic aerosol particles using CCSEM-EDX (Eriksen Hammer et al., 2019). However, identifying the presence of fresh and aged soot is important for determining particle light scattering or absorption (Fierce et al., 2016). Furthermore, determining how the morphology and mixing state of soot changes based on location, distance from sources, and season, will help inform climate impacts (Liu et al., 2017, 2015). Soot particles, either fresh or aged, were observed in many of the studies described herein, including sampling on the North Slope of Alaska for the following studies: Utqiaġvik 2014 (winter), Utqiaġvik 2015 (summer), Utqiaġvik 2016 (spring), Utqiaġvik 2018 (fall), Oliktok 2016 (summer), and Oliktok 2017 (spring). Figure 8.1 shows example SEM and TEM images of fresh soot particles observed during summer at Utqiaġvik. Based on preliminary analysis, fresh soot was observed at Utqiaġvik in spring and summer but not in winter, and at Oliktok during summer but not in spring, demonstrating a seasonal and location-dependent mixing state. Increased concentrations of soot at Utqiaġvik have been correlated with air mass influence from Prudhoe Bay (Gunsch et al., 2017). SEM-EDX analysis on silicon substrates would allow for carbon quantification; a S/C ratio could be used as a measure of soot aging by sulfate. Tilted SEM imaging from TEM grids can also show the three-dimensional particle morphology (Wang et al., 2016), as soot particles do not always

impact flat onto substrates (Fig. 8.2). STXM-NEXAFS analysis over the carbon k-edge would distinguish elemental carbon (soot) from organic carbon and inorganic species (sulfate), providing intraparticle composition and mixing state, as shown in Chapter 3 (Kirpes et al., 2018). Soot particles were also observed during sampling aboard the icebreaker *Araon* in 2016, 2017, and 2018; however, these samples were not collected under automated pollution control, so much of the fresh soot is likely from local ship influence. These samples could be used as a comparison for very fresh soot emissions, if necessary. A comparison could also be made between these Arctic studies and soot observed in midlatitude winter studies, including Ann Arbor 2016, Kalamazoo 2018, and Maine 2019.
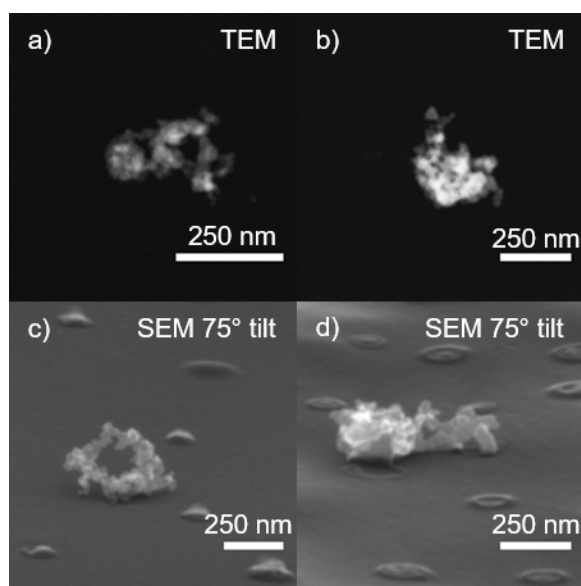
Figure 8.2 TEM images (a and b) and SEM images collected with a 75˚ tilted substrate (c and d) showing representative morphologies of fresh soot particles observed at Utqiaġvik in summer 2015.

8.3.3 Southern Ocean Aerosol Mixing State

In the Southern Ocean, SSA may play a similarly important role in aerosol – cloud – climate feedbacks as in the Arctic Ocean, with few other aerosol sources present (Tomasi et al., 2007). The Arctic and Antarctic are both high albedo environments with influence of local marine emissions and long-range transported aerosol; however, the Antarctic is more isolated from other terrestrial and anthropogenic sources, and can experience extremely low temperatures and high wind events across the continent (Bromwich and Wang, 2008). Alternative mechanisms of SSA production, including blowing snow and frost flowers, have been proposed as important sources of SSA in this region (Giordano et al., 2018; Hara et al., 2004, 2014). In 2018, samples were

collected aboard the icebreaker *Araon* during a Southern Ocean research cruise for offline single particle analysis. There have been few single particle measurements of aerosol composition and mixing state in the Southern Ocean (Eom et al., 2016; Hara et al., 2013, 2014; Ueda et al., 2018). In particular, the influence of marine organics on SSA composition in the Southern Ocean remains unknown (Eom et al., 2016).

8.3.4 Multiphase Reactions with Organic-Coated Chloride-Containing Aerosol

As single particle composition and mixing state are important for determining climate-relevant properties, including reactivity, organic coatings are known to inhibit uptake of trace gases (Ryder et al., 2015). Reactions between chloride-containing aerosol particles and N_2O_5 have been of great interest in the Arctic and in the midlatitudes recently, and these particles (SSA or road salt-derived particles) are likely to exhibit organic coatings, as described in Chapters 2,4,5, and 6. However, the impact of organic coating thickness on reactive uptake is not known (Ryder et al., 2015). This dissertation has demonstrated that SSA organic coatings can vary in thickness based on the SML composition and influence of sea ice biology (Chapter 4). A laboratory study to determine how specific coating thicknesses inhibit N_2O_5 uptake would improve parameterization of these atmospheric reactions and provide better understanding of these mechanisms in both the Arctic and midlatitude environments.

8.3.5 Method Development

Despite the advances in characterization of aerosol mixing state described in this dissertation, challenges still remain, in particular to characterize the composition and mixing state of submicron organic aerosol particles. In the Arctic, this additional knowledge will be crucial for understanding the influence of natural and anthropogenic organic aerosol sources, as well as contributions from primary or secondary marine organics. With SEM-EDX and TEM-EDX analyses, the elemental information provided is often not sufficient to determine organic particle composition and sources. STXM-NEXAFS can often provide complementary information regarding chemical bonding and oxidation states, but access to this technique is limited (Ault and Axson, 2017). While Raman microspectroscopy can provide detailed molecular information, submicron particles are below the diffraction limit and cannot be analyzed, and often, Raman spectra for ambient particles are so complex they are difficult to interpret (Ault and Axson, 2017; Craig et al., 2015). AFM-IR promises to provide detailed chemical characterization of submicron

particles, but additional instrumental and method development is required to improve data quality and speed of analysis (Ault and Axson, 2017; Bondy et al., 2017a). Continuing method improvement is also needed to enable analysis of smaller and thinner particles (Bondy et al., 2017a; Or et al., 2018). Recent developments in AFM-IR and AFM-Raman technologies look promising for continued advancement in this area.

Due to the complexity of ambient particle Raman data, spectral analysis could be improved by employing chemometric methods, including principal component analysis (PCA) or partial least squares (PLS) regression. While χ^2 analysis is a bivariate approach that assesses goodness of fit, PCA and PLS are multivariate methods that can better represent relationships between possibly correlated variables. Application of these statistical methods to single particle data can be challenging due to particle to particle variability in signal intensity, background influence, etc. However, development of these methods for application towards single particle data may be useful to discern the complexity of information provided by Raman analysis.

Comprehensive analysis of single particle composition and aerosol mixing state may also be achieved by coupling microscopic techniques, providing morphological and spatial information, with mass spectrometry methods for detailed chemical analysis. This can be achieved by employing both online mass spectrometry and offline microspectroscopy methods for the same study (Axson et al., 2016a; Gunsch et al., 2017; May et al., 2018b), or by utilizing spatially-resolved mass spectrometric imaging methods. ToF-SIMS has recently been applied to characterization of aerosol particles (Cheng et al., 2014; Chi et al., 2015; Dappe et al., 2018; Huang et al., 2017; Li et al., 2018; Sobanska et al., 2014, 2015; Takami et al., 2013; Tyler et al., 2012; Zhang et al., 2016), and nano-SIMS may be powerful methods for characterization of organics and sulfur species within submicron aerosol particles (Harris et al., 2012a, 2012c, 2013), to determine the composition and sources of primary and secondary organic aerosol.

155

Bibliography

Aliabadi, A. A., Staebler, R. M. and Sharma, S.: Air quality monitoring in communities of the Canadian Arctic during the high shipping season with a focus on local and marine pollution, Atmospheric Chemistry and Physics, 15(5), 2651–2673, doi:10.5194/acp-15-2651-2015, 2015.

Allen, H. M., Draper, D. C., Ayres, B. R., Ault, A., Bondy, A., Takahama, S., Modini, R. L., Baumann, K., Edgerton, E., Knote, C., Laskin, A., Wang, B. and Fry, J. L.: Influence of crustal dust and sea spray supermicron particle concentrations and acidity on inorganic NO3- aerosol during the 2013 Southern Oxidant and Aerosol Study, Atmospheric Chemistry and Physics, 15(18), 10669–10685, doi:10.5194/acp-15-10669-2015, 2015.

Alpert, P. A., Kilthau, W. P., Bothe, D. W., Radway, J. A. C., Aller, J. Y. and Knopf, D. A.: The influence of marine microbial activities on aerosol production: A laboratory mesocosm study, Journal of Geophysical Research, 120(17), 8841–8860, doi:10.1002/2015JD023469, 2015.

Alterskjr, K., Kristjnsson, J. E. and Hoose, C.: Do anthropogenic aerosols enhance or suppress the surface cloud forcing in the Arctic?, Journal of Geophysical Research Atmospheres, 115(22), 1–19, doi:10.1029/2010JD014015, 2010.

Alvarado, M. J., Lonsdale, C. R., MacIntyre, H. L., Bian, H., Chin, M., Ridley, D. A., Heald, C. L., Thornhill, K. L., Anderson, B. E., Cubison, M. J., Jimenez, J. L., Kondo, Y., Sahu, L. K., Dibb, J. E. and Wang, C.: Evaluating model parameterizations of submicron aerosol scattering and absorption with in situ data from ARCTAS 2008, Atmospheric Chemistry and Physics, 16(14), 9435–9455, doi:10.5194/acp-16-9435-2016, 2016.

Anderson, B. J., Musicant, D. R., Ritz, A. M., Ault, A., Gross, D. S., Yuen, M. and Gälli, M.: User-friendly clustering for atmospheric data analysis, Carleton College., 2005.

Anderson, J. R., Buseck, P. R., Saucy, D. A. and Pacyna, J. M.: Characterization of individual fine-fraction particles from the Arctic aerosol at Spitsbergen, May-June 1987, Atmospheric Environment Part A, General Topics, 26(9), 1747–1762, doi:10.1016/0960-1686(92)90072-S, 1992.

Andreae, M. O. and Rosenfeld, D.: Aerosol-cloud-precipitation interactions. Part 1. The nature and sources of cloud-active aerosols, Earth-Science Reviews, 89(1–2), 13–41, doi:10.1016/j.earscirev.2008.03.001, 2008.

Aranami, K., Watanabe, S., Tsunogai, S., Ohki, A., Miura, K. and Kojima, H.: Chemical assessment of oceanic and terrestrial sulfur in the marine boundary layer over the Northern North Pacific during summer, Journal of Atmospheric Chemistry, 41(1), 49–66,

doi:10.1023/A:1013896011709, 2002.

Ardyna, M., Babin, M., Gosselin, M., Devred, E., Rainville, L. and Tremblay, J. É.: Recent Arctic Ocean sea ice loss triggers novel fall phytoplankton blooms, Geophysical Research Letters, 41(17), 6207–6212, doi:10.1002/2014GL061047, 2014.

Arrigo, K. R. and van Dijken, G. L.: Continued increases in Arctic Ocean primary production, Progress in Oceanography, 136, 60–70, doi:10.1016/j.pocean.2015.05.002, 2015.

Arrigo, K. R., Perovich, D. K., Pickart, R. S., Brown, Z. W., Van Dijken, G. L., Lowry, K. E., Mills, M. M., Palmer, M. A., Balch, W. M., Bahr, F., Bates, N. R., Benitez-Nelson, C., Bowler, B., Brownlee, E., Ehn, J. K., Frey, K. E., Garley, R., Laney, S. R., Lubelczyk, L., Mathis, J., Matsuoka, A., Mitchell, B. G., Moore, G. W. K., Ortega-Retuerta, E., Pal, S., Polashenski, C. M., Reynolds, R. A., Schieber, B., Sosik, H. M., Stephens, M. and Swift, J. H.: Massive phytoplankton blooms under arctic sea ice, Science, 336(6087), 1408, doi:10.1126/science.1215065, 2012.

Assmy, P., Fernández-Méndez, M., Duarte, P., Meyer, A., Randelhoff, A., Mundy, C. J., Olsen, L. M., Kauko, H. M., Bailey, A., Chierici, M., Cohen, L., Doulgeris, A. P., Ehn, J. K., Fransson, A., Gerland, S., Hop, H., Hudson, S. R., Hughes, N., Itkin, P., Johnsen, G., King, J. A., Koch, B. P., Koenig, Z., Kwasniewski, S., Laney, S. R., Nicolaus, M., Pavlov, A. K., Polashenski, C. M., Provost, C., Rösel, A., Sandbu, M., Spreen, G., Smedsrud, L. H., Sundfjord, A., Taskjelle, T., Tatarek, A., Wiktor, J., Wagner, P. M., Wold, A., Steen, H. and Granskog, M. A.: Leads in Arctic pack ice enable early phytoplankton blooms below snow-covered sea ice, Scientific Reports, 7, 40850, doi:10.1038/srep40850, 2017.

Atkinson, D. E., Sassen, K., Hayashi, M., Cahill, C. F., Shaw, G., Harrigan, D. and Fuelberg, H.: Aerosol properties over Interior Alaska from lidar, DRUM Impactor sampler, and OPC-sonde measurements and their meteorological context during ARCTAS-A, April 2008, Atmospheric Chemistry and Physics, 13(3), 1293, 2013.

Ault, A. P. and Axson, J. L.: Atmospheric Aerosol Chemistry: Spectroscopic and Microscopic Advances, Analytical Chemistry, 89(1), 430–452, doi:10.1021/acs.analchem.6b04670, 2017.

Ault, A. P., Moore, M. J., Furutani, H. and Prather, K. A.: Impact of Emissions from the Los Angeles Port Region on San Diego Air Quality during Regional Transport Events, Environmental Science & Technology, 43(10), 3500–3506, doi:10.1021/es8018918, 2009.

Ault, A. P., Gaston, C. J., Wang, Y., Dominguez, G., Thiemens, M. H. and Prather, K. A.: Characterization of the Single Particle Mixing State of Individual Ship Plume Events Measured at the Port of Los Angeles, Environmental Science & Technology, 44(6), 1954–1961, doi:10.1021/es902985h, 2010.

Ault, A. P., Peters, T. M., Sawvel, E. J., Casuccio, G. S., Willis, R. D., Norris, G. A. and Grassian, V. H.: Single-particle SEM-EDX analysis of iron-containing coarse particulate matter in an urban environment: Sources and distribution of iron within Cleveland, Ohio, Environmental

Science and Technology, 46(8), 4331–4339, doi:10.1021/es204006k, 2012.

Ault, A. P., Guasco, T. L., Ryder, O. S., Baltrusaitis, J., Cuadra-Rodriguez, L. A., Collins, D. B., Ruppel, M. J., Bertram, T. H., Prather, K. A. and Grassian, V. H.: Inside versus outside: Ion redistribution in nitric acid reacted sea spray aerosol particles as determined by single particle analysis, Journal of the American Chemical Society, 135(39), 14528–14531, doi:10.1021/ja407117x, 2013a.

Ault, A. P., Zhao, D., Ebben, C. J., Tauber, M. J., Geiger, F. M., Prather, K. A. and Grassian, V. H.: Raman microspectroscopy and vibrational sum frequency generation spectroscopy as probes of the bulk and surface compositions of size-resolved sea spray aerosol particles, Physical Chemistry Chemical Physics, 15(17), 6206–6214, doi:10.1039/c3cp43899f, 2013b.

Ault, A. P., Moffet, R. C., Baltrusaitis, J., Collins, D. B., Ruppel, M. J., Cuadra-Rodriguez, L. A., Zhao, D., Guasco, T. L., Ebben, C. J., Geiger, F. M., Bertram, T. H., Prather, K. A. and Grassian, V. H.: Size-dependent changes in sea spray aerosol composition and properties with different seawater conditions, Environmental Science and Technology, 47(11), 5603–5612, doi:10.1021/es400416g, 2013c.

Ault, A. P., Guasco, T. L., Baltrusaitis, J., Ryder, O. S., Trueblood, J. V., Collins, D. B., Ruppel, M. J., Cuadra-Rodriguez, L. A., Prather, K. A. and Grassian, V. H.: Heterogeneous reactivity of nitric acid with nascent sea spray aerosol: Large differences observed between and within individual particles, Journal of Physical Chemistry Letters, 5(15), 2493–2500, doi:10.1021/jz5008802, 2014.

Axson, J. L., May, N. W., Colón-Bernal, I. D., Pratt, K. A. and Ault, A. P.: Lake Spray Aerosol: A Chemical Signature from Individual Ambient Particles, Environmental Science and Technology, 50(18), 9835–9845, doi:10.1021/acs.est.6b01661, 2016a.

Axson, J. L., Shen, H., Bondy, A. L., Landry, C. C., Welz, J., Creamean, J. M. and Ault, A. P.: Transported Mineral Dust Deposition Case Study at a Hydrologically Sensitive Mountain Site: Size and Composition Shifts in Ambient Aerosol and Snowpack, Aerosol and Air Quality Research, 16(3), 555–567, doi:10.4209/aaqr.2015.05.0346, 2016b.

Barnard, W. R., Andreae, M. O. and Iverson, R. L.: Dimethylsulfide and Phaeocystis poucheti in the southeastern Bering Sea, Continental Shelf Research, 3(2), 103–113, doi:10.1016/0278-4343(84)90001-3, 1984.

Barrett, T. E. and Sheesley, R. J.: Year-round optical properties and source characterization of Arctic organic carbon aerosols on the North Slope Alaska, Journal of Geophysical Research: Atmospheres, 122(17), 9319–9331, doi:10.1002/2016JD026194, 2017.

Barrie, L. A. and Barrie, M. J.: Chemical components of lower tropospheric aerosols in the high arctic: Six years of observations, Journal of Atmospheric Chemistry, 11(3), 211–226, doi:10.1007/bf00118349, 1990.

Baustian, K. J., Wise, M. E. and Tolbert, M. A.: Depositional ice nucleation on solid ammonium sulfate and glutaric acid particles, Atmospheric Chemistry and Physics, 10(5), 2307–2317, doi:10.5194/acp-10-2307-2010, 2010.

Baustian, K. J., Cziczo, D. J., Wise, M. E., Pratt, K. A., Kulkarni, G., Hallar, A. G. and Tolbert, M. A.: Importance of aerosol composition, mixing state, and morphology for heterogeneous ice nucleation: A combined field and laboratory approach, Journal of Geophysical Research Atmospheres, 117(6), doi:10.1029/2011JD016784, 2012.

Beitler, J.: Record low extent in the Chukchi Sea | Arctic Sea Ice News and Analysis, National Snow and Ice Data Center [online] Available from: http://nsidc.org/arcticseaicenews/2017/12/record-low-extent-in-the-chukchi-sea/ (Accessed 2 June 2018), 2017.

Beitsch, A., Kaleschke, L. and Kern, S.: Investigating high-resolution AMSR2 sea ice concentrations during the February 2013 fracture event in the beaufort sea, Remote Sensing, 6(5), 3841–3856, doi:10.3390/rs6053841, 2014.

Berkemeier, T., Shiraiwa, M., Pöschl, U. and Koop, T.: Competition between water uptake and ice nucleation by glassy organic aerosol particles, Atmospheric Chemistry and Physics, 14(22), 12513–12531, doi:10.5194/acp-14-12513-2014, 2014.

Bertram, A. K., Martin, S. T., Hanna, S. J., Smith, M. L., Bodsworth, A., Chen, Q., Kuwata, M., Liu, A., You, Y. and Zorn, S. R.: Predicting the relative humidities of liquid-liquid phase separation, efflorescence, and deliquescence of mixed particles of ammonium sulfate, organic material, and water using the organic-to-sulfate mass ratio of the particle and the oxygen-to-carbon ele, Atmospheric Chemistry and Physics, 11(21), 10995–11006, doi:10.5194/acp-11-10995-2011, 2011.

Bigg, E. K. and Leck, C.: Cloud-active particles over the central Arctic Ocean, Journal of Geophysical Research Atmospheres, 106(D23), 32155–32166, doi:10.1029/1999JD901152, 2001a.

Bigg, E. K. and Leck, C.: Properties of the aerosol over the central Arctic Ocean, Journal of Geophysical Research Atmospheres, 106(D23), 32101–32109, doi:10.1029/1999JD901136, 2001b.

Bigg, E. K. and Leck, C.: The composition of fragments of bubbles bursting at the ocean surface, Journal of Geophysical Research, 113(D11), D11209, doi:10.1029/2007JD009078, 2008.

Bikkina, P., Kawamura, K., Bikkina, S., Kunwar, B., Tanaka, K. and Suzuki, K.: Hydroxy Fatty Acids in Remote Marine Aerosols over the Pacific Ocean: Impact of Biological Activity and Wind Speed, ACS Earth and Space Chemistry, 3(3), 366–379, doi:10.1021/acsearthspacechem.8b00161, 2019.

Bikkina, S., Kawamura, K., Imanishi, K., Boreddy, S. K. R. and Nojiri, Y.: Seasonal and longitudinal distributions of atmospheric water-soluble dicarboxylic acids, oxocarboxylic acids, and α-dicarbonyls over the North Pacific, Journal of Geophysical Research, 120(10), 5191–5213, doi:10.1002/2014JD022972, 2015.

Blake, D. R., Hurst, D. F., Smith, T. W., Whipple, W. J., Chen, T.-Y., Blake, N. J. and Rowland, F. S.: Summertime measurements of selected nonmethane hydrocarbons in the Arctic and Subarctic during the 1988 Arctic Boundary Layer Expedition (ABLE 3A), Journal of Geophysical Research, 97(D15), 16559, doi:10.1029/92jd00892, 1992.

Boetius, A., Anesio, A. M., Deming, J. W., Mikucki, J. A. and Rapp, J. Z.: Microbial ecology of the cryosphere: Sea ice and glacial habitats, Nature Reviews Microbiology, 13(11), 677–690, doi:10.1038/nrmicro3522, 2015.

Bond, T. C., Doherty, S. J., Fahey, D. W., Forster, P. M., Berntsen, T., Deangelo, B. J., Flanner, M. G., Ghan, S., Kärcher, B., Koch, D., Kinne, S., Kondo, Y., Quinn, P. K., Sarofim, M. C., Schultz, M. G., Schulz, M., Venkataraman, C., Zhang, H., Zhang, S., Bellouin, N., Guttikunda, S. K., Hopke, P. K., Jacobson, M. Z., Kaiser, J. W., Klimont, Z., Lohmann, U., Schwarz, J. P., Shindell, D., Storelvmo, T., Warren, S. G. and Zender, C. S.: Bounding the role of black carbon in the climate system: A scientific assessment, Journal of Geophysical Research Atmospheres, 118(11), 5380–5552, doi:10.1002/jgrd.50171, 2013.

Bondy, A. L., Kirpes, R. M., Merzel, R. L., Pratt, K. A., Banaszak Holl, M. M. and Ault, A. P.: Atomic Force Microscopy-Infrared Spectroscopy of Individual Atmospheric Aerosol Particles: Subdiffraction Limit Vibrational Spectroscopy and Morphological Analysis, Analytical Chemistry, 89(17), 8594–8598, doi:10.1021/acs.analchem.7b02381, 2017a.

Bondy, A. L., Wang, B., Laskin, A., Craig, R. L., Nhliziyo, M. V., Bertman, S. B., Pratt, K. A., Shepson, P. B. and Ault, A. P.: Inland Sea Spray Aerosol Transport and Incomplete Chloride Depletion: Varying Degrees of Reactive Processing Observed during SOAS, Environmental Science and Technology, 51(17), 9533–9542, doi:10.1021/acs.est.7b02085, 2017b.

Bondy, A. L., Bonanno, D., Moffet, R. C., Wang, B., Laskin, A. and Ault, A. P.: The diverse chemical mixing state of aerosol particles in the southeastern United States, Atmospheric Chemistry and Physics, 18(16), 12595–12612, doi:10.5194/acp-18-12595-2018, 2018.

Boone, E. J., Laskin, A., Laskin, J., Wirth, C., Shepson, P. B., Stirm, B. H. and Pratt, K. A.: Aqueous Processing of Atmospheric Organic Particles in Cloud Water Collected via Aircraft Sampling, Environmental Science and Technology, 49(14), 8523–8530, doi:10.1021/acs.est.5b01639, 2015.

Boucher, O., Randall, D., Artaxo, P., Bretherton, C., Feingold, G., Forster, P., Kerminen, V.-M., Kondo, Y., Liao, H., Lohmann, U., Rasch, P., Satheesh, S. K., Sherwood, S., Stevens, B. and Zhang, X. Y.: Clouds and Aerosols, in Climate Change 2013: The Physical Science Basis. Contribution of Working Group I to the Fifth Assessment Report of the Intergovernmental Panel on Climate Change, pp. 1–4, Cambridge University Press. [online] Available from: www.

climatechange2013.org and www.ipcc.ch., 2013.

Ten Brink, H. M.: Reactive uptake of HNO3 and H2SO4 in sea-salt (NaCl) particles, Journal of Aerosol Science, 29(1–2), 57–64, doi:10.1016/S0021-8502(97)00460-6, 1998.

Bromwich, D. H. and Wang, S.-H.: A review of the temporal and spatial variability of Arctic and Antarctic atmospheric circulation based upon ERA-40, Dynamics of Atmospheres and Oceans, 44(3), 213–243, doi:https://doi.org/10.1016/j.dynatmoce.2007.09.001, 2008.

Brooks, I. M., Yelland, M. J., Upstill-Goddard, R. C., Nightingale, P. D., Archer, S., d'Asaro, E., Beale, R., Beatty, C., Blomquist, B., Bloom, A. A., Brooks, B. J., Cluderay, J., Coles, D., Dacey, J., DeGrandpïe, M., Dixon, J., Drennan, W. M., Gabriele, J., Goldson, L., Hardman-Mountford, N., Hill, M. K., Horn, M., Hsueh, P. C., Huebert, B., De Leeuw, G., Leighton, T. G., Liddicoat, M., Lingard, J. J. N., McNeil, C., McQuaid, J. B., Moat, B. I., Moore, G., Neill, C., Norris, S. J., O'Doherty, S., Pascal, R. W., Prytherch, J., Rebozo, M., Sahlee, E., Salter, M., Schuster, U., Skjelvan, I., Slagter, H., Smith, M. H., Smith, P. D., Srokosz, M., Stephens, J. A., Taylor, P. K., Telszewski, M., Walsh, R., Ward, B., Woolf, D. K., Young, D. and Zemmelink, H.: Physical exchanges at the air-sea interface: UK-SOLAS field measurements, Bulletin of the American Meteorological Society, 90(5), 629–644, doi:10.1175/2008BAMS2578.1, 2009.

Brooks, S. B., Crawford, T. L. and Oechel, W. C.: Measurement of carbon dioxide emissions plumes from Prudhoe Bay, Alaska oil fields, Journal of Atmospheric Chemistry, 27(2), 197–207, doi:10.1023/A:1005890318796, 1997.

Brooks, S. D., Wise, M. E., Cushing, M. and Tolbert, M. A.: Deliquescence behavior of organic/ammonium sulfate aerosol, Geophysical Research Letters, 29(19), 23-1-23–4, doi:10.1029/2002gl014733, 2002.

Browse, J., Carslaw, K. S., Arnold, S. R., Pringle, K. and Boucher, O.: The scavenging processes controlling the seasonal cycle in Arctic sulphate and black carbon aerosol, Atmospheric Chemistry and Physics, 12(15), 6775–6798, doi:10.5194/acp-12-6775-2012, 2012.

Browse, J., Carslaw, K. S., Schmidt, A. and Corbett, J. J.: Impact of future Arctic shipping on high-latitude black carbon deposition, Geophysical Research Letters, 40(16), 4459–4463, doi:10.1002/grl.50876, 2013.

Browse, J., Carslaw, K. S., Mann, G. W., Birch, C. E., Arnold, S. R. and Leck, C.: The complex response of Arctic aerosol to sea-ice retreat, Atmospheric Chemistry and Physics, 14(14), 7543–7557, doi:10.5194/acp-14-7543-2014, 2014.

Burkart, J., Hodshire, A. L., Mungall, E. L., Pierce, J. R., Collins, D. B., Ladino, L. A., Lee, A. K. Y., Irish, V., Wentzell, J. J. B., Liggio, J., Papakyriakou, T., Murphy, J. and Abbatt, J.: Organic Condensation and Particle Growth to CCN Sizes in the Summertime Marine Arctic Is Driven by Materials More Semivolatile Than at Continental Sites, Geophysical Research Letters, 44(20), 10,725-10,734, doi:10.1002/2017GL075671, 2017.

Calhoun, J. A., Bates, T. S. and Charlson, R. J.: Sulfur isotope measurements of submicrometer sulfate aerosol particles over the Pacific Ocean, Geophysical Research Letters, 18(10), 1877–1880, doi:10.1029/91GL02304, 1991.

Callaghan, A. H., Stokes, M. D. and Deane, G. B.: The effect of water temperature on air entrainment, bubble plumes, and surface foam in a laboratory breaking-wave analog, Journal of Geophysical Research: Oceans, 119(11), 7463–7482, doi:10.1002/2014JC010351, 2014.

Carey, W. M., Fitzgerald, J. W., Monahan, E. C. and Wang, Q.: Measurement of the sound produced by a tipping trough with fresh and salt water, The Journal of the Acoustical Society of America, 93(6), 3178–3192, doi:10.1121/1.405702, 1993.

Carslaw, K. S., Boucher, O., Spracklen, D. V., Mann, G. W., L. Rae, J. G., Woodward, S. and Kulmala, M.: A review of natural aerosol interactions and feedbacks within the Earth system, Atmospheric Chemistry and Physics, 10(4), 1701–1737, doi:10.5194/acp-10-1701-2010, 2010.

Carslaw, K. S., Lee, L. A., Reddington, C. L., Pringle, K. J., Rap, A., Forster, P. M., Mann, G. W., Spracklen, D. V., Woodhouse, M. T., Regayre, L. A. and Pierce, J. R.: Large contribution of natural aerosols to uncertainty in indirect forcing, Nature, 503(7474), 67–71, doi:10.1038/nature12674, 2013.

Cartmill, J. W. and Yang Su, M.: Bubble size distribution under saltwater and freshwater breaking waves, Dynamics of Atmospheres and Oceans, 20(1–2), 25–31, doi:10.1016/0377-0265(93)90046-A, 1993.

Cheng, W., Weng, L. T., Li, Y., Lau, A., Chan, C. and Chan, C. M.: Characterization of size-segregated aerosols using ToF-SIMS imaging and depth profiling, Surface and Interface Analysis, 46(7), 480–488, doi:10.1002/sia.5552, 2014.

Cheng, Y., Su, H., Koop, T., Mikhailov, E. and Pöschl, U.: Size dependence of phase transitions in aerosol nanoparticles, Nature Communications, 6, 1–7, doi:10.1038/ncomms6923, 2015.

Chi, J. W., Li, W. J., Zhang, D. Z., Zhang, J. C., Lin, Y. T., Shen, X. J., Sun, J. Y., Chen, J. M., Zhang, X. Y., Zhang, Y. M. and Wang, W. X.: Sea salt aerosols as a reactive surface for inorganic and organic acidic gases in the Arctic troposphere, Atmospheric Chemistry and Physics, 15(19), 11341–11353, doi:10.5194/acp-15-11341-2015, 2015.

Chin, W. C., Orellana, M. V and Verdugo, P.: Spontaneous assembly of marine dissolved organic matter into polymer gels, Nature, 391(6667), 568–572, 1998.

China, S., Scarnato, B., Owen, R. C., Zhang, B., Ampadu, M. T., Kumar, S., Dzepina, K., Dziobak, M. P., Fialho, P., Perlinger, J. A., Hueber, J., Helmig, D., Mazzoleni, L. R. and Mazzoleni, C.: Morphology and mixing state of aged soot particles at a remote marine free troposphere site: Implications for optical properties, Geophysical Research Letters, 42(4), 1243–1250, doi:10.1002/2014GL062404, 2015.

Ciobanu, V. G., Marcolli, C., Krieger, U. K., Weers, U. and Peter, T.: Liquid-liquid phase separation in mixed organic/inorganic aerosol particles, Journal of Physical Chemistry A, 113(41), 10966–10978, doi:10.1021/jp905054d, 2009.

Cochran, R. E., Laskina, O., Jayarathne, T., Laskin, A., Laskin, J., Lin, P., Sultana, C., Lee, C., Moore, K. A., Cappa, C. D., Bertram, T. H., Prather, K. A., Grassian, V. H. and Stone, E. A.: Analysis of Organic Anionic Surfactants in Fine and Coarse Fractions of Freshly Emitted Sea Spray Aerosol, Environmental Science and Technology, 50(5), 2477–2486, doi:10.1021/acs.est.5b04053, 2016.

Cochran, R. E., Laskina, O., Trueblood, J. V., Estillore, A. D., Morris, H. S., Jayarathne, T., Sultana, C. M., Lee, C., Lin, P., Laskin, J., Laskin, A., Dowling, J. A., Qin, Z., Cappa, C. D., Bertram, T. H., Tivanski, A. V., Stone, E. A., Prather, K. A. and Grassian, V. H.: Molecular Diversity of Sea Spray Aerosol Particles: Impact of Ocean Biology on Particle Composition and Hygroscopicity, Chem, 2(5), 655–667, doi:10.1016/j.chempr.2017.03.007, 2017.

Collins, D. B., Ault, A. P., Moffet, R. C., Ruppel, M. J., Cuadra-Rodriguez, L. A., Guasco, T. L., Corrigan, C. E., Pedler, B. E., Azam, F., Aluwihare, L. I., Bertram, T. H., Roberts, G. C., Grassian, V. H. and Prather, K. A.: Impact of marine biogeochemistry on the chemical mixing state and cloud forming ability of nascent sea spray aerosol, Journal of Geophysical Research Atmospheres, 118(15), 8553–8565, doi:10.1002/jgrd.50598, 2013.

Collins, D. B., Bertram, T. H., Sultana, C. M., Lee, C., Axson, J. L. and Prather, K. A.: Phytoplankton blooms weakly influence the cloud forming ability of sea spray aerosol, Geophysical Research Letters, 43(18), 9975–9983, doi:10.1002/2016GL069922, 2016.

Coz, E., Gómez-Moreno, F. J., Pujadas, M., Casuccio, G. S., Lersch, T. L. and Artíñano, B.: Individual particle characteristics of North African dust under different long-range transport scenarios, Atmospheric Environment, 43(11), 1850–1863, doi:10.1016/j.atmosenv.2008.12.045, 2009.

Craig, R. L., Bondy, A. L. and Ault, A. P.: Surface Enhanced Raman Spectroscopy Enables Observations of Previously Undetectable Secondary Organic Aerosol Components at the Individual Particle Level, Analytical Chemistry, 87(15), 7510–7514, doi:10.1021/acs.analchem.5b01507, 2015.

Craig, R. L., Bondy, A. L. and Ault, A. P.: Computer-controlled Raman microspectroscopy (CC-Raman): A method for the rapid characterization of individual atmospheric aerosol particles, Aerosol Science and Technology, 51(9), 1099–1112, doi:10.1080/02786826.2017.1337268, 2017.

Creamean, J. M., Axson, J. L., Bondy, A. L., Craig, R. L., May, N. W., Shen, H., Weber, M. H., Pratt, K. A. and Ault, A. P.: Changes in precipitating snow chemistry with location and elevation in the California Sierra Nevada, Journal of Geophysical Research: Atmospheres, 121(12), 7296–7309, doi:10.1002/2015JD024700, 2016.

Creamean, J. M., Kirpes, R. M., Pratt, K. A., Spada, N. J., Maahn, M., De Boer, G., Schnell, R. C. and China, S.: Marine and terrestrial influences on ice nucleating particles during continuous springtime measurements in an Arctic oilfield location, Atmospheric Chemistry and Physics, 18(24), 18023–18042, doi:10.5194/acp-18-18023-2018, 2018a.

Creamean, J. M., Maahn, M., de Boer, G., McComiskey, A., Sedlacek, A. J. and Feng, Y.: The influence of local oil exploration and regional wildfires on summer 2015 aerosol over the North Slope of Alaska, Atmospheric Chemistry and Physics, 18(2), 555–570, doi:10.5194/acp-18-555-2018, 2018b.

Creamean, J. M., Cross, J. N., Pickart, R., McRaven, L., Lin, P., Pacini, A., Hanlon, R., Schmale, D. G., Ceniceros, J., Aydell, T., Colombi, N., Bolger, E. and DeMott, P. J.: Ice nucleating particles carried from below a phytoplankton bloom to the Arctic atmosphere, Geophysical Research Letters, 0(ja), 2019GL083039, doi:10.1029/2019GL083039, 2019.

Croft, B., Wentworth, G. R., Martin, R. V, Leaitch, W. R., Murphy, J. G., Murphy, B. N., Kodros, J. K., Abbatt, J. P. and Pierce, J. R.: Contribution of Arctic seabird-colony ammonia to atmospheric particles and cloud-albedo radiative effect, Nat Commun, 7, 13444, doi:10.1038/ncomms13444, 2016.

Croft, B., Martin, R. V., Richard Leaitch, W., Burkart, J., Chang, R. Y. W., Collins, D. B., Hayes, P. L., Hodshire, A. L., Huang, L., Kodros, J. K., Moravek, A., Mungall, E. L., Murphy, J. G., Sharma, S., Tremblay, S., Wentworth, G. R., D Willis, M., Abbatt, J. P. D. and Pierce, J. R.: Arctic marine secondary organic aerosol contributes significantly to summertime particle size distributions in the Canadian Arctic Archipelago, Atmospheric Chemistry and Physics, 19(5), 2787–2812, doi:10.5194/acp-19-2787-2019, 2019.

Czamara, K., Majzner, K., Pacia, M. Z., Kochan, K., Kaczor, A. and Baranska, M.: Raman spectroscopy of lipids: A review, Journal of Raman Spectroscopy, 46(1), 4–20, doi:10.1002/jrs.4607, 2015.

Cziczo, D. J. and Abbatt, J. P. D.: Deliquescence, efflorescence, and supercooling of ammonium sulfate aerosols at low temperature: Implications for cirrus cloud formation and aerosol phase in the atmosphere, Journal of Geophysical Research Atmospheres, 104(D11), 13781–13790, doi:10.1029/1999JD900112, 1999.

Dalsøren, S. B., Endresen, Ø., Isaksen, I. S. A., Gravir, G. and Sörgärd, E.: Environmental impacts of the expected increase in sea transportation, with a particular focus on oil and gas scenarios for Norway and northwest Russia, Journal of Geophysical Research Atmospheres, 112(2), doi:10.1029/2005JD006927, 2007.

Dappe, V., Uzu, G., Schreck, E., Wu, L., Li, X., Dumat, C., Moreau, M., Hanoune, B., Ro, C.-U. and Sobanska, S.: Single-particle analysis of industrial emissions brings new insights for health risk assessment of PM, Atmospheric Pollution Research, 9(4), 697–704, doi:10.1016/j.apr.2018.01.016, 2018.

Dazzi, A., Prater, C. B., Hu, Q., Chase, D. B., Rabolt, J. F. and Marcott, C.: AFM-IR: Combining atomic force microscopy and infrared spectroscopy for nanoscale chemical characterization, Applied Spectroscopy, 66(12), 1365–1384, doi:10.1366/12-06804, 2012.

Deane, G. B. and Stokes, M. D.: Air Entrainment Processes and Bubble Size Distributions in the Surf Zone, Journal of Physical Oceanography, 29(7), 1393–1403, doi:10.1175/1520-0485(1999)029<1393:AEPABS>2.0.CO;2, 1999.

Decesari, S., Finessi, E., Rinaldi, M., Paglione, M., Fuzzi, S., Stephanou, E. G., Tziaras, T., Spyros, A., Ceburnis, D., O'Dowd, C., Dall'Osto, M., Harrison, R. M., Allan, J., Coe, H. and Facchini, M. C.: Primary and secondary marine organic aerosols over the North Atlantic Ocean during the MAP experiment, Journal of Geophysical Research Atmospheres, 116(22), doi:10.1029/2011JD016204, 2011.

Decho, A. W. and Gutierrez, T.: Microbial Extracellular Polymeric Substances (EPSs) in Ocean Systems, Front Microbiol, 8(922), 922, doi:10.3389/fmicb.2017.00922, 2017.

Deetz, K., Vogel, H., Haslett, S., Knippertz, P., Coe, H. and Vogel, B.: Aerosol liquid water content in the moist southern West African monsoon layer and its radiative impact, Atmospheric Chemistry and Physics, 18(19), 14271–14295, doi:10.5194/acp-18-14271-2018, 2018.

Demirdjian, B., Ferry, D., Suzanne, J., Popovicheva, O. B., Persiantseva, N. M. and Shonija, N. K.: Heterogeneities in the microstructure and composition of aircraft engine combustor soot: Impact on the water uptake, Journal of Atmospheric Chemistry, 56(1), 83–103, doi:10.1007/s10874-006-9043-9, 2007.

DeMott, P. J., Hill, T. C. J., McCluskey, C. S., Prather, K. A., Collins, D. B., Sullivan, R. C., Ruppel, M. J., Mason, R. H., Irish, V. E., Lee, T., Hwang, C. Y., Rhee, T. S., Snider, J. R., McMeeking, G. R., Dhaniyala, S., Lewis, E. R., Wentzell, J. J. B., Abbatt, J., Lee, C., Sultana, C. M., Ault, A. P., Axson, J. L., Diaz Martinez, M., Venero, I., Santos-Figueroa, G., Stokes, M. D., Deane, G. B., Mayol-Bracero, O. L., Grassian, V. H., Bertram, T. H., Bertram, A. K., Moffett, B. F. and Franc, G. D.: Sea spray aerosol as a unique source of ice nucleating particles., Proceedings of the National Academy of Sciences of the United States of America, 113(21), 5797–803, doi:10.1073/pnas.1514034112, 2016.

Deng, C., Brooks, S. D., Vidaurre, G. and Thornton, D. C. O.: Using Raman Microspectroscopy to Determine Chemical Composition and Mixing State of Airborne Marine Aerosols over the Pacific Ocean, Aerosol Science and Technology, 48(2), 193–206, doi:10.1080/02786826.2013.867297, 2014.

Dette, H. P. and Koop, T.: Glass formation processes in mixed inorganic/organic aerosol particles, Journal of Physical Chemistry A, 119(19), 4552–4561, doi:10.1021/jp5106967, 2015.

Dickson, A. G., Sabine, C. L. and Christian, J. R.: Guide to best practices for ocean CO2 measurements., North Pacific Marine Science Organization., 2007.

Dong, R. and Yu, L. E.: Investigation of suflace changes of nanoparticles using TM-AFM phase imaging, Environmental Science and Technology, 37(12), 2813–2819, doi:10.1021/es034071k, 2003.

Douglas, T. A., Domine, F., Barret, M., Anastasio, C., Beine, H. J., Bottenheim, J., Grannas, A., Houdier, S., Netcheva, S., Rowland, G., Staebler, R. and Steffen, A.: Frost flowers growing in the Arctic ocean-atmosphere-sea ice-snow interface: 1. Chemical composition, Journal of Geophysical Research Atmospheres, 117(3), doi:10.1029/2011JD016460, 2012.

Easter, R. C. and Hobbs, P. V.: The Formation of Sulfates and the Enhancement of Cloud Condensation Nuclei in Clouds, Journal of the Atmospheric Sciences, 31(6), 1586–1594, doi:10.1175/1520-0469(1974)031<1586:tfosat>2.0.co;2, 2002.

Ebben, C. J., Ault, A. P., Ruppel, M. J., Ryder, O. S., Bertram, T. H., Grassian, V. H., Prather, K. A. and Geiger, F. M.: Size-resolved sea spray aerosol particles studied by vibrational sum frequency generation, Journal of Physical Chemistry A, 117(30), 6589–6601, doi:10.1021/jp401957k, 2013.

Eckhardt, S., Quennehen, B., Olivié, D. J. L., Berntsen, T. K., Cherian, R., Christensen, J. H., Collins, W., Crepinsek, S., Daskalakis, N., Flanner, M., Herber, A., Heyes, C., Hodnebrog, Huang, L., Kanakidou, M., Klimont, Z., Langner, J., Law, K. S., Lund, M. T., Mahmood, R., Massling, A., Myriokefalitakis, S., Nielsen, I. E., Nøjgaard, J. K., Quaas, J., Quinn, P. K., Raut, J. C., Rumbold, S. T., Schulz, M., Sharma, S., Skeie, R. B., Skov, H., Uttal, T., Von Salzen, K. and Stohl, A.: Current model capabilities for simulating black carbon and sulfate concentrations in the Arctic atmosphere: A multi-model evaluation using a comprehensive measurement data set, Atmospheric Chemistry and Physics, 15(16), 9413–9433, doi:10.5194/acp-15-9413-2015, 2015.

Engel, A., Bange, H. W., Cunliffe, M., Burrows, S. M., Friedrichs, G., Galgani, L., Herrmann, H., Hertkorn, N., Johnson, M., Liss, P. S., Quinn, P. K., Schartau, M., Soloviev, A., Stolle, C., Upstill-Goddard, R. C., van Pinxteren, M. and Zäncker, B.: The Ocean's Vital Skin: Toward an Integrated Understanding of the Sea Surface Microlayer, Frontiers in Marine Science, 4(165), doi:10.3389/fmars.2017.00165, 2017.

Eom, H. J., Gupta, D., Cho, H. R., Jin Hwang, H., Do Hur, S., Gim, Y. and Ro, C. U.: Single-particle investigation of summertime and wintertime Antarctic sea spray aerosols using low-Z particle EPMA, Raman microspectrometry, and ATR-FTIR imaging techniques, Atmospheric Chemistry and Physics, 16(21), 13823–13836, doi:10.5194/acp-16-13823-2016, 2016.

Eriksen Hammer, S., Ebert, M. and Weinbruch, S.: Comparison of operator- and computer-controlled scanning electron microscopy of particles from different atmospheric aerosol types, Analytical and Bioanalytical Chemistry, 411(8), 1633–1645, doi:10.1007/s00216-019-01614-7, 2019.

Even, A., Smekens, A., Khlystov, A., Berghmans, P., van Grieken, R. and ten Brink, H. M.: Morphology of internally mixed aerosol of ammonium sulfate and soot, Journal of Aerosol

Science, 29, S753–S754, doi:https://doi.org/10.1016/S0021-8502(98)90559-6, 1998.

Facchini, M. C., Rinaldi, M., Decesari, S., Carbone, C., Finessi, E., Mircea, M., Fuzzi, S., Ceburnis, D., Flanagan, R., Nilsson, E. D., de Leeuw, G., Martino, M., Woeltjen, J. and O'Dowd, C. D.: Primary submicron marine aerosol dominated by insoluble organic colloids and aggregates, Geophysical Research Letters, 35(17), L17814, doi:10.1029/2008GL034210, 2008.

Fajardo, O. A., Jiang, J. and Hao, J.: Continuous Measurement of Ambient Aerosol Liquid Water Content in Beijing, Aerosol and Air Quality Research, 16(5), 1152–1164, doi:10.4209/aaqr.2015.10.0579, 2016.

Falk-Petersen, S., Sargent, J. R., Henderson, J., Hegseth, E. N., Hop, H. and Okolodkov, Y. B.: Lipids and fatty acids in ice algae and phytoplankton from the Marginal Ice Zone in the Barents Sea, Polar Biology, 20(1), 41–47, doi:10.1007/s003000050274, 1998.

Farmer, D. K., Cappa, C. D. and Kreidenweis, S. M.: Atmospheric Processes and Their Controlling Influence on Cloud Condensation Nuclei Activity, Chemical Reviews, 115(10), 4199–4217, doi:10.1021/cr5006292, 2015.

Fierce, L., Bond, T. C., Bauer, S. E., Mena, F. and Riemer, N.: Black carbon absorption at the global scale is affected by particle-scale diversity in composition, Nature Communications, 7(1), 12361, doi:10.1038/ncomms12361, 2016.

Fisher, J. A., Jacob, D. J., Wang, Q., Bahreini, R., Carouge, C. C., Cubison, M. J., Dibb, J. E., Diehl, T., Jimenez, J. L., Leibensperger, E. M., Lu, Z., Meinders, M. B. J., Pye, H. O. T., Quinn, P. K., Sharma, S., Streets, D. G., van Donkelaar, A. and Yantosca, R. M.: Sources, distribution, and acidity of sulfate-ammonium aerosol in the Arctic in winter-spring, Atmospheric Environment, 45(39), 7301–7318, doi:10.1016/j.atmosenv.2011.08.030, 2011.

Fitzgerald, E., P. Ault, A., D. Zauscher, M., Mayol-Bracero, O. and Prather, K.: Comparison of the mixing state of long-range transported Asian and African mineral dust, Atmospheric Environment, 115, doi:10.1016/j.atmosenv.2015.04.031, 2015.

Flanner, M. G.: Arctic climate sensitivity to local black carbon, Journal of Geophysical Research Atmospheres, 118(4), 1840–1851, doi:10.1002/jgrd.50176, 2013.

Flanner, M. G., Zender, C. S., Randerson, J. T. and Rasch, P. J.: Present-day climate forcing and response from black carbon in snow, Journal of Geophysical Research Atmospheres, 112(11), doi:10.1029/2006JD008003, 2007.

Forestieri, S. D., Cornwell, G. C., Helgestad, T. M., Moore, K. A., Lee, C., Novak, G. A., Sultana, C. M., Wang, X., Bertram, T. H., Prather, K. A. and Cappa, C. D.: Linking variations in sea spray aerosol particle hygroscopicity to composition during two microcosm experiments, Atmospheric Chemistry and Physics, 16(14), 9003–9018, doi:10.5194/acp-16-9003-2016, 2016.

Forestieri, S. D., Moore, K. A., Martinez Borrero, R., Wang, A., Stokes, M. D. and Cappa,

C. D.: Temperature and Composition Dependence of Sea Spray Aerosol Production, Geophysical Research Letters, 45(14), 7218–7225, doi:10.1029/2018GL078193, 2018.

Frossard, A. A., Russell, L. M., Burrows, S. M., Elliott, S. M., Bates, T. S. and Quinn, P. K.: Sources and composition of submicron organic mass in marine aerosol particles, Journal of Geophysical Research Atmospheres, 119(22), 12977–13003, doi:10.1002/2014JD021913, 2014.

Frost, R. L., Erickson, K. L. and Kloprogge, T. J.: Vibrational spectroscopic study of the nitrate containing hydrotalcite mbobomkulite, Spectrochimica Acta - Part A: Molecular and Biomolecular Spectroscopy, 61(13–14), 2919–2925, doi:10.1016/j.saa.2004.11.002, 2005.

Fu, P., Kawamura, K. and Barrie, L. A.: Photochemical and other sources of organic compounds in the Canadian high Arctic aerosol pollution during winter-spring, Environmental Science and Technology, 43(2), 286–292, doi:10.1021/es803046q, 2009.

Fu, P., Kawamura, K., Chen, J., Qin, M., Ren, L., Sun, Y., Wang, Z., Barrie, L. A., Tachibana, E., Ding, A. and Yamashita, Y.: Fluorescent water-soluble organic aerosols in the High Arctic atmosphere, Sci Rep, 5, 9845, doi:10.1038/srep09845, 2015.

Fu, P. Q., Kawamura, K., Chen, J., Charrière, B. and Sempéré, R.: Organic molecular composition of marine aerosols over the Arctic Ocean in summer: Contributions of primary emission and secondary aerosol formation, Biogeosciences, 10(2), 653–667, doi:10.5194/bg-10-653-2013, 2013.

Fuentes, E., Coe, H., Green, D., De Leeuw, G. and McFiggans, G.: Laboratory-generated primary marine aerosol via bubble-bursting and atomization, Atmospheric Measurement Techniques, 3(1), 141–162, doi:10.5194/amt-3-141-2010, 2010a.

Fuentes, E., Coe, H., Green, D., De Leeuw, G. and McFiggans, G.: On the impacts of phytoplankton-derived organic matter on the properties of the primary marine aerosol - Part 1: Source fluxes, Atmospheric Chemistry and Physics, 10(19), 9295–9317, doi:10.5194/acp-10-9295-2010, 2010b.

Galgani, L., Piontek, J. and Engel, A.: Biopolymers form a gelatinous microlayer at the air-sea interface when Arctic sea ice melts, Scientific Reports, 6(July), doi:10.1038/srep29465, 2016a.

Galgani, L., Piontek, J. and Engel, A.: Biopolymers form a gelatinous microlayer at the air-sea interface when Arctic sea ice melts, Sci Rep, 6(July), 29465, doi:10.1038/srep29465, 2016b.

Gantt, B. and Meskhidze, N.: The physical and chemical characteristics of marine primary organic aerosol: A review, Atmospheric Chemistry and Physics, 13(8), 3979–3996, doi:10.5194/acp-13-3979-2013, 2013.

Gao, Q., Leck, C., Rauschenberg, C. and Matrai, P. A.: On the chemical dynamics of

extracellular polysaccharides in the high Arctic surface microlayer, Ocean Science, 8(4), 401–418, doi:10.5194/os-8-401-2012, 2012.

Gard, E. E., Kleeman, M. J., Gross, D. S., Hughes, L. S., Jonathan, O., Morrical, B. D., Fergenson, D. P., Dienes, T., Gälli, M. E., Robert, J., Cass, G. R., Prather, K. A., Allen, J., Galli, M. E., Prather, A. and Johnson, R. J.: Direct Observation of Heterogeneous Chemistry in the Atmosphere Direct Observation of Heterogeneous Chemistry in the Atmosphere, Science, 279(5354), 1184–1187, doi:10.1126/science.279.5354.1184, 1998.

Garrett, T. J. and Zhao, C.: Increased Arctic cloud longwave emissivity associated with pollution from mid-latitudes, Nature, 440(7085), 787–789, doi:10.1038/nature04636, 2006.

Gautier, A.: Arctic sea ice extent arrives at its minmum, National Snow and Ice Data Center, 2018.

Gautier, D. L., Bird, K. J., Charpentier, R. R., Grantz, A., Houseknecht, D. W., Klett, T. R., Moore, T. E., Pitman, J. K., Schenk, C. J., Schuenemeyer, J. H., Sørensen, K., Tennyson, M. E., Valin, Z. C. and Wandrey, C. J.: Assessment of undiscovered oil and gas in the arctic, Science, 324(5931), 1175–1179, doi:10.1126/science.1169467, 2009.

De Gelder, J., De Gussem, K., Vandenabeele, P. and Moens, L.: Reference database of Raman spectra of biological molecules, Journal of Raman Spectroscopy, 38(9), 1133–1147, doi:10.1002/jrs.1734, 2007.

Geng, H., Ryu, J., Jung, H. J., Chung, H., Ahn, K. H. O. and Ro, C. U. N.: Single-particle characterization of summertime arctic aerosols collected at Ny-Ålesund, Svalbard, Environmental Science and Technology, 44(7), 2348–2353, doi:10.1021/es903268j, 2010.

Ghahremaninezhad, R., Norman, A. L., Abbatt, J. P. D., Levasseur, M. and Thomas, J. L.: Biogenic, anthropogenic and sea salt sulfate size-segregated aerosols in the Arctic summer, Atmospheric Chemistry and Physics, 16(8), 5191–5202, doi:10.5194/acp-16-5191-2016, 2016.

Giamarelou, M., Eleftheriadis, K., Nyeki, S., Tunved, P., Torseth, K. and Biskos, G.: Indirect evidence of the composition of nucleation mode atmospheric particles in the high arctic, Journal of Geophysical Research, 121(2), 965–975, doi:10.1002/2015JD023646, 2016.

Giordano, M. R., Kalnajs, L. E., Douglas Goetz, J., Avery, A. M., Katz, E., May, N. W., Leemon, A., Mattson, C., Pratt, K. A. and DeCarlo, P. F.: The importance of blowing snow to halogen-containing aerosol in coastal Antarctica: Influence of source region versus wind speed, Atmospheric Chemistry and Physics, 18(22), 16689–16711, doi:10.5194/acp-18-16689-2018, 2018.

Goldenson, N., Doherty, S. J., Bitz, C. M., Holland, M. M., Light, B. and Conley, A. J.: Arctic climate response to forcing from light-absorbing particles in snow and sea ice in CESM, Atmospheric Chemistry and Physics, 12(17), 7903–7920, doi:10.5194/acp-12-7903-2012, 2012.

Gong, S. L. and Barrie, L. A.: Simulating the impact of sea salt on global nss sulphate aerosols, Journal of Geophysical Research, 108(D16), 4516, doi:10.1029/2002JD003181, 2003.

Gong, W., Beagley, S. R., Cousineau, S., Sassi, M., Munoz-Alpizar, R., Ménard, S., Racine, J., Zhang, J., Chen, J., Morrison, H., Sharma, S., Huang, L., Bellavance, P., Ly, J., Izdebski, P., Lyons, L. and Holt, R.: Assessing the impact of shipping emissions on air pollution in the Canadian Arctic and northern regions: Current and future modelled scenarios, Atmospheric Chemistry and Physics, 18(22), 16653–16687, doi:10.5194/acp-18-16653-2018, 2018.

Gorkowski, K., Donahue, N. M. and Sullivan, R. C.: Emulsified and Liquid-Liquid Phase-Separated States of α-Pinene Secondary Organic Aerosol Determined Using Aerosol Optical Tweezers, Environmental Science and Technology, 51(21), 12154–12163, doi:10.1021/acs.est.7b03250, 2017.

Gosselin, M., Levasseur, M., Wheeler, P. A., Horner, R. A. and Booth, B. C.: New measurements of phytoplankton and ice algal production in the Arctic Ocean, Deep-Sea Research Part II: Topical Studies in Oceanography, 44(8), 1623–1625, doi:10.1016/S0967-0645(97)00054-4, 1997.

Graham, R. M., Cohen, L., Petty, A. A., Boisvert, L. N., Rinke, A., Hudson, S. R., Nicolaus, M. and Granskog, M. A.: Increasing frequency and duration of Arctic winter warming events, Geophysical Research Letters, 44(13), 6974–6983, doi:10.1002/2017GL073395, 2017.

Guasco, T. L., Cuadra-Rodriguez, L. A., Pedler, B. E., Ault, A. P., Collins, D. B., Zhao, D., Kim, M. J., Ruppel, M. J., Wilson, S. C., Pomeroy, R. S., Grassian, V. H., Azam, F., Bertram, T. H. and Prather, K. A.: Transition metal associations with primary biological particles in sea spray aerosol generated in a wave channel, Environmental Science and Technology, 48(2), 1324–1333, doi:10.1021/es403203d, 2014.

Gunsch, M. J., Kirpes, R. M., Kolesar, K. R., Barrett, T. E., China, S., Sheesley, R. J., Laskin, A., Wiedensohler, A., Tuch, T. and Pratt, K. A.: Contributions of transported Prudhoe Bay oil field emissions to the aerosol population in Utqiaġvik, Alaska, Atmospheric Chemistry and Physics, 17(17), 10879–10892, doi:10.5194/acp-17-10879-2017, 2017.

Haine, T. W. N. and Martin, T.: The Arctic-Subarctic sea ice system is entering a seasonal regime: Implications for future Arctic amplification, Scientific Reports, 7(1), 4618, doi:10.1038/s41598-017-04573-0, 2017.

Hamacher-Barth, E., Leck, C. and Jansson, K.: Size-resolved morphological properties of the high Arctic summer aerosol during ASCOS-2008, Atmospheric Chemistry and Physics, 16(10), 6577–6593, doi:10.5194/acp-16-6577-2016, 2016.

Hancke, K., Lund-Hansen, L. C., Lamare, M. L., Højlund Pedersen, S., King, M. D., Andersen, P. and Sorrell, B. K.: Extreme Low Light Requirement for Algae Growth Underneath Sea Ice: A Case Study From Station Nord, NE Greenland, Journal of Geophysical Research: Oceans, 123(2), 985–1000, doi:10.1002/2017JC013263, 2018.

Hansell, D. A.: Dissolved Organic Carbon Reference Material Program, Eos, Transactions American Geophysical Union, 86(35), 318, doi:10.1029/2005EO350003, 2005.

Hara, K.: Mixing states of individual aerosol particles in spring Arctic troposphere during ASTAR 2000 campaign, Journal of Geophysical Research, 108(D7), 4209, doi:10.1029/2002JD002513, 2003.

Hara, K., Osada, K., Hayashi, M., Matsunaga, K., Shibata, T., Iwasaka, Y. and Furuya, K.: Fractionation of inorganic nitrates in winter Arctic troposphere: Coarse aerosol particles containing inorganic nitrates, Journal of Geophysical Research-Atmospheres, 104(D19), 23671–23679, doi:Doi 10.1029/1999jd900348, 1999.

Hara, K., Osada, K., Matsunaga, K., Iwasaka, Y., Shibata, T. and Furuya, K.: Atmospheric inorganic chlorine and bromine species in Arctic boundary layer of the winter/spring, Journal of Geophysical Research Atmospheres, 107(18), doi:10.1029/2001JD001008, 2002a.

Hara, K., Osada, K., Matsunaga, K., Sakai, T., Iwasaka, Y. and Furuya, K.: Concentration trends and mixing states of participate oxalate in Arctic boundary layer in winter/spring, Journal of Geophysical Research Atmospheres, 107(19), doi:10.1029/2001JD001584, 2002b.

Hara, K., Osada, K., Nishita, C., Yamagata, S., Yamanocuhi, T., Herber, A., Matsunaga, K., Iwasaka, Y., Nagatani, M. and Nakata, H.: Vertical variations of sea-salt modification in the boundary layer of spring Arctic during the ASTAR 2000 campaign, Tellus, Series B: Chemical and Physical Meteorology, 54(4), 361–376, doi:10.1034/j.1600-0889.2002.201253.x, 2002c.

Hara, K., Osada, K., Kido, M., Hayashi, M., Matsunaga, K., Iwasaka, Y., Yamanouchi, T., Hashida, G. and Fukatsu, T.: Chemistry of sea-salt particles and inorganic halogen species in Antarctic regions: Compositional differences between coastal and inland stations, Journal of Geophysical Research D: Atmospheres, 109(20), doi:10.1029/2004JD004713, 2004.

Hara, K., Osada, K. and Yamanouchi, T.: Tethered balloon-borne aerosol measurements: Seasonal and vertical variations of aerosol constituents over Syowa Station, Antarctica, Atmospheric Chemistry and Physics, 13(17), 9119–9139, doi:10.5194/acp-13-9119-2013, 2013.

Hara, K., Nakazawa, F., Fujita, S., Fukui, K., Enomoto, H. and Sugiyama, S.: Horizontal distributions of aerosol constituents and their mixing states in Antarctica during the JASE traverse, Atmospheric Chemistry and Physics, 14(18), 10211–10230, doi:10.5194/acp-14-10211-2014, 2014.

Harrington, J. Y., Reisin, T., Cotton, W. R. and Kreidenweis, S. M.: Cloud resolving simulations of Arctic stratus, Atmospheric Research, 51(1), 45–75, doi:10.1016/s0169-8095(98)00098-2, 2002.

Harris, E., Sinha, B., Hoppe, P., Foley, S. and Borrmann, S.: Fractionation of sulfur isotopes during heterogeneous oxidation of SO 2 on sea salt aerosol: A new tool to investigate

non-sea salt sulfate production in the marine boundary layer, Atmospheric Chemistry and Physics, 12(10), 4619–4631, doi:10.5194/acp-12-4619-2012, 2012a.

Harris, E., Sinha, B., Foley, S., Crowley, J. N., Borrmann, S. and Hoppe, P.: Sulfur isotope fractionation during heterogeneous oxidation of SO2 on mineral dust, Atmospheric Chemistry and Physics, 12(11), 4867–4884, doi:10.5194/acp-12-4867-2012, 2012b.

Harris, E., Sinha, B., Hoppe, P., Crowley, J. N., Ono, S. and Foley, S.: Sulfur isotope fractionation during oxidation of sulfur dioxide: Gas-phase oxidation by OH radicals and aqueous oxidation by H2O2, O3 and iron catalysis, Atmospheric Chemistry and Physics, 12(1), 407–424, doi:10.5194/acp-12-407-2012, 2012c.

Harris, E., Sinha, B., Van Pinxteren, D., Tilgner, A., Fomba, K. W., Schneider, J., Roth, A., Gnauk, T., Fahlbusch, B., Mertes, S., Lee, T., Collett, J., Foley, S., Borrmann, S., Hoppe, P., Herrmann, H., Pinxteren, D. Van, Tilgner, A., Fomba, K. W., Schneider, J., Roth, A., Gnauk, T., Fahlbusch, B., Mertes, S., Lee, T., Collett, J., Foley, S., Borrmann, S., Hoppe, P. and Herrmann, H.: Enhanced role of transition metal ion catalysis during in-cloud oxidation of SO2, Science, 340(6133), 727–730, doi:10.1126/science.1230911, 2013.

Hawkins, L. N. and Russell, L. M.: Polysaccharides, Proteins, and Phytoplankton Fragments: Four Chemically Distinct Types of Marine Primary Organic Aerosol Classified by Single Particle Spectromicroscopy, Advances in Meteorology, 2010, 1–14, doi:10.1155/2010/612132, 2010.

Heintzenberg, J., Leck, C., Birmili, W., Wehner, B., Tjernström, M. and Wiedensohler, A.: Aerosol number-size distributions during clear and fog periods in the summer high Arctic: 1991, 1996 and 2001, Tellus, Series B: Chemical and Physical Meteorology, 58(1), 41–50, doi:10.1111/j.1600-0889.2005.00171.x, 2006.

Heintzenberg, J., Leck, C. and Tunved, P.: Potential source regions and processes of aerosol in the summer Arctic, Atmospheric Chemistry and Physics, 15(11), 6487–6502, doi:10.5194/acp-15-6487-2015, 2015.

Held, A., Brooks, I. M., Leck, C. and Tjernström, M.: On the potential contribution of open lead particle emissions to the central Arctic aerosol concentration, Atmospheric Chemistry and Physics, 11(7), 3093–3105, doi:10.5194/acp-11-3093-2011, 2011.

Hill, V., Ardyna, M., Lee, S. H. and Varela, D. E.: Decadal trends in phytoplankton production in the Pacific Arctic Region from 1950 to 2012, Deep-Sea Research Part II: Topical Studies in Oceanography, 152, 82–94, doi:10.1016/j.dsr2.2016.12.015, 2018.

Hinds, W. C.: Aerosol Technology: Properties, Behavior, and Measurement of Airborne Particles, Wiley. [online] Available from: https://books.google.com/books?id=qIkyjPXfWK4C, 2012.

Hirano, D., Fukamachi, Y., Ohshima, K. I., Watanabe, E., Mahoney, A. R., Eicken, H.,

Itoh, M., Simizu, D., Iwamoto, K., Jones, J., Takatsuka, T., Kikuchi, T. and Tamura, T.: Winter Water Formation in Coastal Polynyas of the Eastern Chukchi Shelf: Pacific and Atlantic Influences, Journal of Geophysical Research: Oceans, 123(8), 5688–5705, doi:10.1029/2017JC013307, 2018.

Hiranuma, N., Brooks, S. D., Moffet, R. C., Glen, A., Laskin, A., Gilles, M. K., Liu, P., MacDonald, A. M., Strapp, J. W. and McFarquhar, G. M.: Chemical characterization of individual particles and residuals of cloud droplets and ice crystals collected on board research aircraft in the ISDAC 2008 study, Journal of Geophysical Research Atmospheres, 118(12), 6564–6579, doi:10.1002/jgrd.50484, 2013.

Hirdman, D., Burkhart, J. F., Sodemann, H., Eckhardt, S., Jefferson, A., Quinn, P. K., Sharma, S., Ström, J. and Stohl, A.: Long-term trends of black carbon and sulphate aerosol in the Arctic: Changes in atmospheric transport and source region emissions, Atmospheric Chemistry and Physics, 10(19), 9351–9368, doi:10.5194/acp-10-9351-2010, 2010.

Holland, M. M. and Bitz, C. M.: Polar amplification of climate change in coupled models, Climate Dynamics, 21(3–4), 221–232, doi:10.1007/s00382-003-0332-6, 2003.

Hopkins, R. J., Desyaterik, Y., Tivanski, A. V., Zaveri, R. A., Berkowitz, C. M., Tyliszczak, T., Gilles, M. K. and Laskin, A.: Chemical speciation of sulfur in marine cloud droplets and particles: Analysis of individual particles from the marine boundary layer over the California current, Journal of Geophysical Research Atmospheres, 113(4), 1–15, doi:10.1029/2007JD008954, 2008.

Huang, D., Xiu, G., Li, M., Hua, X. and Long, Y.: Surface components of PM2.5 during clear and hazy days in Shanghai by ToF-SIMS, Atmospheric Environment, 148, 175–181, doi:10.1016/j.atmosenv.2016.10.036, 2017.

Hultin, K. A. H., Nilsson, E. D., Krejci, R., Mrtensson, E. M., Ehn, M., Hagström, Å. and De Leeuw, G.: In situ laboratory sea spray production during the Marine Aerosol Production 2006 cruise on the northeastern Atlantic Ocean, Journal of Geophysical Research Atmospheres, 115(6), D06201, doi:10.1029/2009JD012522, 2010.

Huntington, H. P., Daniel, R., Hartsig, A., Harun, K., Heiman, M., Meehan, R., Noongwook, G., Pearson, L., Prior-Parks, M., Robards, M. and Stetson, G.: Vessels, risks, and rules: Planning for safe shipping in Bering Strait, Marine Policy, 51, 119–127, doi:10.1016/j.marpol.2014.07.027, 2015.

IPCC: Climate Change 2013 - The Physical Science Basis, edited by Intergovernmental Panel on Climate Change, Cambridge University Press, Cambridge., 2014.

Irish, V. E., Elizondo, P., Chen, J., Choul, C., Charette, J., Lizotte, M., Ladino, L. A., Wilson, T. W., Gosselin, M., Murray, B. J., Polishchuk, E., Abbatt, J. P. D., Miller, L. A. and Bertram, A. K.: Ice-nucleating particles in Canadian Arctic sea-surface microlayer and bulk seawater, Atmospheric Chemistry and Physics, 17(17), 10583–10595, doi:10.5194/acp-17-10583-

2017, 2017.

Jacob, D.: Heterogeneous chemistry and tropospheric ozone, Atmospheric Environment, 34(12–14), 2131–2159, doi:10.1016/S1352-2310(99)00462-8, 2000.

Jacobi, H. W., Voisin, D., Jaffrezo, J. L., Cozic, J. and Douglas, T. A.: Chemical composition of the snowpack during the OASIS spring campaign 2009 at Barrow, Alaska, Journal of Geophysical Research Atmospheres, 117(5), 1–13, doi:10.1029/2011JD016654, 2012.

Jaffe, D. A., Honrath, R. E., Herring, J. A., Li, S. M. and Kahl, J. D.: Measurements of nitrogen oxides at Barrow, Alaska during spring: evidence for regional and Northern Hemispheric sources of pollution, Journal of Geophysical Research, 96(D4), 7395–7405, doi:10.1029/91JD00065, 1991.

Jaffe, D. A., Honrath, R. E., Furness, D., Conway, T. J., Dlugokencky, E. and Steele, L. P.: A determination of the CH4, NOx and CO2 emissions from the Prudhoe Bay, Alaska oil development, Journal of Atmospheric Chemistry, 20(3), 213–227, doi:10.1007/BF00694494, 1995.

Jayarathne, T., Sultana, C. M., Lee, C., Malfatti, F., Cox, J. L., Pendergraft, M. A., Moore, K. A., Azam, F., Tivanski, A. V., Cappa, C. D., Bertram, T. H., Grassian, V. H., Prather, K. A. and Stone, E. A.: Enrichment of Saccharides and Divalent Cations in Sea Spray Aerosol during Two Phytoplankton Blooms, Environmental Science and Technology, 50(21), 11511–11520, doi:10.1021/acs.est.6b02988, 2016.

Jentzsch, P. V., Kampe, B., Ciobotă, V., Rösch, P. and Popp, J.: Inorganic salts in atmospheric particulate matter: Raman spectroscopy as an analytical tool, Spectrochimica Acta - Part A: Molecular and Biomolecular Spectroscopy, 115, 697–708, doi:10.1016/j.saa.2013.06.085, 2013.

Jiang, H., Cotton, W. R., Pinto, J. O., Curry, J. A. and Weissbluth, M. J.: Cloud Resolving Simulations of Mixed-Phase Arctic Stratus Observed during BASE: Sensitivity to Concentration of Ice Crystals and Large-Scale Heat and Moisture Advection, Journal of the Atmospheric Sciences, 57(13), 2105–2117, doi:10.1175/1520-0469(2000)057<2105:crsomp>2.0.co;2, 2002.

Jiang, M. Y., Li, J. Q., Wu, Y. Q., Lin, N. T., Wang, X. M. and Fu, F. F.: Chemical characterization of nanometer-sized elemental carbon particles emitted from diesel vehicles, Journal of Aerosol Science, 42(6), 365–371, doi:10.1016/j.jaerosci.2011.03.002, 2011.

Jodwalis, C. M., Benner, R. L. and Eslinger, D. L.: Modeling of dimethyl sulfide ocean mixing, biological production, and sea-to-air flux for high latitudes, Journal of Geophysical Research Atmospheres, 105(D11), 14387–14399, doi:10.1029/2000JD900023, 2000.

Johnson, M. and Eicken, H.: Estimating Arctic sea-ice freeze-up and break-up from the satellite record: A comparison of different approaches in the Chukchi and Beaufort Seas, Elementa: Science of the Anthropocene, 4(2004), 000124, doi:10.12952/journal.elementa.000124,

2016.

Jones, J., Eicken, H., Mahoney, A., MV, R., Kambhamettu, C., Fukamachi, Y., Ohshima, K. I. and George, J. C.: Landfast sea ice breakouts: Stabilizing ice features, oceanic and atmospheric forcing at Barrow, Alaska, Continental Shelf Research, 126, 50–63, doi:10.1016/j.csr.2016.07.015, 2016.

Kaczor, A. and Baranska, M.: Structural changes of carotenoid astaxanthin in a single algal cell monitored in situ by raman spectroscopy, Analytical Chemistry, 83(20), 7763–7770, doi:10.1021/ac201302f, 2011.

Kanakidou, M., Seinfeld, J. H., Pandis, S. N., Barnes, I., Dentener, F. J., Facchini, M. C., Van Dingenen, R., Ervens, B., Nenes, A., Nielsen, C. J., Swietlicki, E., Putaud, J. P., Balkanski, Y., Fuzzi, S., Horth, J., Moortgat, G. K., Winterhalter, R., Myhre, C. E. L., Tsigaridis, K., Vignati, E., Stephanou, E. G. and Wilson, J.: Organic aerosol and global climate modelling: a review, Atmospheric Chemistry and Physics, 5, 1053–1123, doi:10.5194/acp-5-1053-2005, 2005.

Kane, J.: Multiyear variability of phytoplankton abundance in the Gulf of Maine, ICES Journal of Marine Science, 68(9), 1833–1841, doi:10.1093/icesjms/fsr122, 2011.

Kanji, Z. A., Ladino, L. A., Wex, H., Boose, Y., Burkert-Kohn, M., Cziczo, D. J. and Krämer, M.: Overview of Ice Nucleating Particles, Meteorological Monographs, 58, 1.1-1.33, doi:10.1175/AMSMONOGRAPHS-D-16-0006.1, 2017.

Karl, M., Leck, C., Coz, E. and Heintzenberg, J.: Marine nanogels as a source of atmospheric nanoparticles in the high Arctic, Geophysical Research Letters, 40(14), 3738–3743, doi:10.1002/grl.50661, 2013.

Kawamura, K. and Bikkina, S.: A review of dicarboxylic acids and related compounds in atmospheric aerosols: Molecular distributions, sources and transformation, Atmospheric Research, 170, 140–160, doi:10.1016/j.atmosres.2015.11.018, 2016.

Kawamura, K., Ono, K., Tachibana, E., Charríre, B. and Sempéré, R.: Distributions of low molecular weight dicarboxylic acids, ketoacids and α-dicarbonyls in the marine aerosols collected over the Arctic Ocean during late summer, Biogeosciences, 9(11), 4725–4737, doi:10.5194/bg-9-4725-2012, 2012.

Kawamura, K., Hoque, M. M. M., Bates, T. S. and Quinn, P. K.: Molecular distributions and isotopic compositions of organic aerosols over the western North Atlantic: Dicarboxylic acids, related compounds, sugars, and secondary organic aerosol tracers, Organic Geochemistry, 113, 229–238, doi:10.1016/j.orggeochem.2017.08.007, 2017.

Keene, W. C., Long, M. S., Reid, J. S., Frossard, A. A., Kieber, D. J., Maben, J. R., Russell, L. M., Kinsey, J. D., Quinn, P. K. and Bates, T. S.: Factors That Modulate Properties of Primary Marine Aerosol Generated From Ambient Seawater on Ships at Sea, Journal of Geophysical Research: Atmospheres, 122(21), 11,961-11,990, doi:10.1002/2017JD026872, 2017.

Kerminen, V. M. and Leck, C.: Sulfur chemistry over the central Arctic Ocean during the summer: Gas-to-particle transformation, Journal of Geophysical Research Atmospheres, 106(D23), 32087–32099, doi:10.1029/2000JD900604, 2001.

Kerminen, V. M., Teinilä, K., Hillamo, R. and Pakkanen, T.: Substitution of chloride in sea-salt particles by inorganic and organic anions, Journal of Aerosol Science, 29(8), 929–942, doi:10.1016/S0021-8502(98)00002-0, 1998.

Khlystov, A., Stanier, C. and Pandis, S. N.: An Algorithm for Combining Electrical Mobility and Aerodynamic Size Distributions Data when Measuring Ambient Aerosol Special Issue of Aerosol Science and Technology on Findings from the Fine Particulate Matter Supersites Program, Aerosol Science and Technology, 38(S1), 229–238, doi:10.1080/02786820390229543, 2004.

Kim, B. K., Lee, J. H., Yun, M. S., Joo, H. T., Song, H. J., Yang, E. J., Chung, K. H., Kang, S. H. and Lee, S. H.: High lipid composition of particulate organic matter in the northern Chukchi Sea, 2011, Deep-Sea Research Part II: Topical Studies in Oceanography, 120, 72–81, doi:10.1016/j.dsr2.2014.03.022, 2015a.

Kim, G., Cho, H. J., Seo, A., Kim, D., Gim, Y., Lee, B. Y., Yoon, Y. J. and Park, K.: Comparison of Hygroscopicity, Volatility, and Mixing State of Submicrometer Particles between Cruises over the Arctic Ocean and the Pacific Ocean, Environmental Science and Technology, 49(20), 12024–12035, doi:10.1021/acs.est.5b01505, 2015b.

Kirpes, R. M., Bondy, A. L., Bonanno, D., Moffet, R. C., Wang, B., Laskin, A., Ault, A. P. and Pratt, K. A.: Secondary sulfate is internally mixed with sea spray aerosol and organic aerosol in the winter Arctic, Atmospheric Chemistry and Physics, 18(6), 3937–3949, doi:10.5194/acp-18-3937-2018, 2018.

Kolesar, K. R., Cellini, J., Peterson, P. K., Jefferson, A., Tuch, T., Birmili, W., Wiedensohler, A. and Pratt, K. A.: Effect of Prudhoe Bay emissions on atmospheric aerosol growth events observed in Utqiaġvik (Barrow), Alaska, Atmospheric Environment, 152, 146–155, doi:10.1016/j.atmosenv.2016.12.019, 2017.

Köllensperger, G., Friedbacher, G., Kotzick, R., Niessner, R. and Grasserbauer, M.: In-situ atomic force microscopy investigation of aerosols exposed to different humidities, Fresenius' Journal of Analytical Chemistry, 364(4), 296–304, doi:10.1007/s002160051340, 1999.

Köllner, F., Schneider, J., Willis, M., Klimach, T., Helleis, F., Bozem, H., Kunkel, D., Hoor, P., Burkart, J., Richard Leaitch, W., Aliabadi, A. A., Abbatt, J. P. D., Herber, A. B. and Borrmann, S.: Particulate trimethylamine in the summertime Canadian high Arctic lower troposphere, Atmospheric Chemistry and Physics, 17(22), 13747–13766, doi:10.5194/acp-17-13747-2017, 2017.

Koop, T., Bookhold, J., Shiraiwa, M. and Pöschl, U.: Glass transition and phase state of

organic compounds: Dependency on molecular properties and implications for secondary organic aerosols in the atmosphere, Physical Chemistry Chemical Physics, 13(43), 19238–19255, doi:10.1039/c1cp22617g, 2011.

Korhonen, H., Carslaw, K. S., Spracklen, D. V., Riley, D. A. and Ström, J.: A global model study of processes controlling aerosol size distributions in the Arctic spring and summer, Journal of Geophysical Research Atmospheres, 113(8), doi:10.1029/2007JD009114, 2008.

Krembs, C., Eicken, H., Junge, K. and Deming, J. W.: High concentrations of exopolymeric substances in Arctic winter sea ice: Implications for the polar ocean carbon cycle and cryoprotection of diatoms, Deep-Sea Research Part I: Oceanographic Research Papers, 49(12), 2163–2181, doi:10.1016/S0967-0637(02)00122-X, 2002.

Krembs, C., Eicken, H. and Deming, J. W.: Exopolymer alteration of physical properties of sea ice and implications for ice habitability and biogeochemistry in a warmer Arctic, Proceedings of the National Academy of Sciences, 108(9), 3653–3658, doi:10.1073/pnas.1100701108, 2011.

Kuang, Y., Zhao, C. S., Zhao, G., Tao, J. C., Xu, W., Ma, N. and Bian, Y. X.: A novel method for calculating ambient aerosol liquid water content based on measurements of a humidified nephelometer system, Atmospheric Measurement Techniques, 11(5), 2967–2982, doi:10.5194/amt-11-2967-2018, 2018.

Kwon, D., Or, V. W., Sovers, M. J., Tang, M., Kleiber, P. D., Grassian, V. H. and Young, M. A.: Optical Property Measurements and Single Particle Analysis of Secondary Organic Aerosol Produced from the Aqueous-Phase Reaction of Ammonium Sulfate with Methylglyoxal, ACS Earth and Space Chemistry, 2(4), 356–365, doi:10.1021/acsearthspacechem.8b00004, 2018.

Laimin, Z. and Liqi, C.: China' s first exploration of Chukchi Sea and its adjacent waters in the arctic — A study on lead geochemistry of atmospheric aerosol, Chinese Journal of Geochemistry, 22(1), 23–29, doi:10.1007/bf02831542, 2008.

Laimin, Z., Liqi, C., Xuling, Y., Junmin, D. and Yuanhui, Z.: Chemistry of aerosols over Chukchi Sea and Bering Sea, Chinese Journal of Geochemistry, 23(1), 26–36, doi:10.1007/bf02841133, 2008.

Larkin, P. J.: Infrared and Raman Spectroscopy: Principles and Spectral Interpretation., 2011.

Laskin, A.: Reactions at Interfaces As a Source of Sulfate Formation in Sea-Salt Particles, Science, 301(5631), 340–344, doi:10.1126/science.1085374, 2003.

Laskin, A., Iedema, M. J. and Cowin, J. P.: Quantitative time-resolved monitoring of nitrate formation in sea salt particles using a CCSEM/EDX single particle analysis, Environmental Science and Technology, 36(23), 4948–4955, doi:10.1021/es020551k, 2002.

Laskin, A., Gaspar, D. J., Wang, W., Hunt, S. W., Cowin, J. P., Colson, S. D. and Finlayson-pitts, B. J.: reactions at interfaces as a source of sulfate formation in sea-salt particles, , 301, 340–345, 2003.

Laskin, A., Cowin, J. P. and Iedema, M. J.: Analysis of individual environmental particles using modern methods of electron microscopy and X-ray microanalysis, Journal of Electron Spectroscopy and Related Phenomena, 150(2–3), 260–274, doi:10.1016/j.elspec.2005.06.008, 2006.

Laskin, A., Moffet, R. C., Gilles, M. K., Fast, J. D., Zaveri, R. A., Wang, B., Nigge, P. and Shutthanandan, J.: Tropospheric chemistry of internally mixed sea salt and organic particles: Surprising reactivity of NaCl with weak organic acids, Journal of Geophysical Research: Atmospheres, 117(D15), n/a-n/a, doi:10.1029/2012JD017743, 2012.

Laskin, A., Gilles, M. K., Knopf, D. A., Wang, B. and China, S.: Progress in the Analysis of Complex Atmospheric Particles, Annu Rev Anal Chem (Palo Alto Calif), 9(1), 117–143, doi:10.1146/annurev-anchem-071015-041521, 2016.

Laskina, O., Morris, H. S., Grandquist, J. R., Estillore, A. D., Stone, E. A., Grassian, V. H. and Tivanski, A. V.: Substrate-Deposited Sea Spray Aerosol Particles: Influence of Analytical Method, Substrate, and Storage Conditions on Particle Size, Phase, and Morphology, Environmental Science and Technology, 49(22), 13447–13453, doi:10.1021/acs.est.5b02732, 2015.

Law, K. S. and Stohl, A.: Arctic air pollution: Origins and impacts, Science, 315(5818), 1537–1540, doi:10.1126/science.1137695, 2007.

Leck, C. and Bigg, E. K.: Aerosol production over remote marine areas-A new route, Geophysical Research Letters, 26(23), 3577–3580, doi:10.1029/1999gl010807, 1999.

Leck, C. and Bigg, E. K.: Biogenic particles in the surface microlayer and overlaying atmosphere in the central Arctic Ocean during summer, Tellus, Series B: Chemical and Physical Meteorology, 57(4), 305–316, doi:10.1111/j.1600-0889.2005.00148.x, 2005a.

Leck, C. and Bigg, E. K.: Source and evolution of the marine aerosol - A new perspective, Geophysical Research Letters, 32(19), 1–4, doi:10.1029/2005GL023651, 2005b.

Leck, C. and Keith Bigg, E.: Comparison of sources and nature of the tropical aerosol with the summer high Arctic aerosol, Tellus B: Chemical and Physical Meteorology, 60(1), 118–126, doi:10.1111/j.1600-0889.2007.00315.x, 2008.

Leck, C. and Svensson, E.: Importance of aerosol composition and mixing state for cloud droplet activation over the Arctic pack ice in summer, Atmospheric Chemistry and Physics, 15(5), 2545–2568, doi:10.5194/acp-15-2545-2015, 2015.

Leck, C., Norman, M. and Bigg, E. K.: Chemical composition and sources of the high

Arctic aerosol relevant for cloud formation, Journal of Geophysical Research, 107(D12), 4135, doi:10.1029/2001JD001463, 2002.

Leck, C., Gao, Q., Mashayekhy Rad, F. and Nilsson, U.: Size-resolved atmospheric particulate polysaccharides in the high summer Arctic, Atmospheric Chemistry and Physics, 13(24), 12573–12588, doi:10.5194/acp-13-12573-2013, 2013.

Lee, C., Sultana, C. M., Collins, D. B., Santander, M. V., Axson, J. L., Malfatti, F., Cornwell, G. C., Grandquist, J. R., Deane, G. B., Stokes, M. D., Azam, F., Grassian, V. H. and Prather, K. A.: Advancing Model Systems for Fundamental Laboratory Studies of Sea Spray Aerosol Using the Microbial Loop, Journal of Physical Chemistry A, 119(33), 8860–8870, doi:10.1021/acs.jpca.5b03488, 2015.

Lee, H. D., Ray, K. K. and Tivanski, A. V.: Solid, Semisolid, and Liquid Phase States of Individual Submicrometer Particles Directly Probed Using Atomic Force Microscopy, Analytical Chemistry, 89(23), 12720–12726, doi:10.1021/acs.analchem.7b02755, 2017.

de Leeuw, G., Moerman, M., Cohen, L., Brooks, B., Smith, M. and Vignati, E.: Aerosols, bubbles and sea spray production studies during the RED experiments, 2002.

De Leeuw, G., Andreas, E. L., Anguelova, M. D., Fairall, C. W., Lewis, E. R., O'Dowd, C., Schulz, M. and Schwartz, S. E.: Production flux of sea spray aerosol, Reviews of Geophysics, 49(2), RG2001, doi:10.1029/2010RG000349, 2011.

Lehmpuhl, D. W., Ramirez-Aguilar, K. A., Michel, A. E., Rowlen, K. L. and Birks, J. W.: Physical and chemical characterization of atmospheric aerosols by atomic force microscopy, Analytical Chemistry, 71(2), 379–383, doi:10.1021/ac980849m, 1999.

Letterly, A., Key, J. and Liu, Y.: The influence of winter cloud on summer sea ice in the Arctic, 1983–2013, Journal of Geophysical Research, 121(5), 2178–2187, doi:10.1002/2015JD024316, 2016.

Leu, E., Mundy, C. J., Assmy, P., Campbell, K., Gabrielsen, T. M., Gosselin, M., Juul-Pedersen, T. and Gradinger, R.: Arctic spring awakening - Steering principles behind the phenology of vernal ice algal blooms, Progress in Oceanography, 139, 151–170, doi:10.1016/j.pocean.2015.07.012, 2015.

Li, C., Wang, B., Wang, Z., Li, J., Yang, G., Chen, J., Lin, L., Lyu, Y. and Guo, F.: Spatial and Interannual Variability in Distributions and Cycling of Summer Biogenic Sulfur in the Bering Sea, Geophysical Research Letters, 46(9), 4816–4825, doi:10.1029/2018GL080446, 2019.

Li, M., Yu, X., Kang, H., Xie, Z. and Zhang, P.: Concentrations and size distributions of bacteria-containing particles over oceans from China to the Arctic ocean, Atmosphere, 8(5), 82, doi:10.3390/atmos8050082, 2017.

Li, W., Li, H., Li, J., Cheng, X., Zhang, Z., Chai, F., Zhang, H., Yang, T., Duan, P., Lu, D.

and Chen, Y.: TOF-SIMS surface analysis of chemical components of size-fractioned urban aerosols in a typical heavy air pollution event in Beijing, Journal of Environmental Sciences (China), 69, 61–76, doi:10.1016/j.jes.2017.04.005, 2018.

Lienhard, D. M., Huisman, A. J., Krieger, U. K., Rudich, Y., Marcolli, C., Luo, B. P., Bones, D. L., Reid, J. P., Lambe, A. T., Canagaratna, M. R., Davidovits, P., Onasch, T. B., Worsnop, D. R., Steimer, S. S., Koop, T. and Peter, T.: Viscous organic aerosol particles in the upper troposphere: Diffusivity-controlled water uptake and ice nucleation?, Atmospheric Chemistry and Physics, 15(23), 13599–13613, doi:10.5194/acp-15-13599-2015, 2015.

Lilliefors, H. W.: On the Kolmogorov-Smirnov test for normality with mean and variance unknown, Journal of the American Statistical Association, 62(318), 399–402, 1967.

Lin, F., Chen, M., Tong, J., Cao, J., Qiu, Y. and Zheng, M.: Carbon and nitrogen isotopic composition of particulate organic matter and its biogeochemical implication in the Bering Sea, Acta Oceanologica Sinica, 33(12), 40–47, doi:10.1007/s13131-014-0570-y, 2014.

Liu, D., Whitehead, J., Alfarra, M. R., Reyes-Villegas, E., Spracklen, D. V., Reddington, C. L., Kong, S., Williams, P. I., Ting, Y. C., Haslett, S., Taylor, J. W., Flynn, M. J., Morgan, W. T., McFiggans, G., Coe, H. and Allan, J. D.: Black-carbon absorption enhancement in the atmosphere determined by particle mixing state, Nature Geoscience, 10(3), 184–188, doi:10.1038/ngeo2901, 2017.

Liu, S., Aiken, A. C., Gorkowski, K., Dubey, M. K., Cappa, C. D., Williams, L. R., Herndon, S. C., Massoli, P., Fortner, E. C., Chhabra, P. S., Brooks, W. A., Onasch, T. B., Jayne, J. T., Worsnop, D. R., China, S., Sharma, N., Mazzoleni, C., Xu, L., Ng, N. L., Liu, D., Allan, J. D., Lee, J. D., Fleming, Z. L., Mohr, C., Zotter, P., Szidat, S. and Prevot, A. S.: Enhanced light absorption by mixed source black and brown carbon particles in UK winter, Nat Commun, 6, 8435, doi:10.1038/ncomms9435, 2015.

Liu, Y., Cain, J. P., Wang, H. and Laskin, A.: Kinetic study of heterogeneous reaction of deliquesced NaCl particles with gaseous HNO 3 using particle-on-substrate stagnation flow reactor approach, Journal of Physical Chemistry A, 111(40), 10026–10043, doi:10.1021/jp072005p, 2007.

Lohmann, U. and Leck, C.: Importance of submicron surface-active organic aerosols for pristine Arctic clouds, Tellus, Series B: Chemical and Physical Meteorology, 57(3), 261–268, doi:10.1111/j.1600-0889.2005.00144.x, 2005.

Lovejoy, C., Vincent, W. F., Bonilla, S., Roy, S., Martineau, M. J., Terrado, R., Potvin, M., Massana, R. and Pedrós-Alió, C.: Distribution, phylogeny, and growth of cold-adapted picoprasinophytes in arctic seas, Journal of Phycology, 43(1), 78–89, doi:10.1111/j.1529-8817.2006.00310.x, 2007.

Lundén, J., Svensson, G. and Leck, C.: Influence of meteorological processes on the spatial and temporal variability of atmospheric dimethyl sulfide in the high Arctic summer, Journal of Geophysical Research Atmospheres, 112(13), n/a-n/a, doi:10.1029/2006JD008183, 2007.

Maahn, M., de Boer, G., Creamean, J. M., Feingold, G., McFarquhar, G. M., Wu, W. and Mei, F.: The observed influence of local anthropogenic pollution on northern Alaskan cloud properties, Atmospheric Chemistry and Physics, 17(23), 14709–14726, doi:10.5194/acp-17-14709-2017, 2017.

Mabrouk, K. Ben, Kauffmann, T. H., Aroui, H. and Fontana, M. D.: Raman study of cation effect on sulfate vibration modes in solid state and in aqueous solutions, Journal of Raman Spectroscopy, 44(11), 1603–1608, doi:10.1002/jrs.4374, 2013.

Martin, M., Chang, R. Y. W., Sierau, B., Sjogren, S., Swietlicki, E., Abbatt, J. P. D., Leck, C. and Lohmann, U.: Cloud condensation nuclei closure study on summer arctic aerosol, Atmospheric Chemistry and Physics, 11(22), 11335–11350, doi:10.5194/acp-11-11335-2011, 2011.

Mashayekhy Rad, F., Leck, C., Ilag, L. L. and Nilsson, U.: Investigation of ultrahigh-performance liquid chromatography/travelling-wave ion mobility/time-of-flight mass spectrometry for fast profiling of fatty acids in the high Arctic sea surface microlayer, Rapid Communications in Mass Spectrometry, 32(12), 942–950, doi:10.1002/rcm.8109, 2018.

Mashayekhy Rad, F., Zurita, J., Gilles, P., Rutgeerts, L. A. J., Nilsson, U., Ilag, L. L. and Leck, C.: Measurements of Atmospheric Proteinaceous Aerosol in the Arctic Using a Selective UHPLC/ESI-MS/MS Strategy, Journal of the American Society for Mass Spectrometry, 30(1), 161–173, doi:10.1007/s13361-018-2009-8, 2019.

Maslanik, J., Stroeve, J., Fowler, C. and Emery, W.: Distribution and trends in Arctic sea ice age through spring 2011, Geophysical Research Letters, 38(13), n/a-n/a, doi:10.1029/2011GL047735, 2011.

Massey Jr, F. J.: The Kolmogorov-Smirnov test for goodness of fit, Journal of the American Statistical Association, 46(253), 68–78, 1951.

Matrai, P. A., Tranvik, L., Leck, C. and Knulst, J. C.: Are high Arctic surface microlayers a potential source of aerosol organic precursors?, Marine Chemistry, 108(1–2), 109–122, doi:10.1016/j.marchem.2007.11.001, 2008.

Mauritsen, T., Sedlar, J., Tjernstrãm, M., Leck, C., Martin, M., Shupe, M., Sjogren, S., Sierau, B., Persson, P. O. G., Brooks, I. M. and Swietlicki, E.: An Arctic CCN-limited cloud-aerosol regime, Atmospheric Chemistry and Physics, 11(1), 165–173, doi:10.5194/acp-11-165-2011, 2011.

May, N. W., Axson, J. L., Watson, A., Pratt, K. A. and Ault, A. P.: Lake spray aerosol generation: A method for producing representative particles from freshwater wave breaking, Atmospheric Measurement Techniques, 9(9), 4311–4325, doi:10.5194/amt-9-4311-2016, 2016a.

May, N. W., Quinn, P. K., McNamara, S. M. and Pratt, K. A.: Multiyear study of the

dependence of sea salt aerosol on wind speed and sea ice conditions in the coastal Arctic, Journal of Geophysical Research, 121(15), 9208–9219, doi:10.1002/2016JD025273, 2016b.

May, N. W., Olson, N. E., Panas, M., Axson, J. L., Tirella, P. S., Kirpes, R. M., Craig, R. L., Gunsch, M. J., China, S., Laskin, A., Ault, A. P. and Pratt, K. A.: Aerosol Emissions from Great Lakes Harmful Algal Blooms, Environmental Science and Technology, 52(2), 397–405, doi:10.1021/acs.est.7b03609, 2018a.

May, N. W., Gunsch, M. J., Olson, N. E., Bondy, A. L., Kirpes, R. M., Bertman, S. B., China, S., Laskin, A., Hopke, P. K., Ault, A. P. and Pratt, K. A.: Unexpected Contributions of Sea Spray and Lake Spray Aerosol to Inland Particulate Matter, Environmental Science and Technology Letters, 5(7), 405–412, doi:10.1021/acs.estlett.8b00254, 2018b.

Mayot, N., Matrai, P., Ellingsen, I. H., Steele, M., Johnson, K., Riser, S. C. and Swift, D.: Assessing Phytoplankton Activities in the Seasonal Ice Zone of the Greenland Sea Over an Annual Cycle, Journal of Geophysical Research: Oceans, 123(11), 8004–8025, doi:10.1029/2018JC014271, 2018.

McCluskey, C. S., Hill, T. C. J., Malfatti, F., Sultana, C. M., Lee, C., Santander, M. V., Beall, C. M., Moore, K. A., Cornwell, G. C., Collins, D. B., Prather, K. A., Jayarathne, T., Stone, E. A., Azam, F., Kreidenweis, S. M. and DeMott, P. J.: A Dynamic Link between Ice Nucleating Particles Released in Nascent Sea Spray Aerosol and Oceanic Biological Activity during Two Mesocosm Experiments, Journal of the Atmospheric Sciences, 74(1), 151–166, doi:10.1175/jas-d-16-0087.1, 2016.

McLaughlin, R. P., Bird, B. and Reid, P. J.: Vibrational analysis of isopropyl nitrate and isobutyl nitrate, Spectrochimica Acta - Part A Molecular and Biomolecular Spectroscopy, 58(12), 2571–2580, doi:10.1016/S1386-1425(02)00022-7, 2002.

Meier, W.: Rapid ice loss in early April leads to new record low, National Snow and Ice Data Center [online] Available from: http://nsidc.org/arcticseaicenews/category/analysis/ (Accessed 2 May 2019), 2019.

Mertes, S., Dippel, B. and Schwarzenböck, A.: Quantification of graphitic carbon in atmospheric aerosol particles by Raman spectroscopy and first application for the determination of mass absorption efficiencies, Journal of Aerosol Science, 35(3), 347–361, doi:10.1016/j.jaerosci.2003.10.002, 2004.

Miyazaki, Y., Yamashita, Y., Kawana, K., Tachibana, E., Kagami, S., Mochida, M., Suzuki, K. and Nishioka, J.: Chemical transfer of dissolved organic matter from surface seawater to sea spray water-soluble organic aerosol in the marine atmosphere, Scientific Reports, 8(1), 14861, doi:10.1038/s41598-018-32864-7, 2018.

Moffet, R. C. and Prather, K. A.: In-situ measurements of the mixing state and optical properties of soot with implications for radiative forcing estimates, Proceedings of the National Academy of Sciences, 106(29), 11872–11877, doi:10.1073/pnas.0900040106, 2009.

Moffet, R. C., Henn, T., Laskin, A. and Gilles, M. K.: Automated chemical analysis of internally mixed aerosol particles using X-ray spectromicroscopy at the carbon K-edge, Analytical Chemistry, 82(19), 7906–7914, doi:10.1021/ac1012909, 2010a.

Moffet, R. C., Henn, T. R., Tivanski, A. V., Hopkins, R. J., Desyaterik, Y., Kilcoyne, A. L. D., Tyliszczak, T., Fast, J., Barnard, J., Shutthanandan, V., Cliff, S. S., Perry, K. D., Laskin, A. and Gilles, M. K.: Microscopic characterization of carbonaceous aerosol particle aging in the outflow from Mexico City, Atmospheric Chemistry and Physics, 10(3), 961–976, doi:10.5194/acp-10-961-2010, 2010b.

Monahan, E. C.: Comments on "Bubbles Produced by Breaking Waves in Fresh and Salt Water," Journal of Physical Oceanography, 31(7), 1931–1932, doi:10.1175/1520-0485(2001)031<1931:COBPBB>2.0.CO;2, 2001.

Moore, M. J. K., Furutani, H., Roberts, G. C., Moffet, R. C., Gilles, M. K., Palenik, B. and Prather, K. A.: Effect of organic compounds on cloud condensation nuclei (CCN) activity of sea spray aerosol produced by bubble bursting, Atmospheric Environment, 45(39), 7462–7469, doi:10.1016/j.atmosenv.2011.04.034, 2011.

Movasaghi, Z., Rehman, S. and Rehman, I. U.: Raman spectroscopy of biological tissues, Applied Spectroscopy Reviews, 42(5), 493–541, doi:10.1080/05704920701551530, 2007.

Mungall, E. L., Croft, B., Lizotte, M., Thomas, J. L., Murphy, J. G., Levasseur, M., Martin, R. V., Wentzell, J. J. B., Liggio, J. and Abbatt, J. P. D.: Dimethyl sulfide in the summertime Arctic atmosphere: Measurements and source sensitivity simulations, Atmospheric Chemistry and Physics, 16(11), 6665–6680, doi:10.5194/acp-16-6665-2016, 2016.

Mungall, E. L., Abbatt, J. P. D., Wentzell, J. J. B., Lee, A. K. Y., Thomas, J. L., Blais, M., Gosselin, M., Miller, L. A., Papakyriakou, T., Willis, M. D. and Liggio, J.: Microlayer source of oxygenated volatile organic compounds in the summertime marine Arctic boundary layer, Proceedings of the National Academy of Sciences, 114(24), 6203–6208, doi:10.1073/pnas.1620571114, 2017.

Murphy, S. M., Agrawal, H., Sorooshian, A., Padró, L. T., Gates, H., Hersey, S., Welch, W. A., Jung, H., Miller, J. W., Cocker, D. R., Nenes, A., Jonsson, H. H., Flagan, R. C. and Seinfeld, J. H.: Comprehensive Simultaneous Shipboard and Airborne Characterization of Exhaust from a Modern Container Ship at Sea, Environmental Science & Technology, 43(13), 4626–4640, doi:10.1021/es802413j, 2009.

Murray, B. J., O'Sullivan, D., Atkinson, J. D. and Webb, M. E.: Ice nucleation by particles immersed in supercooled cloud droplets, Chemical Society Reviews, 41(19), 6519–6554, doi:10.1039/c2cs35200a, 2012.

Myhre, G., Bellouin, N., Berglen, T. F., Berntsen, T. K., Boucher, O., Grini, A., Isaksen, I. S. A., Johnsrud, M., Mishchenko, M. I., Stordal, F. and Tanré, D.: Comparison of the radiative

properties and direct radiative effect of aerosols from a global aerosol model and remote sensing data over ocean, Tellus, Series B: Chemical and Physical Meteorology, 59(1), 115–129, doi:10.1111/j.1600-0889.2006.00238.x, 2007.

Nguyen, T. K. V, Zhang, Q., Jimenez, J. L., Pike, M. and Carlton, A. G.: Liquid Water: Ubiquitous Contributor to Aerosol Mass, Environmental Science & Technology Letters, 3(7), 257–263, doi:10.1021/acs.estlett.6b00167, 2016.

Nie, W., Hong, J., Häme, S. A. K., Ding, A., Li, Y., Yan, C., Hao, L., Mikkilä, J., Zheng, L., Xie, Y., Zhu, C., Xu, Z., Chi, X., Huang, X., Zhou, Y., Lin, P., Virtanen, A., Worsnop, D. R., Kulmala, M., Ehn, M., Yu, J., Kerminen, V. M. and Petäjä, T.: Volatility of mixed atmospheric humic-like substances and ammonium sulfate particles, Atmospheric Chemistry and Physics, 17(5), 3659–3672, doi:10.5194/acp-17-3659-2017, 2017.

Niemi, A., Michel, C., Hille, K. and Poulin, M.: Protist assemblages in winter sea ice: Setting the stage for the spring ice algal bloom, Polar Biology, 34(12), 1803–1817, doi:10.1007/s00300-011-1059-1, 2011.

Nilsson, E. D., Rannik, Ü., Swietlicki, E., Leck, C., Aalto, P. P., Zhou, J. and Norman, M.: Turbulent aerosol fluxes over the Arctic Ocean 2. Wind-driven sources from the sea, Journal of Geophysical Research Atmospheres, 106(D23), 32139–32154, doi:10.1029/2000JD900747, 2001.

Norman, A. L., Barrie, L. A., Toom-Sauntry, D., Sirois, A., Krouse, H. R., Li, S. M. and Sharma, S.: Sources of aerosol sulphate at Alert: Apportionment using stable isotopes, Journal of Geophysical Research Atmospheres, 104(D9), 11619–11631, doi:10.1029/1999JD900078, 1999.

Norris, S. J., Brooks, I. M., De Leeuw, G., Sirevaag, A., Leck, C., Brooks, B. J., Birch, C. E. and Tjernström, M.: Measurements of bubble size spectra within leads in the Arctic summer pack ice, Ocean Science, 7(1), 129–139, doi:10.5194/os-7-129-2011, 2011.

Notz, D. and Stroeve, J.: Observed Arctic sea-ice loss directly follows anthropogenic CO2 emission, Science, 354(6313), 747–750, doi:10.1126/science.aag2345, 2016.

O'Brien, R., Wang, B., Kelly, S. T., Lundt, N., You, Y., Bertram, A. K., Leone, S. R., Laskin, A. and Gilles, M. K.: Liquid-liquid phase separation in aerosol particles: Imaging at the nanometer scale, Environmental Science and Technology, 49(8), 4995–5002, doi:10.1021/acs.est.5b00062, 2015a.

O'Brien, R. E., Neu, A., Epstein, S. A., MacMillan, A. C., Wang, B., Kelly, S. T., Nizkorodov, S. A., Laskin, A., Moffet, R. C. and Gilles, M. K.: Physical properties of ambient and laboratory generated secondary organic aerosol, Geophysical Research Letters, 41(12), 4347–4353, doi:10.1002/2014GL060219, 2014.

O'Brien, R. E., Wang, B., Laskin, A., Riemer, N., West, M., Zhang, Q., Sun, Y., Yu, X.-Y., Alpert, P., Knopf, D. A., Gilles, M. K. and Moffet, R. C.: Chemical imaging of ambient aerosol particles: Observational constraints on mixing state parameterization, Journal of Geophysical

Research: Atmospheres, 120(18), 9591–9605, doi:10.1002/2015JD023480, 2015b.

Ødemark, K., Dalsøren, S. B., Samset, B. H., Berntsen, T. K., Fuglestvedt, J. S. and Myhre, G.: Short-lived climate forcers from current shipping and petroleum activities in the Arctic, Atmospheric Chemistry and Physics, 12(4), 1979–1993, doi:10.5194/acp-12-1979-2012, 2012.

Or, V. W., Estillore, A. D., Tivanski, A. V and Grassian, V. H.: Lab on a tip: atomic force microscopy – photothermal infrared spectroscopy of atmospherically relevant organic/inorganic aerosol particles in the nanometer to micrometer size range, Analyst, 143(12), 2765–2774, doi:10.1039/C8AN00171E, 2018.

Orellana, M. V. and Leck, C.: Marine Microgels, edited by C. A. Carlson, Biogeochemistry of Marine Dissolved Organic Matter: Second Edition, 4, 451–480, doi:10.1016/B978-0-12-405940-5.00009-1, 2014.

Orellana, M. V., Matrai, P. A., Leck, C., Rauschenberg, C. D., Lee, A. M. and Coz, E.: Marine microgels as a source of cloud condensation nuclei in the high Arctic, Proceedings of the National Academy of Sciences, 108(33), 13612–13617, doi:10.1073/pnas.1102457108, 2011.

Ovadnevaite, J., Ceburnis, D., Leinert, S., Dall'Osto, M., Canagaratna, M., O'Doherty, S., Berresheim, H. and O'Dowd, C.: Submicron NE Atlantic marine aerosol chemical composition and abundance: Seasonal trends and air mass categorization, Journal of Geophysical Research-Atmospheres, 119(20), 11850–11863, doi:10.1002/2013jd021330, 2014.

Overland, J. E. and Wang, M.: When will the summer Arctic be nearly sea ice free?, Geophysical Research Letters, 40(10), 2097–2101, doi:10.1002/grl.50316, 2013.

Pakulski, J. D. and Benner, R.: Abundance and distribution of carbohydrates in the ocean, Limnology and Oceanography, 39(4), 930–940, doi:10.4319/lo.1994.39.4.0930, 1994.

Patterson, J. P., Collins, D. B., Michaud, J. M., Axson, J. L., Sultana, C. M., Moser, T., Dommer, A. C., Conner, J., Grassian, V. H., Stokes, M. D., Deane, G. B., Evans, J. E., Burkart, M. D., Prather, K. A. and Gianneschi, N. C.: Sea spray aerosol structure and composition using cryogenic transmission electron microscopy, ACS Central Science, 2(1), 40–47, doi:10.1021/acscentsci.5b00344, 2016.

Pearson, C. S. and Beyer, K. D.: Solid/liquid phase diagram of the ammonium sulfate/succinic acid/water system, Journal of Physical Chemistry A, 119(19), 4317–4328, doi:10.1021/jp506902q, 2015.

Peters, G. P., Nilssen, T. B., Lindholt, L., Eide, M. S., Glomsrod, S., Eide, L. I. and Fuglestvedt, J. S.: Future emissions from shipping and petroleum activities in the Arctic, Atmospheric Chemistry and Physics, 11(11), 5305–5320, doi:10.5194/acp-11-5305-2011, 2011.

Petters, M. D. and Kreidenweis, S. M.: A single parameter representation of hygroscopic growth and cloud condensation nucleus activity - Part 2: Including solubility, Atmospheric

Chemistry and Physics, 8(20), 6273–6279, doi:10.5194/acp-8-6273-2008, 2008.

Petters, S. S. and Petters, M. D.: Surfactant effect on cloud condensation nuclei for two-component internally mixed aerosols, Journal of Geophysical Research, 121(4), 1878–1895, doi:10.1002/2015JD024090, 2016.

Pham, D. Q., O'Brien, R., Fraund, M., Bonanno, D., Laskina, O., Beall, C., Moore, K. A., Forestieri, S., Wang, X., Lee, C., Sultana, C., Grassian, V., Cappa, C. D., Prather, K. A. and Moffet, R. C.: Biological Impacts on Carbon Speciation and Morphology of Sea Spray Aerosol, ACS Earth and Space Chemistry, 1(9), 551–561, doi:10.1021/acsearthspacechem.7b00069, 2017.

Phelps, A. D. and Leighton, T. G.: Oceanic bubble population measurements using a buoy-deployed combination frequency technique., 1998.

Phelps, A. D., Ramble, D. G. and Leighton, T. G.: The use of a combination frequency technique to measure the surf zone bubble population, The Journal of the Acoustical Society of America, 101(4), 1981–1989, doi:10.1121/1.418199, 2002.

Pilson, M. E. Q.: An introduction to the chemistry of the sea, Cambridge University Press., 2013.

Pithan, F. and Mauritsen, T.: Arctic amplification dominated by temperature feedbacks in contemporary climate models, Nature Geoscience, 7(3), 181–184, doi:10.1038/ngeo2071, 2014.

Polissar, A. V., Hopke, P. K., Paatero, P., Kaufmann, Y. J., Hall, D. K., Bodhaine, B. A., Dutton, E. G. and Harris, J. M.: The aerosol at Barrow, Alaska: Long-term trends and source locations, Atmospheric Environment, 33(16), 2441–2458, doi:10.1016/S1352-2310(98)00423-3, 1999.

Pöschl, U.: Atmospheric aerosols: Composition, transformation, climate and health effects, Angewandte Chemie - International Edition, 44(46), 7520–7540, doi:10.1002/anie.200501122, 2005.

Pósfai, M. and Buseck, P. R.: Nature and Climate Effects of Individual Tropospheric Aerosol Particles, in Annual Review of Earth and Planetary Sciences, vol. 38, edited by R. Jeanloz and K. H. Freeman, pp. 17–43., 2010.

Prather, K. A., Hatch, C. D. and Grassian, V. H.: Analysis of Atmospheric Aerosols, Annual Review of Analytical Chemistry, 1(1), 485–514, doi:10.1146/annurev.anchem.1.031207.113030, 2008.

Prather, K. A., Bertram, T. H., Grassian, V. H., Deane, G. B., Stokes, M. D., DeMott, P. J., Aluwihare, L. I., Palenik, B. P., Azam, F., Seinfeld, J. H., Moffet, R. C., Molina, M. J., Cappa, C. D., Geiger, F. M., Roberts, G. C., Russell, L. M., Ault, A. P., Baltrusaitis, J., Collins, D. B., Corrigan, C. E., Cuadra-Rodriguez, L. A., Ebben, C. J., Forestieri, S. D., Guasco, T. L., Hersey, S. P., Kim, M. J., Lambert, W. F., Modini, R. L., Mui, W., Pedler, B. E., Ruppel, M. J., Ryder, O.

S., Schoepp, N. G., Sullivan, R. C. and Zhao, D.: Bringing the ocean into the laboratory to probe the chemical complexity of sea spray aerosol, Proceedings of the National Academy of Sciences, 110(19), 7550–7555, doi:10.1073/pnas.1300262110, 2013.

Quinn, P. K., Miller, T. L., Bates, T. S., Ogren, J. A., Andrews, E. and Shaw, G. E.: A 3-year record of simultaneously measured aerosol chemical and optical properties at Barrow, Alaska, Journal of Geophysical Research: Atmospheres, 107(D11), AAC 8-1-AAC 8-15, doi:10.1029/2001jd001248, 2002.

Quinn, P. K., Shaw, G., Andrews, E., Dutton, E. G., Ruoho-Airola, T. and Gong, S. L.: Arctic haze: current trends and knowledge gaps, Tellus Series B-Chemical and Physical Meteorology, 59(1), 99–114, doi:10.1111/j.1600-0889.2006.00238.x, 2007.

Quinn, P. K., Bates, T. S., Baum, E., Doubleday, N., Fiore, A. M., Flanner, M., Fridlind, A., Garrett, T. J., Koch, D., Menon, S., Shindell, D., Stohl, A. and Warren, S. G.: Short-lived pollutants in the Arctic: Their climate impact and possible mitigation strategies, Atmospheric Chemistry and Physics, 8(6), 1723–1735, doi:10.5194/acp-8-1723-2008, 2008.

Quinn, P. K., Bates, T. S., Schulz, K. S., Coffman, D. J., Frossard, A. A., Russell, L. M., Keene, W. C. and Kieber, D. J.: Contribution of sea surface carbon pool to organic matter enrichment in sea spray aerosol, Nature Geoscience, 7(3), 228–232, doi:10.1038/ngeo2092, 2014.

Quinn, P. K., Collins, D. B., Grassian, V. H., Prather, K. A. and Bates, T. S.: Chemistry and Related Properties of Freshly Emitted Sea Spray Aerosol, Chemical Reviews, 115(10), 4383–4399, doi:10.1021/cr500713g, 2015.

Raatikainen, T., Brus, D., Hyvärinen, A. P., Svensson, J., Asmi, E. and Lihavainen, H.: Black carbon concentrations and mixing state in the Finnish Arctic, Atmospheric Chemistry and Physics, 15(17), 10057–10070, doi:10.5194/acp-15-10057-2015, 2015.

Ravishankara, A. R.: Heterogeneous and Multiphase Chemistry in the Troposphere, Science, 276(5315), 1058–1065 [online] Available from: http://www.jstor.org/stable/2893505, 1997.

Rebotier, T. P. and Prather, K. A.: Aerosol time-of-flight mass spectrometry data analysis: A benchmark of clustering algorithms, Analytica Chimica Acta, 585(1), 38–54, doi:https://doi.org/10.1016/j.aca.2006.12.009, 2007.

Reid, J. P., Bertram, A. K., Topping, D. O., Laskin, A., Martin, S. T., Petters, M. D., Pope, F. D. and Rovelli, G.: The viscosity of atmospherically relevant organic particles, Nature Communications, 9(1), 956, doi:10.1038/s41467-018-03027-z, 2018.

Renbaum-Wolff, L., Grayson, J. W., Bateman, A. P., Kuwata, M., Sellier, M., Murray, B. J., Shilling, J. E., Martin, S. T. and Bertram, A. K.: Viscosity of -pinene secondary organic material and implications for particle growth and reactivity, Proceedings of the National Academy of Sciences, 110(20), 8014–8019, doi:10.1073/pnas.1219548110, 2013.

Richard Leaitch, W., Russell, L. M., Liu, J., Kolonjari, F., Toom, D., Huang, L., Sharma, S., Chivulescu, A., Veber, D. and Zhang, W.: Organic functional groups in the submicron aerosol at 82.5° N, 62.5° W from 2012 to 2014, Atmospheric Chemistry and Physics, 18(5), 3269–3287, doi:10.5194/acp-18-3269-2018, 2018.

Richter-Menge, J. A. and Farrell, S. L.: Arctic sea ice conditions in spring 2009-2013 prior to melt, Geophysical Research Letters, 40(22), 5888–5893, doi:10.1002/2013GL058011, 2013.

Riemer, N., Ault, A. P., West, M., Craig, R. L. and Curtis, J. H.: Aerosol Mixing State: Measurements, Modeling, and Impacts, Reviews of Geophysics, 0(0), 2018RG000615, doi:10.1029/2018RG000615, 2019.

Riva, M., Bell, D. M., Hansen, A. M. K., Drozd, G. T., Zhang, Z., Gold, A., Imre, D., Surratt, J. D., Glasius, M. and Zelenyuk, A.: Effect of Organic Coatings, Humidity and Aerosol Acidity on Multiphase Chemistry of Isoprene Epoxydiols, Environmental Science and Technology, 50(11), 5580–5588, doi:10.1021/acs.est.5b06050, 2016.

Roiger, A., Thomas, J. L., Schlager, H., Law, K. S., Kim, J., Schäfler, A., Weinzierl, B., Dahlkötter, F., Risch, I. K., Marelle, L., Minikin, A., Raut, J. C., Reiter, A., Rose, M., Scheibe, M., Stock, P., Baumann, R., Bouarar, I., Lerbaux, C. C., George, M., Onishi, T. and Flemming, A. J.: Quantifying emerging local anthropogenic emissions in the arctic region: The access aircraft campaign experiment, Bulletin of the American Meteorological Society, 96(3), 441–460, doi:10.1175/BAMS-D-13-00169.1, 2015.

Roscoe, H. K., Brooks, B., Jackson, A. V., Smith, M. H., Walker, S. J., Obbard, R. W. and Wolff, E. W.: Frost flowers in the laboratory: Growth, characteristics, aerosol, and the underlying sea ice, Journal of Geophysical Research Atmospheres, 116(12), doi:10.1029/2010JD015144, 2011.

Ruehl, C. R. and Wilson, K. R.: Surface organic monolayers control the hygroscopic growth of submicrometer particles at high relative humidity, Journal of Physical Chemistry A, 118(22), 3952–3966, doi:10.1021/jp502844g, 2014.

Russell, L. M., Hawkins, L. N., Frossard, A. A., Quinn, P. K. and Bates, T. S.: Carbohydrate-like composition of submicron atmospheric particles and their production from ocean bubble bursting, Proceedings of the National Academy of Sciences, 107(15), 6652–6657, doi:10.1073/pnas.0908905107, 2010.

Ryder, O. S., Campbell, N. R., Morris, H., Forestieri, S., Ruppel, M. J., Cappa, C., Tivanski, A., Prather, K. and Bertram, T. H.: Role of Organic Coatings in Regulating N2O5 Reactive Uptake to Sea Spray Aerosol, Journal of Physical Chemistry A, 119(48), 11683–11692, doi:10.1021/acs.jpca.5b08892, 2015.

Sakerin, S. M., Bobrikov, A. A., Bukin, O. A., Golobokova, L. P., Pol'Kin, V. V., Pol'Kin, V. V., Shmirko, K. A., Kabanov, D. M., Khodzher, T. V., Onischuk, N. A., Pavlov, A. N.,

Potemkin, V. L. and Radionov, V. F.: On measurements of aerosol-gas composition of the atmosphere during two expeditions in 2013 along the Northern Sea Route, Atmospheric Chemistry and Physics, 15(21), 12413–12443, doi:10.5194/acp-15-12413-2015, 2015.

Salter, M. E., Nilsson, E. D., Butcher, A. and Bilde, M.: On the seawater temperature dependence of the sea spray aerosol generated by a continuous plunging jet, Journal of Geophysical Research, 119(14), 9052–9072, doi:10.1002/2013JD021376, 2014.

Salter, M. E., Zieger, P., Acosta Navarro, J. C., Grythe, H., Kirkevåg, A., Rosati, B., Riipinen, I. and Nilsson, E. D.: An empirically derived inorganic sea spray source function incorporating sea surface temperature, Atmospheric Chemistry and Physics, 15(19), 11047–11066, doi:10.5194/acp-15-11047-2015, 2015.

Salter, M. E., Hamacher-Barth, E., Leck, C., Werner, J., Johnson, C. M., Riipinen, I., Nilsson, E. D. and Zieger, P.: Calcium enrichment in sea spray aerosol particles, Geophysical Research Letters, 43(15), 8277–8285, doi:10.1002/2016GL070275, 2016.

Sander, R. and Bottenheim, J.: A compilation of tropospheric measurements of gas-phase and aerosol chemistry in polar regions, Earth System Science Data, 4(1), 215–282, doi:10.5194/essd-4-215-2012, 2012.

Scalabrin, E., Zangrando, R., Barbaro, E., Kehrwald, N. M., Gabrieli, J., Barbante, C. and Gambaro, A.: Amino acids in Arctic aerosols, Atmospheric Chemistry and Physics, 12(21), 10453–10463, doi:10.5194/acp-12-10453-2012, 2012.

Schill, G. P. and Tolbert, M. A.: Heterogeneous ice nucleation on phase-separated organic-sulfate particles: Effect of liquid vs. glassy coatings, Atmospheric Chemistry and Physics, 13(9), 4681–4695, doi:10.5194/acp-13-4681-2013, 2013.

Schill, S. R., Collins, D. B., Lee, C., Morris, H. S., Novak, G. A., Prather, K. A., Quinn, P. K., Sultana, C. M., Tivanski, A. V., Zimmermann, K., Cappa, C. D. and Bertram, T. H.: The impact of aerosol particle mixing state on the hygroscopicity of sea spray aerosol, ACS Central Science, 1(3), 132–141, doi:10.1021/acscentsci.5b00174, 2015.

Schmitz, I., Schreiner, M., Friedbacher, G. and Grasserbauer, M.: Phase imaging as an extension to tapping mode AFM for the identification of material properties on humidity-sensitive surfaces, Applied Surface Science, 115(2), 190–198, doi:10.1016/S0169-4332(97)80204-8, 1997.

Schneider, J., Mertes, S., Van Pinxteren, D., Herrmann, H. and Borrmann, S.: Uptake of nitric acid, ammonia, and organics in orographic clouds: Mass spectrometric analyses of droplet residual and interstitial aerosol particles, Atmospheric Chemistry and Physics, 17(2), 1571–1593, doi:10.5194/acp-17-1571-2017, 2017.

Schwier, A. N., Rose, C., Asmi, E., Ebling, A. M., Landing, W. M., Marro, S., Pedrotti, M. L., Sallon, A., Iuculano, F., Agusti, S., Tsiola, A., Pitta, P., Louis, J., Guieu, C., Gazeau, F. and Sellegri, K.: Primary marine aerosol emissions from the Mediterranean Sea during pre-bloom and

oligotrophic conditions: Correlations to seawater chlorophyll a from a mesocosm study, Atmospheric Chemistry and Physics, 15(14), 7961–7976, doi:10.5194/acp-15-7961-2015, 2015.

Schwier, A. N., Sellegri, K., Mas, S., Charrière, B., Pey, J., Rose, C., Temime-Roussel, B., Jaffrezo, J. L., Parin, D., Picard, D., Ribeiro, M., Roberts, G., Sempéré, R., Marchand, N. and D'Anna, B.: Primary marine aerosol physical flux and chemical composition during a nutrient enrichment experiment in mesocosms in the Mediterranean Sea, Atmospheric Chemistry and Physics, 17(23), 14645–14660, doi:10.5194/acp-17-14645-2017, 2017.

Scott, W. D. and Levin, Z. E. V.: Open channels in sea ice (Leads) as ion sources, Science, 177(4047), 425–426, doi:10.1126/science.177.4047.425, 1972.

Seinfeld, J. H. and Pandis, S. N.: Atmospheric Chemistry and Physics: From Air Pollution to Climate Change, John Wiley & Sons., 2012.

Sellegri, K., O'Dowd, C. D., Yoon, Y. J., Jennings, S. G. and de Leeuw, G.: Surfactants and submicron sea spray generation, Journal of Geophysical Research Atmospheres, 111(22), D22215, doi:10.1029/2005JD006658, 2006.

Serreze, M. C. and Barry, R. G.: Processes and impacts of Arctic amplification: A research synthesis, Global and Planetary Change, 77(1–2), 85–96, doi:10.1016/j.gloplacha.2011.03.004, 2011.

Sharma, S., Barrie, L. A., Plummer, D., McConnell, J. C., Brickell, P. C., Levasseur, M., Gosselin, M. and Bates, T. S.: Flux estimation of oceanic dimethyl sulfide around North America, Journal of Geophysical Research Atmospheres, 104(D17), 21327–21342, doi:10.1029/1999JD900207, 1999.

Sharma, S., Chan, E., Ishizawa, M., Toom-Sauntry, D., Gong, S. L., Li, S. M., Tarasick, D. W., Leaitch, W. R., Norman, A., Quinn, P. K., Bates, T. S., Levasseur, M., Barrie, L. A. and Maenhaut, W.: Influence of transport and ocean ice extent on biogenic aerosol sulfur in the Arctic atmosphere, Journal of Geophysical Research Atmospheres, 117(12), doi:10.1029/2011JD017074, 2012.

Shaw, G. E.: X-ray spectrometry of polar aerosols, Atmospheric Environment (1967), 17(2), 329–339, doi:10.1016/0004-6981(83)90049-5, 1983.

Shaw, P. M., Russell, L. M., Jefferson, A. and Quinn, P. K.: Arctic organic aerosol measurements show particles from mixed combustion in spring haze and from frost flowers in winter, Geophysical Research Letters, 37(10), L10803, doi:10.1029/2010GL042831, 2010.

Shen, H., Peters, T. M., Casuccio, G. S., Lersch, T. L., West, R. R., Kumar, A., Kumar, N. and Ault, A. P.: Elevated Concentrations of Lead in Particulate Matter on the Neighborhood-Scale in Delhi, India As Determined by Single Particle Analysis, Environmental Science & Technology, 50(10), 4961–4970, doi:10.1021/acs.est.5b06202, 2016.

Shen, Z., Liu, J., Horowitz, L. W., Henze, D. K., Fan, S., H., L. I., Mauzerall, D. L., Lin, J.-T. and Tao, S.: Analysis of transpacific transport of black carbon during HIPPO-3: implications for black carbon aging, Atmospheric Chemistry and Physics, 14(12), 6315–6327, doi:10.5194/acp-14-6315-2014, 2014.

Shipp, D. W., Sinjab, F. and Notingher, I.: Raman spectroscopy: techniques and applications in the life sciences, Advances in Optics and Photonics, 9(2), 315–428, 2017.

Shiraiwa, M., Yee, L. D., Schilling, K. A., Loza, C. L., Craven, J. S., Zuend, A., Ziemann, P. J. and Seinfeld, J. H.: Size distribution dynamics reveal particle-phase chemistry in organic aerosol formation, Proceedings of the National Academy of Sciences, 110(29), 11746–11750, doi:10.1073/pnas.1307501110, 2013.

Shiraiwa, M., Li, Y., Tsimpidi, A. P., Karydis, V. A., Berkemeier, T., Pandis, S. N., Lelieveld, J., Koop, T. and Pöschl, U.: Global distribution of particle phase state in atmospheric secondary organic aerosols, Nature Communications, 8, 1–7, doi:10.1038/ncomms15002, 2017.

Sierau, B., Chang, R. Y. W., Leck, C., Paatero, J. and Lohmann, U.: Single-particle characterization of the high-Arctic summertime aerosol, Atmospheric Chemistry and Physics, 14(14), 7409–7430, doi:10.5194/acp-14-7409-2014, 2014.

Sirois, A. and Barrie, L. A.: Arctic lower tropospheric aerosol trends and composition at Alert, Canada: 1980-1995, Journal of Geophysical Research Atmospheres, 104(D9), 11599–11618, doi:10.1029/1999JD900077, 1999.

Slade, J. H., Ault, A. P., Bui, A. T., Ditto, J. C., Lei, Z., Bondy, A. L., Olson, N. E., Cook, R. D., Desrochers, S. J., Harvey, R. M., Erickson, M. H., Wallace, H. W., Alvarez, S. L., Flynn, J. H., Boor, B. E., Petrucci, G. A., Gentner, D. R., Griffin, R. J. and Shepson, P. B.: Bouncier Particles at Night: Biogenic Secondary Organic Aerosol Chemistry and Sulfate Drive Diel Variations in the Aerosol Phase in a Mixed Forest, Environmental Science & Technology, 53(9), 4977–4987, doi:10.1021/acs.est.8b07319, 2019.

Sobanska, S., Coeur, C., Maenhaut, W. and Adams, F.: SEM-EDX characterisation of trophospheric aerosols in the Negev desert (Israel), Journal of Atmospheric Chemistry, 44(3), 299–322, doi:10.1023/A:1022969302107, 2003.

Sobanska, S., Hwang, H., Choël, M., Jung, H. J., Eom, H. J., Kim, H., Barbillat, J. and Ro, C. U.: Investigation of the chemical mixing state of individual asian dust particles by the combined use of electron probe X-ray microanalysis and raman microspectrometry, Analytical Chemistry, 84(7), 3145–3154, doi:10.1021/ac2029584, 2012.

Sobanska, S., Falgayrac, G., Rimetz-Planchon, J., Perdrix, E., Brémard, C. and Barbillat, J.: Resolving the internal structure of individual atmospheric aerosol particle by the combination of Atomic Force Microscopy, ESEM-EDX, Raman and ToF-SIMS imaging, Microchemical Journal, 114(0), 89–98, doi:10.1016/j.microc.2013.12.007, 2014.

Sobanska, S., Barbillat, J., Moreau, M., Nuns, N., De Waele, I., Petitprez, D., Tobon, Y. and Brémard, C.: Influence of stearic acid coating of the NaCl surface on the reactivity with NO_2 under humidity, Physical Chemistry Chemical Physics, 17(16), 10963–10977, doi:10.1039/c4cp05655h, 2015.

Song, X. H., Hopke, P. K., Fergenson, D. P. and Prather, K. A.: Classification of single particles analyzed by ATOFMS using an artificial neural network, ART-2A, Analytical Chemistry, 71(4), 860–865, doi:10.1021/ac9809682, 1999.

Sprenger, M. and Wernli, H.: The LAGRANTO Lagrangian analysis tool - Version 2.0, Geoscientific Model Development, 8(8), 2569–2586, doi:10.5194/gmd-8-2569-2015, 2015.

Stokes, M. D., Deane, G. B., Prather, K., Bertram, T. H., Ruppel, M. J., Ryder, O. S., Brady, J. M. and Zhao, D.: A Marine Aerosol Reference Tank system as a breaking wave analogue for the production of foam and sea-spray aerosols, Atmospheric Measurement Techniques, 6(4), 1085–1094, doi:10.5194/amt-6-1085-2013, 2013.

Stroeve, J. C., Kattsov, V., Barrett, A., Serreze, M., Pavlova, T., Holland, M. and Meier, W. N.: Trends in Arctic sea ice extent from CMIP5, CMIP3 and observations, Geophysical Research Letters, 39(16), doi:10.1029/2012GL052676, 2012.

Stroeve, J. C., Markus, T., Boisvert, L., Miller, J. and Barrett, A.: Changes in Arctic melt season and implications for sea ice loss, Geophysical Research Letters, 41(4), 1216–1225, doi:10.1002/2013GL058951, 2014.

Struthers, H., Ekman, A. M. L., Glantz, P., Iversen, T., Kirkevag, A., Martensson, E. M., Seland, O. and Nilsson, E. D.: The effect of sea ice loss on sea salt aerosol concentrations and the radiative balance in the Arctic, Atmospheric Chemistry and Physics, 11(7), 3459–3477, doi:10.5194/acp-11-3459-2011, 2011.

Sturges, W. T. and Barrie, L. A.: Chlorine, Bromine and Iodine in Arctic Aerosols, Atmospheric Environment, 22(6), 1179–1194, doi:Doi 10.1016/0004-6981(88)90349-6, 1988.

Subramanian, B., Tchoukanova, N., Djaoued, Y., Pelletier, C., Ferron, M. and Robichaud, J.: Investigations on the geometrical isomers of astaxanthin: Raman spectroscopy of conjugated polyene chain with electronic and mechanical confinement, Journal of Raman Spectroscopy, 45(4), 299–304, doi:10.1002/jrs.4459, 2014.

Takami, A., Mayama, N., Sakamoto, T., Ohishi, K., Irei, S., Yoshino, A., Hatakeyama, S., Murano, K., Sadanaga, Y., Bandow, H., Misawa, K. and Fujii, M.: Structural analysis of aerosol particles by microscopic observation using a time-of-flight secondary ion mass spectrometer, Journal of Geophysical Research Atmospheres, 118(12), 6726–6737, doi:10.1002/jgrd.50477, 2013.

Taketani, F., Miyakawa, T., Takashima, H., Komazaki, Y., Pan, X., Kanaya, Y. and Inoue, J.: Shipborne observations of atmospheric black carbon aerosol particles over the Arctic Ocean,

Bering Sea, and North Pacific Ocean during september 2014, Journal of Geophysical Research, 121(4), 1914–1921, doi:10.1002/2015JD023648, 2016.

Tang, M., Alexander, J. M., Kwon, D., Estillore, A. D., Laskina, O., Young, M. A., Kleiber, P. D. and Grassian, V. H.: Optical and Physicochemical Properties of Brown Carbon Aerosol: Light Scattering, FTIR Extinction Spectroscopy, and Hygroscopic Growth, Journal of Physical Chemistry A, 120(24), 4155–4166, doi:10.1021/acs.jpca.6b03425, 2016.

Taylor, P., Hand, J. L. and Kreidenweis, S. M.: A New Method for Retrieving Particle Refractive Index and Effective Density from Aerosol Size Distribution Data, Aerosol Science & Technology, 6826(December), 37–41, doi:10.1080/0278682029009227, 2012.

Tervahattu, H., Juhanoja, J. and Kupiainen, K.: Identification of an organic coating on marine aerosol particles by TOF-SIMS, Journal of Geophysical Research-Atmospheres, 107(D16), ACH 18-1-ACH 18-7, doi:Artn 431910.1029/2001jd001403, 2002.

Thompson, B., Perry, M. J. and Davis, C.: Phytoplankton in the Damariscotta River Estuary. [online] Available from: https://digitalcommons.library.umaine.edu/seagrant_pub/6, 2006.

Tian, Y., Pan, X., Yan, J., Lin, Q., Sun, Y., Li, M., Xie, C., Uno, I., Liu, H., Wang, Z., Fu, P. and Wang, Z.: Size Distribution and Depolarization Properties of Aerosol Particles over the Northwest Pacific and Arctic Ocean from Shipborne Measurements during an R/V Xuelong Cruise, Environmental Science & Technology, 53(14), 7984–7995, doi:10.1021/acs.est.9b00245, 2019.

Tjernström, M., Leck, C., Birch, C. E., Bottenheim, J. W., Brooks, B. J., Brooks, I. M., Bäcklin, L., Chang, R. Y. W., de Leeuw, G., Di Liberto, L., de la Rosa, S., Granath, E., Graus, M., Hansel, A., Heintzenberg, J., Held, A., Hind, A., Johnston, P., Knulst, J., Martin, M., Matrai, P. A., Mauritsen, T., Müller, M., Norris, S. J., Orellana, M. V., Orsini, D. A., Paatero, J., Persson, P. O. G., Gao, Q., Rauschenberg, C., Ristovski, Z., Sedlar, J., Shupe, M. D., Sierau, B., Sirevaag, A., Sjogren, S., Stetzer, O., Swietlicki, E., Szczodrak, M., Vaattovaara, P., Wahlberg, N., Westberg, M. and Wheeler, C. R.: The Arctic Summer Cloud Ocean Study (ASCOS): overview and experimental design, Atmospheric Chemistry and Physics, 14(6), 2823–2869, doi:10.5194/acp-14-2823-2014, 2014.

Tomasi, C., Vitale, V., Lupi, A., Di Carmine, C., Campanelli, M., Herber, A., Treffeisen, R., Stone, R. S., Andrews, E., Sharma, S., Radionov, V., von Hoyningen-Huene, W., Stebel, K., Hansen, G. H., Myhre, C. L., Wehrli, C., Aaltonen, V., Lihavainen, H., Virkkula, A., Hillamo, R., Ström, J., Toledano, C., Cachorro, V. E., Ortiz, P., de Frutos, A. M., Blindheim, S., Frioud, M., Gausa, M., Zielinski, T., Petelski, T. and Yamanouchi, T.: Aerosols in polar regions: A historical overview based on optical depth and in situ observations, Journal of Geophysical Research: Atmospheres, 112(D16), doi:10.1029/2007JD008432, 2007.

Tremblay, S., Picard, J. C., Bachelder, J. O., Lutsch, E., Strong, K., Fogal, P., Richard Leaitch, W., Sharma, S., Kolonjari, F., Cox, C. J., Chang, R. Y. W. and Hayes, P. L.:

Characterization of aerosol growth events over Ellesmere Island during the summers of 2015 and 2016, Atmospheric Chemistry and Physics, 19(8), 5589–5604, doi:10.5194/acp-19-5589-2019, 2019.

Tyler, B. J., Dambach, S., Galla, S., Peterson, R. E. and Arlinghaus, H. F.: Investigation of the Utility of Laser-Secondary Neutral Mass Spectrometry for the Detection of Polyaromatic Hydrocarbons in Individual Atmospheric Aerosol Particles, Analytical Chemistry, 84(1), 76–82, doi:10.1021/ac2008338, 2012.

U.S. Energy Information Administration, I. S. A.: Top 100 U.S. Oil and Gas Fields, U.S. Department of Energy, Washington, D.C., 2015.

Ueda, S., Osada, K., Hara, K., Yabuki, M., Hashihama, F. and Kanda, J.: Morphological features and mixing states of soot-containing particles in the marine boundary layer over the Indian and Southern oceans, Atmospheric Chemistry and Physics, 18(13), 9207–9224, doi:10.5194/acp-18-9207-2018, 2018.

Unga, F., Choël, M., Derimian, Y., Deboudt, K., Dubovik, O. and Goloub, P.: Microscopic Observations of Core-Shell Particle Structure and Implications for Atmospheric Aerosol Remote Sensing, Journal of Geophysical Research: Atmospheres, 123(24), 13,944-13,962, doi:10.1029/2018JD028602, 2018.

Vancoppenolle, M., Meiners, K. M., Michel, C., Bopp, L., Brabant, F., Carnat, G., Delille, B., Lannuzel, D., Madec, G., Moreau, S., Tison, J. L. and van der Merwe, P.: Role of sea ice in global biogeochemical cycles: Emerging views and challenges, Quaternary Science Reviews, 79, 207–230, doi:10.1016/j.quascirev.2013.04.011, 2013.

Veghte, D. P., Altaf, M. B. and Freedman, M. A.: Size dependence of the structure of organic aerosol, Journal of the American Chemical Society, 135(43), 16046–16049, doi:10.1021/ja408903g, 2013.

Veghte, D. P., Bittner, D. R. and Freedman, M. A.: Cryo-transmission electron microscopy imaging of the morphology of submicrometer aerosol containing organic acids and ammonium sulfate, Analytical Chemistry, 86(5), 2436–2442, doi:10.1021/ac403279f, 2014.

de Velde, K., Boutron, C. F., Ferrari, C. P., Moreau, A.-L., Delmas, R. J., Barbante, C., Bellomi, T., Capodaglio, G. and Cescon, P.: A two hundred years record of atmospheric cadmium, copper and zinc concentrations in high altitude snow and ice from the French-Italian Alps, Geophysical Research Letters, 27(2), 249–252, 2000.

Vernet, M., Matrai, P. A. and Andreassen, I.: Synthesis of particulate and extracellular carbon by phytoplankton at the marginal ice zone in the Barents Sea, Journal of Geophysical Research: Oceans, 103(C1), 1023–1037, doi:10.1029/97jc02288, 1998.

De Villepin, J., Novak, A. and Bougeard, D.: α- And β Phases of oxalic acid, H2C2O4: Vibrational spectra, normal-coordinate calculations, and intermolecular forces, Chemical Physics,

73(3), 291–312, doi:10.1016/0301-0104(82)85170-7, 1982.

Vizcarra, N.: Arctic Sea Ice Maximum at Second Lowest in the Satellite Record, Arctic Sea Ice News and Analysis, National Snow and Ice Data Center [online] Available from: https://nsidc.org/arcticseaicenews/2018/03/arctic-sea-ice-maximum-second-lowest/ (Accessed 23 March 2018), 2018.

Walden, V. P., Rowe, P. M., Shupe, M. D. and Cox, C. J.: Humidity trends imply increased sensitivity to clouds in a warming Arctic, Nature Communications, 6, 1–8, doi:10.1038/ncomms10117, 2015.

Wang, B., Aller, J. Y., Knopf, D. a. and Alpert, P. a.: Stimulation of ice nucleation by marine diatoms, Nature Geoscience, 4(2), 88–90, doi:10.1038/ngeo1037, 2011.

Wang, B., Harder, T. H., Kelly, S. T., Piens, D. S., China, S., Kovarik, L., Keiluweit, M., Arey, B. W., Gilles, M. K. and Laskin, A.: Airborne soil organic particles generated by precipitation, Nature Geoscience, 9(6), 433–437, doi:10.1038/ngeo2705, 2016.

Wang, J., Cubison, M. J., Aiken, A. C., Jimenez, J. L. and Collins, D. R.: The importance of aerosol mixing state and size-resolved composition on CCN concentration and the variation of the importance with atmospheric aging of aerosols, Atmospheric Chemistry and Physics, 10(15), 7267–7283, doi:10.5194/acp-10-7267-2010, 2010.

Wang, Q. and Monahan, E. C.: The Influence of Salinity on the Spectra of Bubbles Formed in Breaking Wave Simulations, Sea Surface Sound, 312–319 [online] Available from: papers3://publication/uuid/C44B5C53-E615-40D0-8D54-4883EFC61386, 1995.

Wang, X., Sultana, C. M., Trueblood, J., Hill, T. C. J., Malfatti, F., Lee, C., Laskina, O., Moore, K. A., Beall, C. M., McCluskey, C. S., Cornwell, G. C., Zhou, Y., Cox, J. L., Pendergraft, M. A., Santander, M. V., Bertram, T. H., Cappa, C. D., Azam, F., DeMott, P. J., Grassian, V. H. and Prather, K. A.: Microbial control of sea spray aerosol composition: A tale of two blooms, ACS Central Science, 1(3), 124–131, doi:10.1021/acscentsci.5b00148, 2015a.

Wang, X., Jing, B., Tan, F., Ma, J., Zhang, Y. and Ge, M.: Hygroscopic behavior and chemical composition evolution of internally mixed aerosols composed of oxalic acid and ammonium sulfate, Atmospheric Chemistry and Physics, 17(20), 12797–12812, doi:10.5194/acp-17-12797-2017, 2017a.

Wang, X., Deane, G. B., Moore, K. A., Ryder, O. S., Stokes, M. D., Beall, C. M., Collins, D. B., Santander, M. V., Burrows, S. M., Sultana, C. M. and Prather, K. A.: The role of jet and film drops in controlling the mixing state of submicron sea spray aerosol particles, Proceedings of the National Academy of Sciences, 114(27), 6978–6983, doi:10.1073/pnas.1702420114, 2017b.

Wang, Z., Su, H., Wang, X., Ma, N., Wiedensohler, A., Pöschl, U. and Cheng, Y.: Scanning supersaturation condensation particle counter applied as a nano-CCN counter for size-resolved analysis of the hygroscopicity and chemical composition of nanoparticles, Atmospheric

Measurement Techniques, 8(5), 2161–2172, doi:10.5194/amt-8-2161-2015, 2015b.

Weinbruch, S., Wiesemann, D., Ebert, M., Schütze, K., Kallenborn, R. and Ström, J.: Chemical composition and sources of aerosol particles at Zeppelin Mountain (Ny ålesund, Svalbard): An electron microscopy study, Atmospheric Environment, 49, 142–150, doi:10.1016/j.atmosenv.2011.12.008, 2012.

Weinbruch, S., Benker, N., Kandler, K., Schütze, K., Kling, K., Berlinger, B., Thomassen, Y., Drotikova, T. and Kallenborn, R.: Source identification of individual soot agglomerates in Arctic air by transmission electron microscopy, Atmospheric Environment, 172, 47–54, doi:10.1016/j.atmosenv.2017.10.033, 2018.

Wentworth, G. R., Murphy, J. G., Croft, B., Martin, R. V., Pierce, J. R., Côté, J. S., Courchesne, I., Tremblay, J. É., Gagnon, J., Thomas, J. L., Sharma, S., Toom-Sauntry, D., Chivulescu, A., Levasseur, M. and Abbatt, J. P. D.: Ammonia in the summertime Arctic marine boundary layer: Sources, sinks, and implications, Atmospheric Chemistry and Physics, 16(4), 1937–1953, doi:10.5194/acp-16-1937-2016, 2016.

Wernecke, A. and Kaleschke, L.: Lead detection in Arctic sea ice from CryoSat-2: Quality assessment, lead area fraction and width distribution, Cryosphere, 9(5), 1955–1968, doi:10.5194/tc-9-1955-2015, 2015.

Wex, H., Fuentes, E., Tsagkogeorgas, G., Voigtländer, J., Clauss, T., Kiselev, A., Green, D. H., Coe, H., McFiggans, G. and Stratmann, F.: The Influence of Algal Exudate on the Hygroscopicity of Sea Spray Particles, Advances in Meteorology, 2010, 1–11, doi:10.1155/2010/365131, 2010.

Williams, J., De Reus, M., Krejci, R., Fischer, H. and Ström, J.: Application of the variability-size relationship to atmospheric aerosol studies: Estimating aerosol lifetimes and ages, Atmospheric Chemistry and Physics, 2(2), 133–145, doi:10.5194/acp-2-133-2002, 2002.

Willis, M. D., Köllner, F., Burkart, J., Bozem, H., Thomas, J. L., Schneider, J., Aliabadi, A. A., Hoor, P. M., Schulz, H., Herber, A. B., Leaitch, W. R. and Abbatt, J. P. D.: Evidence for marine biogenic influence on summertime Arctic aerosol, Geophysical Research Letters, 44(12), 6460–6470, doi:10.1002/2017GL073359, 2017.

Willis, M. D., Leaitch, W. R. and Abbatt, J. P. D.: Processes Controlling the Composition and Abundance of Arctic Aerosol, Reviews of Geophysics, 56(4), 621–671, doi:10.1029/2018RG000602, 2018.

Willis, R. D., Blanchard, F. T. and Conner, T. L.: Guidelines for the Application of SEM / EDX Analytical Techniques to Particulate Matter Samples, Environmental Protection Agency, Research Triangle Park, NC. National Exposure Research Lab., 2002.

Wilson, T. W., Ladino, L. A., Alpert, P. A., Breckels, M. N., Brooks, I. M., Browse, J., Burrows, S. M., Carslaw, K. S., Huffman, J. A., Judd, C., Kilthau, W. P., Mason, R. H.,

McFiggans, G., Miller, L. A., Najera, J. J., Polishchuk, E., Rae, S., Schiller, C. L., Si, M., Temprado, J. V., Whale, T. F., Wong, J. P. S., Wurl, O., Yakobi-Hancock, J. D., Abbatt, J. P. D., Aller, J. Y., Bertram, A. K., Knopf, D. A. and Murray, B. J.: A marine biogenic source of atmospheric ice-nucleating particles, Nature, 525(7568), 234–238, doi:10.1038/nature14986, 2015.

Van Wyngarden, A. L., Pérez-Montaño, S., Bui, J. V. H., Li, E. S. W., Nelson, T. E., Ha, K. T., Leong, L. and Iraci, L. T.: Complex chemical composition of colored surface films formed from reactions of propanal in sulfuric acid at upper troposphere/lower stratosphere aerosol acidities, Atmospheric Chemistry and Physics, 15(8), 4225–4239, doi:10.5194/acp-15-4225-2015, 2015.

Xiao, H. S., Dong, J. L., Wang, L. Y., Zhao, L. J., Wang, F. and Zhang, Y. H.: Spatially resolved micro-raman observation on the phase separation of effloresced sea salt droplets, Environmental Science and Technology, 42(23), 8698–8702, doi:10.1021/es801181f, 2008.

Xie, Z., Sun, L., Blum, J. D., Huang, Y., He, W., Utsunomiya, S., Ewing, R. C., Wang, X. and Sun, L.: Summertime aerosol chemical components in the marine boundary layer of the Arctic Ocean, Journal of Geophysical Research Atmospheres, 112(10), doi:10.1029/2006JD007247, 2006.

Xie, Z., Blum, J. D., Utsunomiya, S., Ewing, R. C., Wang, X. and Sun, L.: Summertime carbonaceous aerosols collected in the marine boundary layer of the Arctic Ocean, Journal of Geophysical Research Atmospheres, 112(2), doi:10.1029/2006JD007247, 2007.

Xu, J., Imre, D., McGraw, R. and Tang, I.: Ammonium Sulfate: Equilibrium and Metastability Phase Diagrams from 40 to −50 °C, The Journal of Physical Chemistry B, 102(38), 7462–7469, doi:10.1021/jp981929x, 2002.

Yamashita, S., Kikkawa, J., Yanagisawa, K., Nagai, T., Ishizuka, K. and Kimoto, K.: Atomic number dependence of Z contrast in scanning transmission electron microscopy, Scientific Reports, 8(1), 12325, doi:10.1038/s41598-018-30941-5, 2018.

Yang, X., Neděla, V., Runštuk, J., Ondrušková, G., Krausko, J., Vetráková, L. and Heger, D.: Evaporating brine from frost flowers with electron microscopy and implications for atmospheric chemistry and sea-salt aerosol formation, Atmospheric Chemistry and Physics, 17(10), 6291–6303, doi:10.5194/acp-17-6291-2017, 2017.

Ye, P., Xie, Z., Yu, J. and Kang, H.: Spatial distribution of methanesulphonic acid in the Arctic aerosol collected during the Chinese Arctic Research Expedition, Atmosphere, 6(5), 699–712, doi:10.3390/atmos6050699, 2015.

Yool, A., Popova, E. E. and Coward, A. C.: Future change in ocean productivity: Is the Arctic the new Atlantic, Journal of Geophysical Research: Oceans, 120(12), 7771–7790, doi:10.1002/2015JC011167, 2015.

Young, G., Jones, H. M., Darbyshire, E., Baustian, K. J., McQuaid, J. B., Bower, K. N., Connolly, P. J., Gallagher, M. W. and Choularton, T. W.: Size-segregated compositional analysis of aerosol particles collected in the European Arctic during the ACCACIA campaign, Atmospheric Chemistry and Physics, 16(6), 4063–4079, doi:10.5194/acp-16-4063-2016, 2016.

Zábori, J., Krejci, R., Ekman, A. M. L., Märtensson, E. M., Ström, J., De Leeuw, G. and Nilsson, E. D.: Wintertime Arctic Ocean sea water properties and primary marine aerosol concentrations, Atmospheric Chemistry and Physics, 12(21), 10405–10421, doi:10.5194/acp-12-10405-2012, 2012.

Zangmeister, C. D. and Pemberton, J. E.: Raman Spectroscopy of the Reaction of Sodium Chloride with Nitric Acid: Sodium Nitrate Growth and Effect of Water Exposure, The Journal of Physical Chemistry A, 105(15), 3788–3795, doi:10.1021/jp003374n, 2001.

Zawadowicz, M. A., Proud, S. R., Seppalainen, S. S. and Cziczo, D. J.: Hygroscopic and phase separation properties of ammonium sulfate/organics/water ternary solutions, Atmospheric Chemistry and Physics, 15(15), 8975–8986, doi:10.5194/acp-15-8975-2015, 2015.

Zhang, T., Zhuang, Y., Jin, H., Li, K., Ji, Z., Li, Y. and Bai, Y.: Comparison of Phytoplankton Communities Between Melt Ponds and Open Water in the Central Arctic Ocean, Journal of Ocean University of China, 18(3), 573–579, doi:10.1007/s11802-019-3871-0, 2019.

Zhang, Y., Chen, Y., Lambe, A. T., Olson, N. E., Lei, Z., Craig, R. L., Zhang, Z., Gold, A., Onasch, T. B., Jayne, J. T., Worsnop, D. R., Gaston, C. J., Thornton, J. A., Vizuete, W., Ault, A. P. and Surratt, J. D.: Effect of the Aerosol-Phase State on Secondary Organic Aerosol Formation from the Reactive Uptake of Isoprene-Derived Epoxydiols (IEPOX), Environmental Science and Technology Letters, 5(3), 167–174, doi:10.1021/acs.estlett.8b00044, 2018.

Zhang, Z., Li, H., Liu, H., Ni, R., Li, J., Deng, L., Lu, D., Cheng, X., Duan, P. and Li, W.: A preliminary analysis of the surface chemistry of atmospheric aerosol particles in a typical urban area of Beijing, Journal of Environmental Sciences (China), 47, 71–81, doi:10.1016/j.jes.2016.01.025, 2016.

Zhou, S., Hwang, B. C. H., Lakey, P. S. J., Zuend, A., Abbatt, J. P. D. and Shiraiwa, M.: Multiphase reactivity of polycyclic aromatic hydrocarbons is driven by phase separation and diffusion limitations, Proceedings of the National Academy of Sciences, 116(24), 11658–11663, doi:10.1073/pnas.1902517116, 2019.

Zhuang, H., Chan, C. K., Fang, M. and Wexler, A. S.: Formation of nitrate and non-sea-salt sulfate on coarse particles, Atmospheric Environment, 33(26), 4223–4233, doi:10.1016/S1352-2310(99)00186-7, 1999.

Ziemba, L. D., Dibb, J. E., Griffin, R. J., Huey, L. G. and Beckman, P.: Observations of particle growth at a remote, Arctic site, Atmospheric Environment, 44(13), 1649–1657, doi:https://doi.org/10.1016/j.atmosenv.2010.01.032, 2010.